Recombinant sFRPs in Wnt/β-Catenin Signaling Targeted Cancer Therapy

A Thesis

Submitted in Partial Fulfillment of the

Requirements for the award of the degree of

Doctor of Philosophy

by

ARCHITA GHOSHAL

Roll no - 11610607

Department of Biosciences and Bioengineering

Indian Institute of Technology Guwahati

Guwahati 781039, Assam, India

July 2016

Recombinant sFRPs in Wnt/β-Catenin Signaling Targeted Cancer Therapy

A Thesis

Submitted in Partial Fulfillment of the

Requirements for the award of the degree of

Doctor of Philosophy

by

ARCHITA GHOSHAL

Roll no - 11610607

Department of Biosciences and Bioengineering

Indian Institute of Technology Guwahati

Guwahati 781039, Assam, India

July 2016

Dedicated to

My Parents & My Grandma

DECLARATION

I, hereby, declare that the matter embodied in this thesis titled "**Recombinant sFRPs in Wnt/β-Catenin Signaling Targeted Cancer Therapy**" is the result of investigations carried out by me under the supervision of Prof. Siddhartha Sankar Ghosh, Department of Biosciences and Bioengineering, Indian Institute of Technology Guwahati, India for the award of the degree of Doctor of Philosophy. This work has not been submitted elsewhere for any degree, diploma, associateship or membership etc. of any institute or university to the best of my knowledge and belief.

July 2016

Archita Ghoshal

Roll no. - 11610607

INDIAN INSTITUTE OF TECHNOLOGY GUWAHATI

DEPARTMENT OF BIOSCIENCES AND BIOENGINEERING

CERTIFICATE

This is to certify that the thesis titled "**Recombinant sFRPs in Wnt/β-Catenin Signaling Targeted Cancer Therapy**" being submitted to the Indian Institute of Technology Guwahati by **Archita Ghoshal** for the award of the degree of Doctor of Philosophy in Department of Biosciences and Bioengineering, is a bonafide record of research work carried out by her. The contents of this thesis have not been submitted to any other University or Institute for the award of any degree or diploma.

Prof. Siddhartha Sankar Ghosh

Thesis Supervisor

ACKNOWLEDGEMENT

I would like to take this once-in-a-lifetime opportunity to express my heartfelt gratitude to all the people who have helped me through the tenure of my PhD as well as to all those who helped me get here in the first place. My family, my teachers and my friends have all played an immensely important role in my life, for which I shall be forever indebted to them.

First of all, I would express my deepest gratitude to my thesis supervisor Prof. Siddhartha Sankar Ghosh, who has been a guide to me in every sense of the term. I will never forget all those times when he has provided endless moral support, especially at times when research failed me and positive results refused to come. With due respect to all my teachers, I believe that one can hardly hope to be inducted under the guidance of such a human being as I was fortunate enough to be. Thank you Sir, for all your motivation, encouragement and support.

I am also enormously grateful to my doctoral committee members- Prof. Pranab Goswami, Dr. Biplab Bose, and Dr. Vaibhav V. Goud, for their valuable suggestions and critical inputs throughout the course of these five years. I am also highly obliged to Prof. Arun Chattopadhyay, who has always readily agreed to give his critical suggestions, whenever I have approached him.

I am grateful to the Department of Biosciences and Bioengineering, Centre for Nanotechnology, and Central Instrumentation Facility, IIT Guwahati, for providing me with all the support required for carrying out my thesis work. I would like to thank all the staff members as well. Also, I am grateful to the Department of Biotechnology (DBT), India and the Centre for International Co-operation in Science (CICS) for granting me financial support for participating in an international conference in Germany.

Next, I would like to express my sincerest gratitude to the seniors of my lab- Kohila di, Chocks bhaiya, Subhamoy da and Nidhi di for painstakingly, yet lovingly, imparting to me all their gathered knowledge. I will always remember the affection bestowed upon me by my beloved seniors. I am also thankful to my seniors- Amaresh da, Mitun da, Amit da, Shilpa

di, Pallab da, Pojul da, Ashok da, Ashim da, Mohitosh da, Debomitra di, Damini di, Rumi di, Ankana di, and Rama for all their help and advice.

Moreover, I am extremely thankful to current lab-members, who are also some of the closest friends that I have here- Sharmi, Asif, Neha, Anil, Srirupa, Gavya and few former lab-mates- Vanitha and Gargi. They are the ones who have made our lab my second home and I will forever appreciate the numerous times when they have assisted me in my experimental work and provided moral support in times of need. I would also deeply appreciate my other colleagues and friends- Upashi, Bandhan, Deepanjalee, Anita, Srestha, Anushree, Sunil. I also take this moment to thank my other friends and neighboring-lab-mates- Sambhavi, Nivedita, Priyamvada, Babina, Poulomi, Aruna, Mahesh, Thiyagarajan, Sandipan, Sanjeev, Vimal, Arun, Himanshu, Yoganand, Shruti, Vijya, Ruchi and many more... I will also carry with me all those precious moments spent with my seniors and my friends, in enjoying the aspects of life other than work.

Last but definitely not the least, I would like to thank my parents for all their love, incessant support, guidance through every step of my way, for putting up with all my tantrums, and for fulfilling all my wishes. I am grateful to my family members, especially my Dibhai, as well as to my best friends. Thank you God, for everything that You have given me.

CONTENTS

ABBREVIATIONS xix

ABSTRACT xxiii

CHAPTER 1: Introduction and Review of Literature 1

1.1 Recombinant proteins 3

1.2 Recombinant proteins in cancer therapy 5

1.3 Recombinant proteins 6

1.3.1 Wnt signaling 7

1.3.2 Role of Secreted Frizzled-related Proteins (sFRPs) in Wnt signaling 10

1.4 Composite nanoparticles in therapy 13

1.4.1 Polymeric nanoparticles 15

1.4.2 Fluorescent nanoclusters 16

1.5 Nanoparticles and Recombinant proteins: an interplay 16

1.6 Key questions and scope of research 17

1.7 Objectives of the thesis 18

1.8 Salient features of this work 18

CHAPTER 2: Expression, Purification, and Therapeutic Implications of Recombinant sFRP1

2.1 Introduction 21

2.2 Material and Methods 22

2.2.1 Cell culture 22

2.2.2 Cloning of sFRP1 23

2.2.3 Expression of GST-sFRP1 in *E.coli* BL21 (DE3) 23

2.2.4 Solubilization, Purification and Refolding of GST-sFRP1 protein 24

2.2.5 Homology modeling and docking studies 25

2.2.6 Western blotting 25

2.2.7 Secondary structure characterization with circular dichroism 26

2.2.8 MALDI TOF-TOF analysis 26

2.2.9 Cell viability assay 26

2.2.10 Combination therapy 27

2.2.11 Cell cycle analysis 27

2.2.12 Statistical tests 28

2.3 Results and Discussion 28

2.3.1 Cloning, expression and purification of GST-sFRP1 28

2.3.2 Homology modeling and docking studies 32

2.3.3 Western blot analysis 39

2.3.4 Secondary structure characterization with circular dichroism 40

2.3.5 Analysis of MALDI TOF-TOF data 41

2.3.6 Cell viability assay 42

2.3.7 Combination therapy 44

2.3.8 Cell cycle analysis 47

2.3.9. Effect of GST-SFRP1 on non-cancerous cell line HEK-293 50

2.4 Conclusions 51

CHAPTER 3: Targeting Wnt Canonical Signaling by Recombinant sFRP1 Bound Luminescent Au-Nanocluster Embedded Nanoparticles in Cancer Theranostics

3.1 Introduction 55

3.2 Material and Methods 57

3.2.1 Synthesis of Chitosan-Au NC-Alginate NPs (Chi-Au NC-Alg NPs) 57
3.2.2 Expression, purification of GST tagged human sFRP1 58
3.2.3 Characterization of Chi-Au NC-Alg NPs 58
3.2.4 Imaging of Chi-Au NC-Alg NPs with TEM and fluorescence Microscope 58
3.2.5 Binding studies of NPs with protein 58
3.2.6 Release studies of protein 59
3.2.7 Mammalian cell culture 59
3.2.8 Stability studies of NPs and tracking the release of protein 59
3.2.9 Assessment of cell viability 60
3.2.10 Tracking NPs with high-end deconvolution microscopy 60
3.2.11 Preparation of whole cell protein lysate and western blotting 60
3.2.12 Acridine orange (AO) / Ethidium bromide (EB) dual staining 61
3.2.13 Expression profiling for downstream genes 62
3.2.14 Combination therapy with cisplatin 62
3.2.15 Cell cycle analysis 62
3.2.16 Detection of apoptosis by fluorescein isothiocyanate (FITC) conjugated Annexin V/ PI 63
3.3 Results and Discussion 63
3.3.1 Recombinant GST-sFRP1 bound to Chi-Au NC-Alg NPs 63
3.3.2 Binding and release studies of recombinant protein 69
3.3.3 Stability of Au NCs in cell culture media studied by probing Luminescence 72
3.3.4 Tracking NPs for anti-cancer function 73
3.3.5 Targeting the Wnt signaling pathway 76

3.3.6 Molecular mechanisms in combination module 79

3.4 Conclusions 82

CHAPTER 4: Antagonizing Canonical Wnt Signaling Pathway by Recombinant Human sFRP4 Purified from *E. coli* and its Implications in Cancer Therapy

4.1 Introduction 87

4.2 Material and Methods 90

4.2.1 Cell culture 90

4.2.2 Materials 90

4.2.3 Cloning of sFRP4 90

4.2.4 Expression of sFRP4 in *E.coli* BL21(DE3) 90

4.2.5 Purification of sFRP4 from bacterial system 91

4.2.6 Homology modeling and docking analyses 92

4.2.7 MALDI TOF/TOF analysis 92

4.2.8 Secondary structure analysis using circular dichroism 92

4.2.9 Expression profile analysis of genes involved in the Wnt pathway in three different cell lines 93

4.2.10 Western blotting 93

4.2.11 Combination therapy 93

4.2.12 Cell viability assay 94

4.2.13 Cell cycle analysis 94

4.2.14 Apoptosis detection assay 95

4.2.15 AO/EB dual staining for detection of apoptosis 95

4.2.16 Real-time PCR analysis (List of primers) 95

4.2.17 Statistical tests 96

4.3 Results and Discussion 96

4.3.1 Expression profile analysis of genes associated with Wnt family 96

4.3.2 Cloning, expression, and purification of sFRP4 98

4.3.3 Characterization of recombinant GST-sFRP4 101

4.3.4 Prediction of 3-D structure of GST-sFRP4 and its docking with Wnt7a 102

4.3.5 Anti-proliferative effect of GST-sFRP4 106

4.3.6 Anti-proliferative effect of GST-sFRP4 in combination with GST-sFRP1 107

4.3.7 Targeting classical Wnt/β-catenin signaling with GST-sFRP4 107

4.3.8 Efficacy of co-therapy 110

4.3.9 Determination of cell cycle arrest by flow cytometry 111

4.3.10 Induction of apoptosis in a co-therapy module 114

4.3.11 Quantitative expression profiling of Wnt downstream genes by Real-time PCR 118

4.3.12 Effect on GST-sFRP4 on normal cell line 3T3-L1 121

4.4 Conclusions 122

CHAPTER 5: Recombinant sFRP4 bound Chitosan-Alginate Composite Nanoparticles Embedded with Silver Nanoclusters for Wnt/ β-catenin targeting in Cancer Theranostics

5.1 Introduction 127

5.2 Material and Methods 129

5.2.1 Chemicals 129

5.2.2 Synthesis of Chi-Ag NC-Alg NPs 129

5.2.3 Expression and Purification of GST tagged sFRP4 129

5.2.4 Characterization of Chi-Ag NC-Alg NPs 130
5.2.5 Binding and release studies of NPs with GST-sFRP4 130
5.2.6 Mammalian Cell Culture 131
5.2.7 Cytotoxicity assays 131
5.2.8 Estimation of cellular uptake of NPs 132
5.2.9 Western blotting for confirmation of affected signaling Pathway 132
5.2.10 Studying the mode of cell death 133
5.2.11 ROS generation 133
5.2.12 Cell cycle analysis 133
5.2.13 Annexin V-FITC / PI Apoptosis detection assay 133
5.2.14 Dual staining with AO/ EB 134
5.2.15 FESEM analysis 134
5.3 Results and Discussion 135
5.3.1 Expression of functional GST-sFRP4 135
5.3.2 Binding of sFRP4 with Ag NC-Chitosan-Alginate NPs based on electrostatic interactions 135
5.3.3 Characterization of Ag NC-Chi-Alg NPs 136
5.3.4 Therapeutic efficacy determined by cell viability assays 141
5.3.5 Cellular uptake of luminescent NPs assessed by Confocal microscopy and Flow cytometry 142
5.3.6 Targeting the Wnt/ β-catenin signaling by recombinant sFRP4 145
5.3.7 Cytotoxic effect of Ag NC embedded NPs 147
5.3.8 Co-therapeutic efficacy of sFRP4 bound NPs 149
5.4 Conclusion 151

CONCLUSION AND FUTURE PROSPECTS 155

REFERENCES 158

LIST OF PUBLICATIONS 180

CONFERENCES ATTENDED 181

APPENDIX 182

ABBREVIATIONS

Ag NC-Chi-Alg NPs	- Silver nanoclusters-chitosan-alginate nanoparticles
AO	- Acridine orange
APC	- Adenomatous polyposis coli
β-cat	- β-catenin
βTrCP	- β-transducin repeat-containing protein
BSA	- Bovine serum albumin
CD52	- Cluster of differentiation 52
cDNA	- Complementary deoxyribonucleic acid
Chi-Au NC-Alg NPs	- Chitosan- gold nanoclusters-alginate nanoparticles
CRD	- Cysteine-rich domain
DCFDA	- Dichlorofluorescin diacetate
DLS	- Dynamic light scattering
DMEM	- Dulbecco's Modified Eagle's Medium
DMSO	- Dimethyl sulfoxide
DNA	- Deoxyribose nucleic acid
Dsh	- Dishevelled
EB	- Ethidium bromide
EDTA	- Ethylenediaminetetraacetic acid
EGFR	- Epidermal growth factor receptor
FACS	- Fluorescence-activated cell sorting
FBS	- Fetal bovine serum
FDA	- Food and Drug Administration
FESEM	- Field Emission Scanning Electron Microscopy

FITC	- Fluorescein isothiocyanate
FTIR	- Fourier transform infrared spectroscopy
Fzd	- Frizzled
GSK3β	- Glycogen synthase kinase 3β
GST	- Glutathione S-transferase
HER2	- Human epidermal growth factor receptor 2
HRP	- Horseradish peroxidase
IAP	- Inhibitors of apoptosis
IPTG	- Isopropyl β-D-1-thiogalactopyranoside
LB	- Luria Bertani
LEF	- Lymphoid enhancer-binding factor
LRP	- Low density lipoprotein receptor-related protein
MALDI TOF	- Matrix-assisted laser desorption/ionization time-of-flight
MPA	- 2-mercaptopropionic acid
MPS	- Mononuclear phagocyte system
MTT	-3-(4,5-dimethylthiazol-2-yl)-2,5diphenyltetrazolium bromide
NIR	- Near-infrared
NLD	- Netrin-like domain
NP	- Nanoparticle
OD	- Optical density
PBS	- Phosphate-buffered saline
PBST	- PBS with 1% Tween-20
PCR	- Polymerase chain reaction
PEG	- Polyethylene glycol
PI	- Propidium iodide

PLGA	- Poly lactide-co-glycolide
PLA	- Polylactic acid
PMSF	- Phenylmethylsulfonyl fluoride
PVDF	- Polyvinylidene difluoride
RNA	- Ribonucleic acid
ROS	- Reactive oxygen species
SDS-PAGE	- Sodium dodecyl sulfate polyacrylamide gel electrophoresis
siRNA	- Small interfering RNA
sFRP	- Secreted frizzled-related protein
SPR	- Surface plasmon resonance
TBS	- Tris-buffered saline
TBST	- TBS with 1% Tween-20
TCF	- T cell-specific transcription factor
TEM	- Transmission electron microscopy
VEGF	-Vascular endothelial growth factor
WIF1	- Wnt-inhibitory factor-1

ABSTRACT

Cancer cells are known to lack regulation of cell proliferation due to the aberrant behavior of a myriad of signaling pathways. One such pathway is the Wnt signal cascade, which is one of the multiple facets responsible for the upregulation of several pro-proliferative genes in cancer. In non-cancerous cells, this Wnt pathway is blocked by a family of secretory glycoproteins playing a role in cell growth arrest, called the secreted frizzled-related proteins (sFRPs). However, these sFRPs are typically silenced in cancer due to promoter hypermethylation.

The current thesis aims to exploit the anti-proliferative role of sFRPs to regulate cancer cell proliferation *in vitro* by targeted protein therapeutics. More specifically, the two most promising sFRPs, viz., sFRP1 and sFRP4, were selected for the development of novel co-therapeutic and theranostic models for combating cancer in cell culture model. In **Chapter 1,** the burgeoning field of recombinant protein therapeutics has been delved into. Essentially, the role of recombinant proteins in regulating signal networks, their potential clinical usage as well as the advantages they hold over current modes of cancer therapy, have been encompassed in this chapter. More specifically, the role of sFRPs in regulating cell growth by modulation of the Wnt pathway has been deliberated. The use of nanomaterials for stability and sustained release of the recombinant proteins, while enabling their tracking and delivery to desired sites, has also been discussed herein. In **Chapter 2,** the cloning, expression, and purification of recombinant human sFRP1 using *Escherichia coli* has been reported. Further, the therapeutic implications of the GST tagged sFRP1, alone and in combination with conventional chemotherapeutic drugs, viz. cisplatin and doxorubicin, in two different cancer cell lines were deciphered by cell viability assay and cell cycle analysis. In **Chapter 3**, the fabrication of a versatile novel sFRP1 bound composite nanoparticles has been demonstrated. In this approach, gold nanoclusters-embedded nanoparticles were utilized for analysis of binding, tracking, and sustained release of sFRP1 from the nanoparticles. Inferences were drawn based on luminescence detection using fluorescence spectrometry, flow cytometry, and high-end deconvolution microscopy. The stability imparted by the nanoparticles to the protein resulted in enhanced anti-tumor efficacy. Most

importantly, this method implied targeted cancer therapy, as the protein component sFRP1 ensured the targeting of the Wnt pathway in cancer cells. Studies using Western blotting and semi-quantitative PCR-based expression of essential molecules of the Wnt pathway validated the molecular mechanisms. A co-therapy module with cisplatin was also exhibited by extensive cell-based assays for further augmentation of anti-cancer activity. In **Chapter 4**, the cloning of human sFRP4 from a novel source- ACHN renal carcinoma cell line has been reported, along with its bacterial expression, purification, characterization, and anti-proliferative effect. Expression analysis of downstream Wnt pathway molecules by Western blotting and quantitative real-time PCR showed that the functional recombinant sFRP4 inhibited the canonical Wnt signaling. Improved cellular responses upon combination therapy with cisplatin/doxorubicin were revealed by cell cycle analysis and dual staining-based assays. In **Chapter 5,** the theranostic potential of a sFRP4 bound silver nanoclusters-embedded nanoparticle platform has been illustrated. While the extraordinary luminescence properties of the nanoclusters enabled binding, imaging, and uptake studies, Western blotting documented the targeting of Wnt signaling by the GST-sFRP4 released from the NPs. Furthermore, co-therapeutic benefits of sFRP4 and silver clusters were examined. The effects on cancer cells were elaborately delineated by cell viability assays, flow cytometry-based cell cycle, apoptosis detection assays as well as microscopy-based experiments. Time dependent uptake of luminescent silver clusters was demonstrated by confocal microscopy and flow cytometry. In the final section on **Conclusion and Future Prospects,** the thrust areas of this study have been highlighted and the importance of these findings has been emphasized.

In brief, human sFRP1 and sFRP4 have been cloned and expressed in bacterial system. The expression and purification procedure was extensively optimized to obtain the proteins in soluble form. Glutathione agarose-based affinity chromatography was used to purify both the recombinant proteins. Thereafter, the therapeutic efficacy of the proteins on mammalian cancer cells was determined, alone as well as in co-therapy module. Binding with noble metal nanoclusters enhanced the efficacy of the proteins and enabled luminescence-based binding, imaging, and uptake studies. Further the functionality of the proteins was evaluated by their role in inhibiting the Wnt/ β-catenin signaling pathway and induction of apoptosis

of the cells was investigated by various assays. The current therapeutic approach holds immense promise in the field of *in vivo* cancer theranostics.

CHAPTER 1

Introduction and Review of Literature

CHAPTER 1

Introduction and Review of Literature

1.1 Recombinant proteins

Proteins play the most dynamic roles in biological functioning- constituting the physical support system of cells, participating in a myriad of biochemical reactions, forming membrane receptors and channels, and carrying out molecular trafficking. While this dependency of the human body on proteins poses a major challenge to the medical world when any gene or protein behaves abnormally, this also provides a large window of opportunity for exploiting proteins for treatment of these diseases. The advent of protein therapy was a significant breakthrough in research, whereby proteins began to be administered exogenously to target cells. Proteins offer several advantages over small molecule drugs; they can perform complex functions, elicit reduced or negligible immune responses without interfering with normal biological functions and are highly specific in their targeting. However, isolation of these proteins from animal sources has several disadvantages; the limited availability of animal sources raises the cost of production, not to mention the immunogenic reaction of the human body to animal proteins. This limitation was surmounted when the first recombinant protein-insulin was produced by genetically engineering *Escherichia coli*. The approval of insulin in 1982 by the US FDA (Food and Drug Administration) ushered in the era of recombinant therapeutic proteins. Since then, over 100 such recombinant proteins have been given consent for clinical usage and many more are in the pipeline. Examples of recombinant proteins (examples in **Table 1.1**) already in the market include growth hormone somatotrophin used to treat growth failure, blood coagulation factors VIII and IX for hemophilia, β-glucocerebrosidase for gaucher's disease, erythropoietin, interferons, pancreatic enzymes, albumin, osteoporosis, streptokinase etc [1].

Recombinant protein drug	Clinical use
Teriparatide (parathyroid hormone)	Osteoporosis
β-glucocerebrosidase	Gaucher's disease
Erythropoietin	Certain types of anaemia
Oprelvekin (Interleukin11)	Thrombocytopenia
Human follicle-stimulating hormone	Assisted reproduction
Interferon-α2a	Chronic hepatitis C/ types of leukemia
Factor VII	Certain types of haemorrhaging
Hyaluronidase	Adjuvant for anesthesia
Adalimumab	Rheumatoid arthritis

Table 1.1. Few examples of recombinant protein therapy currently in clinical usage.

Immunotherapy-based treatment options have been in the process of being perfected for decades.[2] Interleukin-2 is the first effective adoptive immunotherapy, which involves boosting the patient's immune system by expanding the T-cell population [3, 4]. **Figure 1.1** and **Figure 1.2** depict the market analysis of protein drugs as presented by various groups.

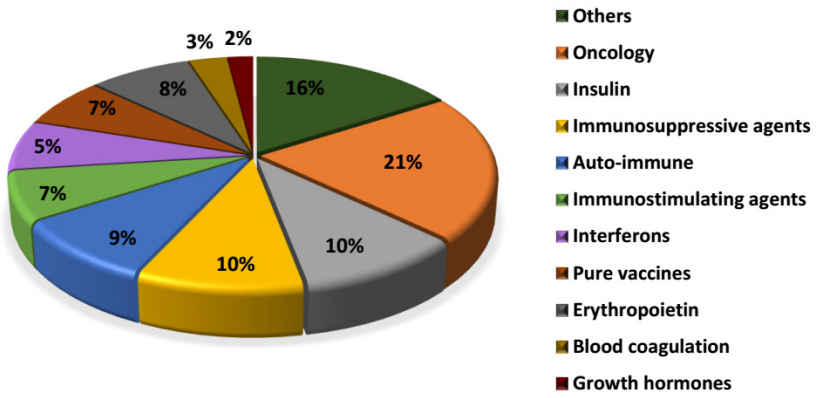

Figure 1.1. Redrawn from the information provided in the 'Global Protein Therapeutics Market Forecast to 2015'. The pie chart shows the market share of the protein therapy drug classes, as estimated for the year 2015 (http://laborant.pl/index.php/recombinant-protein-therapeutics-the-future-is-here).

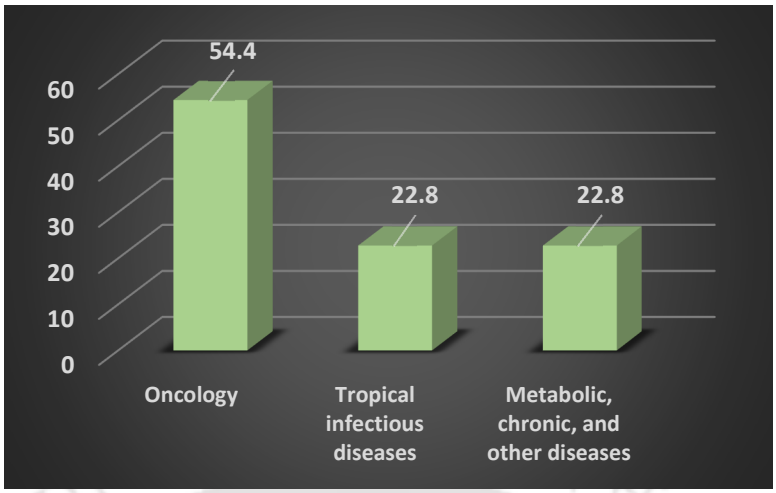

Figure 1.2. Redrawn from the market analysis data by Frost and Sullivan (http://www.frost.com/prod/servlet/market-insight-print.pag?docid=265837953). The bar graph shows the percentage of therapeutic vaccine candidates in different stages of clinical pipeline.

1.2 Recombinant proteins in cancer therapy

In the past few decades, an array of novel strategies, designed and aimed to treat cancer, have surfaced. Of them, recombinant protein therapeutics is one such modality that has emerged for the treatment of this complex and diverse diseases. Yet, the only recombinant proteins available for the treatment of cancer are monoclonal antibodies against cell surface molecules [1]. The categories of protein-based vaccines in various stages of clinical trial have been demonstrated in **Figure 1.3**.

Although a deep insight into the molecular basis of human malignancies has initiated the implementation of protein therapy in treatment of human cancers, cure of cancer has proven to be greatly elusive to molecular biologists and chemists alike. A major challenge in curing cancer lies in the fact that non-malignant cells need to be preserved while cancer cells are being targeted. Adverse side effects of conventional chemotherapeutic drugs, like doxorubicin [5, 6] and cisplatin [7], along with the development of multi-drug resistance have led to the search for alternatives.

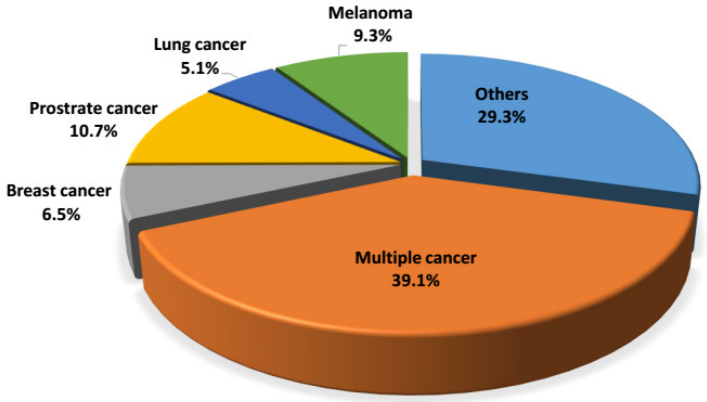

Figure 1.3. Redrawn from the market analysis data by Frost and Sullivan (http://www.frost.com/prod/servlet/market-insight-print.pag?docid=265837953). The bar graph shows the percentage of vaccine candidates for cancer therapy in different stages of clinical pipeline.

1.3 Recombinant proteins in targeting signaling pathways

The approach of recombinant protein therapy to target specific cell signaling pathways in cancer is an increasingly exciting avenue of research. Intricately woven signaling networks have been targeted using humanized monoclonal antibodies designed against tyrosine kinase receptor Human epidermal growth factor receptor 2 (HER2) [8] in metastatic breast cancers, Vascular Endothelial Growth Factor Receptor (VEGFR) in colorectal cancers [9], and Epidermal Growth Factor Receptor (EGFR) [10]. Till date, the only options of protein drugs available in the market for cancer therapy are these monoclonal antibodies (**Table 1.2**) developed against various molecules that are typically overexpressed in specific cancer types, such as cell surface receptors [1, 8-16].

Cancer type	Proteins (receptors) against which humanized monoclonal antibodies have been generated
Colorectal cancer	VEGF, EGFR
Head and neck cancer	EGFR
Chronic lymphocytic leukemia	CD52 antigen
Breast cancer	HER2/Neu receptor
Lymphoma/ Non-Hodgkin's lymphoma	CD20 antigen
Hodgkin's lymphoma	CD30 antigen
Acute myelogenous leukemia	CD33 antigen
Epithelial tumors	EpCAM glycoprotein
Colorectal carcinoma	gpA133 glycoprotein
Neuroectodermal tumors	Gangliosides (GD2, GD3 etc.)
Tumor vasculature	Integrins
Colon, lung and pancreas tumours, haematological malignancies	TRAILR1/R2
Colon, breast, lung, pancreas, head and neck tumours	FAP

Table 1.2. Examples of drugs marketed for cancer therapy [17].

1.3.1 Wnt signaling

One pathway that has been strongly associated with cancer is the Wnt signal transduction pathway [18]. Its aberrant upregulation in a multitude of cancers culminates in the activation

of several pro-proliferative genes [18, 19]. Initiated by Wnt ligand binding to corresponding Frizzled (Fzd) receptors, the Wnt pathway plays an active role in differentiation events during normal embryonic developmental processes. Comprising of a family of 19 members, these Wnt ligands are secreted glycoproteins differentially expressed by different types of cancer. The signal transduction is initiated by the binding of Wnt ligands to their corresponding Fzd receptors, which belong to the G-protein-coupled receptor superfamily. While there are other Wnt receptors reported in literature, such as receptor tyrosine kinases ROR1 and ROR2, Fzd receptors are the ones more common. Of the family of 10 Fzd members, several have been known to be overexpressed in certain cancer types, such as Fzd6 [19] and Fzd7 [20], and may contribute to carcinogenesis. The binding of Wnt ligands to Fzd receptors is facilitated by coreceptor Low density lipoprotein receptor-related protein (LRP) - LRP5 or LRP6.

Wnt pathway has traditionally been classified into two categories that two have been found to be active in tumor formation and angiogenesis [21]:

- The classical or canonical Wnt pathway, better known as the β-catenin dependent Wnt signaling, is primarily observed in tumorigenesis. Mutations in Wnt genes or Wnt pathway component genes result in constitutive, redundant transduction of the Wnt pathway in cancer, central to which, is the stabilization of cytoplasmic β-catenin. Regulation of β-catenin levels is maintained by a destruction complex comprising of intermediate molecules like Axin, serine/threonine kinase GSK3β (glycogen synthase kinase 3β), tumor suppressor gene APC (adenomatous polyposis coli), CKI (casein kinase I) and Dishevelled (Dsh). In absence of Wnt ligand binding with its Fzd receptor, these proteins maintain a low level of cytoplasmic β-catenin by continuous proteasome-mediated ubiquitination. More specifically, GSK3β is responsible for priming β-catenin for β-transducin repeat-containing protein (β-TrCP) mediated proteosomal degradation, by phosphorylating serine residues at different sites. When Wnt binds to Fzd receptor, in presence of LRP5 or 6, Axin and Dsh bind to LRP and abandon the destruction complex, thereby inhibiting the degradation of β-catenin. This results in accumulation of cytoplasmic and nuclear β-catenin, which in turn, translocates to the nucleus and interacts with transcription factors LEF/TCF (Lymphoid enhancer-binding factor/T cell-specific transcription

factor) to activate expression of downstream target genes like survivin, c-jun, cyclin D1 and c-myc [22-25]. Transcription of these pro-proliferative genes results in anomalous cell cycle progression. The Wnt signaling pathway has been delineated in brief in **Figure 1.4**.

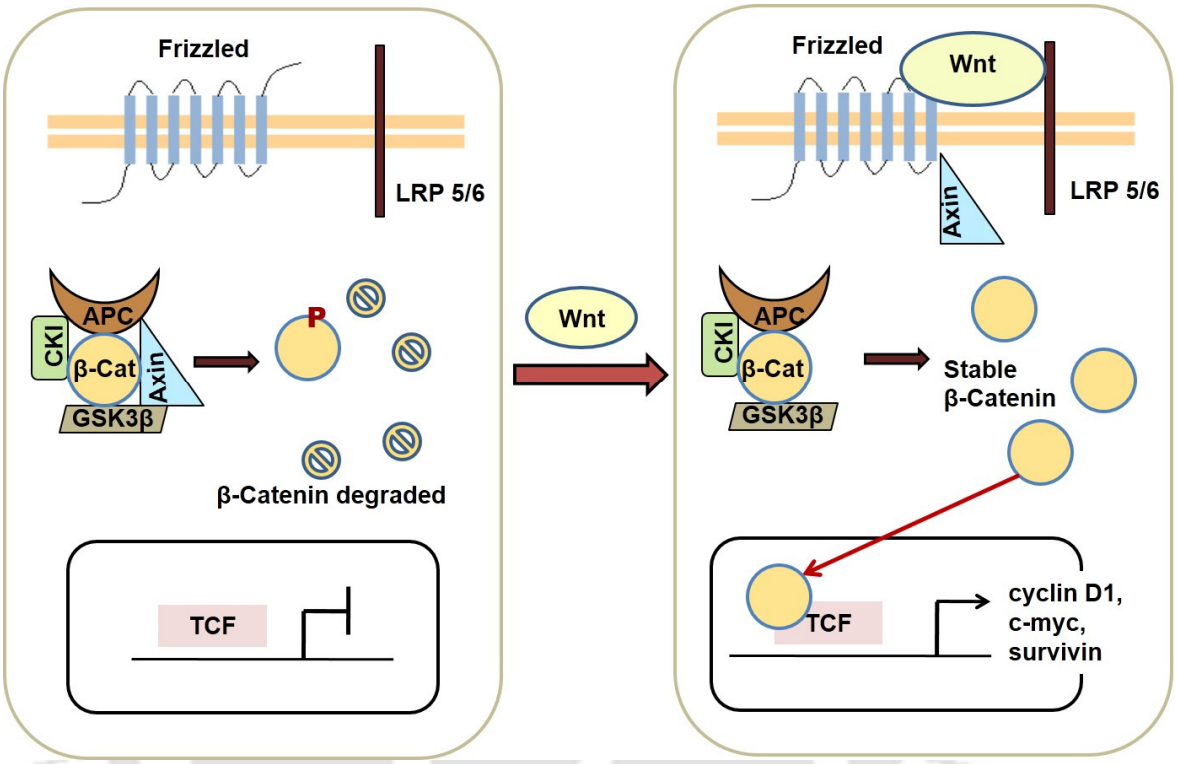

Figure 1.4. Wnt pathway in absence and presence of Wnt ligand. (APC- adenomatous polypsis coli, β-Cat- β-catenin, CKI-casein kinase I, GSK3β-glycogen synthase kinase 3β, LRP-low-density lipid receptor, TCF-T-cell factor).

- The Wnt/Ca^{2+} pathway, also known as the β-catenin independent or the non-canonical Wnt pathway, revolves round the stimulation of Ca^{2+} sensitive signaling components due to activation by Wnt5a and Wnt11. Implication of this branch of Wnt in cancer is, till date, indistinct.

Understanding the underlying details of this pathway may prove to be pivotal for the future of cancer therapy [19]. This may involve binding of inhibitory molecules to Wnt ligands to prevent its functioning via canonical and non-canonical pathways [26, 27], or targeting downstream entities in the canonical Wnt pathway [28]. Natural blockers of the Wnt pathway are divided into two classes-the first class includes the secreted frizzled-related

proteins (sFRPs) [29-32], WIF-1 (Wnt-inhibitory factor-1), and Cerberus. The second class includes members of the Dickkopf family, which bind to the LRPs and inhibit the canonical Wnt signaling [33]. Exploiting these inhibitors has opened up an evolving prospect in cancer therapy that is still in its very nascent stage of development.

1.3.2 Role of Secreted Frizzled-related Proteins (sFRPs) in Wnt signaling

Explorations into the world of sFRP superfamily and their implications in cancer have commenced only recently. Human sFRP was first purified and identified from human embryonic lung fibroblast culture fluid and was believed to be an antagonizer of the Wnt pathway [34]. These sFRPs are approximately 300 amino acids in length and have been found to share sequence similarity with the extracellular cysteine-rich domain (CRD) of Fzd receptors. Hence, they act as putative binding sites for Wnt proteins [34]. As sFRPs lack transmembrane domain for Wnt signal transduction within the cell, they serve to inhibit the Wnt pathway by blocking the binding of Wnt ligands to respective Fzd receptors in normal human tissue (**Figure 1.5**) [32]. However, in various cancers, such as, colorectal cancers [30], gastric cancers [35], invasive breast tumors [36], bladder cancer, [31] and tumors of mesenchymal origin [29], these sFRPs have been found to be downregulated due to promoter hypermethylation. In absence of these sFRPs, β-catenin, a downstream molecule of the Wnt pathway, escapes proteasome degradation and accumulates in the cytoplasm. Thereafter, it translocates to the nucleus, where it is involved in transcriptional upregulation of genes activating cell proliferation (such as c-myc and cyclin D1 [18]) or genes inhibiting apoptosis (such as survivin [37]).

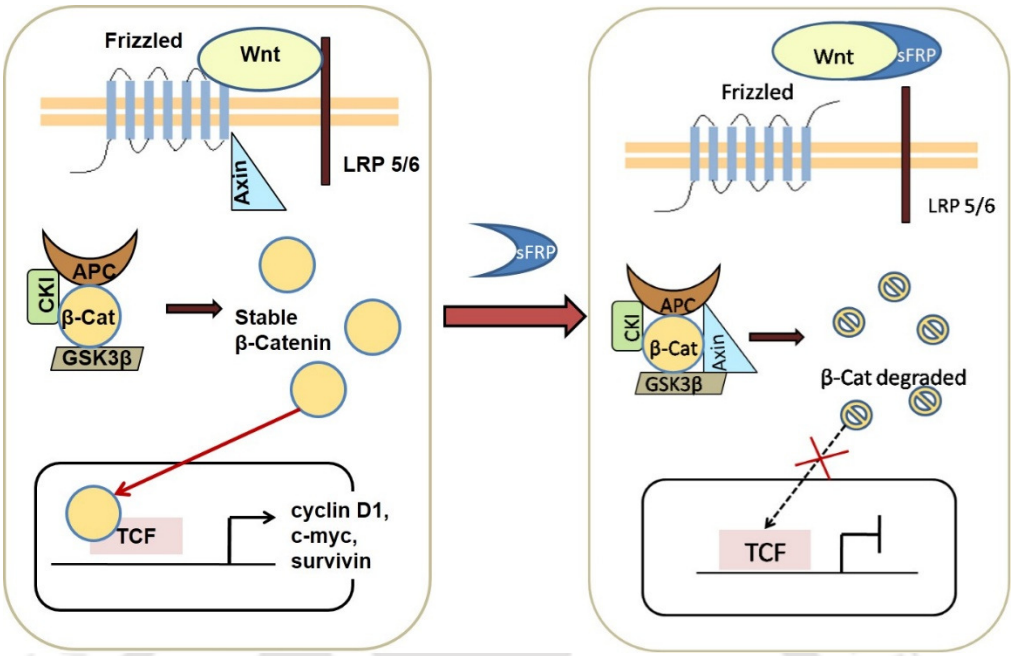

Figure 1.5. Effect of binding of sFRP to Wnt ligands on the Wnt signaling pathway.

Although the epigenetic silencing of sFRP family members is well-documented in cancer, there have been quite a few contradictory reports challenging the same [38, 39]. However, in cancers where sFRPs are suppressed, their expression has been restored by means of transfection of sFRP [40-43] or demethylating chemical agents [44] and anti-cell proliferative effects have been observed. It has been established that sFRP1, sFRP2, sFRP4 and sFRP5 are the ones most commonly implicated in tumorigenesis due to silencing [45]. However, for utilizing the sFRPs in negative regulation of Wnt pathway in cancer, a deeper understanding of their functioning is imperative.

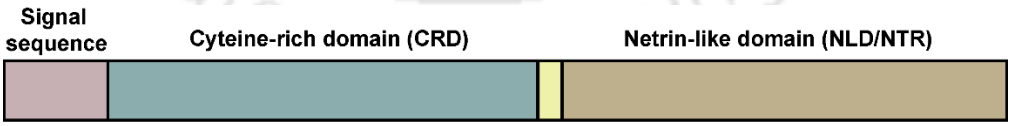

Figure 1.6. The domain architecture of sFRP family members.

From the structural point of view (**Figure 1.6**), sFRPs have an N-terminal signal sequence that enables their extracellular secretion, followed by the CRD, which is responsible for binding to Wnt ligands or in some cases, Fzd receptors. The CRD has 10 conserved cysteine

residues and shares sequence similarity with CRD of Fzd receptors, thus serving as putative binding sites for Wnt ligands. However, the sFRPs lack transmembrane and cytosolic domains, distinguishing them from their receptor counterparts [33]. The hydrophilic C-terminal domain, called the Netrin-like domain (NLD), may also function in promoting cell death, which may or may not be via canonical Wnt pathway [46, 47]. While not much is known about the NLD, functional CRD alone has been shown to be sufficient to suppress Wnt signaling [45]. Post-translational modifications in the form of N-linked glycosylations have been found in the sFRPs, a number of putative sites being in the NLD [48]. Although a few potential sites are present in the CRD as well, glycosylation is not essential for binding to Wnt ligand [49]. This suggested that if recombinant human sFRPs are expressed in a bacterial system, they may be purified in functional form. If the limitation of eukaryotic protein folding can be overcome, expression in bacterial system has the advantage of lower cost and potential for production in bulk, which makes it a lucrative option for potential therapeutic applications. Possible means of regulating the Wnt signaling with sFRPs have been outlined in **Figure 1.7**, of which transfection studies have been done by a few groups reporting a positive outcome [41, 50, 51].

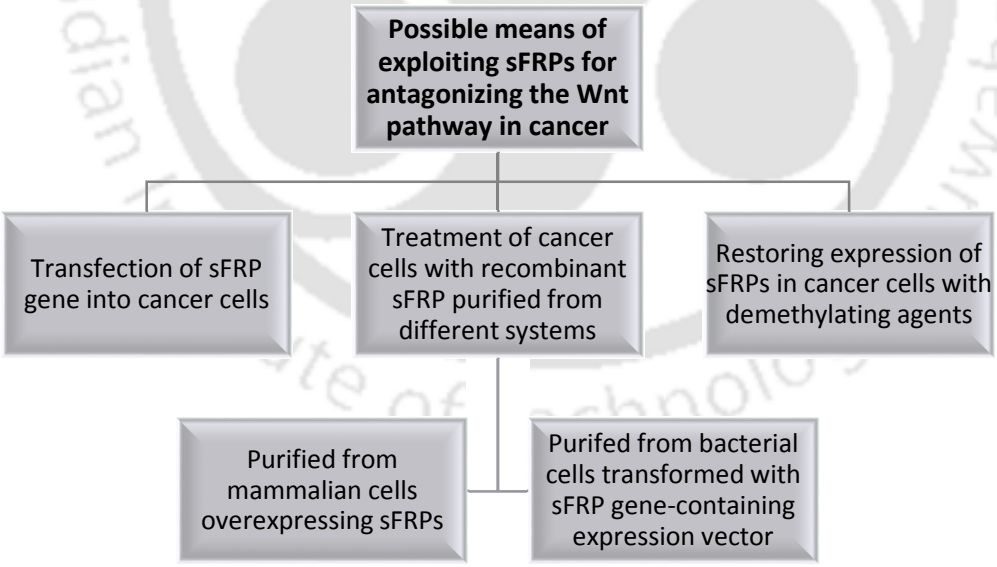

Figure 1.7. Possible means of exploiting the sFRPs for antagonizing Wnt pathway in cancer.

1.4 Composite nanoparticles (NPs) in therapy

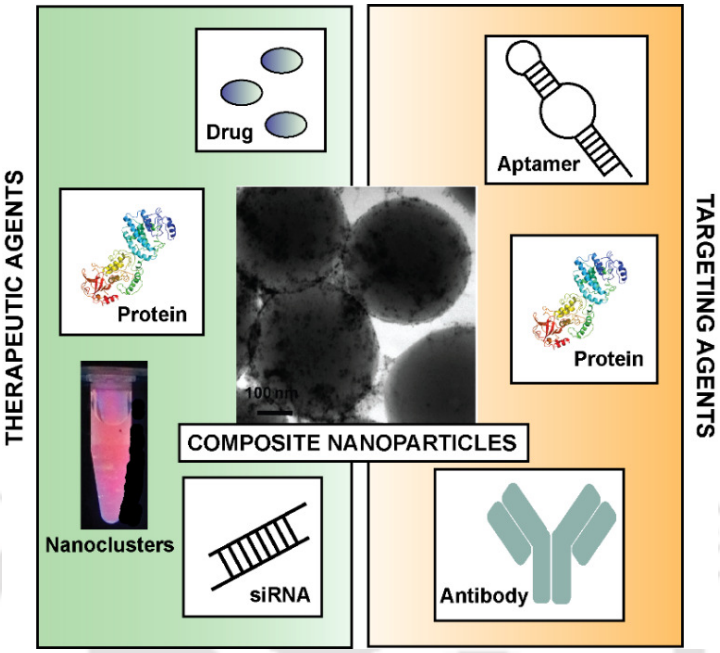

Figure 1.8. Application of theranostic nanoparticles in targeting and therapy; idea of the image conceptualized from Reference [52].

Since the inception of nanotechnology, the now burgeoning field has been entwined with the area of medicine in a multitude of ways. With their ideal size for biological applications, size tunable properties, and easily modifiable surface chemistry, NPs have found a place in clinical applications, giving rise to the interdisciplinary domain of 'nanomedicine'. Several of these have attained fruition, viz., Doxil™ and Abraxane™. Moreover, diverse nano-sized building blocks possessing different functional properties can be assembled into one multifunctional composite with the precise requirements desirable for a particular application. Additionally, biomacromolecules, such as DNA, siRNA, and protein, as well as chemical drugs, metals can be multiplexed with the NPs to attain a plethora of objectives (**Figure 1.8**).

The nanoparticles can be broadly classified into- drug conjugates, micelles, vesicles, core-shell NPs, carbon nanotubes [53] etc, which have been employed to engineer clinically effective formulations. Currently, nanosystems that can be used for both therapeutic and diagnostic purposes are in vogue. These 'theranostic' NPs have promising clinical relevance

as they can be used for treating heterogeneous diseases like cancer, while at the same time providing a 'quick, high-fidelity snapshot of the living system' [53].

- For decades, cancer therapy has been primarily achieved with small-molecule drugs, such as 5-fluorouracil, taxol, doxorubicin etc. However, in the past decade, efforts have been made to encapsulate these drugs in nanocarriers, to attain better pharmacokinetics, targeted delivery, and enhanced therapeutic benefits [54]. These drugs may also be conjugated to a diagnostic component to effectuate a dual-modality theranostic system [55]. Biomolecules like therapeutic siRNA have also accomplished a similar purpose, with the added advantage of overcoming the negative side-effects of drugs, thereby making them a more attractive solution [56].
- For monitoring purposes, optical, magnetic resonance, radionucleotide-based, and ultrasound-based modalities have been implemented. Of them, optical imaging is most common due to their ease of usage, designing, applicability, in addition to their cost-effectiveness. The spectrum from visible to near-infrared (NIR) window that is harmless to users and provides excellent spatial resolution, has been expertly exploited in various studies. To overcome the hindrance due to autofluorescence of biological moieties and to enhance the signal-to-noise ratio, the NIR spectrum has been specifically focused on [57]. The common underlying factor that weds diagnosis with therapy is that both require accumulation in the diseased location of the body, for instance, the tumor tissue.
- Targeting the theranostic moieties to the tumor site necessitates the use of a targeting agent, which may be the diagnostic or the therapeutic moiety, or an altogether different component of the composite NP system. Targeting strategies will be particularly useful in the conception of 'personalized medicine', where quick and effective tactics can be administered for various cancer types. A prevailing approach of active targeting in cancer has been the employment of agents to detect biomarkers on the cell surface, such as growth factor receptors and G-protein-coupled receptors for angiogenesis-modulating proteins [58].

1.4.1 Polymeric nanoparticles

Composite nanoparticles have been implemented for therapy, biological imaging, diagnostics, and targeting of cancer cells. Of the repertoire of substances that can be used as matrices for NP-synthesis, biodegradable polymeric matrices are highly desirable; they are amenable to the integration of different functional entities, which can be released in the biological system once the matrix has disintegrated, causing minimum side-effects. Stable in aqueous environment, these NPs having enhanced half-life and disintegrating to non-toxic metabolites, are given preference for clinical usage [59]. Their biological inertness and cost-effectiveness coupled to their ease of availability are the major causes of their attraction. Moreover, they can interact with the cell membrane in a surface charge-dependent fashion, which is easy to modulate as per the suitability of the application. Also, temperature and pH dependent degradation of the NPs to facilitate controlled release of payload have been reported. Commonly used polymeric NPs include chitosan, sodium alginate, gelatin, albumin, poly lactic acid (PLA), poly lactide-co-glycolide (PLGA) etc. However, so far most marketed drug-loaded NPs or those in the pipeline suffer from the inaccessible predicaments of low loading efficiency and burst release of drug in the *in vivo* system. These ensue the complications of requirement of a larger amount of NPs leading to toxicity and the release of the drug before reaching the tumor site causing side-effects [60]. Hence, the search for alternatives to conventional chemotherapy has resulted in a surge of interest in the application of therapeutic biomacromolecules, such as proteins, siRNA and aptamers.

Among them, the natural polymers-chitosan and sodium alginate have found a consolidated place in NP-synthesis, due to their biocompatibility, high loading efficiency, water-retention capabilities, and bio-adhesiveness [61]. While chitosan is a cationic polysaccharide obtained from chitin present in crustacean animals comprising of β-(1–4)-2-acetamido-2-deoxy-β-D-glucose and β-(1-4)-2-amine-2-deoxyb-β-D-glucose, alginate is an algal-derived anionic polysaccharide made up of 1, 4-linked β-D-mannuronic and α-L-guluronic acid. Interestingly, the electrostatic interactions between the amine group of chitosan and the carboxyl group of alginate has long been exploited for manipulation of polymeric NPs to conform to specific requirements [61, 62].

1.4.2 Fluorescent nanoclusters

As discussed previously, fluorescent moieties may be attached to polymeric templates to enable optical tracking and monitoring of the nanocarriers. Fluorescent NPs are evolving as a promising tool for theranostic purposes [63, 64]. However, the last few years have witnessed an upsurge in the scientific appreciation of a milieu of particles of size less than 2 nm. These particles were termed 'nanoclusters' and they differ widely in physicochemical properties from their nanoparticle counterparts. While metal NPs exhibit surface plasmon resonance (SPR), the nanoclusters do not. Noble-metal nanoclusters, which contain only a few atoms, possess discrete energy levels as the particle size approaches Fermi wavelength of an electron and the continuous band splits. As a result, they lose their plasmonic properties, becoming somewhat similar to molecules. Additionally, they display optical fluorescence via electronic transitions owing to the quantum confinement effect [65]. The most commonly used noble-metal nanoclusters, especially for biological implementation, are the gold and silver nanoclusters, which possess very mild or even negligible toxicity.

1.5 Nanoparticles and Recombinant proteins: an interplay

Cancer, being a phenotypically lethal disease, is still wreaking havoc even in the modern world of highly progressive technology. Naturally, it is the aim of many research groups working in the fields of biology and nanomedicine to eradicate this complex disease. In the novel area of theranostics, cell signaling molecule-loaded NPs have attracted tremendous attention for targeting and combating cancer [66, 67]. The treatment with exogenously administered therapeutic protein may have certain limitations pertaining to the fact that slight changes in its micro-environment during delivery can destabilize the protein, resulting in its loss of function. The constraints, thus arising, can be circumvented by fabricating a system ensemble to stabilize and enhance the efficacy of the protein, for sustained release of payload as well as to probe and quantify the release profile of the protein. However, maintenance of the structural and functional integrity of the macromolecules should be given prime importance for the design of these delivery systems. Delivery of therapeutic proteins for cancer has been successfully done using nanocarriers, such as hydrogel NPs [68]. Co-therapeutic regime, combining the immune-acceptability of recombinant proteins with the potency of chemotherapy to reduce exacerbated side-effects, has also been established [69].

In addition to these systems, which ferry potentially therapeutic proteins, such as Interferon-γ, IκBα, Caspase-3 [70], and RNase A/saporin [71], cancer biomarker-targeting proteins are being extensively researched. For instance, some breast cancers have been specifically targeted by NP formulations targeting the overexpressed HER2 receptors [54, 72]. Similar targeted delivery regimes have been implemented for cancer cells overexpressing VEGF receptors [73], transferrin receptors [74], folic acid receptors [75]. Therapeutic polypeptides have also been employed to design co-therapeutic regimes with traditional drugs [76, 77]. Presently, in healthcare, these challenges are being encountered by the advancements in nanomedicine, where nanocarriers are in the process of taking centre stage in modern clinical applications.

1.6 Key questions and scope of research

- The domain of sFRPs and Wnts and their interactions is largely an uncharted territory, till date.
- Functionality of the recombinant sFRPs expressed and purified from the bacterial system needs to be evaluated.
- Expression of sFRPs in bacterial systems may open up new avenues in combination therapy, where protein therapy may be coupled with conventional chemotherapy to achieve greater efficacy at reduced drug concentrations.
- Since the sFRP isoforms are known to behave in conflicting manner, their behavior in each cancer cell type needs to be arduously monitored before proposing their use as cancer therapeutics.
- Increasing stability of recombinant sFRPs with composite nanoparticles may enhance their efficacy.
- Nanoparticles having fluorescent component may enable their usage in biological imaging, tracking and other analytical studies.

1.7 Objectives of the thesis

1. Cloning, expression and purification of recombinant proteins to target cell surface signaling pathways using Secreted Frizzled-related Protein (sFRP) isoforms, sFRP1 and sFRP4.

2. Studying anti-proliferative effects of the recombinant sFRP1 and sFRP4.

3. Examination of synergistic anti-proliferative properties of recombinant sFRP1 and sFRP4 in combination with anticancer drugs.

4. Evaluation of recombinant sFRP1 and sFRP4-bound composite nanoparticles embedded with metal nanoclusters for bioimaging and targeting Wnt/ β-catenin signaling.

1.8 Salient features of this work

- Cloning, expression and purification of recombinant glutathione S-transferase (GST) tagged sFRP isoforms- sFRP1 and sFRP4
- Structural and functional characterization of sFRP1 and sFRP4
- Anti-proliferative activity of GST-sFRP tested on cancer cell lines
- Targeting the Wnt/ β-catenin signaling pathway with the GST-sFRPs
- Chemosensitization of cancer cells toward conventional anti-cancer drugs with the sFRPs
- Synthesis of sFRP-bound novel nanocluster-based composite nanoparticles for biological imaging, uptake analyses, binding studies and sustained delivery
- Enhanced anti-cancer benefits of sFRP-bound nanoparticles
- Investigation into the mode of cell death

CHAPTER 2

Expression, Purification, and Therapeutic Implications of Recombinant sFRP1

CHAPTER 2

2.1 Introduction

sFRP1, the first discovered sFRP, is the most promising candidate for cancer therapy and forms the stepping stone for investigations. Accumulating evidence suggests that sFRP1 is downregulated in colorectal, breast, ovarian, malignant mesothelioma, and lung cancer [29, 40, 78-80]. Specifically in lung carcinoma, loss of heterozygosity has also been reported in the sFRP1 gene locus, which may contribute to the absence of gene expression [40]. Interestingly, chain terminating mutations have also been found to exist in colorectal tumors [78], in addition to epigenetic inactivation. SFRP1 transfection led to reduced colony formation and decreased transcriptional activity of β-catenin in non-small-cell lung cancer [40]. However, a discrepancy has been reported in prostate tumor, where elevated expression of sFRP1 has been observed, as compared to adult prostate [81]. This evidence correlated with the finding that when human prostatic epithelial cells were treated with sFRP1, they exhibited increased proliferation and decreased apoptosis. A similar discrepancy was also found in gastric cancer, where high levels of sFRP1 have been shown to promote tumor formation [82]. Recently, transfection studies have revealed growth inhibitory effects of sFRP1 on few breast cancer cell lines [50] and hepatoma cell lines [41] with wild type β-catenin or β-catenin containing point mutations, but not in those containing truncated β-catenin.

In this chapter, an endeavor has been made to delineate the impact of bacterially expressed GST-sFRP1 on cancer cell types. For this purpose, the expression, purification and re-folding conditions of the recombinant protein were optimized before adding it onto the cells. This is the first expedition aimed at illustrating the anti-cell proliferative effect of bacterially expressed GST tagged sFRP1 on cancer cells, which may have significant prospective in cancer therapeutics. The idea has been schematically conceptualized in **Scheme 2.1**.

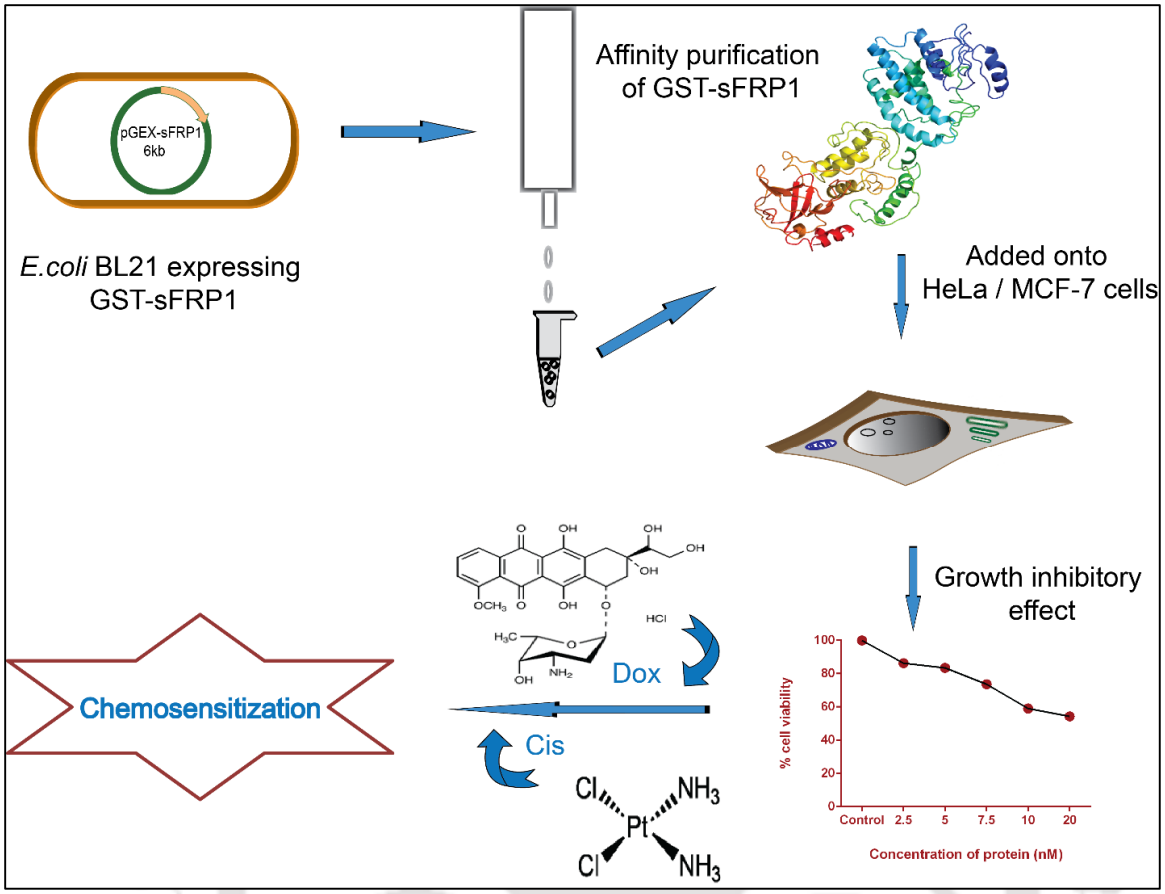

Scheme 2.1. Schematic representation of the concept of this chapter.

2.2 Material and Methods

2.2.1 Cell Culture and Materials

The cancer cell lines HeLa (cervical), MCF-7 (breast), human embryonal kidney (HEK-293) were obtained from National Centre for Cell Science (NCCS), India. The cells were cultured under conventional conditions in Dulbecco's Modified Eagle's Medium (DMEM), supplemented with 10% Fetal bovine serum (FBS, PAA Laboratories), 100 U/ml Penicillin, 100 µg/ml Streptomycin and maintained in humidified atmosphere in a 5% carbon dioxide incubator at 37 °C.

All items (materials and kits) were purchased from Sigma-Aldrich, unless mentioned otherwise.

2.2.2 Cloning of sFRP1

The 945 bp human sFRP1 gene was obtained from DNASU Plasmid Repository, USA in pDNR-Dual vector. The gene was amplified by Polymerase Chain Reaction (PCR) using gene-specific forward primer 5'- GTAGGATCCATGGGCATCGGGCGCA-3' with a *Bam*HI overhang and reverse primer 5'-GTTCTCGAGTCACTTAAACACGGACTGAAAG-3' with a *Xho*I overhang. Taq polymerase (Bioline) was used for the PCR amplification. Conditions for the PCR reaction were as follows: denaturation at 95 ℃ for 50 sec, annealing at 60 ℃ for 40 sec and extension at 72 ℃ for 1.5 min. The amplified and eluted product as well as the bacterial expression vector pGEX-4T2 (GE Healthcare) were then digested with the mentioned restriction enzymes (New England Biolabs) and ligated using Quick Ligase kit (New England Biolabs). The ligation product was transformed into *E. coli* DH5α. Sequencing was done by Xcelris Labs Ltd. for clone confirmation. Digestion was carried out with the above restriction enzymes *Bam*HI and *Xho*I for the same purpose.

2.2.3 Expression of GST-sFRP1 in E. coli BL21 (DE3)

The recombinant vector was transferred into *E. coli* BL21(DE3) (procured from Institute of Microbial Technology, India). The same was then cultured in small scale in Luria Bertani (LB) media, containing 100 μg/ml ampicillin. It was kept overnight in a 37 °C shaker incubator, at 180 rpm. This was used as inoculum at a dilution of 1:100 for 100 ml of the secondary culture, which was allowed to reach mid log phase (an O.D. of 0.6) before induction with 0.2 mM isopropyl β-D-1-thiogalactopyranoside (IPTG, Sisco Research Laboratories Pvt. Ltd., India). The induced culture was kept at temperatures ranging from 16 ℃ to 37 ℃ in a shaker incubator to acquire maximum expression of sFRP1 protein. For each of the temperatures tested for protein expression, induction times were varied from 4 h to 12 h (data not shown). Eventually, the cells were harvested by centrifuging under chilled conditions at 6500 rpm for 5 min. Cells were lysed in 10 mM phosphate-buffered saline (PBS) and 1 mM phenylmethylsulfonyl fluoride (PMSF) by sonication. Samples were run on 12% sodium dodecyl sulfate-polyacrylamide gel electrophoresis (SDS-PAGE) to observe the expression of protein for the varying conditions of temperature and time duration mentioned previously.

2.2.4 Solubilization, Purification and Refolding of GST-sFRP1 protein

Maximum protein expression was achieved with induction at 28 °C for 8 h. These conditions were hence followed throughout. However, when the cells were lysed by sonicator and centrifuged, the expressed protein was obtained in the insoluble fraction, perhaps as inclusion bodies. In order to solubilize the protein from pellet fraction, several modifications were made to the lysis buffer composition and sonication conditions. Finally, maximum solubilization was attained under the following conditions. Pellet was resuspended in 10 ml lysis buffer containing 10 mM PBS, 1 mM ethylenediaminetetraacetic acid (EDTA, SRL), 0.32% N-lauroylsarcosine and 1 mM PMSF. Cells were then sonicated using a probe sonicator, while keeping the sample on ice. Lysed cells were centrifuged at 20,100 g for 25 min at 4 °C. 1% Triton X-100 was added to the supernatant, which was then stirred for 1 h in cold. Thereafter, it was diluted three times with 10 mM PBS and filtered using 0.45 µm syringe filter. Then it was loaded batch-wise onto a glutathione agarose affinity chromatography column and incubated for 30 min each at 4 °C. The column was then washed with one column volume (approximately 12 ml) of 10 mM PBS for fourteen times before elution of desired protein. Elution buffer was composed of 15 mM L-reduced glutathione in 50 mM Tris-HCl (pH 9.5). All steps were performed under cold conditions. Samples were analyzed on 12% SDS-PAGE. The protein was refolded by subjecting it to step-wise dialysis against Tris-HCl, pH 7.4 for 6 h. The buffer concentration was decreased from an initial 100 mM to a final 10 mM, with three rounds of buffer replacement. Concentration was done with PEG 8000. After two changes of buffer during dialysis, the dialysis bag containing the protein was covered with PEG, which absorbs water, and kept at 4 °C for half an hour. It was replaced by fresh PEG after every 5 min. At the end of this concentration procedure, the protein was again dialyzed against 10 mM Tris-HCl buffer, pH 7.4.

2.2.5 Homology modeling and docking studies

The structures of CRD of sFRP1, sFRP1 and GST tagged sFRP1 were predicted using Phyre2 (Protein Homology/analogY Recognition Engine V 2.0) [83]. The structure of Wnt7a, which has been found to bind with sFRP1, was predicted using I-Tasser server [84-86]. The structure of CRD-sFRP1 hence predicted was compared to that predicted by SWISSMODEL (http://www.proteinmodelportal.org/query/uniprot/Q6FHJ7) and the crystal structure of CRD of sFRP3 (PDB ID: 1ijxA) by overlapping the respective structures using PyMOL and generating a root mean square deviation value. This was done in order to validate the structure of CRD-sFRP1. This was then overlapped with the predicted structures of full length sFRP1 and GST-sFRP1 (again by using PyMOL), in order to compare the binding domain of CRD-sFRP1, full length sFRP1 and GST-sFRP1. Next each of these three structures was docked with Wnt7a using ClusPro web interface. The docked structures hence obtained were modified using PDBEditor and analyzed with PDBsum Generate. The generated data for docked structures, viz., CRD-sFRP1:Wnt7a, sFRP1:Wnt7a and GST-sFRP1:Wnt7a were compared.

2.2.6 Western blotting

Western blotting was done to validate the presence of GST-sFRP1 using anti-GST antibody. Purified GST-sFRP1 was electrophoresed on 12% SDS-PAGE and transferred onto polyvinylidene difluoride (PVDF, Millipore, USA) membrane. After confirming the transfer with Ponceau S staining, membrane was washed with PBST (1% Tween-20 in 10 mM PBS) and subsequent blocking was done with 3% BSA in PBST. Thereafter, the membrane was incubated overnight with monoclonal anti-GST primary antibody raised in rat. Then, it was washed with PBST four times, before being incubated for 2 h with Anti-Rat IgG (whole molecule) Peroxidase antibody produced in goat. After thorough washing with PBST, blot was developed using Chemiluminescent Peroxidase Substrate. GST protein alone was also purified by affinity chromatography and blotted as control following the same protocol. The uninduced cell lysate (negative control) and induced cell fractions were also blotted.

2.2.7 Secondary structure characterization with circular dichroism

The secondary structure of GST-sFRP1 was assessed with the help of circular dichroism spectra obtained with JASCO-815 spectrometer (Jasco, Japan). This was carried out in order to analyze whether the purified, dialyzed and concentrated protein retained its secondary structure. After step-wise dialysis, the final concentration of Tris-HCl buffer was 10 mM (pH 7.4). The concentration of GST-sFRP1 analyzed in spectrometer was 0.3 μM. Spectra were recorded for protein in cuvette of 0.2 cm path length, under constant nitrogen gas purging at a flow rate of 5 L/min and at a temperature of 25 ℃ maintained by circulating water-bath. Scanning was done from wavelength 240 nm to 190 nm at a speed of 50 nm/min, with 4 accumulations. Background spectrum of corresponding buffer was subtracted from the sample spectrum.

2.2.8 MALDI TOF-TOF analysis

MALDI MS-MS analysis was performed in order to characterize and confirm sFRP1 protein by tryptic digestion. In situ gel digestion of protein band was carried out using Trypsin Profile In-gel digestion kit following manufacturer's protocol. The processed sample was mixed in a ratio of 5:3 with matrix α-cyano-4-hydroxycinnamic acid and spotted onto analyzer plate. MS-MS analysis was done with 4700 Proteomics Analyzer with TOF/TOF Optics (Applied Biosystems), which uses a diode pumped solid state class I laser. MS/MS data were acquired in automatic mode using acquisition method MS MS 1kV positive.

2.2.9 Cell viability assay

The effect of GST-sFRP1 was ascertained on two different cancer cell lines, viz., HeLa and MCF-7. The protein was dialyzed, concentrated and quantified by Bradford protein estimation assay before being added onto the cells. Cells were seeded in 96-well plate at a density of 7000 cells per well in DMEM containing 10% FBS. After allowing them to attach for about 8 h, media was removed and the protein was added in serum-free media at varying concentrations ranging from 1.6 nM to 20 nM. Under these conditions, the cells were incubated at 37 °C in 5% carbon dioxide incubator for 48 h. Thereafter, MTT assay was performed, where MTT (3-(4,5-dimethylthiazol-2-yl)-2,5 diphenyltetrazolium bromide) is converted to purple formazan crystals by dehydrogenase enzymes in mitochondria of

healthy, respiring cells. Dimethyl sulfoxide (DMSO, SRL) was added to dissolve the formazan, and absorbance was measured at 550 nm. Background measurement was done at 650 nm. The experiment was also conducted with purified GST protein as control, up to a concentration of 40 nM, to eliminate any probability of its effect on cell viability. Percentage cell viability was measured by the following equation:

$$\% \text{ of cell viability} = \frac{(A_{550} - A_{655})_{\text{sample}}}{(A_{550} - A_{655})_{\text{control}}} \times 100$$

2.2.10 Combination therapy

Combination therapy of GST-sFRP1 with conventional chemotherapeutic drugs, namely, cisplatin, under the commercial name Platin 50 (Cadila Pharmaceuticals Limited), and doxorubicin hydrochloride, under the commercial name Adriamycin (Pfizer), was also performed. Cisplatin was used in the range of 0.5-5 µg/ml and 3-10 µg/ml, whereas doxorubicin was used in the range of 0.1-0.5 µg/ml and 0.09-0.2 µg/ml, for HeLa and MCF-7 cells, respectively. The range, in which the effect was observed, is in accordance with the range reported in literature [87, 88]. Both HeLa and MCF-7 cells were tested for the above combinations with MTT assay following the same protocol. Control and treated cells were observed under microscope (Nikon ECLIPSE TS100). Both HeLa and MCF-7 cells were treated with 12 nM of protein, alone and in combination with cisplatin (2 µg/ml and 5 µg/ml respectively) or doxorubicin (0.4 µg/ml and 0.2 µg/ml respectively).

2.2.11 Cell cycle analysis

Cell cycle analysis was performed using Fluorescence Activated Cells Sorter (FACSCalibur, BD Biosciences, NJ, USA) to measure the DNA content of cells upon treatment with GST-sFRP1, alone and in conjunction with chemotherapeutic agents, namely, cisplatin and doxorubicin. Cells were seeded at a density of around 10^5 cells per well, in a six-well tissue culture plate. After allowing the cells to grow for 8 h, the media was replaced by serum-free media containing GST-sFRP1, cisplatin, doxorubicin or a combination of GST-sFRP1 with cisplatin/doxorubicin. For treatment of the HeLa cells, concentrations of protein, cisplatin and doxorubicin used for this experiment were 12 nM, 1 µg/ml and 0.2 µg/ml, respectively.

For the MCF-7 cells, the treatment was done with 12 nM GST-sFRP1, 5 µg/ml cisplatin and 0.1 µg/ml doxorubicin. The concentrations were determined on the basis of the results yielded in the MTT assays. The dose of protein, exerting the maximum effect on cell viability, was chosen; for the drugs, a concentration at which around 80% of the cells were viable was selected. Treatment was done for 48 h, after which, the cells were collected by trypsinization. Floating cells in media were collected by centrifugation at 650 g for 6 min at 4 °C, whereas trypsinized cells were centrifuged at 450 g for 6 min at 4 °C. Cells were then fixed in cold, by adding 70% ethanol drop-wise and stored at -20 °C. Subsequently, cells were centrifuged, washed with cold PBS and incubated with 0.2 mg/ml RNase A (Amresco) at 37 °C for 1 h. Thereafter, propidium iodide (PI) was added at a final concentration of 10 µg/ml and incubated for 20 min in dark, at 4 °C. Cells were analyzed in FACSCalibur. 10,000 cells were acquired and analyzed for each sample, using the software CellQuest Pro.

2.2.12 Statistical tests

Statistical tests were carried out for the results obtained for all MTT assays using Graphpad Prism software. One-way or two-way ANOVA analysis was performed, as per requirement.

2.3 Results and Discussion

2.3.1 Cloning, expression and purification of GST-sFRP1

The coding sequence of human sFRP1 comprising of 945 bp was subcloned into pGEX-4T2 bacterial expression vector, as demonstrated in **Figure 2.1A**. PCR amplification was carried out using pDNR-Dual vector harboring sFRP1 gene, as template DNA; the amplified band at the desired position is shown in **Figure 2.1B**. The clone was confirmed by digestion with the restriction enzymes *Bam*HI and *Xho*I (**Figure 2.1C**) as well as by sequencing (the sequence is given in **Figure 2.1D**), as mentioned in subsection 2.2.2.

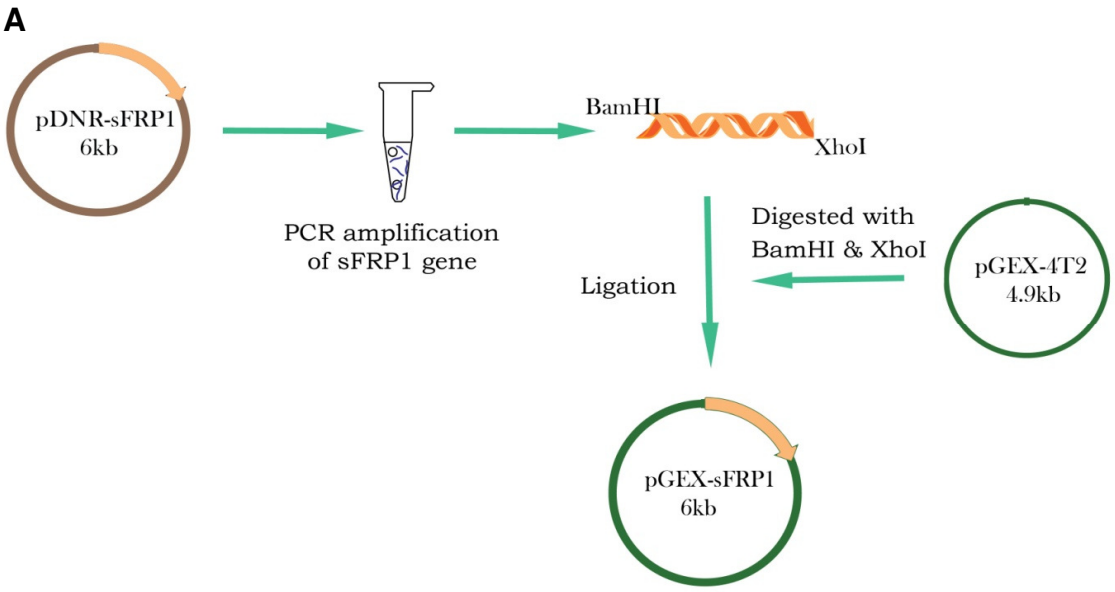

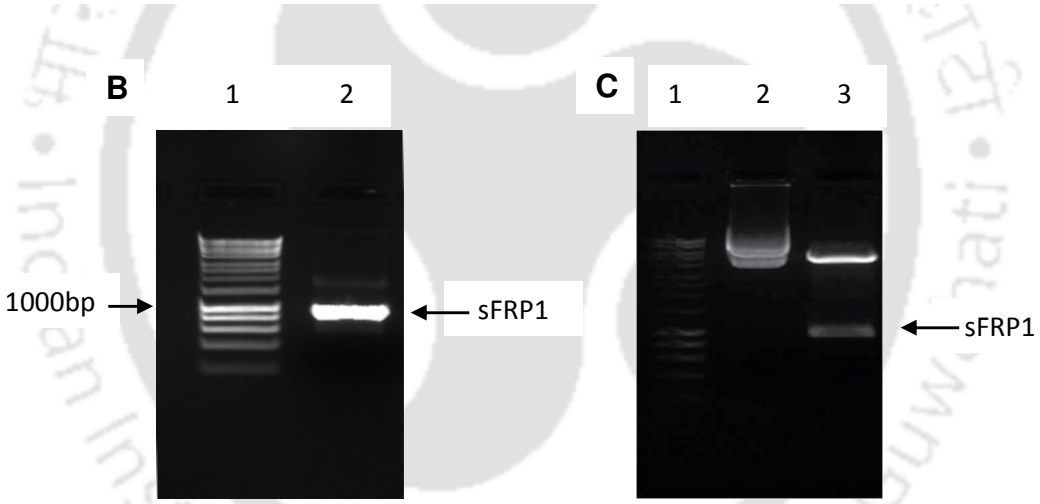

D

ATGGGCATCGGGCGCAGCGAGGGGGGCCGCCGCGGGGCAGCCCTGGGCGTGCTGCTGGCGCTGGGCGCGGCGC
TTCTGGCCGTGGGCTCGGCCAGCGAGTACGACTACGTGAGCTTCCAGTCGGACATCGGCCCGTACCAGAGCGG
GCGCTTCTACACCAAGCCACCTCAGTGCGTGGACATCCCCGCGGACCTGCGGCTGTGCCACAACGTGGGCTAC
AAGAAGATGGTGCTGCCCAACCTGCTGGAGCACGAGACCATGGCGGAGGTGAAGCAGCAGGCCAGCAGCTGGG
TGCCCCTGCTCAACAAGAACTGCCACGCCGGCACCCAGGTCTTCCTCTGCTCGCTCTTCGCGCCCGTCTGCCT
GGACCGGCCCATCTACCCGTGTCGCTGGCTCTGCGAGGCCGTGCGCGACTCGTGCGAGCCGGTCATGCAGTTC
TTCGGCTTCTACTGGCCCGAGATGCTTAAGTGTGACAAGTTCCCCGAGGGGGACGTCTGCATCGCCATGACGC
CGCCCAATGCCACCGAAGCCTCCAAGCCCCAAGGCACAACGGTGTGTCCTCCCTGTGACAACGAGTTGAAATC
TGAGGCCATCATTGAACATCTCTGTGCCAGCGAGTTTGCACTGAGGATGAAAATAAAAGAAGTGAAAAAAGAA
AATGGCGACAAGAAGATTGTCCCCAAGAAGAAGAAGCCCCTGAAGTTGGGGCCCATCAAGAAGAAGGACCTGA
AGAAGCTTGTGCTGTACCTGAAGAATGGGGCTGACTGTCCCTGCCACCAGCTGGACAACCTCAGCCACCACTT
CCTCATCATGGGCCGCAAGGTGAAGAGCCAGTACTTGCTGACGGCCATCCACAAGTGGGACAAGAAAAACAAG
GAGTTCAAAAACTTCATGAAGAAAATGAAAAACCATGAGTGCCCCACCTTTCAGTCCGTGTTTAAGTGA

Figure 2.1. (A) Schematic of the method followed for subcloning sFRP1 into PGEX-4T2. Agarose (1%) gel analysis, **(B)** Lane 1 shows 1kb DNA ladder and lane 2 shows sFRP1 gene amplified with gene specific primers using pDNR-sFRP1 as template. **(C)** Lane 1 is the DNA ladder, lane 2 is undigested pGEX-sFRP1, lane 3 is pGEX-sFRP1 digested with *Bam*HI and *Xho*I. **(D)** Sequencing results in pGEX-4T2.

The recombinant plasmid containing N-terminal GST tagged sFRP1 was eventually transformed into *E. coli* BL21 (DE3). Induction conditions were optimized, where maximum protein expression was found at 28 °C for 8 h (**Figure 2.2A**). However, nearly the entire recombinant protein was present as inclusion bodies. Solubilization of this protein from the pellet fraction was attempted by various means, such as, cloning and expression in Rosetta-gami2(DE3) [89], cloning in other bacterial expression vectors, induction at reduced temperatures and varying durations of time, usage of detergents like Triton X-100, Tween 20 and sodium deoxycholate at different concentrations. Earlier investigations by various groups reveal the use of various detergents, which were modified and implemented in this study as mentioned above [90, 91]. However, urea and guanidine HCl, although found to be greatly effective in solubilizing proteins from inclusion bodies, were not tried, as their usage leads to a highly disordered protein structure that usually requires extensive refolding processes [92]. Also, the GST-protein fusion system has been shown to enhance the stability and solubility of recombinant protein. Even in cases where it is not soluble, addition of

detergents is sufficient for this purpose [93]. Here, substantial solubilization was accomplished with N-lauroylsarcosine and Triton X-100, using the protocol mentioned earlier in subsection 2.2.4. A single band of GST-sFRP1 corresponding to molecular weight 61 kDa was obtained after purification, at the desired position in a 12% SDS-PAGE (**Figure 2.2B**). The method optimized for the expression and purification has been illustrated in **Scheme 2.2**. The yield of purified protein, estimated by Bradford assay, was found to be approximately 0.5 mg from 100 ml of starter culture.

Refolding of purified protein to obtain it in a functionally active form is an essential requirement for therapeutic applications. Since solubilization of proteins from inclusion bodies demands the presence of strong detergents, the protein itself gets completely unfolded in the process. Therefore, refolding is indispensable to attaining native conformation. For this purpose, different modes of dialysis have been previously used [92].

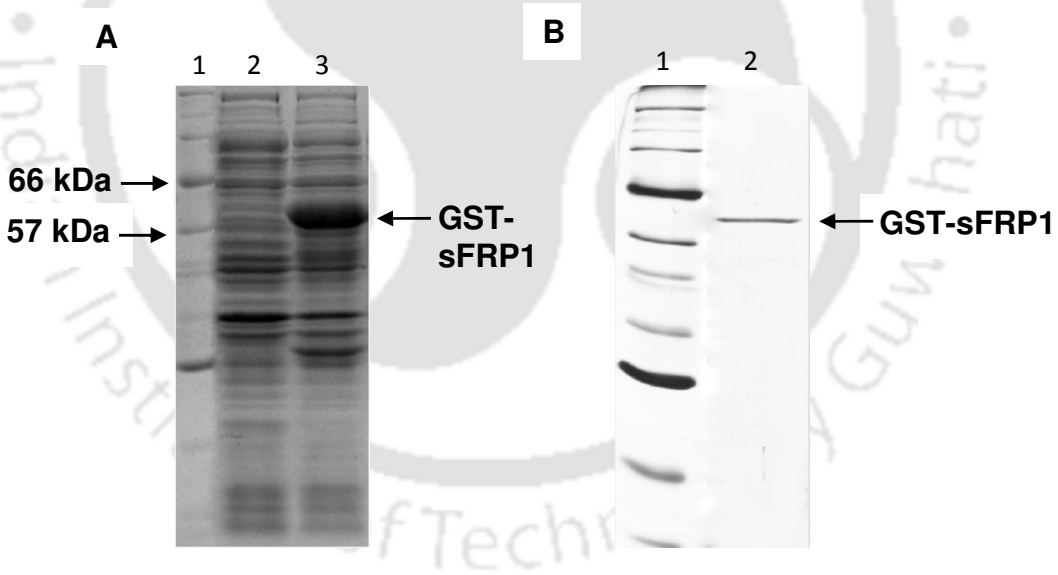

Figure 2.2. 12% SDS-PAGE depicting expression and purification of GST-sFRP1. **(A)** Lane 1 shows the protein molecular weight marker (2-212 kDa), lane 2 shows the uninduced cell lysate of *E. coli* containing pGEX-sFRP1, lane 3 shows the expressed GST-sFRP1 in pellet fraction. **(B)** Lane 1 shows protein molecular weight marker and Lane 2 shows the purified single band at the legitimate position.

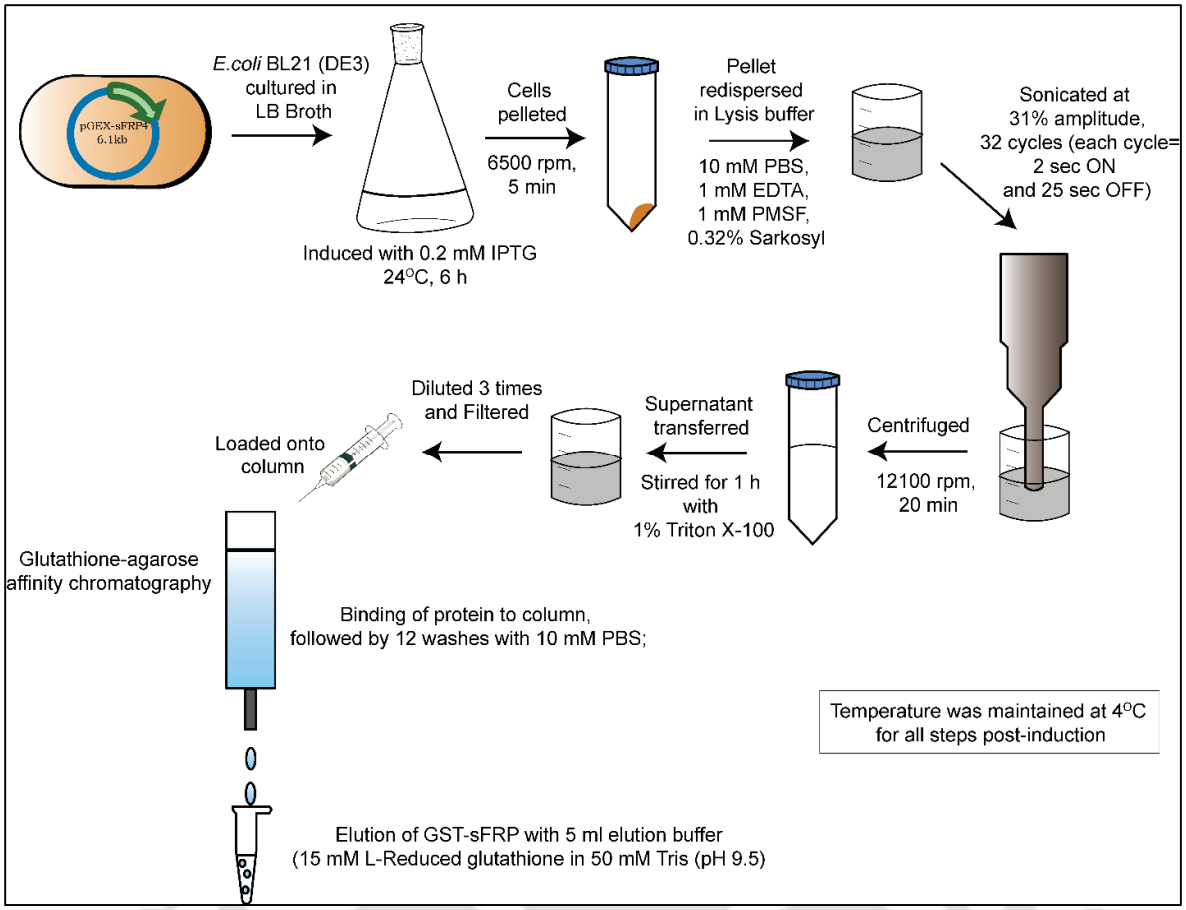

Scheme 2.2. Schematic illustration of the method optimized for expression and purification of GST-sFRP1.

2.3.2 Homology modeling and docking studies

Since functional activity of GST-sFRP1 has not been demonstrated yet, docking studies were performed to computationally confirm the functionality of GST-sFRP1, before conducting experiments in order to prove the same. As the only crystal structure available for the sFRP superfamily is that of the binding domain (CRD) of sFRP3 (PDB ID: 1ijxA), binding studies of sFRP1 with Wnt could only be performed after predicting the structures of CRD-sFRP1, sFRP1, GST-sFRP1 and Wnt7a. Wnt7a was selected for the docking studies with sFRP1 as they have previously been shown to bind to each other. The 3-D structures for CRD-sFRP1 (**Figure 2.3A**), sFRP1 (**Figure 2.3B**) and GST-sFRP1 (**Figure 2.3C**) were modeled using Phyre2, whereas Wnt7a was modeled with I-TASSER server (**Figure 2.3D**).

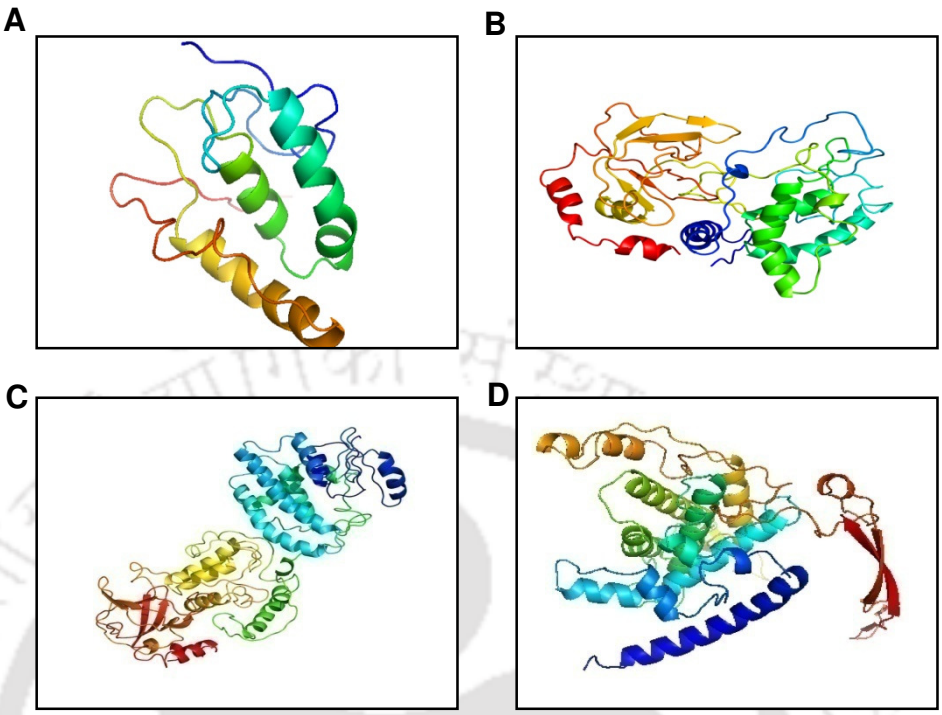

Figure 2.3. Three dimensional structures predicted with homology modeling servers. **(A)** CRD-sFRP1**. (B)** sFRP1. **(C)** GST-sFRP1. **(D)** Wnt7a.

CRD-sFRP1 hence predicted was confirmed by aligning with the structure of CRD-sFRP3 available in PDB in PyMOL (**Figure 2.4A**) and that of CRD-sFRP1 predicted in SWISSMODEL website (**Figure 2.4B**). The structural integrity of the binding domain in the predicted whole molecule structure of sFRP1 as well as in GST-sFRP1 was confirmed by the same method (**Figure 2.4C** and **Figure 2.4D**, respectively). Also, the crystal structure of GST obtained from PDB (ID: 1UA5) was aligned with the predicted GST-sFRP1 to confirm the reliability of the predicted model (**Figure 2.4E**). In each of the above cases, a root mean square deviation value was generated by PyMOL, which have been mentioned in the figure captions.

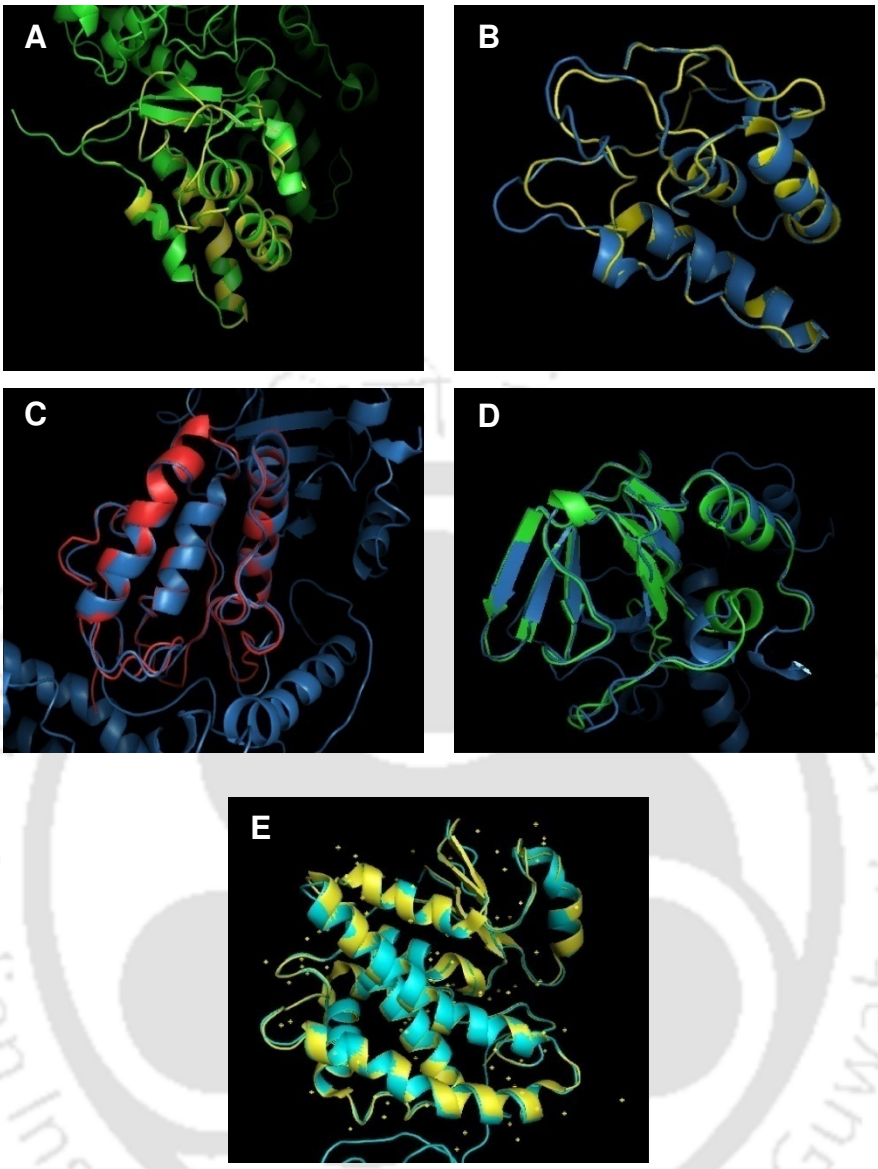

Figure 2.4. Overlapping alignment of three dimensional structures using PyMol **(A)** CRD-sFRP3:CRD-sFRP1 (Swissmodel) with RMSD=0.085 **(B)** CRD-sFRP1 (Swissmodel):CRD-sFRP1 (Phyre2) with RMSD=0.5 **(C)** GST-sFRP1:CRD_sFRP1 with RMSD=1.69 **(D)** GST-sFRP1:NTR_sFRP1 with RMSD=1.70 **(E)** GST-sFRP1:GST (PDB) with RMSD=0.842.

Thereafter, each of the predicted structures- CRD-sFRP1, sFRP1 and GST-sFRP1, was docked with Wnt7a by means of the protein-protein docking server ClusPro 2.0 (**Figure**

2.5A, **Figure 2.5B** and **Figure 2.5C**). This revealed that GST possibly did not participate in binding or hinder the binding of sFRP1 to Wnt7a, as it remained separated.

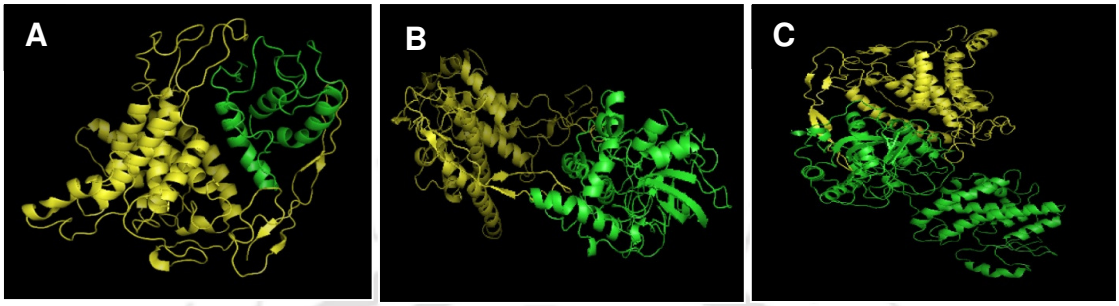

Figure 2.5. Docking studies using ClusPro server. **(A)** CRD-sFRP1 with Wnt7a. **(B)** sFRP1 with Wnt7a. **(C)** GST-sFRP1 with Wnt7a.

The docked structures were then subjected to analysis of interacting residues using PDBsum Generate online server. The residues in the CRD responsible for interaction with Wnt7a have been found to interact in a like manner in case of GST-sFRP1, which revealed that GST-sFRP1 may exhibit similar functional activity as sFRP1 alone. The summary of the results are outlined in **Table 2.1**, while the details are given in **Figure 2.6**, **Figure 2.7** and **Figure 2.8**.

CRD-sFRP1	GST-sFRP1
Ala 63	Ala 289
Asp 64	Asp 364
Leu 65	Leu 291
Arg 66	Arg 292
Lys 91	Lys 317
Arg 130	Arg 356
Trp 131	Trp 357
Glu 134	Glu 360
Arg 137	Arg 363
Asp 138	Asp 364
Glu 141	Glu 367
Gln 145	Gln 371
Phe 146	Phe 372
Phe 147	Phe 373
Phe 149	Phe 375
Tyr 150	Tyr 376
Glu 162	Glu 388

Table 2.1. A summary of results generated by PDBsum Generate (elaborated in Figure 2.6, 2.7, 2.8) is given here. It lists all the interacting residues common for CRD-sFRP1 binding with Wnt7a and GST-sFRP1 binding with sFRP1, showing that binding of CRD possibly remains unhindered. CRD denotes Cysteine Rich Domain or binding domain of sFRP1.

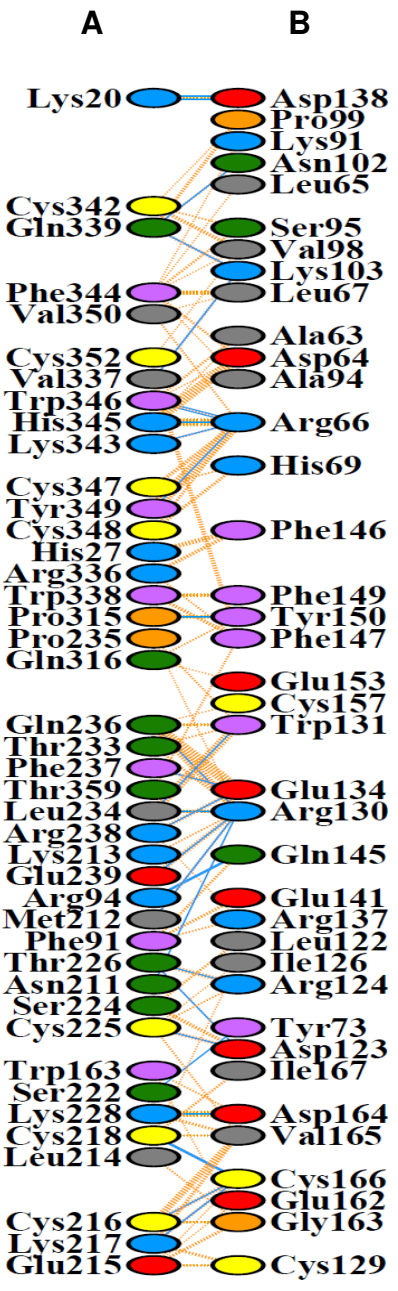

Figure 2.6. Analysis of docking studies performed with PDBsum generate server **(A)** Wnt7a **(B)** CRD-sFRP1.

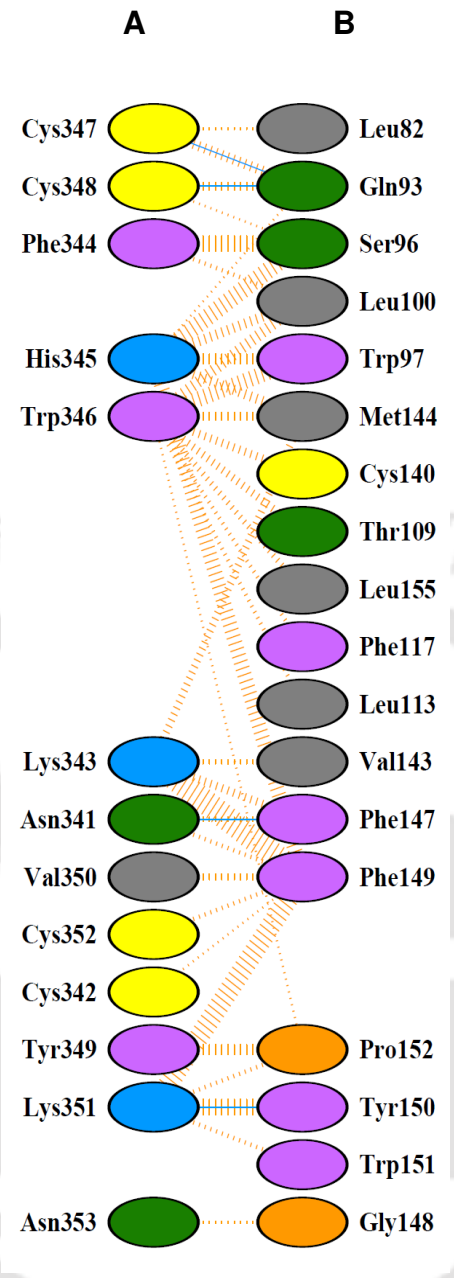

Figure 2.7. Analysis of docking studies performed with PDBsum generate server **(A)** Wnt7a **(B)** sFRP1.

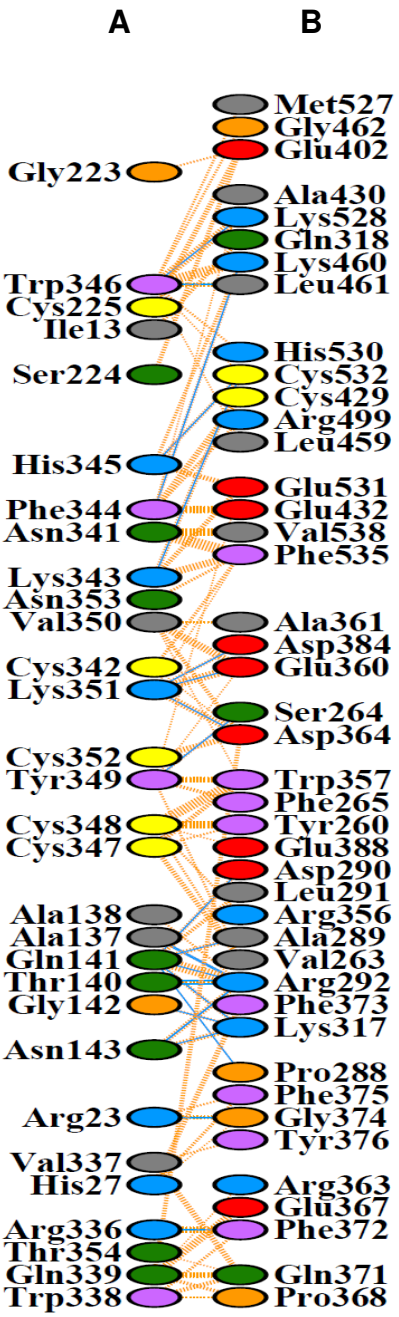

Figure 2.8. Analysis of docking studies performed with PDBsum generate server **(A)** Wnt7a **(B)** GST-sFRP1.

2.3.3 Western blot analysis

Western blotting with anti-GST monoclonal antibody generated legitimate band of GST-sFRP1 of approximately 61kDa (**Figure 2.9**). Purified GST alone was also blotted, which

developed a band corresponding to the molecular weight of GST (**Figure 2.9**). The uninduced cell lysate and induced cell fraction were blotted, as shown in **Figure 2.10**.

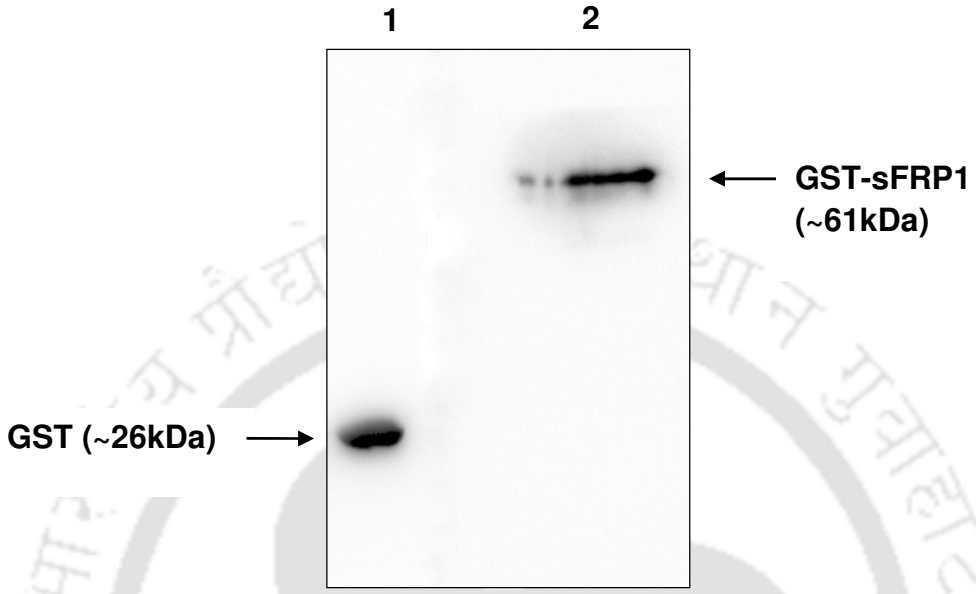

Figure 2.9. Western blotting with anti-GST monoclonal antibody; Lane 1- Purified GST; Lane 2- Purified GST-sFRP1.

Figure 2.10. Western blotting was performed for **(A)** uninduced cell lysate as negative control, **(B)** Induced cell fraction.

2.3.4 Secondary structure characterization with circular dichroism

The secondary structure of GST-sFRP1, suspended in 10 mM Tris-HCl (pH 7.4), was characterized by far-UV circular dichroism. The CD spectrum was obtained with millidegree on the Y-axis, which was converted to mean residue ellipticity (mdeg.cm^{2}dmol^{-1}) by the formula

Mean residue ellipticity (Θ) = (100*θ)/Cnl

Where, θ is the ellipticity in millidegree, C is the concentration of the sample protein, n is the number of residues and l is the path length [94]. **Figure 2.11** shows the obtained spectrum. The secondary structure analysis was done by employing Yang's reference, which revealed the α-helix content to be 20.7%, β-sheet content to be 33.5% and random coil to be 29.5%.

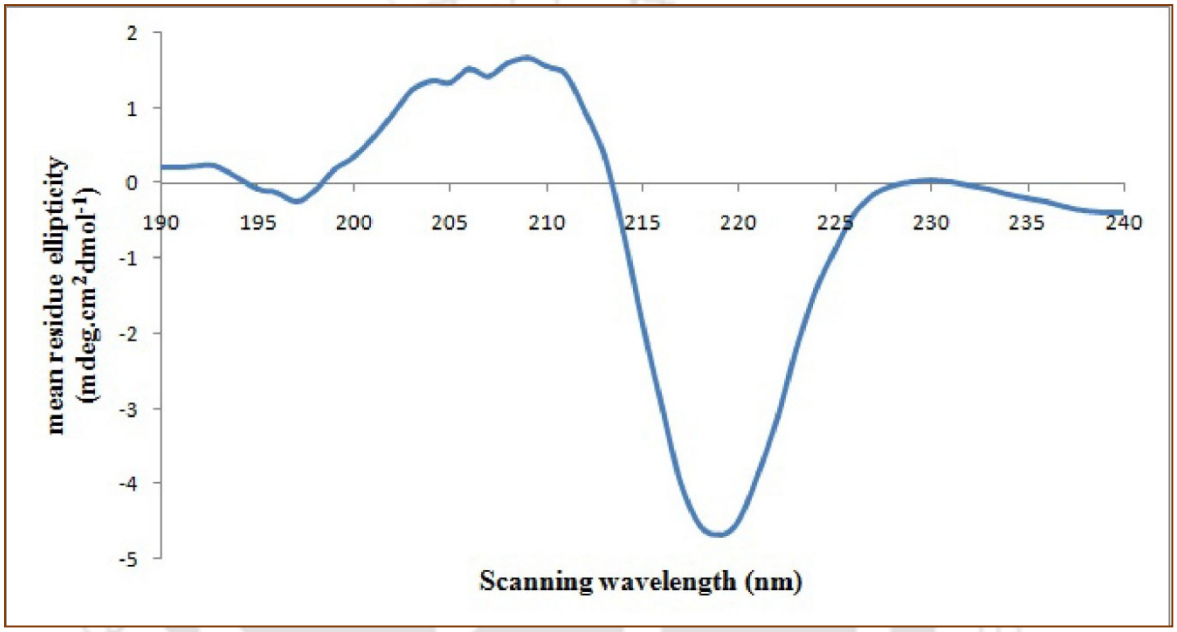

Figure 2.11. Far-UV circular dichroism spectra of GST-sFRP1 in 10 mM Tris-HCl at pH 7.4.

2.3.5 Analysis of MALDI TOF-TOF data

Soft ionization techniques in mass spectrometry have been employed in conjunction with database searching algorithms [95, 96] for protein identification and characterization since the past two decades. Here, MALDI coupled with time-of-flight analysis was used for characterizing the recombinant sFRP1; the mass spectrometry data is shown in **Figure 2.12**. MS/MS study of each peptide fragment obtained by tryptic digestion of GST-sFRP1 generated a match with the MASCOT database, with a score of 104. This sequence similarity confirmed the identity of the sFRP1 protein.

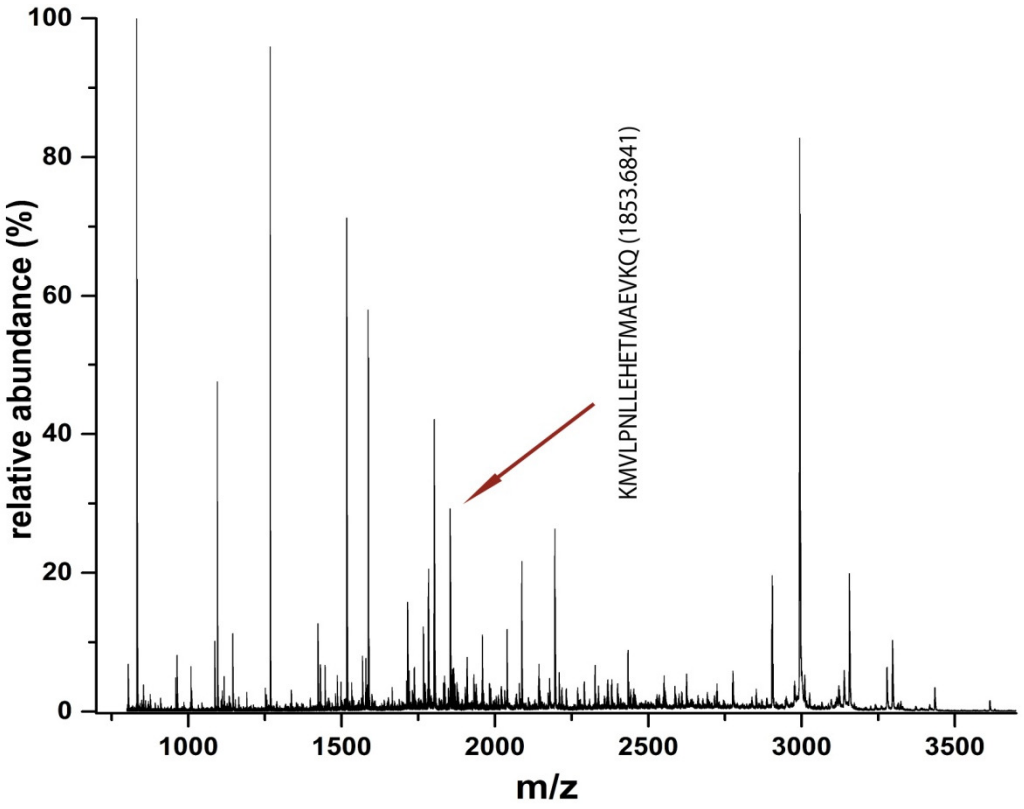

Figure 2.12. MALDI TOF/TOF analysis of GST-sFRP1 upon tryptic digestion generated a peptide match of the following sequence KMVLPNLLEHETMAEVKQ.

2.3.6 Cell viability assay

sFRP1 has been found to be downregulated due to promoter hypermethylation in various cancer types [29-31]. Hence, it can be hypothesized that its overexpression may lead to anti-proliferative activity by inhibiting the Wnt pathway. Binding of sFRP1 to Wnt ligands is known to inhibit the interaction of Wnt with corresponding Fzd receptors, which is necessary for Wnt signal transduction [35]. In non-small-cell lung cancer, sFRP1 was demonstrated to inhibit the transcriptional activity of β-catenin [40], which is a downstream molecule in the Wnt canonical pathway. Although, the non-canonical pathway of Wnt has not been properly implicated in carcinogenesis, there is one report, for colorectal cancer, hypothesizing the

same [78]. Also, treatment of sFRP1 with demethylating agents, like 5-aza-2'-deoxycytidine, restored the expression of sFRP1 [79, 97] and suppressed tumor growth [41].

In this study, functional activity of recombinant sFRP1 was determined by adding it onto two different cancer cell lines HeLa and MCF-7. In both cases, the protein was found to display significant dose-dependent cell growth inhibitory effect. After 48 h of treatment, less than 60% of cell viability was achieved with approximately 10 nM of GST-sFRP1 in case of HeLa (**Figure 2.13A**) and 20 nM in case of MCF-7 (**Figure 2.13B**), respectively.

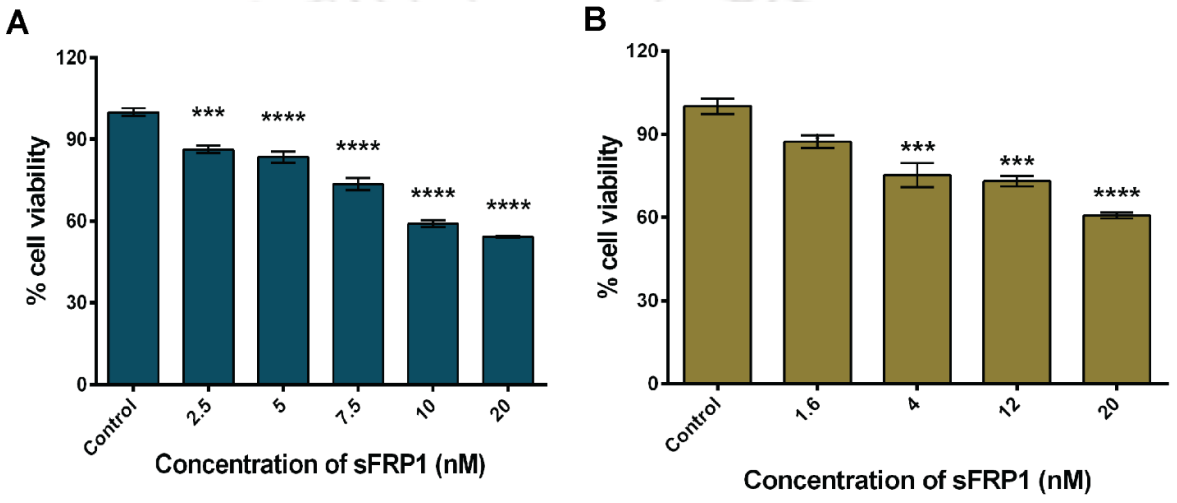

Figure 2.13. Effect of GST-sFRP1 in terms of reduction in percentage of viable cells as demonstrated by MTT assay. Statistical significance has been determined by one-way ANOVA, where * refers to $p<0.05$, ** refers to $p<0.01$, *** refers to $p<0.001$, **** refers to $p<0.0001$. **(A)** HeLa cells. **(B)** MCF-7 cells.

Cell viability was unchanged when purified GST alone (up to a concentration of 40 nM) was added onto cells (**Figure 2.14**).

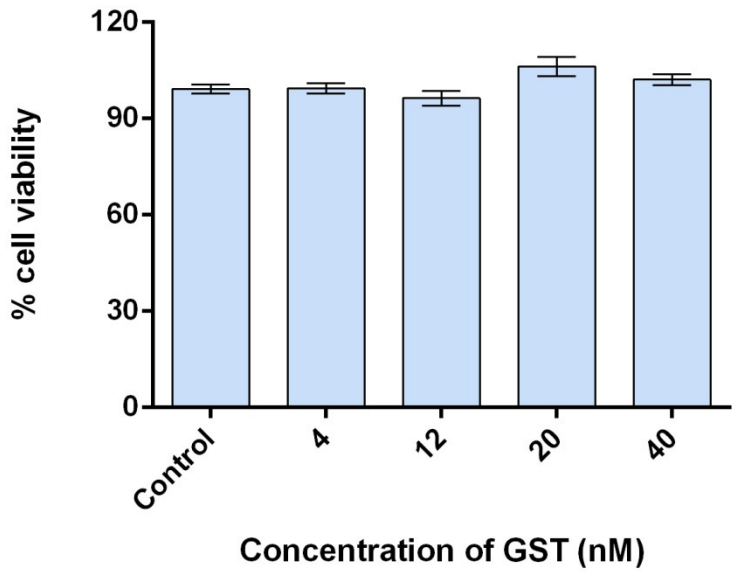

Figure 2.14. Effect of only purified GST on HeLa cells as demonstrated by MTT assay.

The fact that the treatment with recombinant sFRP1 alone had displayed cell growth inhibition could potentially contribute to the domain of combination therapy for the treatment of cancer. Hence, the following experiments were conducted to test this hypothesis.

2.3.7 Combination therapy

Combination therapy was attempted to check if administration of the recombinant sFRP1 enhances sensitization of cells toward conventional chemotherapeutic drugs. Till date, there has been no report of the combinatorial effect of sFRP1 with any anti-cancer drug. However, another member of the sFRP family, namely sFRP4, has been shown to significantly increase the sensitivity of transfected chemoresistant ovarian cancer cell lines to treatment with cisplatin [98].

Various concentrations of protein and drug were tested in order to optimize the ratio required for maximum impact on cell viability. The optimized ratio obtained via MTT assays in case of HeLa and MCF-7, when treated with GST-sFRP1 along with cisplatin (**Figure 2.15A** and **Figure 2.15B** respectively) and doxorubicin (**Figure 2.16A** and **Figure 2.16B** respectively)

have been shown. Significant differences in cell viability were observed between treatment with only drug and that of drug with protein in each of the following cases.

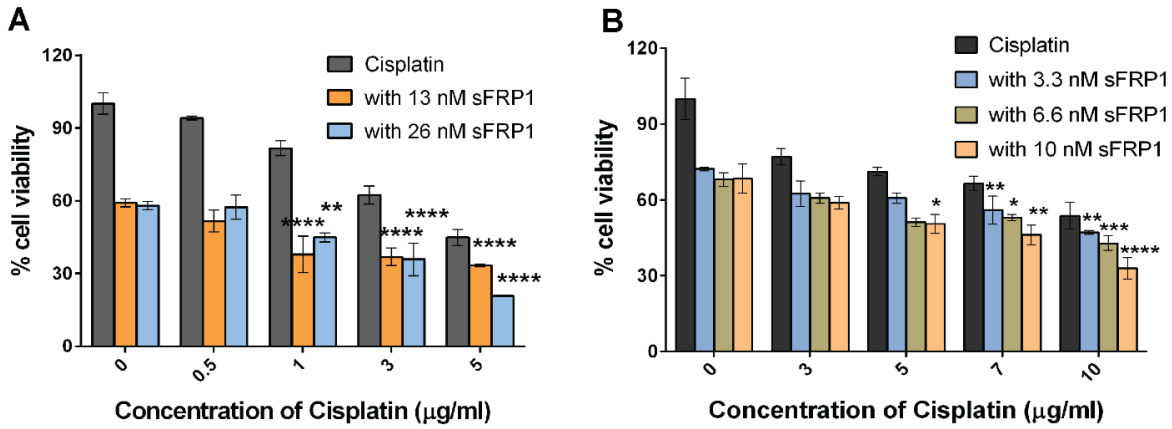

Figure 2.15. Treatment of cells with increasing dosage of cisplatin alone and in combination with specified concentrations of GST-sFRP1. **(A)** in case of HeLa cells **(B)** in case of MCF-7 cells. Statistical significance has been determined by two-way ANOVA, where * refers to $p<0.05$, ** refers to $p<0.01$, *** refers to $p<0.001$, **** refers to $p<0.0001$.

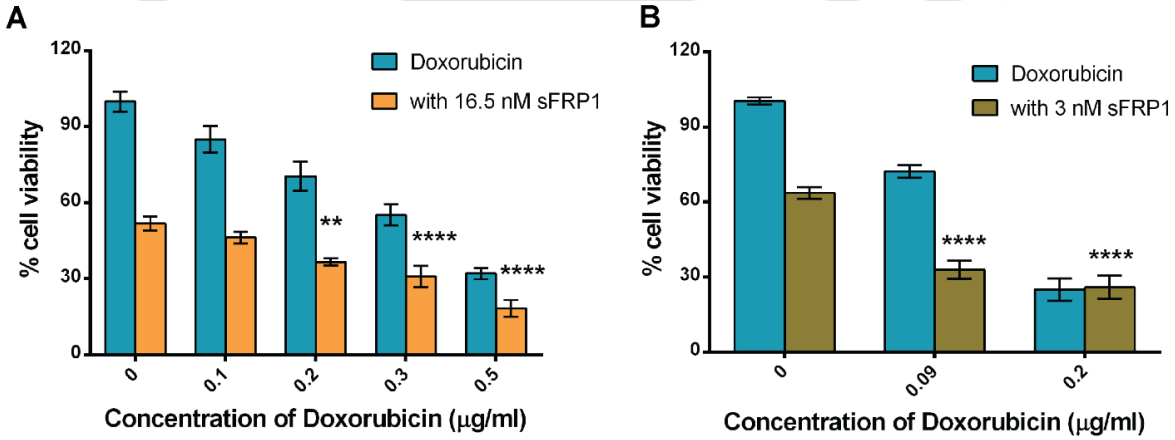

Figure 2.16. Treatment of cells with increasing dosage of doxorubicin alone and in combination with specified concentration of GST-sFRP1. **(A)** in case of HeLa cells **(B)** in case of MCF-7 cells. Statistical significance has been determined by two-way ANOVA, where * refers to $p<0.05$, ** refers to $p<0.01$, *** refers to $p<0.001$, **** refers to $p<0.0001$.

Microscopic images of control and treated HeLa and MCF-7 cells have been illustrated in **Figure 2.17** and **Figure 2.18**, respectively. Treatment with GST-sFRP1 did not seem to damage cell morphology, although the number of cells appeared to be decreased considerably. However, the chemotherapeutic drugs caused a significant damage to the cells, which was further augmented in case of combination therapy.

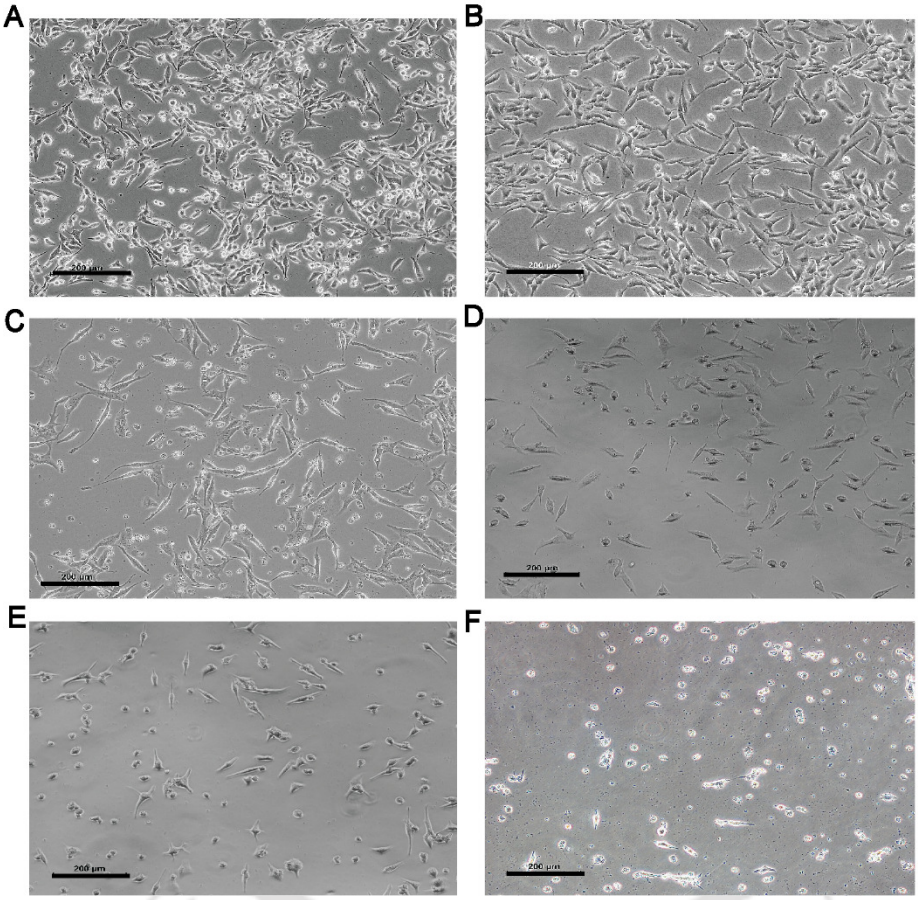

Figure 2.17. Microscopic imaging of HeLa cells **(A)** Untreated. Treated with **(B)** 12 nM GST-sFRP1. **(C)** 2 µg/ml cisplatin. **(D)** 2 µg/ml cisplatin and 12 nM GST-sFRP1. **(E)** 0.4 µg/ml doxorubicin. **(F)** 0.4 µg/ml doxorubicin and 12 nM GST-sFRP1. Scale bar represents 200 µm.

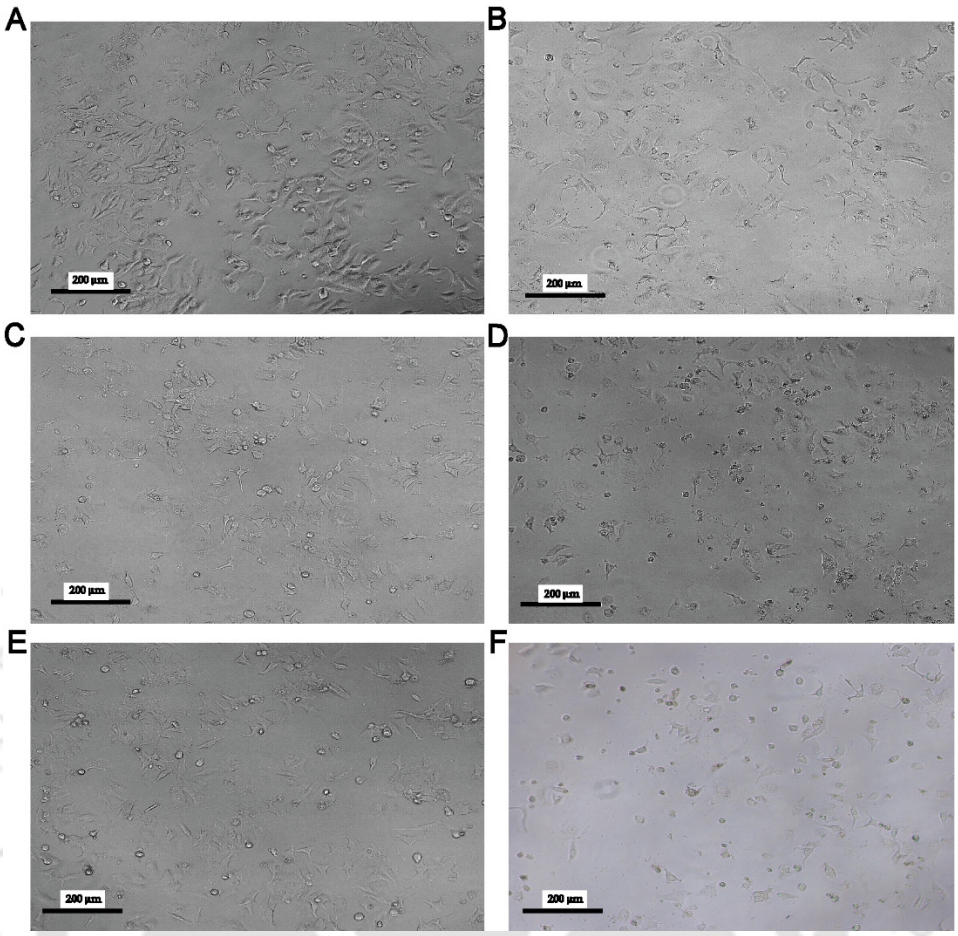

Figure 2.18. Microscopic imaging of MCF-7 cells **(A)** Untreated. Treated with **(B)** 12 nM GST-sFRP1. **(C)** 5 µg/ml cisplatin. **(D)** 5 µg/ml cisplatin and 12 nM GST-sFRP1. **(E)** 0.2 µg/ml doxorubicin. **(F)** 0.2 µg/ml doxorubicin and 12 nM GST-sFRP1. Scale bar represents 200 µm.

2.3.8 Cell cycle analysis

FACS-based analysis was performed to delineate the impact of GST-sFRP1 (alone and in combination with chemotherapeutic drugs) on cell cycle of HeLa (**Figure 2.19A** and **Figure 2.19B**) and MCF-7 (**Figure 2.19C** and **Figure 2.19D**) cells. The treatment of HeLa cells with protein substantially reduced the number of cells in G1 phase and increased the cell population in G2/M phase, as compared to untreated cells. A small population of cells (3.99%) was found to appear in the sub-G1 phase even in control cells, which was possibly due to incubation in serum-free media for 48 h. The percentage of this cell population was

increased to 5.89% in the HeLa cells treated with GST-sFRP1. Treatment with chemotherapeutic drugs significantly increased G2/M population, which was further augmented by combination therapy of the respective drugs with protein. In case of MCF-7 cells, GST-sFRP1 treatment resulted in a significant apoptotic cell population (7.49%), which was further increased during combination therapy with either of the two drugs. Addition of either drug as well as combination therapy with protein caused a significant decrease in G1 population and increase in G2/M population in both cell lines. All the results indicated that the recombinant protein induced cell growth inhibition, partly through cell cycle arrest and partly through apoptosis in HeLa cells, whereas apoptosis seemed to be the more prominent mechanism in MCF-7 cells. Combination therapy was effective in augmenting the impact of the protein. These findings correlated with the results observed in MTT assays and morphology studies. It should be mentioned here, that the concentrations of chemotherapeutic drugs used for this experiment were much lower than their respective IC_{50} dosage, in an attempt to reduce their adverse side-effects.

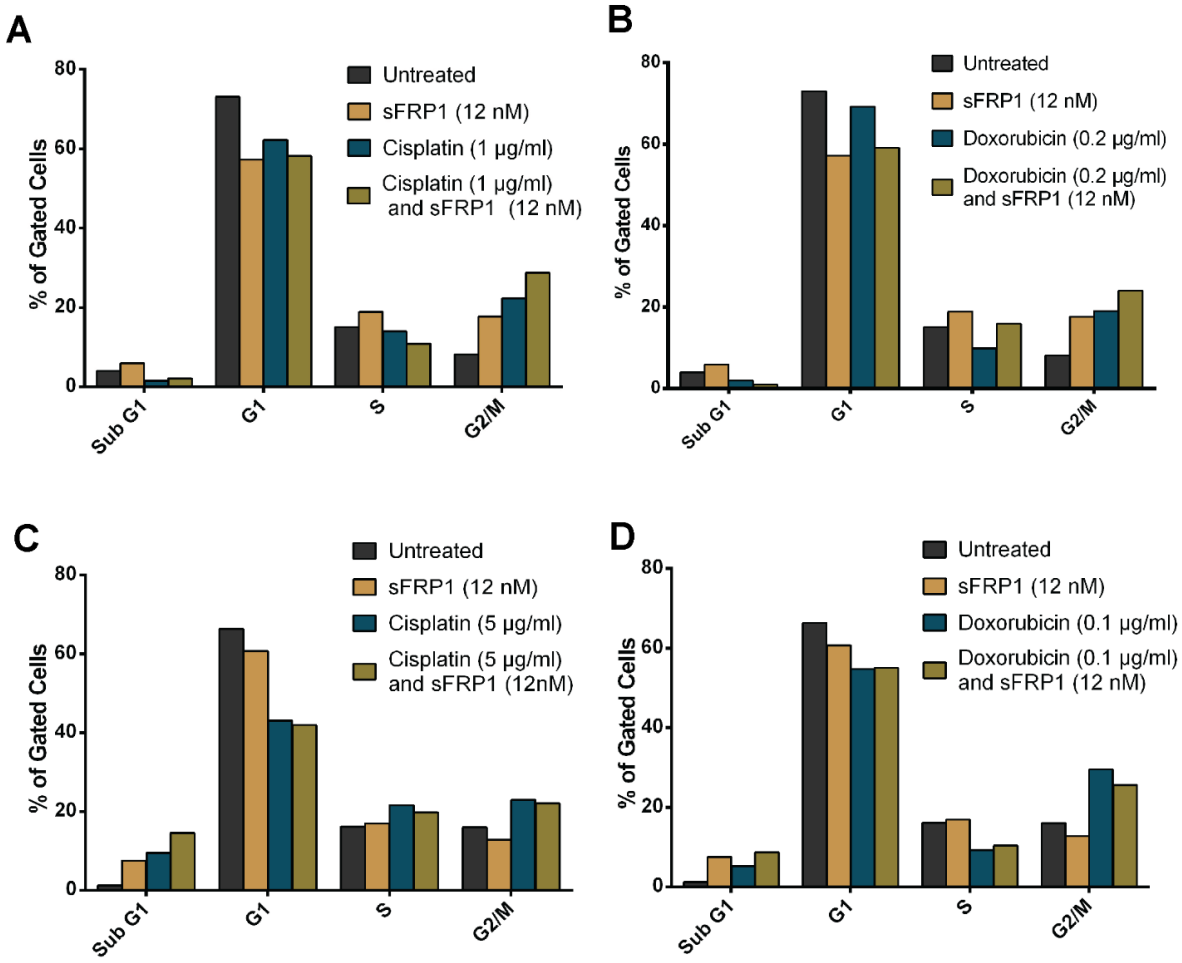

Figure 2.19. Flow cytometry-based cell cycle analysis **(A)** HeLa cells treated with sFRP1 (12 nM), cisplatin (1 µg/ml) and their combination, **(B)** HeLa cells treated with sFRP1 (12 nM), doxorubicin (0.2 µg/ml) and their combination, **(C)** MCF-7 cells treated with sFRP1 (12 nM), cisplatin (5 µg/ml) and their combination, **(D)** MCF-7 cells treated with sFRP1 (12 nM), doxorubicin (0.1 µg/ml) and their combination.

2.3.9. Effect of GST-SFRP1 on non-cancerous cell line HEK-293

Finally the effect of the recombinant sFRP1 was tested on a non-cancerous cell line HEK-293. It was found that as high as 30 nM of protein did not bring about any difference in cell viability (**Figure 2.20**).

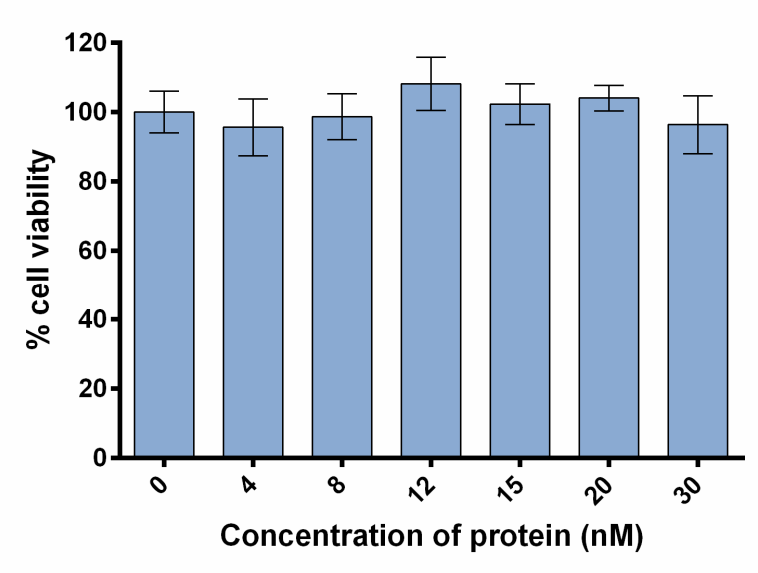

Figure 2.20. Cell viability assay of HEK-293 cells showed that there is no significant effect of recombinant sFRP1.

The development of resistance and severe side-effects of chemotherapy and radiotherapy have led to the evolution of gene therapy and protein therapeutics. However, these, by themselves, often do not exert sufficiently adequate anti-tumor responses. Hence, treatment of cancer has witnessed a paradigm shift culminating in the emergence of combination therapy.

Cell signaling pathways are intricately designed processes, where often certain genes/proteins are found to perform multiple roles. As cisplatin and doxorubicin both act by inhibiting the mechanism of DNA synthesis, whereas the sFRPs inhibit the Wnt signaling pathway, there seems to be no direct interaction between them. However, the cells may have been chemosensitized toward the drugs due to the inhibition of the Wnt pathway by sFRP1. Stress conditions resulting from cell cycle arrest may render the cells more sensitive toward the chemotherapeutic drugs, resulting in increased cell death. Whether the effect on cells is

due to the independent functions of GST-sFRP1 and drugs or whether their actions are somehow intertwined can only be concluded after extensive analysis. One group had reported that adriamycin upregulated hsFRP protein in a non-cancerous cell line (HBL-100). The study concluded that hsFRP brings about both apoptosis and cell cycle regulation but did not explicitly explain the link between the two networks [36].

Although further explorations into this field are essential to draw definitive conclusions, these experiments demonstrate that this combination therapy may be used for chemosensitization of cancer cells toward conventional anti-cancer drugs.

2.4 Conclusions

Targeting the Wnt family, which constitutes a largely uncharted territory, holds great promises in cancer therapy. This chapter has reported expression, purification and functional characterization of the recombinant sFRP1 protein. Molecular docking studies provided evidence of sFRP1 interactions with Wnt molecules in Wnt pathway. Experimental studies on cell viability and flow cytometry-based assays corroborated anti-cell proliferative effect of the recombinant sFRP1. Finally, combination therapy with conventional chemotherapeutic drugs augmented anti-cell proliferative responses of the recombinant sFRP1. This study may pave the way for clinical translation of the potential of recombinant sFRP1 in the upcoming field of protein therapeutics.

CHAPTER 3

Targeting Wnt Canonical Signaling by Recombinant sFRP1 Bound Luminescent Au-Nanocluster Embedded Nanoparticles in Cancer Theranostics

CHAPTER 3

3.1 Introduction

Metal nanoclusters (NCs) have the potential to revolutionize the current therapeutic modality by virtue of their extraordinary physical and chemical properties [99-101]. Of the metal NCs, gold nanoclusters (Au NCs) have transpired as an attractive option due to their stability, non-toxicity, remarkable fluorescence properties, and large Stokes shift, thus overcoming the limitations of organic dyes and quantum dots [102-105]. Their emission in red/near-infrared (NIR) region prevents interference from biological entities during cellular imaging [106-108]. Biodegradable polymers, acting as templates for hosting Au NCs, may qualify as versatile platforms for drug delivery, as they can be used as probe for detection of binding and release of cargo. In addition, tunable fluorescence imaging studies can provide a thorough understanding of its mechanism of action, making it an attractive solution for a grave problem. The synthesis of chitosan-based Au NC-containing nanocarriers has been previously reported, displaying simultaneous red, green and blue fluorescence, which has been favorably exploited for optical imaging and as flow cytometry probe [109]. Combination therapy has also been implemented using Au NCs for fluorescent/ X-ray computed tomography imaging and radiotherapy [110, 111].

Recent material innovations have propagated a paradigm shift toward the unique concept of co-delivery of drug and therapeutic molecules conjugated to nanocarriers [112]. Studies have revealed that these therapeutic molecules by themselves may not be toxic enough to eradicate cancer completely, but they may be used in combination with chemotherapy to help reduce the dosage of drugs and diminish their side effects [68, 113]. Ligand-targeted NPs loaded with chemotherapeutic drugs are increasingly finding application in remedy of cancer, with the common targets being receptors overexpressed by cancer cells, such as folate and transferrin receptors [114-116]. However, even though aberrant upregulation of Wnt pathway is one of the highlights in cancer, till date there has been no report documenting the targeting of Wnt pathway with NPs for cancer therapy.

In the current study, a novel system consisting of recombinant therapeutic protein sFRP1 bound chitosan-Au NC-alginate composite NPs (henceforth referred to as protein-NPs) was established for specific targeting of the Wnt pathway in cervical cancer cells (HeLa). The anti-proliferative effect of the sFRP1-NPs was determined by treating HeLa cells. Here, the theranostic NPs were constructed by a quick and facile method, whereby, Au NCs were synthesized keeping biopolymer chitosan as template, and converted to NPs using polysaccharide alginate. Size and surface charge of these multifunctional NPs were modulated keeping in mind that recombinant sFRP1 binds to its target Wnt ligand in the extracellular space and hence, the composite ideally should not penetrate the cell membrane. Luminescence properties of Au NCs fortified its role as a fluorescent signal indicator for *in media* probing of protein, monitoring its binding, stability as well as imaging over a prolonged time period. Binding of sFRP1 with NPs resulted in its enhanced anti-proliferative activity, as shown by cell viability assay, dual staining by acridine orange (AO) and ethidium bromide (EB), cell cycle analysis, and apoptosis detection assay of treated HeLa cells. Targeting of the Wnt ligands with sFRP1-NPs successfully blocked the Wnt signaling cascade, which plays a predominant role in carcinogenesis. The uniqueness of this regime lies in the feature that the therapeutic protein-NPs will simultaneously serve the purposes of both targeting cancer cells and arresting their growth. In addition, synergistic effect of sFRP1-NPs with traditional chemotherapeutic agent cisplatin brought about a drastic increase in apoptotic cell population. This novel approach of co-therapy exploited the benefits of NP-mediated protein therapeutics to augment the efficacy of chemotherapy via targeted cancer cell signaling. While sFRP1 possesses the therapeutic potential, composite NPs provide stability to the system. The crux of the concept of this work has been illustrated in **Scheme 3.1**.

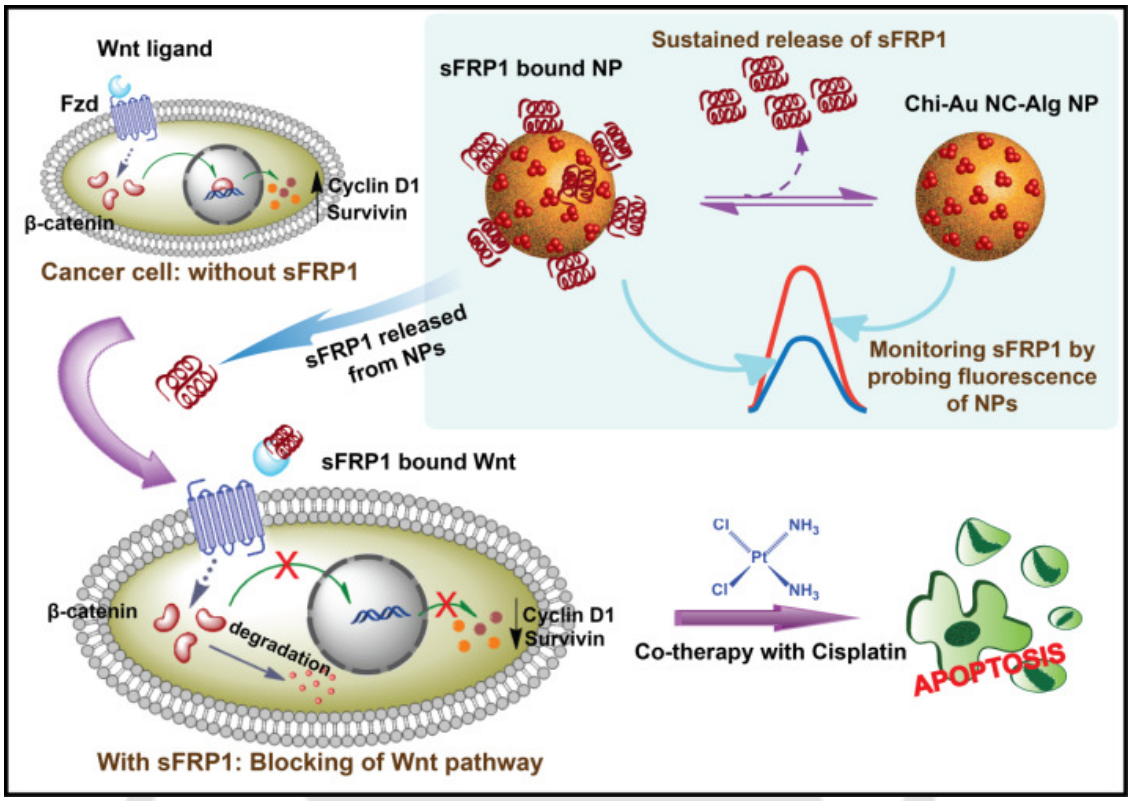

Scheme 3.1. The findings reported in this chapter are represented schematically.

3.2 Material and Methods

3.2.1 Synthesis of Chitosan-Au NC-Alginate NPs (Chi-Au NC-Alg NPs)

Chitosan solution was prepared at a concentration of 0.5% in 0.1% (v/v) acetic acid. It was then filtered to attain homogeneous solution of chitosan. The pH was adjusted to 6.2 with NaOH. 2 ml of this solution was added to 10 ml of Milli-Q water, to which 80 µl of 0.11 M MPA was added. Au NCs were synthesized by adding 180 µl of 10 mM gold(III) chloride to the above solution and stirring for 15 min at room temperature. After checking the luminescence of the Au NCs in UV transilluminator, 2 ml of the synthesized chitosan-Au NC was taken in a separate tube. To make negatively charged NPs, 1 ml of liquid paraffin oil was added to it, along with 0.5 ml of 1% sodium alginate. It was then sonicated with a probe sonicator for 3 min, under cold conditions. After sonication, the top layer of oil was discarded and rest was centrifuged at 11,500 g for 5 min at room temperature. Pellet obtained

on centrifugation was resuspended in 1 ml Milli-Q water. This washing step was crucial for complete removal of oil and hence was repeated three times. After the final round of centrifugation, the pellet was dissolved in 500 µl Milli-Q water to get negatively charged Chitosan -Au NCs -Alginate NPs.

3.2.2 Expression, purification of GST tagged human sFRP1

Protein was expressed in *E. coli* BL21 (DE3) cells transformed with recombinant vector pGEX-4T2 containing human sFRP1 gene. GST-sFRP1 was purified to near homogeinity by affinity chromatography, using glutathione-agarose beads, which bind to GST.[27] The purified GST tagged human SFRP1 protein was dialyzed against 10 mM tris buffer at pH 7.5 for 7 h. The protein concentration was estimated by Bradford assay for all experiments.

3.2.3 Characterization of Chi-Au NC-Alg NPs

The NPs were characterized, alone as well as after binding to GST-sFRP1, by means of dynamic light scattering (DLS) and zeta potential measurement using Malvern Zetasizer Nano ZS, to determine hydrodynamic diameter and net surface charge respectively. Fourier transform infrared (FTIR) spectroscopic analysis was also performed for NPs, protein, and protein-NPs. Samples were lyophilized, pellets were prepared with potassium bromide, and thereafter, spectral measurements were taken in the range of 400 to 4000 cm^{-1} using Perkin-Elmer Spectral One. Quantum yield of Chi-Au NC-Alg NPs was calculated using established formula [117] (details given in subsection 3.3.1).

3.2.4 Imaging of Chi-Au NC-Alg NPs with TEM and fluorescence microscope

Transmission electron microscopy (JEM 2100 TEM) was done, at an accelerating voltage of 200 keV, to capture images of NPs, alone and bound to GST-sFRP1. For this purpose, samples were drop-casted on carbon-coated copper grid and dried at room temperature. Fluorescence microscopy was also used to record images of NPs at different emission wavelengths by drying the samples on a glass slide.

3.2.5 Binding studies of NPs with protein

The same batch of NPs was loaded with different amounts of dialyzed protein for studying their binding efficiency. Volume was made up to 1 ml with 10 mM tris buffer (pH 7.5) for

all samples. Incubation was done at 37 °C for 3 h, at the end of which, samples were centrifuged and pellet was redispersed in 1 ml Milli-Q. Luminescence of NPs was probed at excitation wavelength of 320 nm using Fluorolog-3. Binding efficiency was calculated by the following formula –

$$\text{Binding efficiency (\%)} = \frac{\text{Intensity}_{NP} - \text{Intensity}_{protein\text{-}NP}}{\text{Intensity}_{NP}} \text{ X } 100$$

Circular dichroism spectral analysis was conducted with JASCO-815 spectrometer (Jasco, Japan), at flow rate of 5 L/min, temperature of 25 °C and scanning wavelengths of 240 nm to 190 nm.

3.2.6 Release studies of protein

From the previous experiment, the concentration of protein displaying maximum binding to the NPs was selected. After binding, samples were centrifuged, pellets were redispersed in PBS, and incubated at 37 °C for different time periods ranging from 0 h to 48 h. Each sample was centrifuged at various time points, supernatant was collected, which will contain the released protein. For this experiment, fluorescence intensity of released protein was probed by tracking the emission wavelength at 360 nm, on excitation at 280 nm using fluorescence spectrophotometer LS55 Perkin-Elmer.

3.2.7 Mammalian cell culture

Human cervical cancer (HeLa) and human embryonal kidney (HEK-293) cell lines were obtained from National Centre for Cell Sciences, Pune. Cells were maintained in DMEM, containing 10% FBS, 100 U/ml Penicillin, 100 µg/ml Streptomycin in humidified atmosphere at 37 °C in a 5% carbon dioxide incubator.

3.2.8 Stability studies of NPs and tracking the release of protein

The luminescence property of Au NCs was utilized for probing the stability of NPs and release of protein in culture media, over a span of 48 h. For this purpose, HeLa cells were seeded in six-well plate at a density of 10^5 cells per well and allowed to attach for 8 h. Thereafter, media was replaced by serum-free media containing only NPs as well as NPs

bound to GST-sFRP1 in separate wells. One set of NPs and protein-bound NPs, was collected at each time point in their culture media. Luminescence intensity was measured with Fluorolog-3, Horiba JobinYvon, USA, at 2 h, 14 h, 24 h and 48 h respectively.

3.2.9 Assessment of cell viability

The effect of sFRP1-NPs on HeLa cells was determined by MTT assay. HeLa cells were seeded in a 96-well plate at a density of 7000 cells per well. After allowing the cells to attach for 8 h, they were treated with Chi-Au NC-Alg NPs, GST-sFRP1 and sFRP1-NPs respectively, for 48 h. The activity of recombinant protein was also tested on non-cancerous cell line HEK-293. Then MTT assay was performed, whereby MTT was converted to purple formazan crystals by healthy cells. These crystals were dissolved in DMSO and absorbance was recorded at 550 nm, with background reference measured at 655 nm. All concentrations were added in triplicates and the experiment was performed three times. Cell viability was calculated using the following formula and statistical tests were performed.

$$\% \text{ of cell viability} = \frac{(A_{550} - A_{655})_{\text{sample}}}{(A_{550} - A_{655})_{\text{control}}} \times 100$$

3.2.10 Tracking NPs with high-end deconvolution microscopy

Tracking the localization of NPs was essential to confirm whether they remained in the media or were uptaken by the cells. For this purpose, they were viewed after incubation with sFRP1-NPs under high-end deconvolution microscope (DeltaVision, GE Healthcare Life Sciences).

3.2.11 Preparation of whole cell protein lysate and Western blotting

Western blotting was done to analyze the signaling pathway responsible in bringing about the detrimental effects of GST-sFRP1 on the growth of HeLa cells. In particular, phosphorylation status of β-catenin protein, which is central to the Wnt pathway, was checked. Cells treated with protein-NPs were also analyzed in order to evaluate the functionality of protein in the two cases. With this intent, cells were treated with both for 24 h in 60 mm culture petridishes containing serum-free media. A control sample with cells incubated in serum-free media for 24 h was also kept. Thereafter the media were discarded

and the cells were washed two times with PBS. RIPA buffer supplemented with protease inhibitor cocktail was added to each plate, and incubated for 5 min in cold under mild shaking. The cell lysate was then sonicated for 10 sec with probe sonicator in ice. Thereafter, samples were centrifuged at 8000 g for 10 min at 4 °C to pellet down the cell debris. The respective supernatants, containing all soluble proteins, were collected and the amount of protein in each was quantified using Lowry's method of protein estimation. Then an equal amount of each of the three samples (untreated, treated with protein, treated with protein-NPs) was electrophoresed in triplicates on 12% SDS-PAGE and transferred to a PVDF membrane. Blocking of the membrane was done with 4% bovine serum albumin (BSA, HiMedia, India) in PBST for 2 h. It should be mentioned here that all steps followed for detection of phosphorylated protein require the usage of TBST (50 mM tris, 150 mM sodium chloride, 0.1% tween 20) instead of PBST. Eventually, membrane was cut such that each replicate sample was incubated overnight with either of primary antibody against human β-catenin, phosphorylated form of β-catenin ($pSer^{33}$/ $pSer^{37}$) and β-actin as endogenous control. Next, membrane was washed with PBST/TBST five times and incubated with corresponding peroxidase labeled secondary antibodies. Again, washing was done five times with PBST/TBST, before the blots were developed with Chemiluminescent Peroxidase Substrate.

3.2.12 AO/ EB dual staining

To distinguish between healthy and membrane compromised cells, the cells were simultaneously stained with AO and EB. In this pursuit, the cells were grown in a 96-well plate, as before. Recombinant protein, alone and after being bound to Chi-Au NC-Alg NPs, were added at concentrations for which maximum effect was observed in the MTT assay. At the end of the treatment period of 48 h, media was discarded, the cells were washed thoroughly with 10 mM PBS, and AO and EB were added at concentrations of 2 µg/ml and 10 µg/ml, respectively. After incubation for 5 min in dark, the cells were washed with fresh PBS and visualized under fluorescence microscope (Nikon ECLIPSE TS100).

3.2.13 Expression profiling for downstream genes

Expression of two genes- cyclin D1 and survivin, functioning downstream of β-catenin in the Wnt pathway, was also studied to further confirm the implication of this signaling pathway. RNA was isolated with the Tri reagent-based method and cDNA was synthesized with RevertAid H-minus Reverse Transcriptase kit (Fermentas). A 220 bp fragment of the gene for cyclin-D1 was amplified from the cDNA using forward primer 5´-CGCCCCACCCCTCCAG- 3´and reverse primer 5´-CGCCCAGACCCTCAGACT- 3´, whereas a 170 bp fragment of the survivin gene was amplified using forward primer 5´-AGAACTGGCCCTTCTTGGAGG-3´and reverse primer 5´-CTTTTTATGTTCCTCTATGGGGTC-3´.

3.2.14 Combination therapy with cisplatin

Cisplatin was also added in combination with the above samples, to determine if the protein-NPs have the potential to induce sensitization of HeLa cells toward cisplatin. MTT assay was conducted following the above protocol. The range of concentration of cisplatin used was 1 µg/ml to 5 µg/ml.

3.2.15 Cell cycle analysis

The effect of the protein conjugated NPs on the cell cycle pattern of HeLa cells was evaluated by FACS using PI. Also, its impact in combination with cisplatin was ascertained in the same manner. Cells were seeded at a density of 10^5 cells per well in a six-well plate and allowed to attach overnight. Thereafter, the cells were treated separately with recombinant sFRP1 and sFRP1-NPs, alone and in combination with cisplatin. The concentration used for GST-sFRP1 was 10 nM and equivalent concentration of protein-NPs was used. Concentration of cisplatin used was 3 µg/ml. All concentrations were decided based on the data obtained from MTT assays. Samples were treated for 48 h at the end of which, cells were harvested by trypsinization, and fixed with 70% ethanol in ice for 1 h. Then they were centrifuged at 650 g for 5 min at 4 °C. Pellets thus formed were washed with cold PBS before being incubated in 0.4 mg/ml RNase solution for 1 h at 37 °C. PI was added to each sample at a concentration of 10 µg/ml and incubated in dark till the time of analysis in FACSCalibur.

3.2.16 Detection of apoptosis by fluorescein isothiocyanate (FITC) conjugated Annexin V/ PI

This assay was performed to distinguish among the healthy, early apoptotic and late apoptotic cells, following treatment. HeLa cells were grown and treated following the same method as above. Cells were collected by trypsinization, washed with PBS and stained with Annexin V-FITC and PI, following the manufacturer's protocol provided with Annexin V-FITC apoptosis detection kit (BD Biosciences). Finally, the cells were analyzed by FACS. All concentrations used were same as the previous experiment.

3.3 Results and Discussion

3.3.1 Recombinant GST-sFRP1 bound to Chi-Au NC-Alg NPs

The recombinant vector pGEX-4T2 with the cloned human sFRP1 was transformed into *E. coli* BL21(DE3). GST tagged sFRP1 protein was expressed and purified from the bacterial culture using affinity chromatography column, which generated a discrete single band at 61 kDa corresponding to GST-sFRP1, in SDS-PAGE (**Figure 3.1A**). The pI (isoelectric pH) of GST-sFRP1 calculated theoretically using ExPASy pI calculator, was found to be 8.73, which meant that the recombinant protein would have a net positive surface charge at physiological pH. Also, its mechanism of action requires its presence outside the cells, in the culture media, where it binds to Wnt ligands [33]. In non-cancerous cells, sFRP1 is known to bind to Wnt ligands, which are extracellular secretory proteins, and prevent it from carrying out its downstream signaling [118]. In cancer cells, sFRP1 is downregulated [119, 120] and hence, Wnt binds to its cell surface receptor Fzd to transduce the Wnt cell signaling pathway, resulting in upregulation of pro-proliferative genes like cyclin D1, survivin and c-myc. Exogenous addition of GST-sFRP1 to cervical cancer cells led to its binding to Wnt ligand in the extra-cellular medium [27]. In order to overcome the limitations of treatment with recombinant protein alone, biocompatible composite NPs were formulated. Additionally, for real time monitoring of protein luminescent Au NCs were incorporated owing to their enhanced photophysical activity. Prior to formation of the composite NPs, Au NCs were synthesized with gold(III) chloride, on biopolymer chitosan, in the presence of

reducing agent 2-mercaptopropionic acid (MPA), based on the method developed earlier [109]. They were converted to NPs using biopolymer alginate, which being negatively charged at physiological pH, helped in the formation of spherical NPs by electrostatic interactions with positively charged amine groups of chitosan. As synthesized composite NPs revealed characteristic emission of the Au NCs at 610 nm when excited by 320 nm UV light as depicted in **Figure 3.1B**.

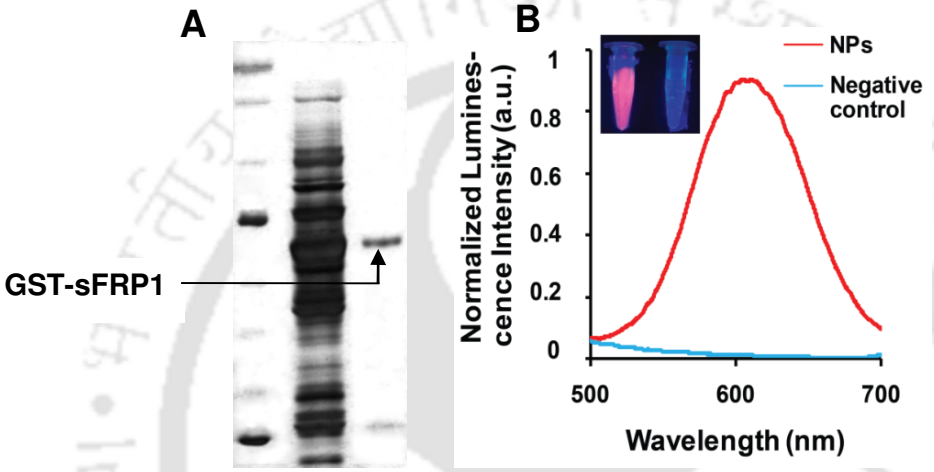

Figure 3.1. (A) 12% SDS-PAGE showed a single band of purified GST-sFRP1 at its legitimate size of 61 kDa, **(B)** Emission spectrum of Chi-Au NC-Alg NPs displaying bright luminescence when excited with 320 nm wavelength of light; negative control containing all the constituents of the NPs excepting gold chloride.

MALDI-TOF data showed a prominent peak at m/z equaling to 5310.98 (**Figure 3.2A**), which corresponds to [Au_{20}+ $(MPA)_{12}$+ 5 Na^+]. This was a confirmation of the organization of gold cluster, comprising of 20 gold atoms. The extinction spectrum of the synthesized NPs did not display any peak in the range of 400-800 nm, ruling out the possibility of formation of SPR positive gold NPs [106, 109] (**Figure 3.2B**).

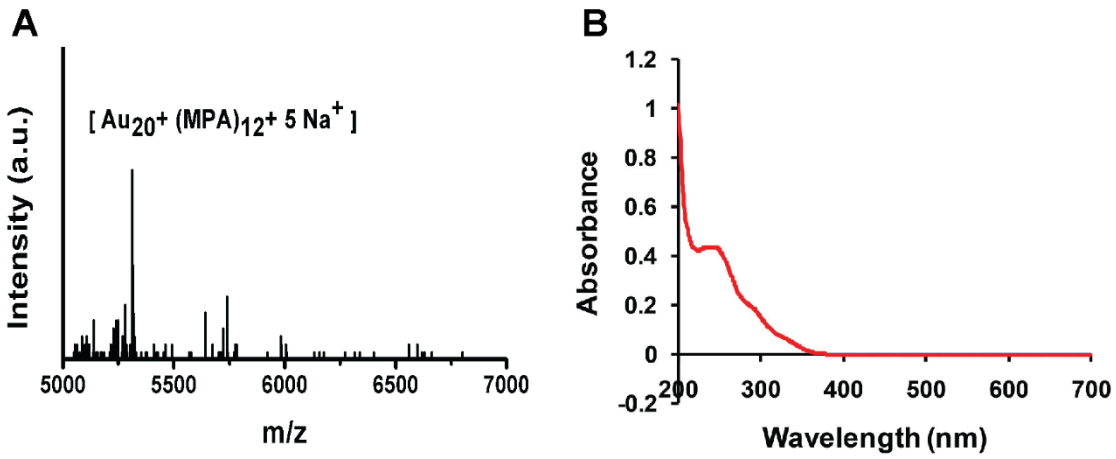

Figure 3.2. (A) MALDI TOF analysis of composite NPs demonstrated the molecular formula of the Au NCs to be $[Au_{20} + (MPA)_{12} + 5\ Na^+]$. **(B)** UV-visible absorption spectrum of Au nanoclusters.

The size and surface charge of the composite NPs were optimized by varying the concentration of chitosan to alginate ratio to attain bigger and negatively charged NPs, which possessed reduced capability of penetrating the cell membrane. This was necessary as the recombinant protein binds to Wnt ligands in the extracellular medium to exert its activity. Average hydrodynamic diameter of the NPs was 599 nm (**Figure 3.3A**) and that of protein-NPs was 767 nm (**Figure 3.3B**), as analyzed by DLS. Zeta potential studies revealed that the positively charged chitosan Au NCs were converted to negatively charged NPs (-26.6 mV) by addition of alginate (**Figure 3.3C**). Interaction of NPs with GST-sFRP1 caused a further reduction in its negative charge from -26.6 mV to -15.8 mV (**Figure 3.3D**). The negative charge of the NPs would possibly help to reduce the endocytic uptake of protein-NP conjugate by the negatively charged cell membrane [121]. Besides, this decrease in negative charge may enhance the circulation time of the NPs by reducing uptake by macrophages. Literature also suggests that positive NPs are cleared more quickly from the body by the mononuclear phagocyte system (MPS), as compared to neutral or negatively charged NPs [121]. It may be emphasized here that the features of size and surface charge tunability of the composite NPs greatly widen the scope of its clinical application.

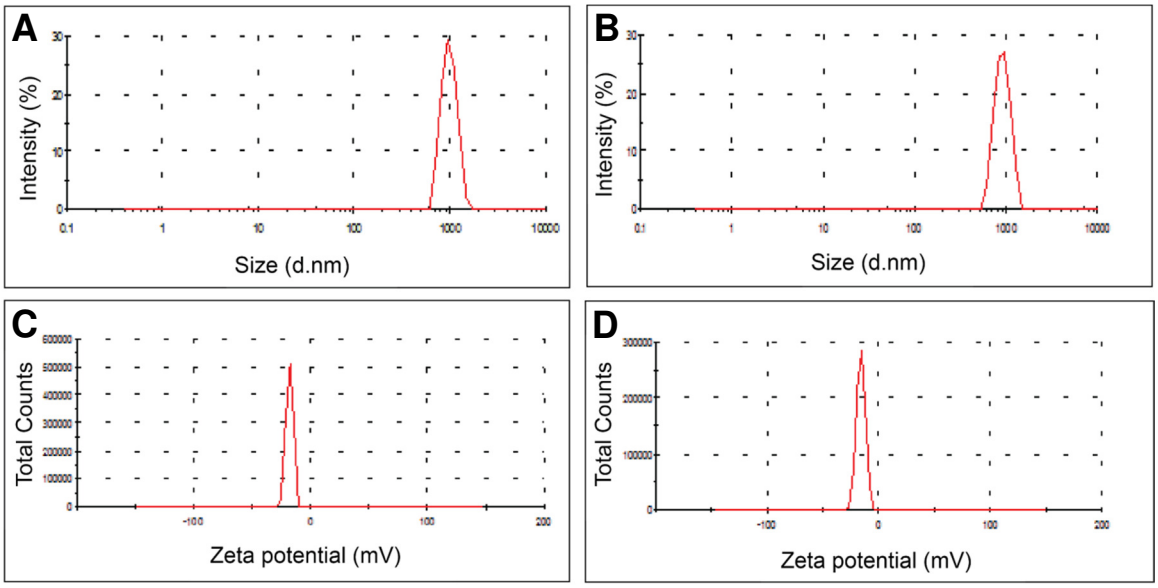

Figure 3.3. Hydrodynamic diameter was found to be **(A)** 599 nm for Chi-AuNC-Alg NPs. and **(B)** 767 nm for sFRP1-NPs. Zeta potential studies showed that net surface charge of **(C)** NPs was -26.6 mV. **(D)** Protein-NPs was -15.8 mV.

TEM images revealed the formation of nearly uniform spherical NPs of average diameter of 320 ± 15 nm (**Figure 3.4A**). The difference in size of NPs as observed in TEM images, showing dried samples, and DLS analysis, with samples in solution, was probably due to the swelling of NPs in solution. Both chitosan and alginate have been reported to swell in aqueous solution, depending on their concentration and degree of cross-linking [122]. The Au NCs are clearly visible in the magnified image (**Figure 3.4B**). Interestingly, the composite NPs remained intact even after interaction with protein (**Figure 3.4C** and **Figure 3.4D**), which implied that the protein structure did not interfere with the chemistry of the NPs. This finding is quite remarkable as it unveils the potential of this system for the delivery of therapeutic proteins in future. The particle size distribution profile shown in **Figure 3.4E**.

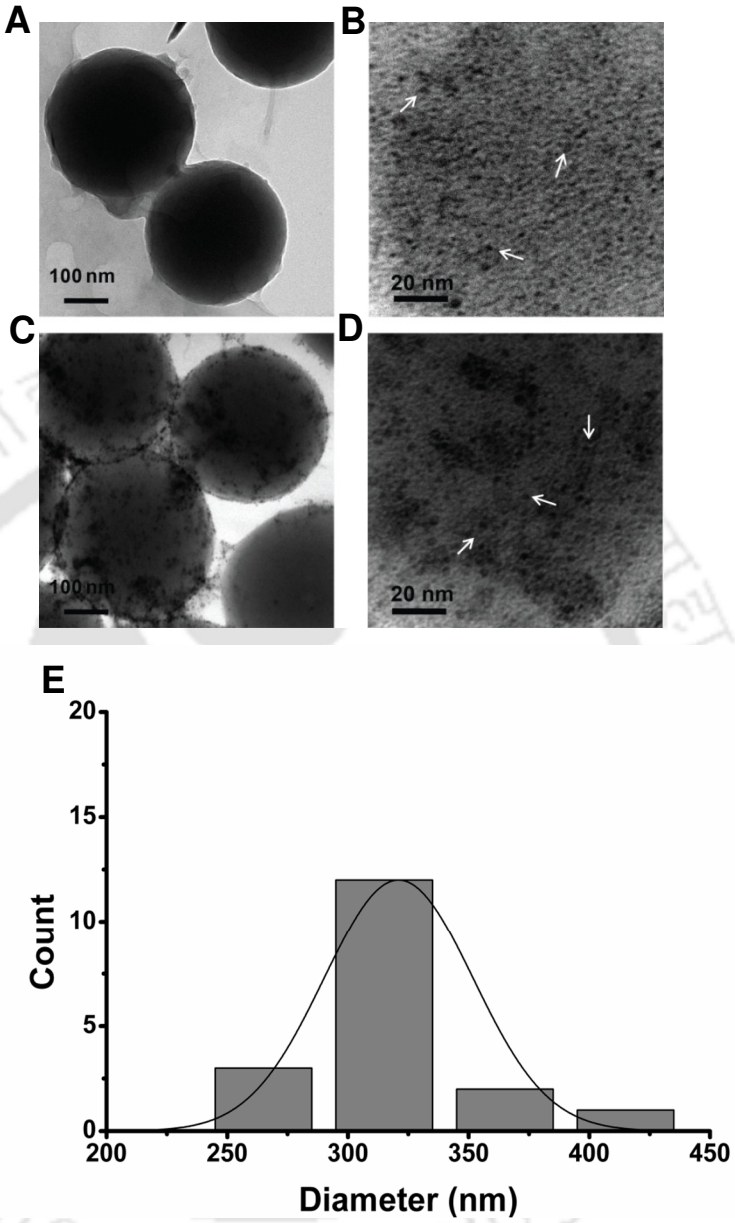

Figure 3.4. **(A)** As synthesized NPs were drop casted, dried and imaged with TEM image, which depicted spherical NPs of around 350 nm diameter and, **(B)** Magnified image to show Au NCs, **(C)** Binding of NPs with protein was done in Tris buffer for 2 h. Thereafter, the sample was dried on a TEM grid and imaged and, **(D)** Magnified image to show Au NCs after binding of protein. **(E)** Particle size distribution data based on TEM images.

Another important necessity for drug or protein delivery is the tracking of its path after its administration. The extraordinary luminescence properties of the Au NCs in the composite

NPs enable its use as a luminescent probe for imaging and tracking purposes [105]. The quantum yield of Chi-Au NC-Alg NPs was calculated to be 1.3%, using quinine sulfate as standard, using established one-step method:

$$Q = Q_R \frac{I \quad OD_R \quad n^2}{I_R \; OD \quad n_R^2}$$

Where, Q is the fluorescence quantum yield, I is the integrated fluorescence intensity, OD is the optical density (absorption), n is the refractive index. The subscript R denotes the standard compound used, which in this case, is quinine sulfate. The quantum yield of quinine sulfate is 54%.

Furthermore, epi-fluorescence microscopy showed discrete particles displaying green and red images with blue and green filters respectively (**Figure 3.5**). This fascinating feature can be exploited for optical imaging studies, especially if more than one fluorescent molecule is required for any experiment. Also, previous investigations have demonstrated that Au NCs undergo photobleaching to a far lesser degree than organic dyes, which further enriches the credibility of Au NCs [105, 109].

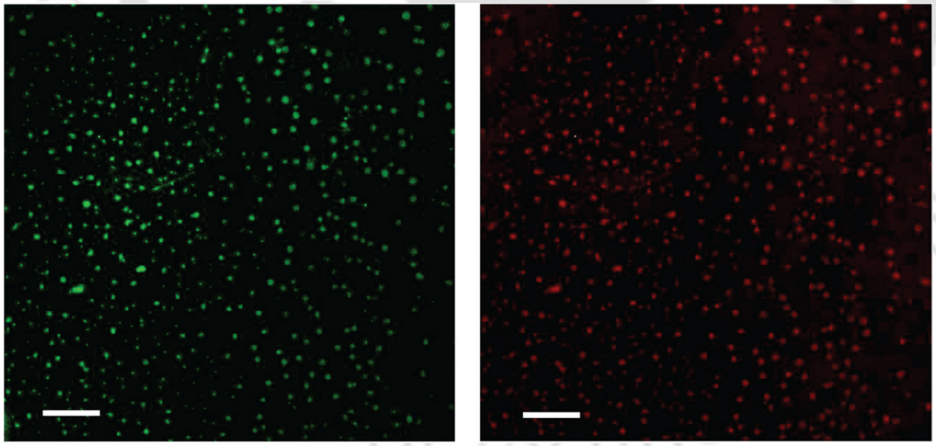

Figure 3.5. Composite NPs emitting green and red fluorescence under microscope when excited with blue and green light, respectively. Scale bar is 10 μm.

3.3.2 Binding and release studies of recombinant protein

Binding studies of the GST-sFRP1 were conducted by probing the luminescence of Au NCs. Maximum binding efficiency was calculated to be approximately 70.6% in Tris buffer at pH 7.4 (**Figure 3.6A** and **Figure 3.6B**).

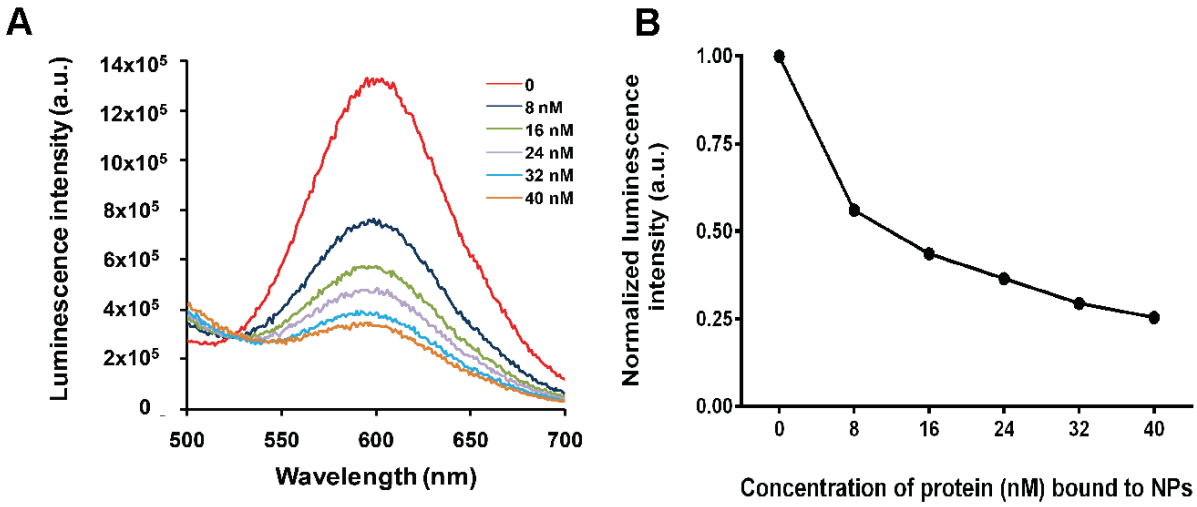

Figure 3.6. **(A & B)** Binding of NPs with increasing concentrations of protein was done for 2 h in Tris buffer (pH 7.4). Probing the luminescence of Au NCs yielded protein concentration dependent quenching of luminescence, with a maximum binding efficiency of 70.6% for a protein concentration of 32 nM, after which saturation was attained.

Binding of protein to the NPs was further substantiated by FTIR spectroscopy (**Figure 3.7**) and circular dichroism spectral analysis. In the FTIR spectra, binding of protein to Chi-Au NC-Alg NPs was represented by a shift in the characteristic peak for amide I from 1609 cm^{-1} to 1613 cm^{-1}, with the appearance of a second peak at 1524 cm^{-1} signifying amide II.

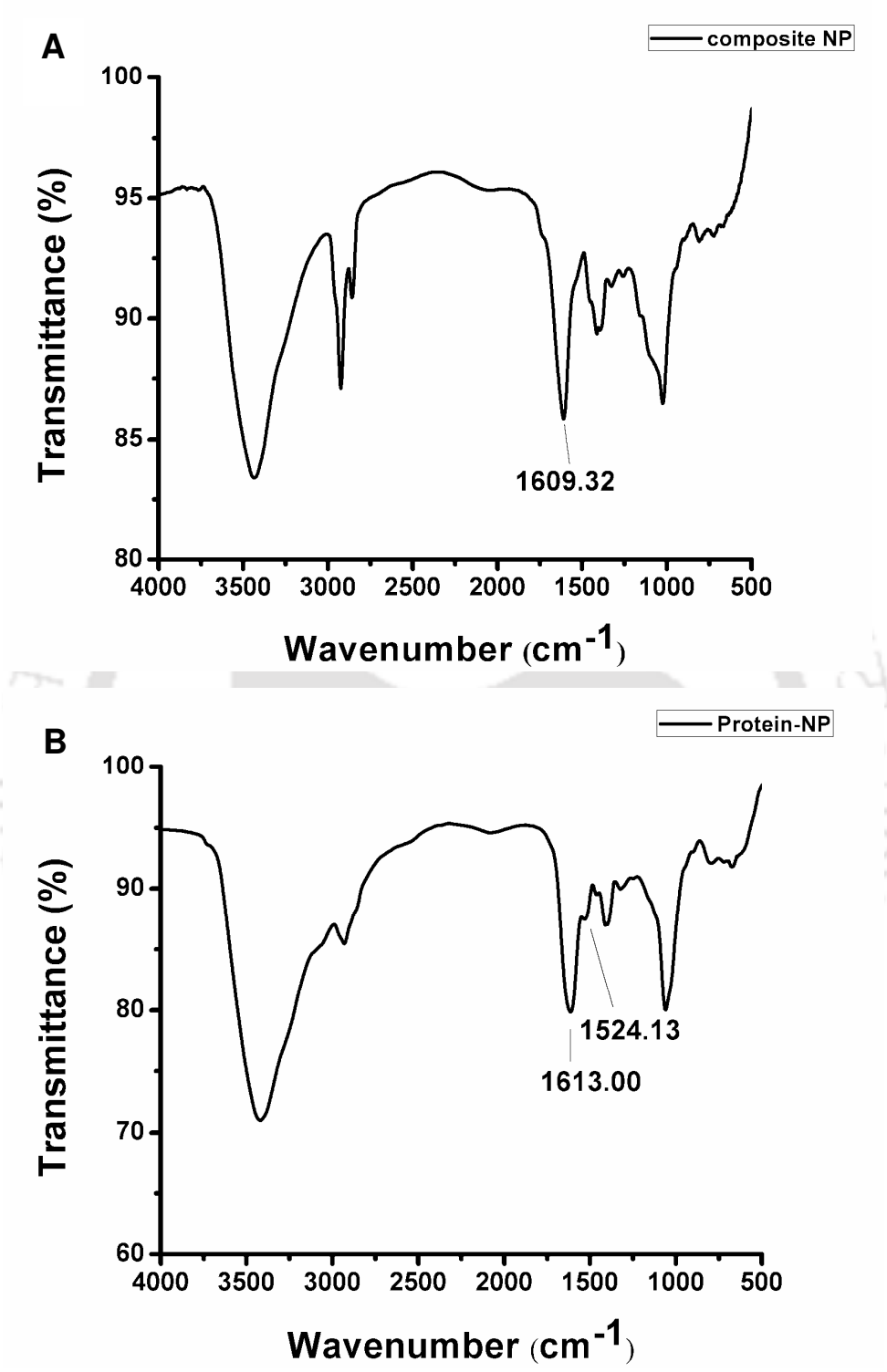

Figure 3.7. FTIR analyses of **(A)** Chi-AuNC-Alg NPs. **(B)** sFRP1-NPs after binding for 2 h in Tris buffer. Both samples were lyophilized before analysis.

Circular dichroism analysis was performed to study the conformational change of protein after binding with NPs. As reported in the previous chapter, α- helical structures and β-sheets of GST-sFRP1 were 20.7% and 33.5%, respectively [27]. Upon binding to NPs, α-helix was found to reduce to 9.3% and β-sheets were increased to 60.6% (**Figure 3.8**). This indicated that although the protein underwent some conformational changes upon binding to NPs, its secondary structures were intact to a significant extent. Subsequent experiments confirmed that the functionality of the protein was retained.

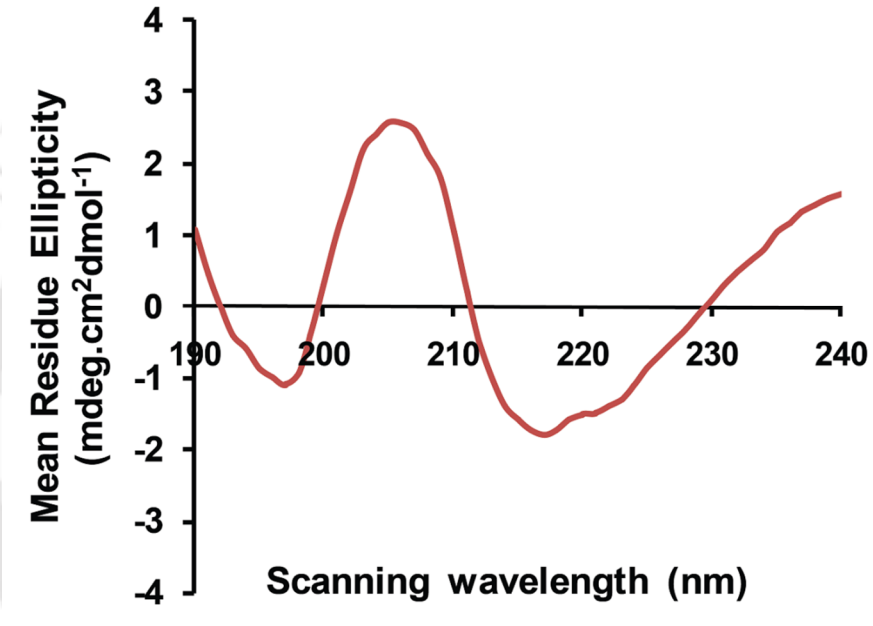

Figure 3.8. CD spectrum of GST-sFRP1 bound to NPs performed in Tris buffer pH 7.4.

Release profile of GST-sFRP1 from Chi-Au NC-Alg NPs was examined in PBS (pH 7.4) by probing intrinsic luminescence of protein. It demonstrated a sustained release of about 40% of the bound protein from composite NPs after 48 h (**Figure 3.9A**). It can be anticipated that the bound protein may also interact with its target i.e., Wnt ligand through protein-protein interaction in the extracellular media and generate desired cell inhibitory effects. The sustained release profile obtained in this case is ideal for prolonged activity of the protein.

3.3.3 Stability of Au NCs in cell culture media studied by probing luminescence

As an *in vitro/in vivo* biological system contains an assortment of proteins, the stability of the protein- NPs in cell culture media, was also conducted by probing the luminescence of Au NCs. In this pursuit, luminescence of the NPs was quenched by 20% in the initial hours possibly due to instability of the NPs (in absence of protein) in media (**Figure 3.9B**). However, interaction of the NPs with different components of medium, such as, amino acids, resulted in the stabilization and constancy of the luminescence due to Au NCs over longer period of time. However, the interaction of the protein with NPs significantly stabilized the NPs and the luminescence intensity remained undiminished, where the emission intensities due to both bound and unbound NPs were normalized to emphasize the difference in their stability.

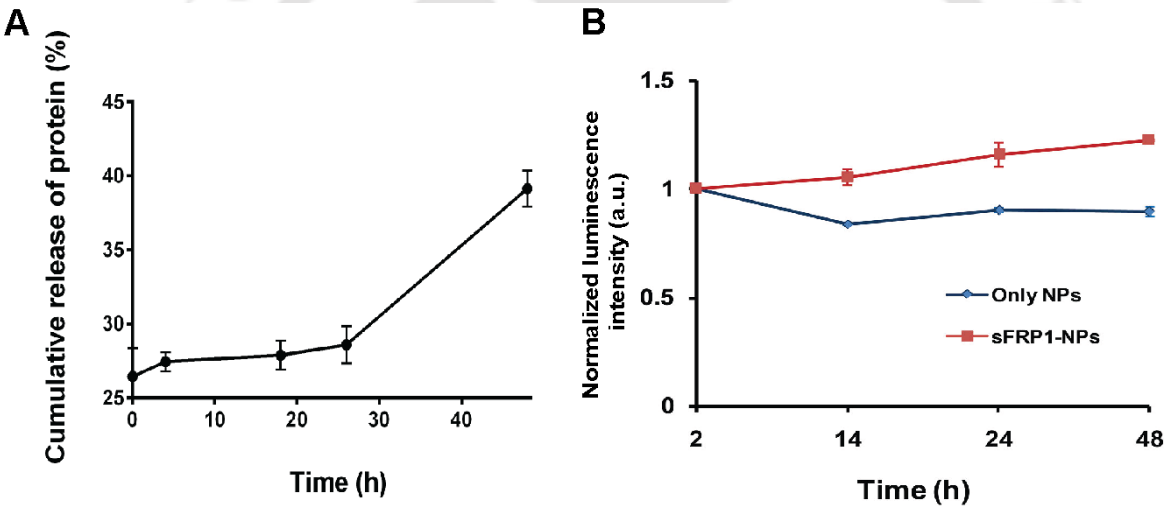

Figure 3.9. (A) After 2 h of binding of NPs with protein in Tris, time dependent release profile was investigated in PBS (pH 7.4) , which illustrated a maximum of 40% release of bound protein from the NPs in 48 h, **(B)** Stability studies in growth media displayed enhanced stability of the protein-NPs, as compared to unbound NPs. For this experiment, cells were treated with NPs, with or without bound protein, and the culture media were collected for analysis of luminescence, at different time points up to 48 h.

Figure 3.10 depicted that binding of protein to NPs in culture media quenched the luminescence of the clusters, corroborating the results obtained from the binding studies in

Tris buffer, pH 7.4. However, maximum luminescence quenching was observed at 2 h, which decreased gradually in a time dependent fashion. This may prove to be an excellent tool to perform relative quantification studies using stable and labelled payload *in vitro,* by using Au NCs as luminescent probe [123].

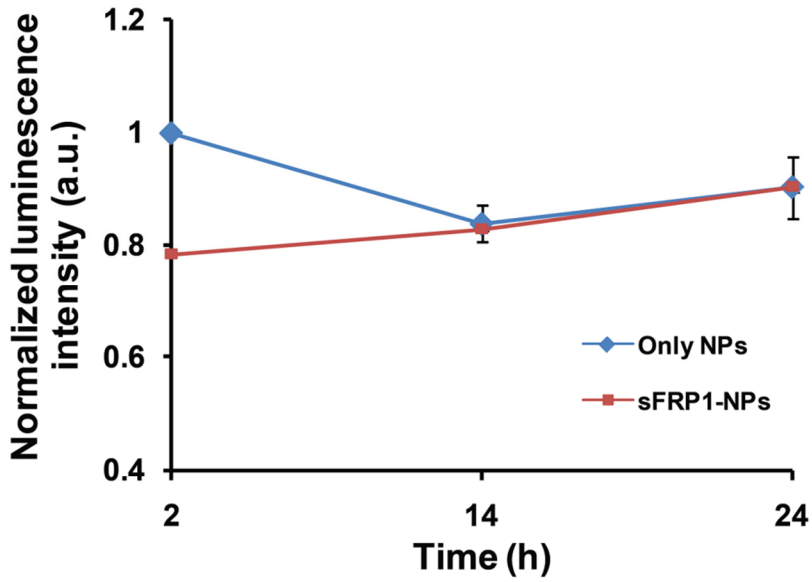

Figure 3.10. Binding of sFRP1 with composite NPs in cell culture media quenched the luminescence of the clusters at initial hours.

3.3.4 Tracking NPs for anti-cancer function

Researchers have reported that transfection of sFRP1 gene in mammalian cancer cells leads to reduced cell growth and proliferation [41, 50]. In the previous chapter, the inhibitory effects of GST-sFRP1 on cancer cell lines were demonstrated [27]. In this chapter, it has been established that the protein after being bound to NPs, not only retained its functionality, but also displayed improved cell inhibitory effect, as compared to protein alone. This can be attributed to the stability and sustained release of protein from the NPs, resulting in the prolonged presence of functional sFRP1 in the medium, as compared to the protein alone. Cell viability was reduced to 50% for protein-NPs, while corresponding concentration of protein (12 nM) showed a viability of 61% (**Figure 3.11A**). Composite NPs were found to

be completely non-toxic even at high concentrations, making them ever more suitable for clinical applications in tracking and delivery of cargo. Moreover, GST-sFRP1 did not exert any inhibitory action on non-cancerous cell line HEK-293 (**Figure 3.11B**). This would imply reduced side effects, making this protein ideal for cancer therapy.

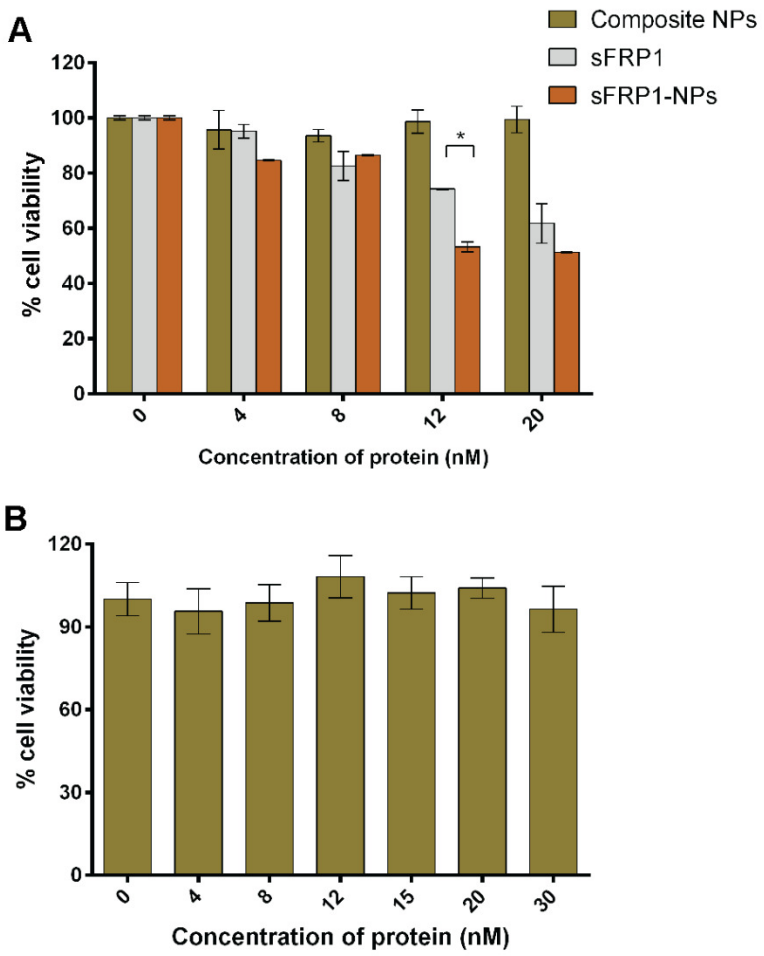

Figure 3.11. **(A)** Treatment with protein-NPs showed profound effect on viability of HeLa cells, compared to protein alone, as deduced from cell viability assay. Cells were also treated with NPs of corresponding concentrations. **(B)** Cell viability assay showed that recombinant sFRP1 has no effect on HEK-293 cells, even after 48 h of treatment at high concentrations.

Herein, it should be mentioned that sFRP1 exerts its activity in the extracellular medium. To determine the fate of NPs, the particles were tracked using deconvolution microscope at 60X magnification (**Figure 3.12A**). The images clearly deciphered that NPs remained in

media with red luminescence and thus the criteria for synthesizing the NPs were met. This was corroborated by flow cytometry-based quantitative analysis of HeLa cells treated with luminescent NPs. Analysis was performed in FL3-H channel for recording red fluorescence upon excitation with 488 nm laser. No shifting of peak along the FL3-H axis in the treated cell population was observed, as compared to the control cells (**Figure 3.12B**). This proved that the cells had not taken up the luminescent NPs, which corroborated Figure 3.12A.

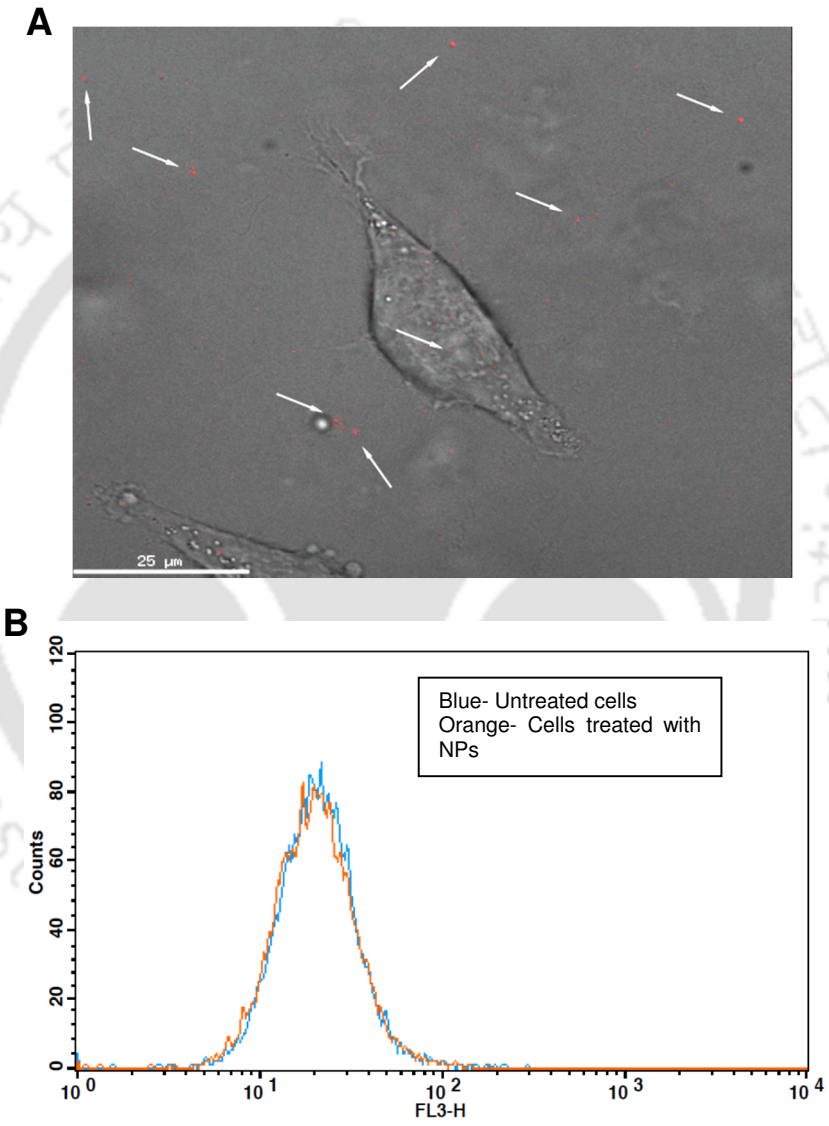

Figure 3.12. **(A)** Imaging NPs in cell culture media showed that they remained in the media and were not uptaken by cells at 2 h. **(B)** Quantitative analysis by flow cytometry demonstrated that HeLa cells did not show uptake of luminescent NPs.

3.3.5 Targeting the Wnt signaling pathway

The downstream Wnt pathway was studied to elucidate the mechanism of the growth inhibitory effect of recombinant sFRP1 on HeLa cells and to prove that the Wnt pathway was indeed being targeted by the sFRP1-NPs. As sFRP1 is reported to block Wnt pathway in normal adult cells, expression profile of a few crucial molecules of the Wnt cascade was explored. The most prominent member lying downstream of Wnt is the β-catenin protein. In cancer cells, Wnt pathway is active, where β-catenin is stabilized by several proteins and accumulates in the cytoplasm. Subsequently, it translocates into the nucleus and transcriptionally upregulates the expression of certain pro-proliferative genes like cyclin D1 and survivin. In presence of active sFRP1 in normal cells, β-catenin is phosphorylated to mark it for degradation by ubiquitination, and expressions of cyclin D1 and survivin are decreased. Hence, the β-catenin protein level as well as gene expression of cyclin D1 and survivin were examined by Western blotting and semi-quantitative PCR, respectively. For Western blotting, 53 µg of whole cell protein from each of three samples (control, GST-sFRP1, Chi-Au NC-Alg conjugated GST-sFRP1) was loaded into each well of a 12% SDS-PAGE, after quantifying them with Lowry assay. β-actin was used as loading control for all samples. β-catenin was significantly downregulated and phosphorylated β-catenin was significantly upregulated in both sFRP1 (**Figure 3.13A**) and sFRP1-NP treated cells (**Figure 3.13B**), as compared to the control cells. Ratio of phosphorylated to total β-catenin was negligible in control cells, whereas it increased 47 folds and 73 folds in protein and protein-NP treated cells, respectively (represented graphically in **Figure 3.13C**). Gene expression levels decreased for cyclin D1 (1.03 times and 1.78 times for protein and protein-NPs respectively). Similarly, expression of survivin gene also decreased (1.43 fold and 3.45 folds respectively), as illustrated in **Figure 3.13D**. Graphical representation of fold-change in gene expression is given **Figure 3.13E**. These experiments provided conclusive evidence that GST-sFRP1 exerted its anti-cancer effect by targeting the Wnt pathway. Also, they confirmed that the recombinant protein entirely retained its functional integrity after being bound to Chi-Au NC-Alg NPs.

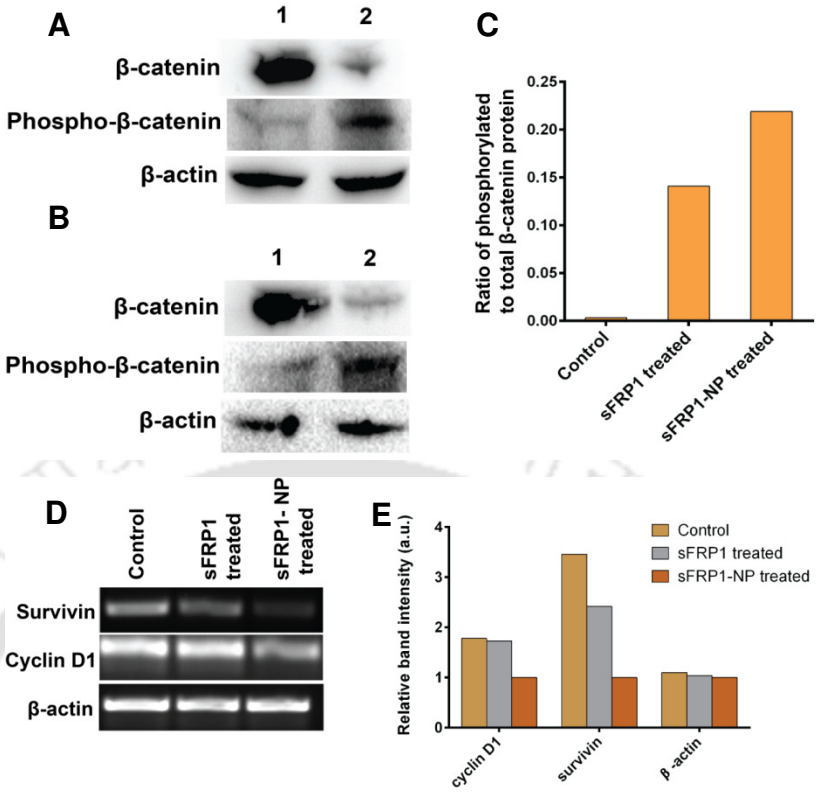

Figure 3.13. Western blotting to detect β-catenin, phosphorylated β-catenin and β-actin protein levels in HeLa cells **(A)** lane-1: untreated control, lane 2: treated with sFRP1 for 24 h and, **(B)** lane-1: untreated control, lane 2: treated with sFRP1-NPs for 24 h, **(C)** Graphical representation of fold change in ratio of phosphorylated β-catenin to β-catenin protein, **(D)** Expression analysis of downstream survivin and cyclin D1 genes in cells treated with sFRP1 and sFRP1-NPs for 24 h, as compared to untreated cells, **(E)** Graphical representation of fold change of cyclin D1, survivin and β-actin.

Furthermore, the effect of the recombinant sFRP1, with and without conjugation to nanocomposite, was delineated by a series of experiments. A preliminary examination of the damage sustained by the HeLa cells was done by simultaneous staining with two fluorescent dyes-AO and EB. AO is a cationic, cell permeable dye that stains the entire cell including nucleus. It has an emission maximum at 525 nm (green), when exposed to blue light. EB has an emission maximum at 605 nm (intense orange) on intercalating with DNA, when excited with ultraviolet light. However, it is cell impermeable and can bind to the DNA of membrane compromised cells only. Hence, dual staining with AO and EB was employed to distinguish

between healthy and membrane compromised cells. Further, apoptotic and necrotic cells can be differentiated based on the fact that necrotic cells will only be stained by EB as they undergo autolysis and do not have intact membrane. Visualization in epi-fluorescence microscopy demonstrated that the treatment with GST-sFRP1 triggered membrane damage of cells. The effect was enhanced on treatment with sFRP1-NPs, where a significant population of the cells showed staining with AO and EB (**Figure 3.14**). It is evident from the images that treated HeLa cells undergo apoptosis, which is the preferred mode of cell death. Hence, it may be surmised that the sFRP1-NPs successfully damaged cancer cells by targeting the Wnt cascade.

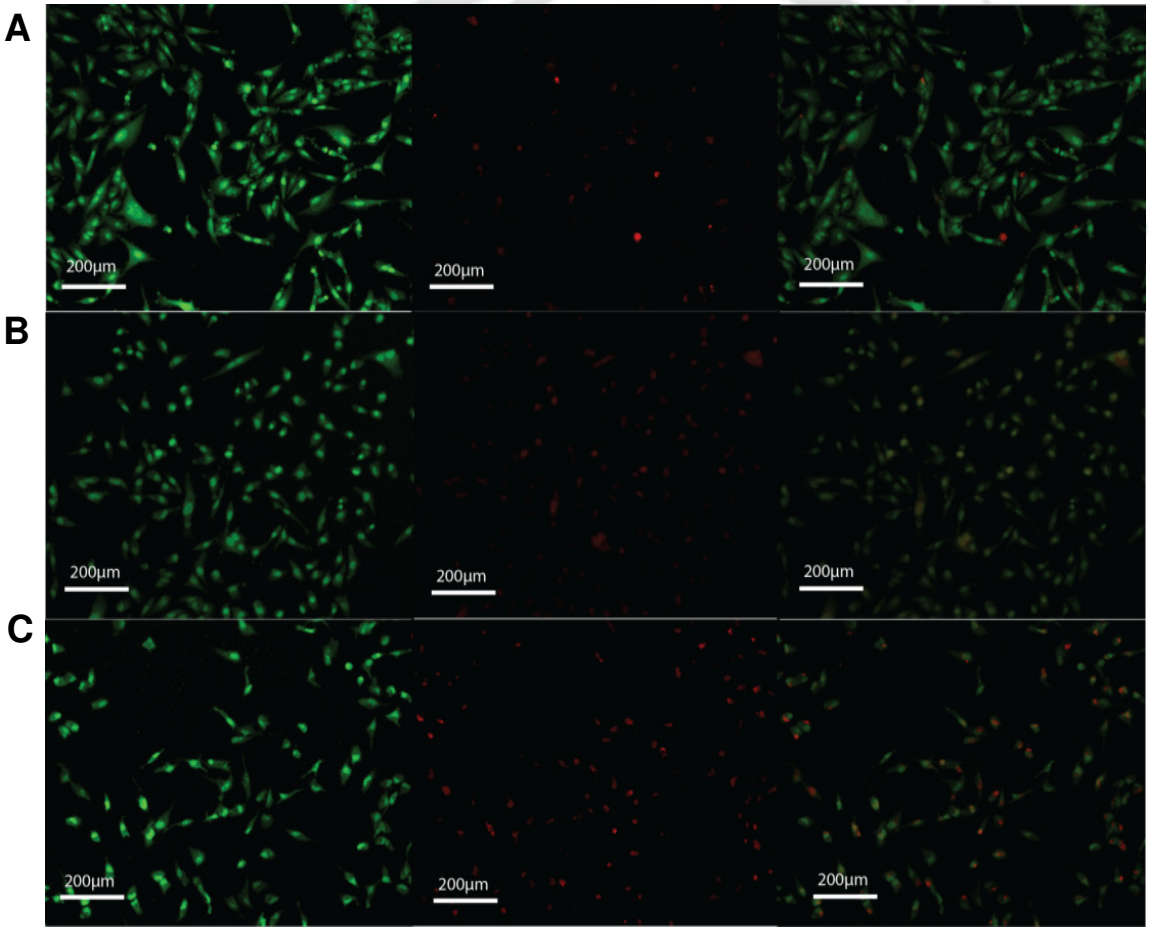

Figure 3.14. AO/EB staining of **(A)** control HeLa cells, **(B)** cells treated with protein and, **(C)** treated with protein-NP, respectively, depict membrane compromised cells in treated population, with damage being maximum in case of treatment with protein bound to composite NPs.

3.3.6 Molecular mechanisms in combination module

Studies have elaborated the phenomenon of chemosensitization of cancer cells toward a conventional chemotherapeutic agent by over-expression of a relevant gene [124] or addition of a therapeutic protein [109]. This fact has been exploited in this work, whereby, binding of protein to Chi-Au NC-Alg was found to considerably sensitize HeLa cells toward cisplatin. MTT assay exhibited a sharp reduction in cell viability in case of combination therapy (cisplatin with protein-NPs), as compared to only protein-NPs or only cisplatin treated cells (**Figure 3.15A**). The concept of combination therapy, such as chemotherapy followed by radiotherapy, has been prevalent for decades [125, 126]. Although this mode of treatment has accomplished some degree of success in certain types of cancers [127-129], the aftermaths concerning exacerbated side effects and development of resistance are yet to be addressed. Hence, the module of co-therapy demonstrated herein, combining protein therapeutics with chemotherapy provided a new facet to this work. It has the potential to augment the efficacy, reduce side effects and avoid development of resistance, thereby outweighing the benefits of monotherapy [130] or prevalent combination therapies.

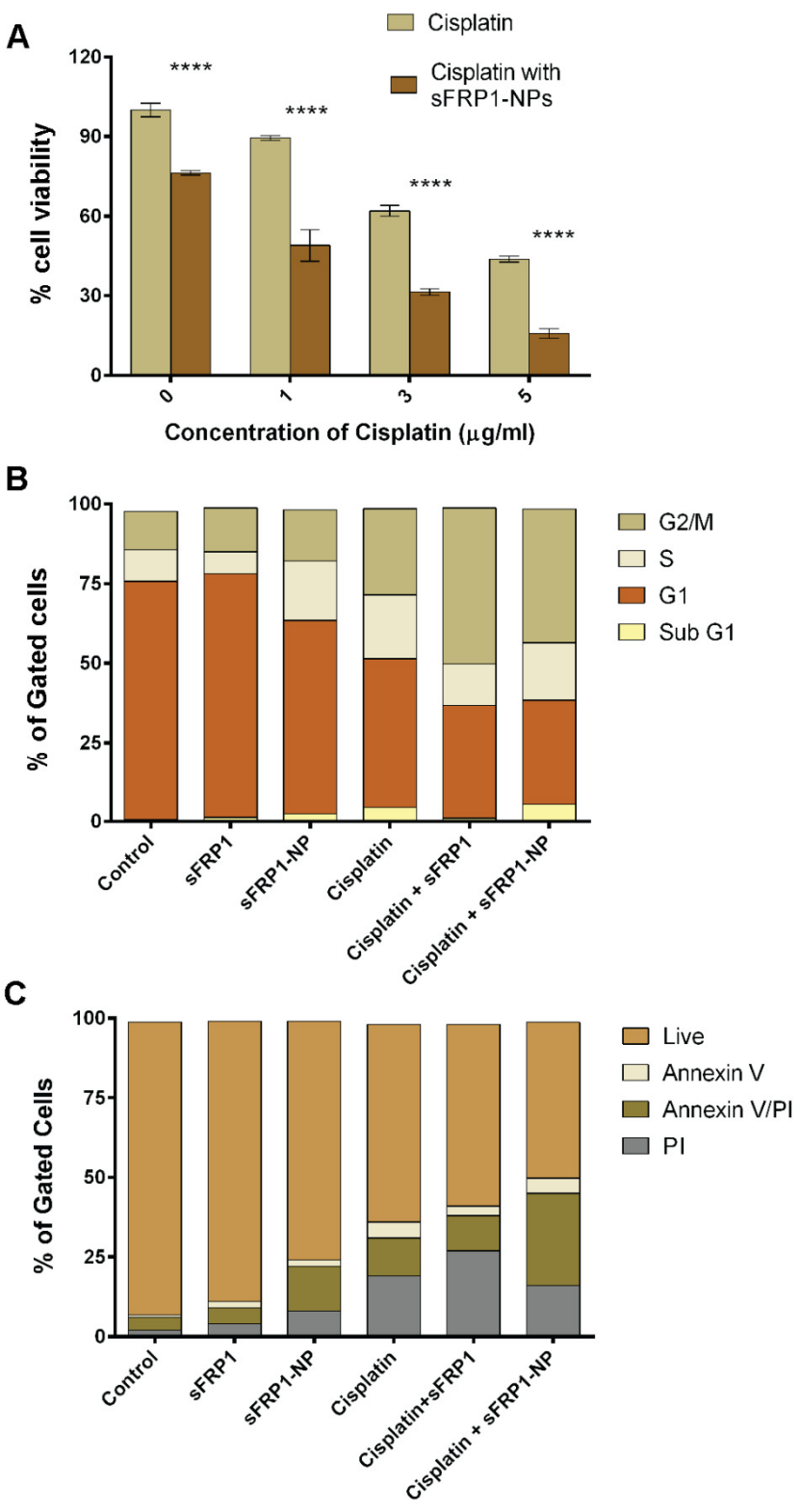
A
Cisplatin
Cisplatin with sFRP1-NPs
% cell viability
120
90
60
30
0
****
****
****
****
0
1
3
5
Concentration of Cisplatin (µg/ml)
B
% of Gated cells
100
75
50
25
0
G2/M
S
G1
Sub G1
Control
sFRP1
sFRP1-NP
Cisplatin
Cisplatin + sFRP1
Cisplatin + sFRP1-NP
C
% of Gated Cells
100
75
50
25
0
Live
Annexin V
Annexin V/PI
PI
Control
sFRP1
sFRP1-NP
Cisplatin
Cisplatin+sFRP1
Cisplatin + sFRP1-NP

Figure 3.15. **(A)** MTT assay showing viability of HeLa cells after combination therapy of protein-NPs with cisplatin for 48 h, **(B)** cell cycle analysis of HeLa cells of control and treated cells by FACS, performed 48 h after treatment with sFRP1, sFRP1-NPs and their respective combination with cisplatin, **(C)** Annexin V-FITC /PI staining of HeLa cells showing a decrease in population of live cells in samples treated for 48 h, with respect to untreated control cells.

To investigate the mode of impact of the protein-NP conjugate on the cell cycle progression of HeLa cells, flow cytometric analysis with PI was conducted. PI is a DNA intercalating agent that is employed to measure DNA content of cells, which in turn, indicates the phase of cell cycle. Treatment of HeLa cells with a low concentration of protein (10 nM), bound to NPs or otherwise, induced a slight increase in G2/M phase and a decrease in G1 phase. In combination with cisplatin (3 µg/ml), the G2/M population of cells treated with protein-NPs combined with cisplatin increased dramatically; increase being over 1.5 fold (42%) as compared to only cisplatin treated cells (27%), depicting a G2/M arrest (**Figure 3.15B**). A prominent sub-G1 population (5.4%) was also observed, indicating apoptosis. Cisplatin has been previously reported to arrest cells in G2/M phase of the cell cycle [131]. However, the significantly enhanced efficacy of co-therapy may be attributed to the blockage of the Wnt pathway by the sFRP1-NPs. As the Wnt cascade plays a prominent role in cell proliferation, disrupting the pathway by the sFRP1-NPs possibly sensitizes the cancer cells to treatment with chemotherapy. Correlating with the results obtained in MTT assay, it can be concluded that even a low concentration of sFRP1-NPs is sufficient to greatly sensitize the cancer cells toward cisplatin.

For detection of mechanism of cell death, cells were stained with FITC Annexin V and counter-staining with PI. Annexin V-FITC stains the cells by labeling phosphatidylserine sites on the cell membrane in early or late apoptotic stage, prior to complete loss of cytoplasm. PI stains cells with damaged membrane as it is cell impermeable; staining late apoptotic or necrotic cells. This difference forms the basis of the assay for detection of apoptosis. Early apoptotic cells are Annexin V-FITC positive, whereas late apoptotic cells are positive for both dyes. This FACS-based experiment showed that the percentage of live

cells decreased (from 92% in control to 75% in treated) and late apoptotic cells increased (from 6% in control to 22% in treated) substantially upon treatment with GST-sFRP1 (10 nM)-NPs. These data were found to be completely in agreement with the dual staining results with AO and EB observed previously. Moreover, this effect was augmented greatly in case of combination therapy (49% live and 45% late apoptotic) of protein-NPs and cisplatin, as opposed to either of them alone (**Figure 3.15C**). Although the protein alone did not exhibit significant difference with control cells, combination therapy with cisplatin yielded a high population of late apoptotic cells. These results corroborated the previous observations and proved that the above treatments enforce the apoptotic mode of cell death. Chemosensitization of the HeLa cells mediated by co-therapy of sFRP1-NPs and cisplatin is a novel mode of targeting two different pathways for treating cancer.

3.4 Conclusions

In this study, a nanocarrier has been successfully engineered comprising of recombinant therapeutic protein bound to novel NPs embedded with highly fluorescent gold nanoclusters. The luminescence properties of Au NCs were exploited for the purpose of tracking, imaging, and profiling the release of protein from NPs. Features of the composite NPs were effectively modulated to meet the criteria of protein binding, release, and its function. Also, GST-sFRP1 was delivered in its functionally active form and exerted its anti-cancerous activities on HeLa cells by blocking the Wnt signal cascade. Interaction of the protein with the NPs considerably augmented its efficiency. Herein, fabrication of the nanocarrier to target and simultaneously block Wnt signaling pathway in cancer was first of its kind. Moreover, combination of sFRP1-NPs and traditional drug cisplatin demonstrated the sensitization of the cancer cells toward cisplatin, providing a novel regime of co-therapy. Cell based assays, dual staining methods and apoptosis detection experiments provided detailed characteristics of the mode of cell death. The results obtained distinctly exhibited that the co-therapy caused significantly greater damage to the cancer cells than chemotherapy or NP-mediated protein therapy alone. Hereby, two different pathways were targeted- the Wnt pathway playing a prominent role in cancer, and the established apoptotic induction by cisplatin [132]. Hence, it paves a new path of generating composite nanoparticles to modulate signaling

mechanisms, which reduces the required dosage of chemotherapeutic drugs by aiming at two independent pathways for the remedy of cancer. It can be concluded that these biocompatible and non-toxic NPs may prove to be archetypical for tracking and sustained release of functionally active therapeutic sFRP1 for blocking Wnt signals, which holds immense prospect in cancer theranostics.

CHAPTER 4

Antagonizing Canonical Wnt Signaling Pathway by Recombinant Human sFRP4 Purified from *E. coli* and its Implications in Cancer Therapy

CHAPTER 4

4.1 Introduction

sFRP4 is one of the promising isoforms of the sFRP superfamily, having serious implications in tumorigenesis [133]. In normal adult cells, it binds to Wnt morphogens and prevents their binding to corresponding transmembrane Frizzled receptor, thereby impeding the canonical Wnt pathway. However, loss of expression of sFRP4 due to promoter hypermethylation has been found in several types of cancer, such as, colorectal cancer [30], bladder cancer [134], mesothelioma [29], cervical cancer [135], and ovarian cancer [136]. This promotes the upregulation of Wnt signaling, resulting in the stabilization of a cytoplasmic pool of β-catenin protein, which is the signaling node of the canonical Wnt pathway. β-catenin, in turn, transcriptionally activates pro-proliferative genes like cyclin D1 [23], survivin [22], and c-myc [24], thereby deregulating cell proliferation. In non-cancerous cells, sFRPs block the Wnts; subsequently, β-catenin is phosphorylated and marked for degradation, leading to downregulation of pro-proliferative genes. This gives rise to the possibility of mimicking this scenario in case of cancer cells as well by blocking the Wnt ligands either with functional recombinant sFRP4 added to the cell culture media. If such a system is designed, alterations in expression levels of downstream molecules may be used as a tool for quantitative estimation of the extent of inhibition of the Wnt pathway. Moreover, it raises the question of clinical application of the recombinant sFRP4; if aberrant proliferation of cancer cells can be restricted by blocking the Wnt pathway with sFRP4, then this protein may have a great potential in the field of recombinant protein therapeutics.

Recent investigations into the interactions of sFRP4 with several Wnt ligands have created a surge of interest in exploring its anti-proliferative activity. Both transfection studies and exogenous addition of sFRP4 to culture have demonstrated that it is accountable for keratinocyte differentiation and apoptosis [51]. In breast cancer cell line MCF-7, sFRP4 conditioned media were found to diminish cell proliferation and downregulated Wnt signaling genes [42]. In a similar study, transfection of sFRP4 was found to reduce proliferation via the canonical Wnt pathway in prostate cancer cells [43]. Interestingly, it has

also been shown to induce apoptosis in β-catenin deficient mesothelioma cells, suggesting that canonical Wnt pathway independent signaling phenomena may also be at play [29]. However, intriguing discrepancies have been reported, challenging the generally accepted antagonistic function of sFRPs [33]. For instance, sFRP4 was found overexpressed in colorectal cancer patient samples, revealing that sFRP4 may have entirely different biological roles in different cancer types [137]. These investigations reflect the bewilderingly complex behavior of this signaling system. The fact that it varies so widely in different cell types and growth conditions necessitates further explorations into this field.

Another compelling facet of sFRP4 that has surfaced is its ability to chemosensitize cancer cells to conventional drugs. So far documented in ovarian cancer cells [98] and glioma stem cells [138], this phenomenon has the potential to find a place for sFRP4 in the transforming field of combination therapy, which could reduce the exacerbated side-effects of chemotherapeutic agents, while enhancing the anti-cancer efficacy. However, the same may not be applicable for bacterially expressed recombinant sFRP4 or in case of other forms of cancer. If the Wnt blocking efficiency of bacterially produced sFRP4 is retained in conjunction with drugs, while the drugs induce apoptosis via other interconnected signaling pathways, then this system may indeed prove to be successful in a combination module.

In this chapter, it has been reported that the sFRP4 gene was cloned from a novel source into bacterial expression vector pGEX-4T2 containing GST tag. The GST-sFRP4 protein, purified from *E. coli* BL21(DE3) cells, was characterized by Matrix-assisted laser desorption/ionization time-of-flight (MALDI TOF/TOF), circular dichroism spectra and Western blot analyses. The functionality of recombinant protein was assessed on two different cancer cell lines- cervical carcinoma (HeLa) and lung carcinoma (A549). This was the first report interpreting the structural and functional characterization of bacterially expressed GST-sFRP4. Further, targeting of canonical Wnt pathway was proven by analyzing levels of β-catenin and phosphorylated β-catenin protein as well as gene expression analysis of cyclin D1, survivin, and c-myc. In addition, combination module was designed with traditional chemotherapeutic drugs for augmented efficiency, which also showed that functionality of sFRP4 in blocking the Wnt pathway was retained even in conjunction with drugs. Anti-cancer effect was ascertained by cell viability assay, dual

staining, and flow cytometry based cell cycle and apoptosis analyses. These data inspire the possibility of exploiting this recombinant sFRP4 in the avenue of possible protein therapeutics. The concept of this chapter has been represented schematically in **Scheme 4.1**.

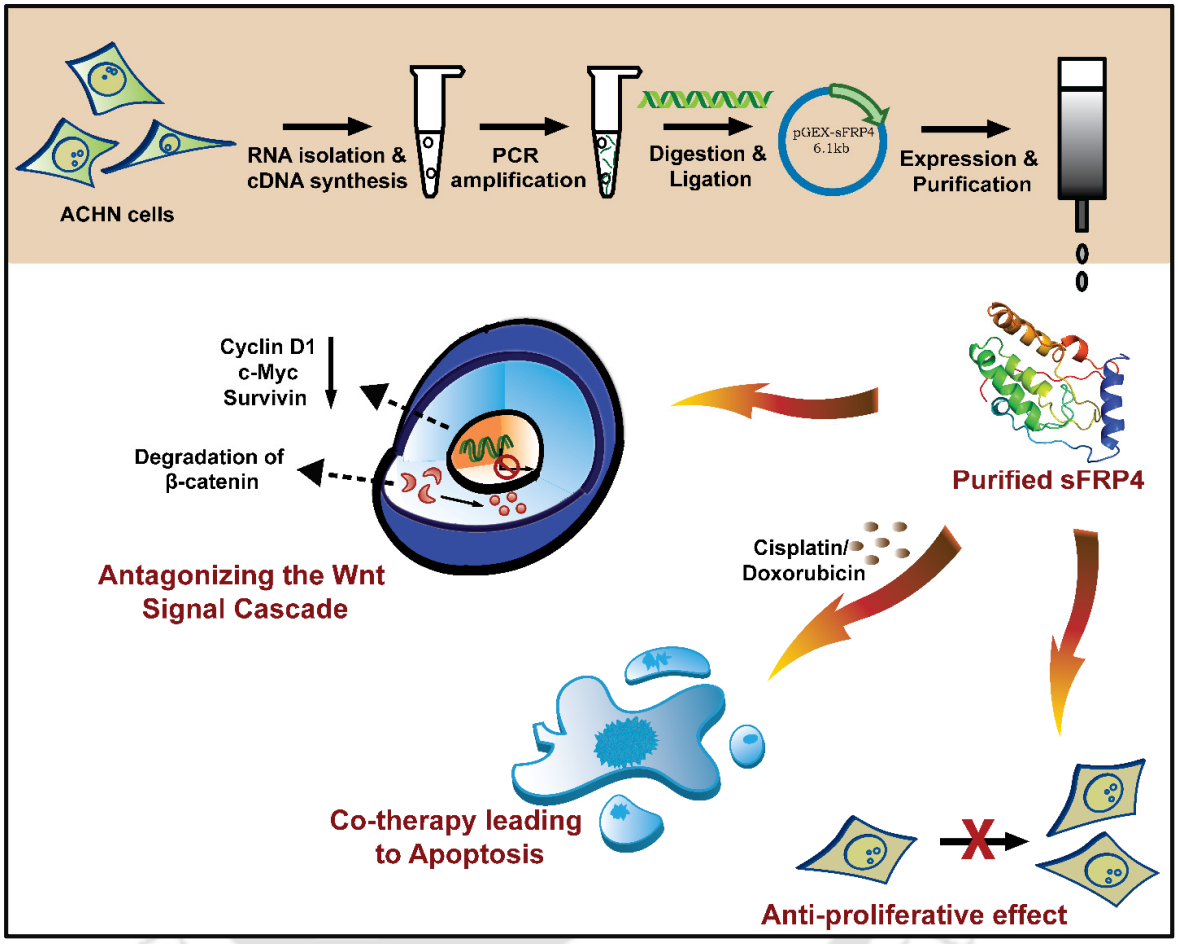

Scheme 4.1. Schematic representation of the work described in this chapter.

4.2 Material and Methods

4.2.1 Cell culture

Cervical cancer (HeLa), lung cancer (A549), renal cancer (ACHN), non-cancerous human embryonal kidney (HEK-293) cells, normal mouse fibroblast cells (3T3-L1) were purchased from National Centre for Cell Science, India. Cells were grown in DMEM, with 10% FBS, 100 U/ml Penicillin, 100 µg/ml Streptomycin, in 5% carbon dioxide incubator with controlled humidity at 37 °C.

4.2.2 Materials

All items were purchased from Sigma-Aldrich unless mentioned otherwise.

4.2.3 Cloning of sFRP4

Total RNA was isolated from human renal cell carcinoma cell line (ACHN) using Tri reagent. cDNA was synthesized with Verso cDNA kit (Thermo Scientific), according to manufacturer's protocol. The 1041 bp gene of sFRP4 was amplified from the cDNA pool using forward primer5'- ATGTTCCTCTCCATCCTAGTGGCGCT -3' and reverse primer 5'- GCTCACACTCTTTTCGGGTTTGTTCTC -3'. The gene was incorporated into pGEMT Easy vector (Promega) after overnight ligation at 4°C. From this clone, sFRP4 gene was PCR amplified with gene specific forward primer 5'- GGCGGATCCATGTTCCTCTCCATCCT -3' and reverse primer 5'- GCCCTCGAGTCACACTCTTTTCGGGT -3' containing overhangs for *Bam*HI and *Xho*I restriction sites. Subsequently, the amplified product was subcloned into expression vector pGEX-4T2 by digestion with *Bam*HI and *Xho*I restriction enzymes, followed by its ligation to the digested vector at 37 °C. Ligated product was transformed into *E. coli* DH5α. Clone was confirmed by sequencing at Xcelris Labs Ltd., India.

4.2.4 Expression of sFRP4 in E. coli BL21(DE3)

Clone was transformed into *E. coli* BL21(DE3), which is suitable for protein expression. Primary culture was grown in Luria-Bertani media overnight at 37 °C under shaking conditions. Secondary culture was given with 1% of primary culture as inoculum. When an

O.D. of 0.6 was attained, sFRP4 protein was induced by IPTG. Expression was optimized by varying induction time, temperature, shaking speed, and concentration of IPTG. Maximum expression was obtained at induction temperature and time of 28 °C and 8 h respectively. However, upon lysis of the bacterial cells with 10 mM PBS, 1 mM PMSF and 1 mM EDTA, protein was found to be expressed entirely as inclusion bodies.

4.2.5 Purification of sFRP4 from bacterial system

For the purpose of solubilizing sFRP4 protein from the inclusion bodies, the initial attempts involved varying induction time, temperature, and concentration of IPTG. When the protein was still expressed as insoluble fraction, the pGEX-4T2 holding sFRP4 gene was transformed into different strains of bacteria, viz., Rosetta-gami and *E. coli* BL21 pLysS. When the desired results were still not obtained, the composition of the lysis buffer was modified by using various detergents, such as, Triton X-100, sodium deoxycholate and N-lauroylsarcosine. Eventually, a concentration of 0.32% N-lauroylsarcosine added to the lysis buffer composition yielded in the entire protein being expressed in the soluble fraction. To optimize the binding of GST-sFRP4 to the glutathione-agarose affinity chromatography column, the supernatant obtained after centrifugation of lysed cells was stirred in cold for 1 h, after addition of 1 % Triton X-100. This was then diluted two times with 10 mM PBS, filtered and loaded into the column in three batches, with 30 min incubation time each. Subsequently, the column was washed 12 times with PBS, at the end of which, GST-sFRP4 was eluted with 5 mL elution buffer (50 mM Tris, pH 9.5 and 15 mM L-reduced glutathione). Elution fractions were electrophoresed in a 12% SDS-PAGE to observe expression of GST-sFRP4 in the purified elute. Further, the induction temperature and time were reduced to 24 °C and 6 h respectively, in order to prevent degradation of GST from GST-sFRP4. Before performing each of the experiments, protein was dialyzed in step-wise manner against Tris-HCl buffer (pH 7.4), where the final buffer concentration was maintained as 10 mM. Bradford assay was performed to estimate the protein concentration, using BSA as standard.

4.2.6 Homology modeling and docking analyses

The structure of the binding domain (CRD or Cysteine-rich domain) of sFRP4 was predicted using PHYRE2 Protein Fold Recognition Server, along with those of sFRP4 and GST-sFRP4 [83]. Another protein structure prediction server I-TASSER [84-86] was used to predict the 3-D structure of Wnt7a, which has been documented to bind to sFRP4 [139]. To ascertain whether the CRD remained intact in case of sFRP4 and GST-sFRP4 structures, CRD was individually overlapped with each of the two, using the molecular visualization system PyMOL, and the root mean square deviation value was generated in each case. Also, CRD of sFRP4 was aligned with the crystal structure of sFRP3 (PDB ID: 1ijxA), to verify the integrity of the modeled structure. Thereafter, Wnt7a was docked with each of the three modeled structures, namely CRD-SFRP4, sFRP4 and GST-sFRP4, using ClusPro server [140-143]. The docked structures were analyzed with PDBsum Generate [144, 145].

4.2.7 MALDI TOF/TOF analysis

Confirmation of sFRP4 sequence was done by MALDI TOF/TOF analysis. *In situ* gel tryptic digestion of GST-sFRP4 was performed using Trypsin Profile In-Gel Digestion kit following manufacturer's protocol. Sample was mixed with 10 mg/ml α-cyano-4-hydroxycinnamic acid matrix in 0.1% trifluoroacetic acid, 50% acetonitrile, and spotted on the MALDI target plate. Eventually, it was analyzed with 4700 Proteomics Analyzer with TOF/TOF Optics (Applied Biosystems) equipped with a diode pumped solid state class I laser and MS/MS data were acquired in automatic mode.

4.2.8 Secondary structure analysis using circular dichroism

Formation of secondary structure of GST-sFRP4 was confirmed by circular dichroism analysis using a JASCO-815 spectrometer (Jasco, Japan). Purified and dialyzed protein was analyzed in a cuvette of 1 mm path length, under constant flow of nitrogen gas at a rate of 5 L/min and maintenance of constant temperature at 25 °C. Sample was scanned at a speed of 50 nm/min, from wavelength 250 nm to 180 nm. Background subtraction was done with Tris buffer of concentration equal to that of the protein sample.

4.2.9 Expression profile analysis of genes involved in the Wnt pathway in four different cell lines

The expression levels of five genes relevant to the Wnt signaling cascade were checked in two different cancer cell lines, namely HeLa, A549, and one non-cancerous cell line HEK-293. The genes analyzed were Wnt4, Wnt7b, Wnt10b, co-receptor LRP6, and β-catenin. Based on the results obtained in this expression profiling study, the work was initiated.

4.2.10 Western blotting

The technique of Western blotting was applied to assess if the purified protein was indeed GST-sFRP4 using anti-GST antibody. Purified GST-sFRP4 was electrophoresed on 12% SDS-PAGE. Also, the effect of GST-sFRP4 on the Wnt pathway of cancer cells was also probed using antibodies against β-catenin as well as its phosphorylated form. In this pursuit, cells were treated with GST-sFRP4 for 24 h. Thereafter, whole cell lysate was prepared from treated and untreated cells, with RIPA buffer, supplemented with 1 mM PMSF and 1 mM EDTA. Total protein content was estimated with Lowry assay and 12% SDS-PAGE was done after loading equal amounts of protein for each sample. In all cases, protein was electroblotted onto a PVDF membrane for 3 h at constant voltage, followed by blocking with 4% BSA in PBST for 2 h. Next, the membrane was incubated overnight with the respective primary antibodies under cold conditions. Subsequently, membrane was washed six times with PBST, before being incubated with horseradish peroxidase (HRP) conjugated secondary antibody for 2 h. Then, it was washed six times with PBST and developed with chemiluminescence peroxidase substrate kit. It should be mentioned here that for probing phospho-β-catenin, TBST was used in all steps, instead of PBST.

4.2.11 Combination therapy

Combination therapy of GST-sFRP4 with conventional chemotherapeutic agents, cisplatin and doxorubicin, was attempted. For all of the following experiments, this mode of co-therapy was employed.

4.2.12 Cell viability assay

Cell viability assay was conducted in order to assess the effect of GST-sFRP4 and the co-therapy regime on HeLa and A549 cells. For this purpose, cells were seeded at a density of 7000 cells per well in 96-well plate and allowed to attach for about 8 h. Subsequently, serum media was removed and treatment was done with the dialyzed and quantified GST-sFRP4 (0 nM to 32 nM for HeLa and 0 to 20 nM for A549), alone and in combination with cisplatin (0 µM to 16 µM) or doxorubicin (0 µM to 0.6 µM) in serum-free media for 48 h. At the end of the treatment period, MTT assay was performed, whereby live cells converted MTT to purple formazan crystals, which were dissolved by adding DMSO and absorbance was determined at 550 nm. Percentage of viable cells was calculated using the formula:

$$\% \text{ of cell viability} = \frac{(A_{550} - A_{655})_{\text{sample}}}{(A_{550} - A_{655})_{\text{control}}} \times 100$$

Control experiments were also performed using a Wnt pathway inhibitor XAV939 to show that the Wnt pathway is indeed hyper-active in HeLa and A549 cells. Additionally, the same protocol was followed to determine the effect of GST-sFRP4 on normal mouse cell line 3T3-L1.

4.2.13 Cell cycle analysis

Flow cytometric analysis of cell cycle was performed with FACS to ascertain the occurrence of cell cycle arrest, if any. Cells were seeded in six-well plates at a density of 10^5 cells per well. Treatment was given in the same manner as described previously. Concentrations of GST-sFRP4, cisplatin and doxorubicin added to the cells were 12 nM, 7 µM and 0.2 µM, respectively. After 48 h of treatment, cells were harvested by trypsinization and fixed with 70% ethanol under chilled conditions. Cells were then washed with pre-chilled PBS, RNaseA was added at a concentration of 0.2 mg/ml and incubated for 1 h at 37 °C. Next, cells were incubated with 10 µg/ml of the nucleic acid intercalating dye (PI) for 15 min in dark, before analysis.

4.2.14 Apoptosis detection assay

Apoptosis was detected by flow cytometry using Annexin V- FITC/PI Apoptosis Detection Kit. Cells were seeded and treated as mentioned previously. After the treatment period, cells were harvested, washed with PBS, and incubated with Annexin V-FITC and/or PI, following manufacturer's protocol. Unstained cell samples were also kept for each mode of treatment to check auto-fluorescence. After staining for 30 min, cells were analyzed in BD FACSCalibur.

4.2.15 AO/EB dual staining for detection of apoptosis

Dual staining of cells with AO and EB was done to distinguish between healthy and membrane compromised cells post treatment. Cells were seeded in 96-well plate and treated with the concentrations of protein and/or drugs showing maximum cell-inhibitory effect in MTT assay. Then, media were discarded and cells were incubated with 2 μg/ml of AO and 10 μg/ml of EB in PBS for 5 min in the dark. Eventually, cells were washed with PBS before being visualized under a fluorescence microscope (Nikon ECLIPSE TS100).

4.2.16 Real-time PCR analysis

Real-time PCR analysis was performed to check the expression of crucial pro-proliferative genes downstream of the Wnt pathway, namely cyclin D1, survivin, and c-myc. In this regard, treatment of cells was done with same concentrations of protein/drugs as in the flow cytometry based experiments. RNA was extraction from each sample with the Mammalian Total RNA Isolation kit, following manufacturer's protocol. RNA was quantified with Nanodrop (GE Healthcare Life Sciences) and 1 μg equivalent cDNA was synthesized using First Strand cDNA Synthesis kit (Thermo Scientific). With this cDNA as template, gene specific primers (Table 4.1) and SYBR Green Mastermix as the reporter dye (Power SYBR Green PCR master mix, Applied Biosystems), Real-time PCR (Rotor-Gene Q, Qaigen) was done.

Name of gene	Sequence of primer
Cyclin D1	Forward: 5′-CGCCCCACCCCTCCAG-3′ Reverse: 5′-CGCCCAGACCCTCAGACT-3′
c-Myc	Forward: 5′-CCAGGACTGTATGTGGAGCG-3′ Reverse: 5′-CTTGAGGACCAGTGGGCTGT-3′
Survivin	Forward: 5′-AGAACTGGCCCTTCTTGGAGG-3′ Reverse: 5′-CTTTTTATGTTCCTCTATGGGGTC-3′
β-actin	Forward: 5`-CTGTCTGGCGGCACCACCAT-3` Reverse: 5`-GCAACTAAGTCATAGTCCGC-3`

Table 4.1. Primer sequences used for Q-PCR.

4.2.17 Statistical tests

Statistical tests were performed using GraphPad Prism. Significance of data was determined by One-way or Two-way ANOVA, as applicable.

4.3 Results and Discussion

4.3.1 Expression profile analysis of genes associated with the Wnt family

Before proceeding to experiment with the GST tagged sFRP4, a few cell lines of different origins were screened, to ensure that Wnt ligands were expressed. The expression of five genes associated with the Wnt family was analyzed in three different cell lines (**Figure 4.1A**). Out of the three Wnts, viz., Wnt4, 7b, and 10b, at least two were found expressed in all cell lines screened; prominent expression of coreceptor LRP6, and β-catenin was also

observed. The gene profile obtained was found to be in agreement with previous reports documenting the expression of Wnt ligands in cancer. Encouraged by these data, cloning and purification of sFRP4 was done in order to examine its role in blocking Wnt signaling for possible therapeutic applications.

In addition, a small molecule drug XAV939 (**Figure 4.1B** and **Figure 4.1C**, respectively) was employed, which solely inhibits the Wnt/β-catenin pathway [146]. Cell viability assays revealed that in both cell types, IC_{50} value was attained at approximately 100 μM of XAV939, confirming the functionality of Wnt pathway.

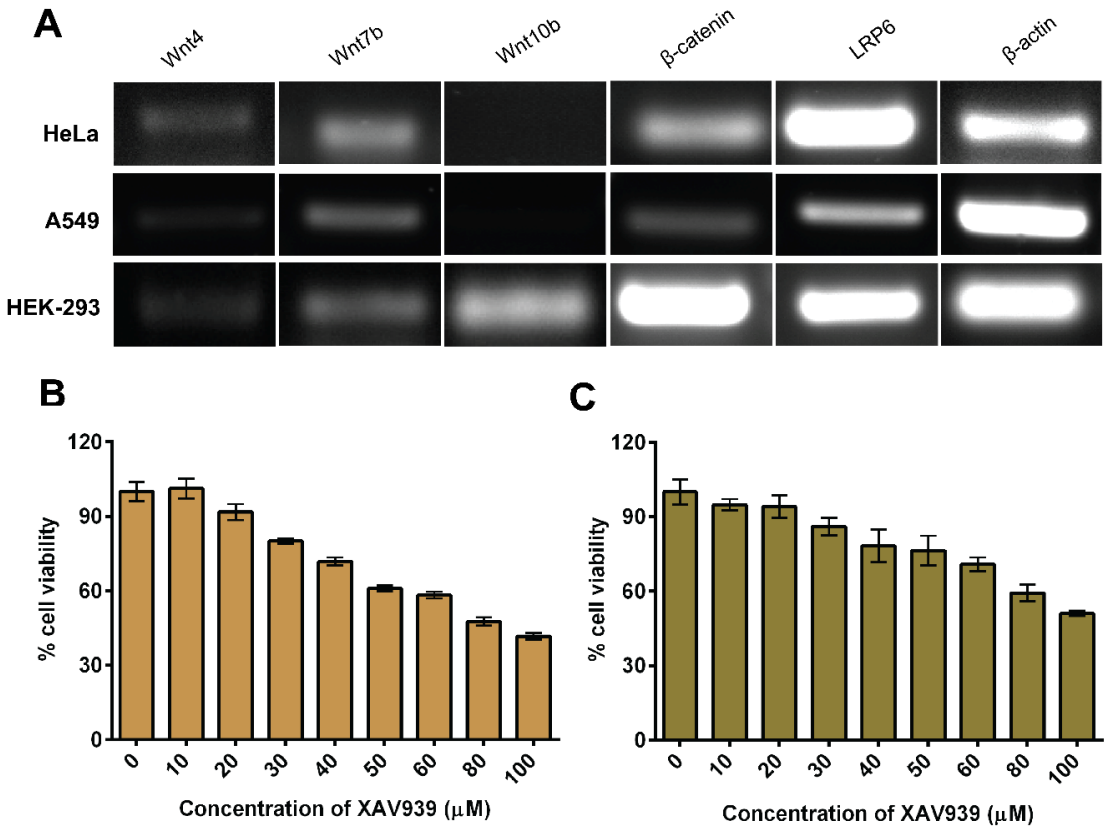

Figure 4.1. **(A)** Expression profiling of genes belonging to Wnt signaling pathway by RT-PCR analysis of three different cell lines. **(B)** MTT assay depicting anti-proliferative activity of Wnt/β-catenin pathway inhibitor XAV939 on HeLa cells, and **(C)** on A549 cells.

4.3.2 Cloning, expression, and purification of sFRP4

Cloning of sFRP4 was done from a hitherto unknown source- ACHN renal carcinoma cells following the procedure described in subsection 4.2.3. As the expression level of sFRP4 in ACHN cells was low, re-PCR was done to obtain sufficient PCR product (**Figure 4.2A**) for subsequent cloning steps. sFRP4 gene was cloned into the pGEX-4T2 via an intermediate TA vector pGEMT-Easy. Clone was confirmed in pGEX-4T2 by digestion with *BamHI* and *XhoI* restriction enzymes, which generated a band corresponding to 1041 bp of sFRP4 gene (**Figure 4.2B**). Clone was also confirmed by sequencing (Xcelris Pvt. Ltd.), which yielded the following sequence-

GCCATGTTCCTCTCCATCCTAGTGGCGCTGTGCCTGTGGCTGCACCTGGCGCTGGGCGTGCGCGGCGCGC
CCTGCGAGGCGGTGCGCATCCCTATGTGCCGGCACATGCCCTGGAACATCACGCGGATGCCCAACCACCT
GCACCACAGCACGCAGGAGAACGCCATCCTGGCCATCGAGCAGTACGAGGAGCTGGTGGACGTGAACTGC
AGCGCCGTGCTGCGCTTCTTCCTCTGTGCCATGTACGCGCCCATTTGCACCCTGGAGTTCCTGCACGACC
CTATCAAGCCGTGCAAGTCGGTGTGCCAACGCGCGCGCGACGACTGTGAGCCCCTCATGAAGATGTACAA
CCACAGCTGGCCCGAAAGCCTGGCCTGCGACGAGCTGCCTGTCTATGACCGTGGCGTGTGCATCTCGCCT
GAAGCCATCGTCACGGACCTCCCGGGAGGATGTTAAGTGGATAGACATCACACCAGACATGATGGTACAG
GAAAGGCCTCTTGATGTTGACTGTAAACGCCTAAGCCCCGATCGGTGCAAGTGTAAAAAGGTGAAGCCAA
CTTCGGCAACGTATCTCAGCAAAAACTACAGCTATGTTATTCATGCCAAAATAAAAGCTGTGCAGAGGAG
TGGCTGCAATGAGGTCACAACGGTGGTGGATGTAAAAGAGATCTTCAAGTCCTCATCACCCATCCCTCGA
ACTCAAGTCCCGCTCATTACAAATTCTTCTTGCCAGTGTCCACACATCCTGCCCCATCAAGATGTTCTCA
TCATGTGTTACGAGTGGCGCTCAAGGATGATGCTTCTTGAAAATTGCTTAGTTGAAAAATGGAGAGATCA
GCTTAGTAAAAGATCCATACAGTGGGAAGAGAGGCTGCAGGAACAGCGGAGAACAGTTCAGGACAAGAA
GAAAACAGCCGGGCGCACCAGTCGTAGTAATCCCCCCAAACCAAAGGGAAAGCCTCCTGCTCCCAAACCA
GCCAGTCCCAAGAAGAACATTAAAACTAGGAGTGCCCAGAAGAGAACAAACCCGAAAAGAGTGTGAGCA
ATCACTAGTGAATTCGC

For the expression of recombinant protein in bacterial system, the common *E. coli* BL21 (DE3) strain was chosen. However, the recombinant protein was completely present as inclusion bodies. Therefore, attempts were made to solubilize the protein by varying induction temperature, time, shaking speed, and concentration of IPTG. Strains specifically engineered for expression of mammalian proteins were also tried in order to solve this problem. Since none of the methods employed seemed to yield protein in soluble form, BL21(DE3) was used and GST-sFRP4 was solubilized from inclusion bodies using detergents [91, 147]. Optimum expression of GST-sFRP4 was observed at 28 °C after carrying out induction at temperatures ranging from 16 °C to 37 °C. Varying the concentration of IPTG and induction time, optimum yield of protein was obtained for 0.2 mM IPTG and 6 h, respectively (**Figure 4.2C**). To obtain the protein in soluble fraction, a number of strategies involving the usage of various detergents were implemented following

literature [91, 147]. Finally, 0.32% of the ionic detergent N-lauroylsarcosine was used to successfully solubilize the protein from inclusion bodies and mild stirring was done in 1% Triton X-100. Triton X-100 is a non-ionic detergent that probably sequestered the N-lauroylsarcosine into its micelles and helped in renaturation of the protein, that had been partially denatured by N-lauroylsarcosine [90]. Eventual washing steps during purification and the subsequent process of dialysis also helped the removal of the detergents from the system. Electrophoresis of the purified GST-sFRP4 yielded a single band at approximately 64 kDa (**Figure 4.2D**). A faint band of GST was also observed at 26 kDa, which could be due to cleavage of the recombinant protein. Reduction of induction temperature from 28 °C to 24 °C was found to yield a fainter band of GST. Quantifying the purified GST-sFRP4 with Bradford assay demonstrated that the total yield of protein from 100 ml of culture was 0.3 mg. Step-wise dialysis against Tris-HCl buffer (pH 7.4) ensured gradual removal of detergents and renaturation of the protein. It was speculated that the use of Triton X-100 to capture N-lauroylsarcosine in its micelle during solubilization of protein as well as subsequent step-wise dialysis helped in the refolding of the recombinant sFRP4. Although it is plausible that expressing of the recombinant sFRP4 using yeast may show better anti-proliferative effect due to protein folding analogous to that in mammalian cells, but functional expression in bacterial host in the present study is an easy approach for generation of recombinant sFRP4.

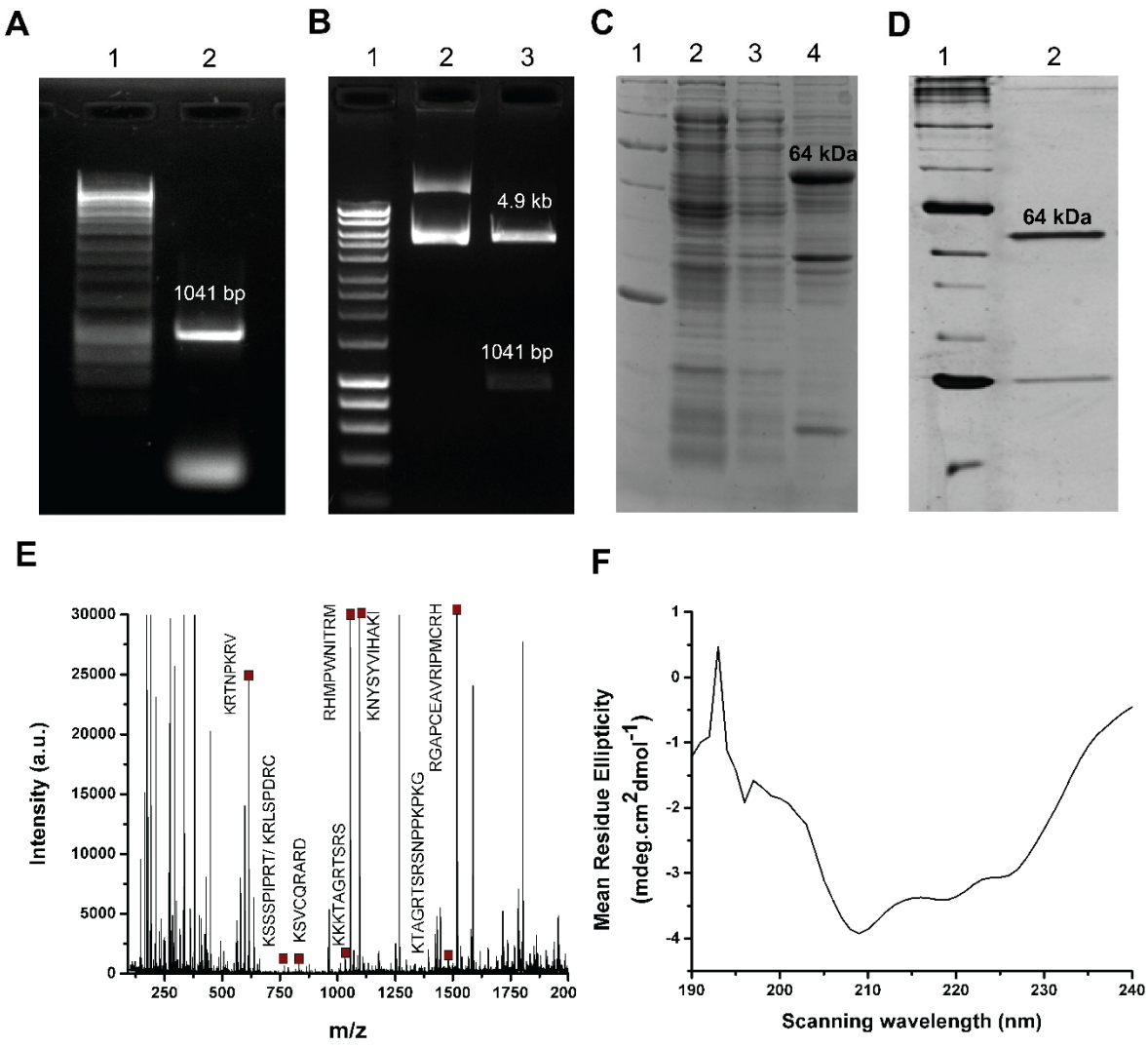

Figure 4.2. **(A)** Lane 1- DNA hyperladder, Lane 2- sFRP4 amplified with gene specific primers from cDNA pool of ACHN cell line, **(B)** Lane 1- DNA hyperladder, Lane 2- Uncut pGEX-4T2 containing sFRP4 gene, Lane 3- Release of band corresponding to 1041 bp of sFRP4 on digestion of sFRP4 pGEX-sFRP4 with *Bam*HI and *Xho*I. **(C)** Expression of GST-sFRP4 in *E. coli* BL21(DE3), Lane 1- Protein marker, Lane 2- Uninduced pGEX-sFRP4, Lane 3- Supernatant after lysis of induced *E. coli* BL21 transformed with sFRP4 gene containing pGEX-4T2, Lane 4- Pellet obtained after lysis, **(D)** Purification of GST-sFRP4, Lane 1- Protein marker, Lane 2- Band corresponding to 64 kDa of purified GST-sFRP4. **(E)** Tryptic digestion of GST-sFRP4 generated a peptide signature corresponding to the specific sequence of sFRP4, on MALDI TOF-TOF mass spectrometric analysis, **(F)** Circular dichroism spectra depicting 20% alpha helix and 11.9% β-sheet.

4.3.3 Characterization of recombinant GST-sFRP4

Soft ionization techniques like MALDI coupled with TOF mass spectrometry have proven to be ideal tools for protein sequencing and fingerprinting. Here, enzymatic digestion of purified recombinant sFRP4 *in situ* yielded peptide fragments, which were analyzed in the MS/MS mode for confirmation of protein identity. The data file was analyzed with FindPept proteomics tool provided with ExPASy (http://web.expasy.org/findpept/) [148, 149], which uses protein databases to compare to experimental masses obtained. The mass spectrometry data is plotted in **Figure 4.2E**, denoting the peptide fragments specific to sFRP4.

Formation of secondary structures of any recombinant protein is crucial for retention of its functionality. After the rigorous process of purification with detergents and subsequent dialysis, involving denaturation, renaturation, and refolding steps, it was essential to know the integrity of secondary structure. Hence, purified and dialyzed GST-sFRP4 was subjected to circular dichroism spectral analysis, which generated a spectrum of scanning wavelength versus millidegree. **Figure 4.2F** depicts the graph of scanning wavelength versus mean residue ellipticity ($mdeg.cm^2dmol^{-1}$), which was obtained by the following formula:

Mean residue ellipticity (Θ) = $(100*\theta)/Cnl$

Here, θ is ellipticity in millidegree, C is concentration of protein, n gives number of residues, and l gives the path length [94]

The percentages of α-helices and β-sheets, as determined by applying Yang's algorithm, were found to be 20% and 11.9%, respectively.

Western blotting with anti-GST antibody confirmed the presence of GST tagged sFRP4 at the legitimate position corresponding to 64 kDa of GST-sFRP4. As a control experiment, GST protein purified from pGEX-4T2 bearing *E. coli* BL21 cells, was also blotted (**Figure 4.3**).

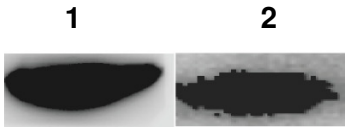

Figure 4.3. Western blotting detected over-expression of GST-sFRP4 (Lane 1) and expression of control GST in empty vector pGEX-4T2 containing *E. coli* BL21 (Lane 2).

4.3.4 Prediction of 3-D structure of GST-sFRP4 and its docking with Wnt7a

Docking studies were carried out for GST-sFRP4 with one of the Wnt ligands known to bind to sFRP4 [139]. The *in silico* study was performed as there was no report available on the functionality of the GST tagged sFRP4 bound with Wnt ligands. Firstly, the 3-D structures of CRD (binding domain) of sFRP4 (henceforth referred to as CRD-sFRP4, **Figure 4.4A**), sFRP4 (**Figure 4.4B**), GST-sFRP4 (**Figure 4.4C**), and Wnt7a (**Figure 4.4D**) were predicted due to a lack of reports on crystal structures of sFRP4 and Wnts. The only available crystal structure of sFRP superfamily is that of CRD of sFRP3 (PDB ID: 1IJXA) [49]. Therefore, CRD of sFRP3 was automatically detected by Phyre2 server as a template for predicting the structure of CRD of sFRP4. 3-D structure of Wnt7a was generated with I-Tasser prediction server. Validation of the predicted structures was done by aligning CRD-sFRP4 with the CRD of sFRP3 in PyMol, which generated a root mean square deviation (rmsd) value of 0.326 (**Figure 4.4E**), indicating nearly similar structural folds. The same comparison was done between CRD-sFRP4 and GST-sFRP4 structures, which generated an rmsd value of 0.584 (**Figure 4.4F**), respectively. Both cases demonstrated that binding domain remained intact in the predicted structures of sFRP4 and GST-sFRP4, as shown by negligible values of rmsd. Moreover, the lower rmsd between CRD-sFRP4 and GST-sFRP4 suggested that tagging of GST to sFRP4 slightly changed the protein conformation in favor of binding. This may be explained on the basis of previous studies, where tagging of GST to recombinant proteins helps to stabilize them [150].

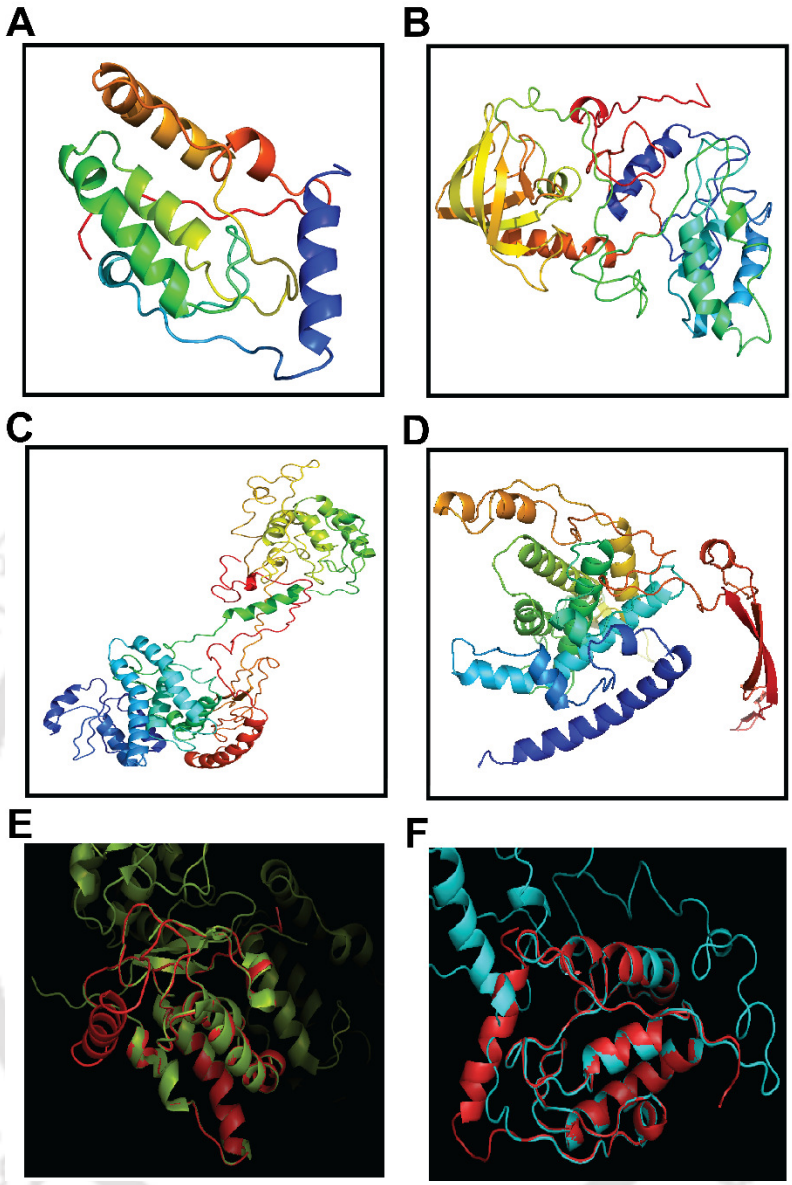

Figure 4.4. Protein 3-D structures of **(A)** CRD-sFRP4 , **(B)** sFRP4, **(C)** GST-sFRP4, and **(D)** Wnt7a. All structures except Wnt7a were predicted with Phyre2, while Wnt7a was predicted with I-tasser structure prediction server. Comparative studies of 3-D structures showing that binding domain (CRD) of sFRP4, shown in red, remains nearly unaltered on tagging with GST, **(E)** Alignment of the generated structure of CRD of sFRP4 (in Phyre2 server) with PDB structure of CRD of sFRP3 gave rmsd value of 0.326, **(F)** Alignment of the generated structure of CRD of sFRP4 with generated structure of GST-sFRP4 (Phyre2) gave rmsd value of 0.584.

After confirming the validity of the binding domain, which is primarily responsible for binding of Wnt ligands, the structures were docked with Wnt. Each of CRD-sFRP4, sFRP4 and GST-sFRP4 was separately docked with Wnt7a using ClusPro (**Figure 4.5A**, **Figure 4.5B**, and **Figure 4.5C**, respectively). Analysis of interactions between the docked structures of lowest binding energies was done using PDBsum Generate (**Figure 4.5D**, **Figure 4.5E**, and **Figure 4.5F**). It should be mentioned here that although there is no report stating that GST tagged protein displays improved binding properties with target ligands, GST is known to enhance stability of the tagged protein [93], which in turn could be responsible for its improved binding capacity.

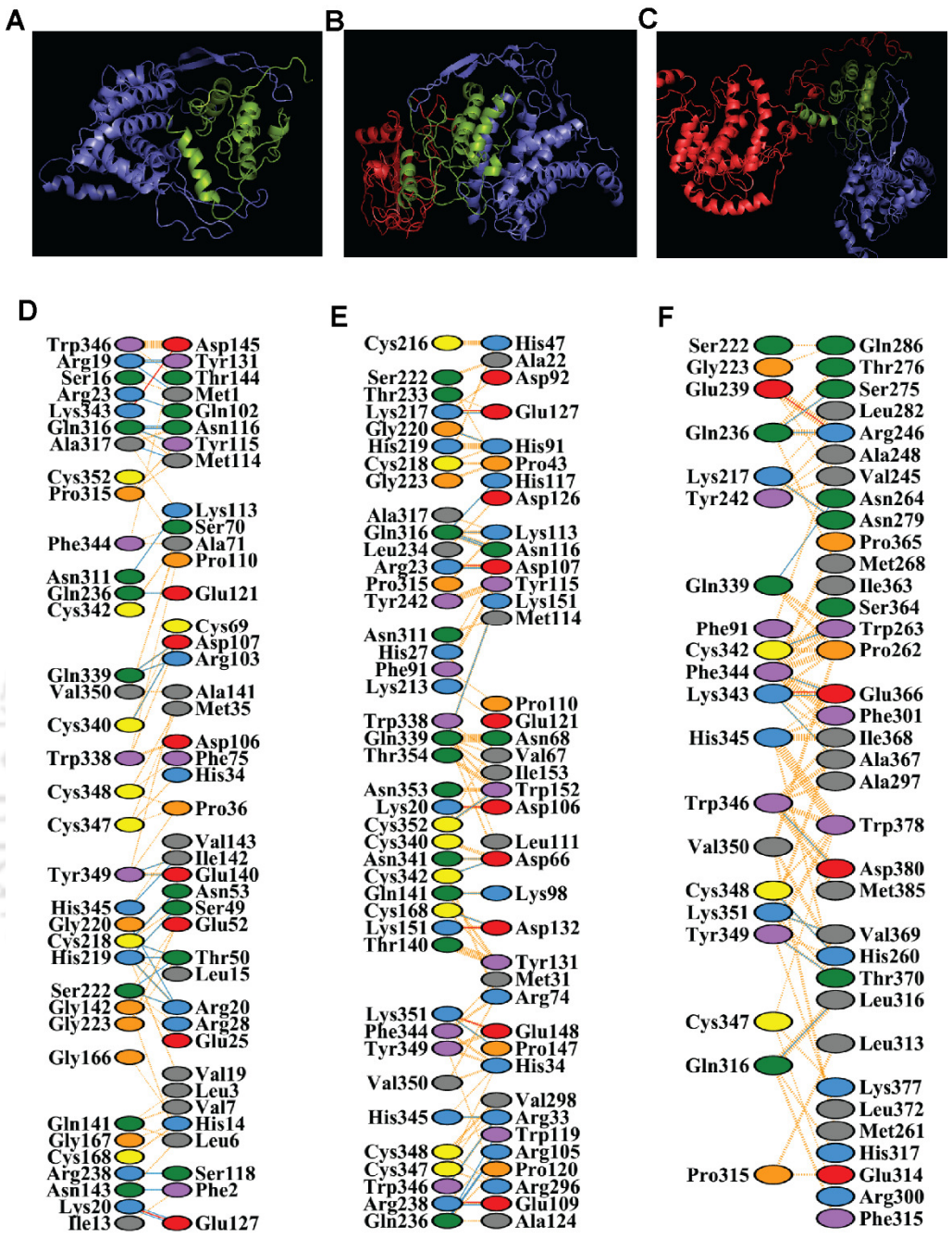

Figure 4.5. Docked structures of Wnt7a with **(A)** CRD-sFRP4, **(B)** sFRP4, **(C)** GST-sFRP4. Docking was done using ClusPro protein-protein docking server. **(D, E, F)** Analysis of docking studies performed with PDBsum generate server showing interaction between residues of **(D)** Wnt7a with CRD-sFRP4, **(E)** Wnt7a with sFRP4, **(F)** Wnt7a with GST-sFRP4.

4.3.5 Anti-proliferative effect of GST-sFRP4

Equipped with the evidence gathered from these data, a holistic approach was assumed in establishing the functionality of recombinant sFRP4 in blocking the Wnt signaling. The Wnt signal transduction is known to be responsible for aberrant proliferation in cancer cells, where inhibitory proteins like sFRP4 are hypermethylated. Although there are a few reports demonstrating that transfection of sFRP4 antagonizes the Wnt pathway, there has been no documentation of the therapeutic effect of bacterially expressed recombinant sFRP4 on cancer cells. In this study, MTT assays revealed that the exogenous addition of GST-sFRP4 to HeLa and A549 cancer cells significantly inhibited cell proliferation in a dose-dependent fashion (**Figure 4.6A** and **Figure 4.6B**, respectively). HeLa cells when treated with up to 32 nM of protein for 48 h resulted in reduction of viable cells to below 60%. In case of A549 cells, a similar effect was seen at a maximum concentration of 20 nM of recombinant protein. Post-dialysis buffer controls were kept for all MTT assays, which confirmed the complete removal of contaminating agents from the purified protein fractions, such as, L-reduced glutathione and detergents (data not shown).

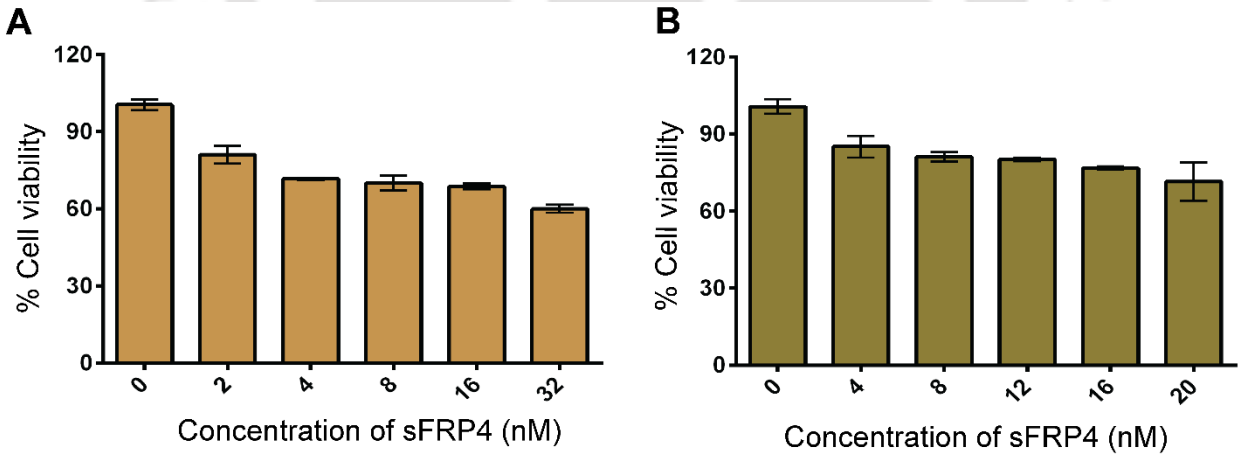

Figure 4.6. MTT assay depicting a significant ($p<0.0001$) dose dependent anti-proliferative effect of GST-sFRP4 on **(A)** HeLa cells, and **(B)** A549 cells.

4.3.6 Anti-proliferative effect of GST-sFRP4 in combination with GST-sFRP1

Cell viability assay of GST-sFRP4 was also performed in combination with GST-sFRP1. The detailed anti-cell proliferative activity of GST-sFRP1 has been described in Chapter 2. However, we find that combination did not show any further reduction of cell viability in various protein conventions (**Figure 4.7**). Hence, it is assumed that one of the isoform was sufficient to bring about significant anti-proliferative effect. Hence we continue with GST-sFRP4 for all subsequent studies in this chapter.

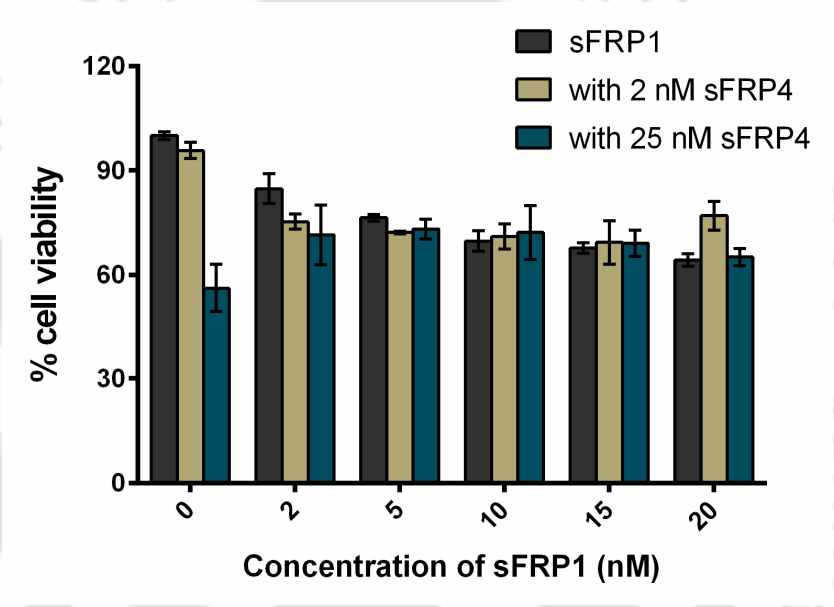

Figure 4.7. Cell viability assay to assess co-therapeutic benefits of recombinant sFRP1 and sFRP4 revealed that either one of the isoforms is sufficient to arrest cell proliferation.

4.3.7 Targeting the classical Wnt/β-catenin signaling with GST-sFRP4

The complex nature of signaling pathways and their intersection with a plethora of other pathways often makes it extremely difficult to decipher their functions. While there are three reported pathways of Wnt activation, the canonical β-catenin dependent signaling has often been implicated in cancer formation and progression. However, there have been contradictory reports stating otherwise [33, 137]. Therefore, the involvement of the Wnt/β-catenin pathway was validated by analyzing key players of the downstream pathway by

Western blotting or quantitative real-time PCR analysis. Activation of the signaling in most forms of cancer leads to stabilization of free pools of β-catenin in the cytoplasm. A similar observation was made by Western blotting of total protein from untreated HeLa and A549 cells, which revealed the presence of total cytoplasmic β-catenin and negligible amounts of phosphorylated β-catenin, that is, β-catenin marked for degradation. Whether the family of sFRPs always targets the canonical Wnt pathway, is a debatable issue, since there have been several reports stating the contrary. Nearly all of the sFRPs, including sFRP4, have been shown to behave in a conflicting manner [33, 81, 82, 137]. In order to understand the underlying mechanism of cell growth inhibition observed in the cell viability assays and to shed some light on the implicated pathway, the expression of certain critical members of the canonical Wnt pathway was probed. One such central molecule is the β-catenin, which has a stable cytosolic expression during Wnt signal transduction and promotes the upregulation of downstream pro-proliferative genes, such as, cyclin D1, survivin, and c-myc. However, when the pathway is shut down due to the presence of some inhibitory molecule, β-catenin is phosphorylated and thus marked for degradation, thereby blocking the transcription of the downstream genes. Therefore, the expression levels of total β-catenin as well as its phosphorylated form were checked in treated and untreated HeLa and A549 cells. After quantifying total protein content of each sample by Lowry assay, 60 µg of protein was loaded in each well. In both cell types, expression of β-catenin was greatly reduced in comparison to control experiments. Specifically in case of HeLa, treated cells possessed negligible amounts of β-catenin protein. When probed with antibody specific for the Ser^{33}/Ser^{37} phosphorylated form of β-catenin, expression was substantially increased in treated cells, with respect to the untreated control cells. Ratio of phosphorylated to total β-catenin increased greatly in sFRP4 treated HeLa cells in comparison to control cells (**Figure 4.8A**). Furthermore, expressions of cyclin D1, survivin, and c-myc genes were analyzed by real-time PCR. In HeLa cells, expression of all of the above three genes was reduced approximately two-fold after treatment with GST-sFRP4, with respect to untreated cells (**Figure 4.8B**). This is in accordance to with the above Western blot analysis data, which demonstrated that β-catenin was degraded on treatment with GST-sFRP4 and was thus unable to transcribe the downstream genes. It can be inferred from these expression analyses that treatment with GST-sFRP4 resulted in antagonizing of the Wnt, thereby blocking

downstream signaling leading to phosphorylation and subsequent ubiquitination of β-catenin. In A549 cells (**Figure 4.8C** and **Figure 4.8D**), a similar trend was observed. Ratio of phosphorylated to total β-catenin increased significantly in sFRP4 treated A549 cells in comparison to the untreated cells. Expression of survivin gene was found to decrease slightly (approximately 1.3 fold) and expression of c-myc was reduced nearly two-fold on treatment with recombinant protein. However, treatment failed to induce changes in the levels of cyclin D1 gene. All values were normalized with respect to expression of β- actin gene. These data provided evidence of β-catenin dependent regulation of the canonical Wnt pathway upon GST-sFRP4 treatment. Although MALDI and circular dichroism results demonstrated the authenticity and intact secondary structure formation of the bacterially expressed GST-sFRP4, blocking of the Wnt cascade proved beyond doubt that the protein retained its functionality even after extensive extraction and purification steps.

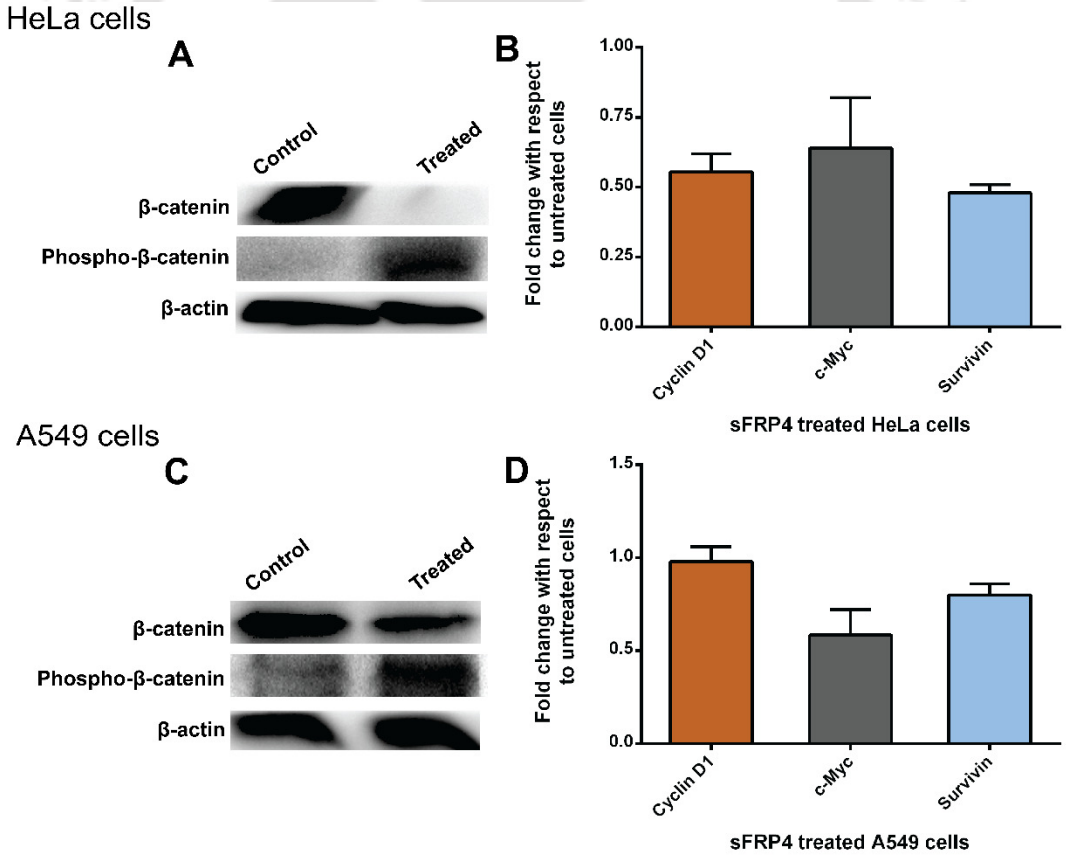

Figure 4.8. Expression analysis of key players of the classical Wnt pathway **(A)** Western blotting showed that ratio of phosphorylated to total β-catenin increased significantly in

sFRP4 treated HeLa cells with respect to control, **(B)** Real-time PCR analysis showed downstream genes cyclin D1, c-myc, and survivin genes were repressed in treated cells, **(C)** Western blotting of control and treated A549 cells revealed that ratio of phospho-β-catenin to total β-catenin increased in treated cells, **(D)** Real-time PCR analysis of A549 cells showed downregulation of c-myc and survivin genes with respect to untreated cells, while cyclin D1 remained nearly unaltered. Each bar represents the fold change in expression of a particular gene (cyclin D1, c-myc, or survivin) in sFRP4 treated cells with respect to untreated cells with a set value of 1.

4.3.8 Efficacy of co-therapy

In the earlier experiment to assess cell viability of sFRP4 treated cells, it was found that increasing the concentration or time of treatment did not lead to any further enhancement of anti-proliferative effect. Therefore, the potential of the recombinant sFRP4 to chemosensitize cancer cells toward conventional anti-cancer drugs was tested, in order to augment the efficacy of recombinant sFRP4. In this pursuit, a module of co-therapy of sFRP4 with conventional anti-tumor drugs, namely cisplatin and doxorubicin, was designed. MTT assays showed a significant increase in enhancement of efficacy in case combination therapy as compared to either the protein or the drug alone. This chemosensitizing effect of recombinant protein would help to greatly minimize the adverse side-effects of the drugs, when implemented clinically. In HeLa cells, 3 nM of protein was sufficient to reduce the percentage of viable cells from 90% in case of only 4 μM cisplatin to 40% in case of combination therapy (**Figure 4.9A**). A similar scenario was observed for A549 cells, where 20-30% reduction of viable cells was observed in combination with protein. (**Figure 4.9B**). In the other instance of doxorubicin (**Figure 4.9C** and **Figure 4.9D** for HeLa and A549, respectively), cell viability was reduced by about 20% when sFRP4 was added to the treatment module, even for very low concentration of doxorubicin (0.1-0.6 μM). These results led us to understand that this mode of co-therapy would be a possible choice for futuristic cancer therapy with minimum side-effects.

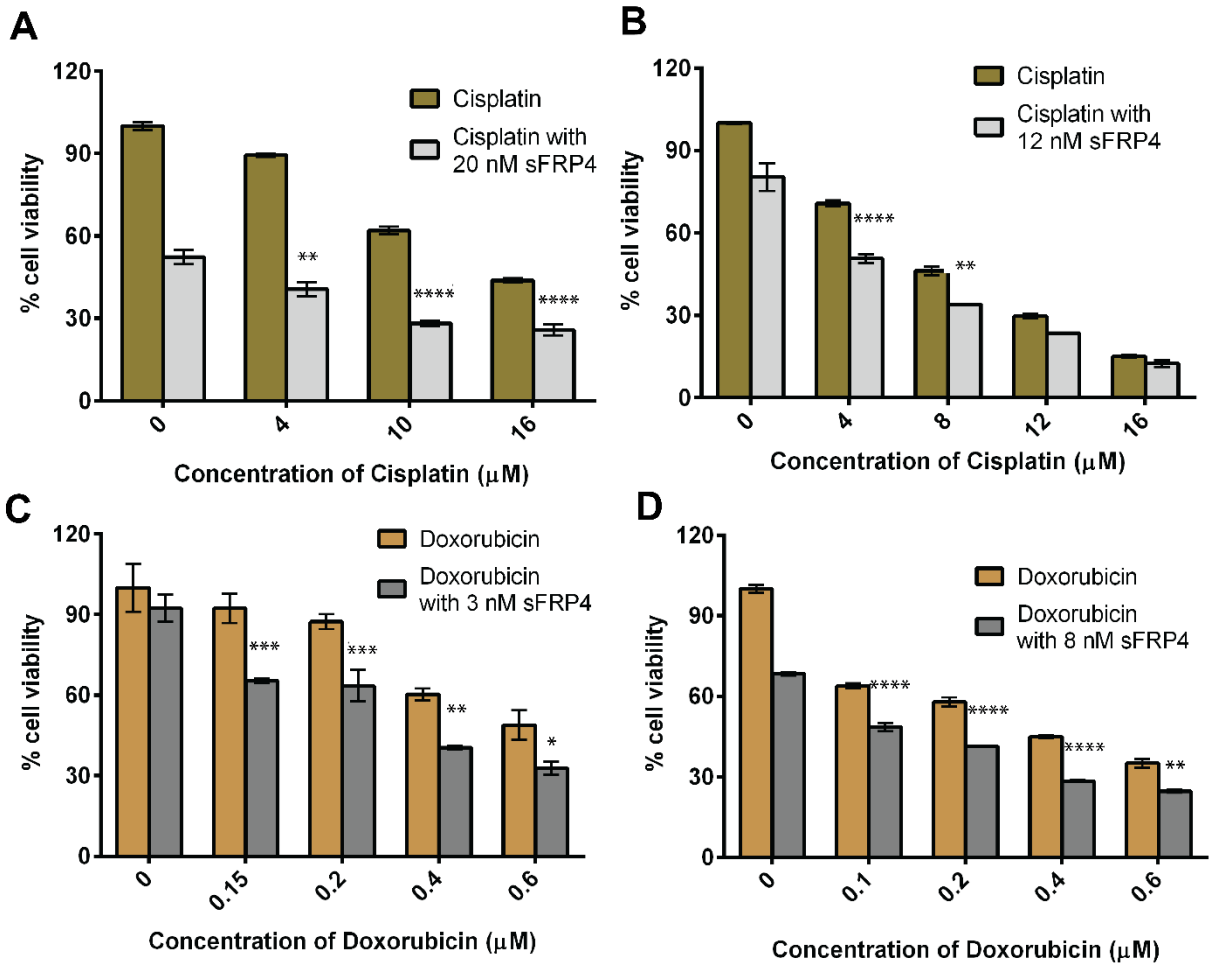

Figure 4.9. Cell viability assay after 48 h of combination therapy, **(A)** HeLa cells treated with increasing concentration of cisplatin and 20 nM of GST-sFRP4, **(B)** A549 cells treated with increasing concentration of cisplatin and 12 nM of GST-sFRP4, **(C)** HeLa cells treated with increasing concentration of doxorubicin and 3 nM of GST-sFRP4, **(D)** A549 cells treated with increasing concentration of doxorubicin and 8 nM of GST-sFRP4.

4.3.9 Determination of cell cycle arrest by flow cytometry

To substantiate the above findings, the mode of anti-proliferative effect was investigated by flow cytometric analysis and dual staining methods. FACS based analysis was performed to ascertain the effect of recombinant sFRP4, alone and in combination with chemotherapeutic drugs on the cell cycle using PI. A low concentration of sFRP4 (12 nM) was found to be sufficient to induce arrest in G2/M phase for both cell lines (15% to 34% in HeLa and

10.19% to 21% in A549) in 48 h. However, in case of A549 cells, there was a significant increase in cells undergoing S phase arrest (5% in control to 16% in treated). A low range of protein concentration was selected to demonstrate the augmented effect of co-therapy. In combination of cisplatin with GST-sFRP4, both cells showed an increase in percentage of cells in G2/M phase by approximately 12%, in comparison to cisplatin alone. For HeLa, 50% of cells exhibited G2/M arrest on this mode of co-therapy, whereas the percentage was 67% for A549. In case of co-therapy with doxorubicin, differential behavior was observed for the two cell types. While HeLa cells exhibited S phase arrest, A549 cells showed G2/M blocking of cell cycle. The cell cycle analysis is depicted in **Figure 4.10A** and **Figure 4.10B**, for HeLa and A549 cells, respectively. Graphical representation of the same is given in **Figure 4.11**.

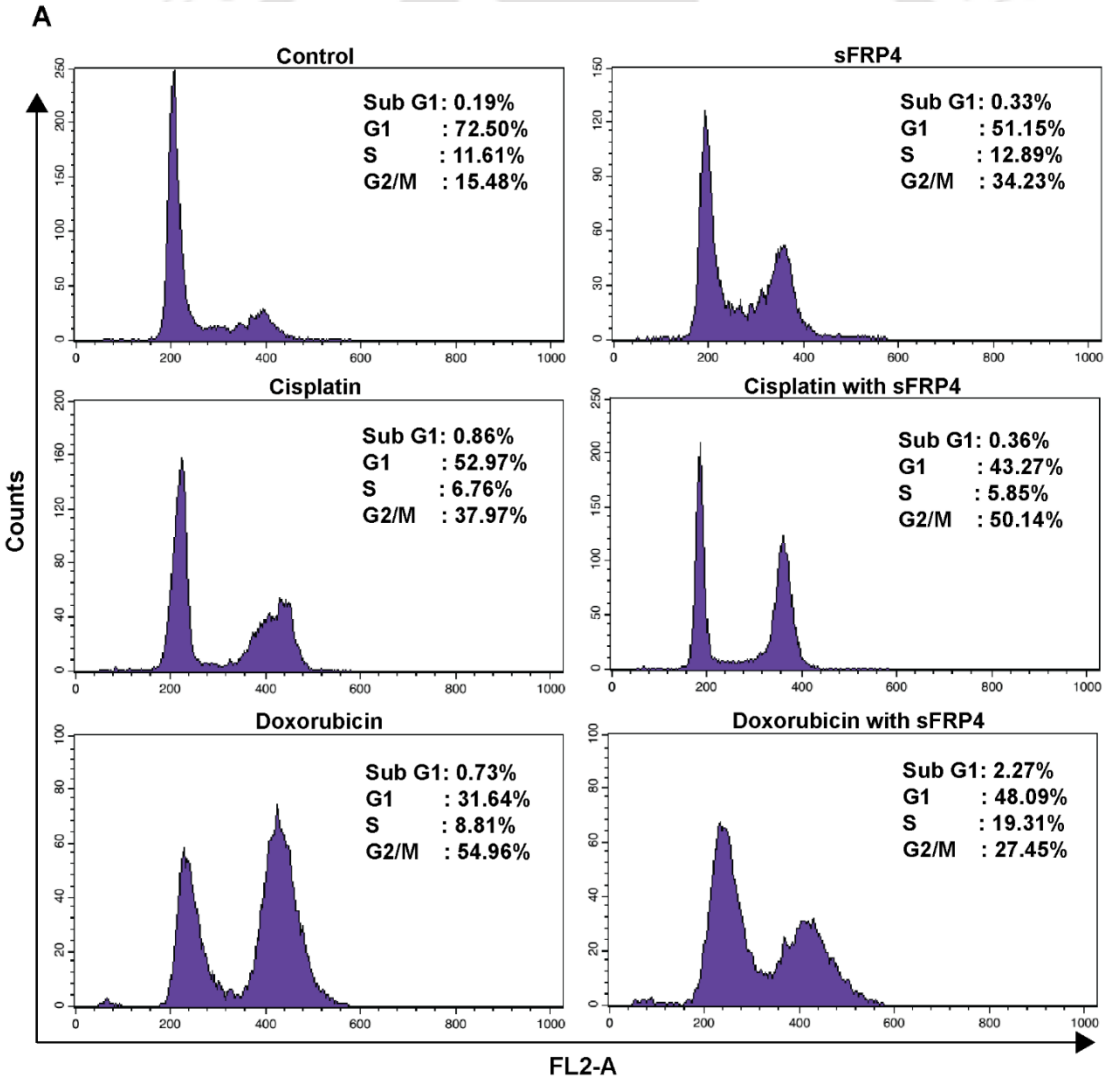

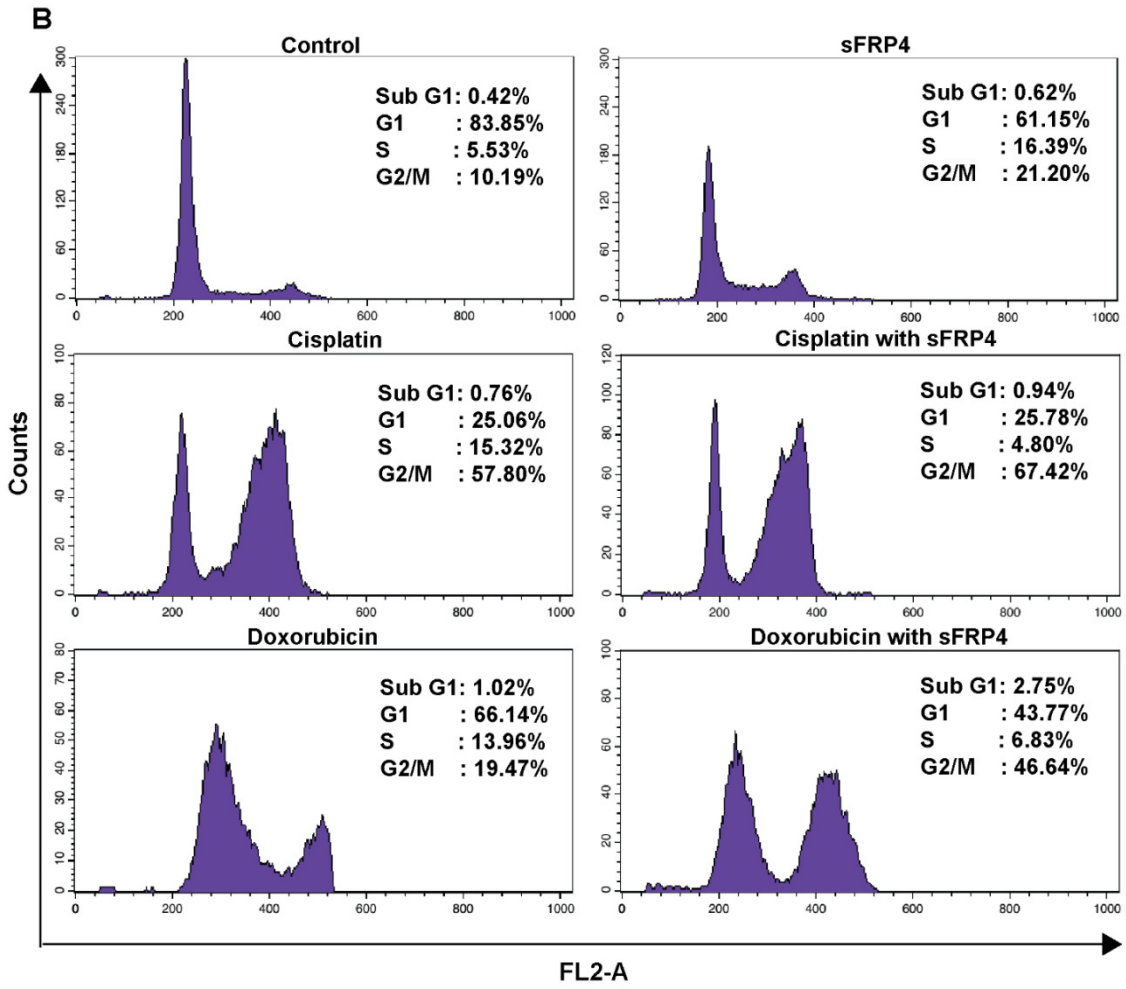

Figure 4.10. Flow cytometry-based cell cycle analysis of untreated and treated **(A)** HeLa cells, **(B)** A549 cells.

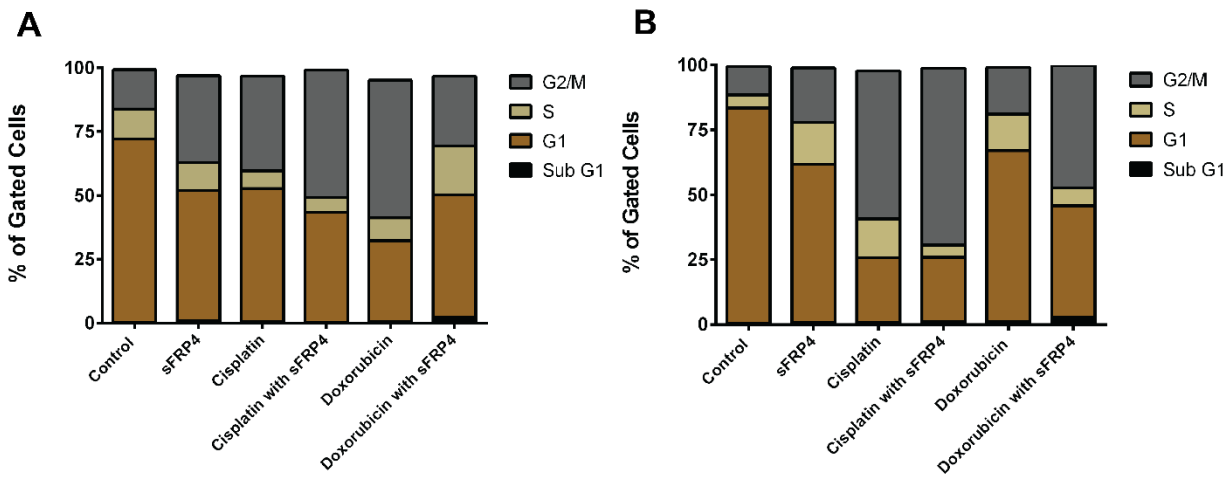

Figure 4.11. Graphical representation of flow cytometry-based cell cycle analysis after co-therapy of **(A)** HeLa cells, **(B)** A549 cells.

4.3.10 Induction of apoptosis in a co-therapy module

Onset of apoptosis was determined by exploiting its underlying mechanism by means of Annexin V-FITC/PI dual staining using flow cytometry. Labelled Annexin V is an indicator of translocation of phosphatidylserine from inner to outer leaflet of cell membrane, a characteristic event of apoptosis. It labels both early and late apoptotic cells till the membrane is completely disintegrated. On the other hand, PI is a membrane impermeable dye, which can intercalate with nucleic acids only when membrane is damaged. Hence, this system was employed to quantitatively ascertain the percentages of viable (Annexin V^-, PI^-), early apoptotic (Annexin V^+, PI^-), late apoptotic (Annexin V^+, PI^+), very late apoptotic /necrotic (Annexin V^-, PI^+) cells by flow cytometric analysis. Percentage of live cells was reduced from 91.4% to 73% for HeLa cells and 92.5% to 82.8% for A549 cells after 48 h of treatment with a very low concentration (12 nM) of GST-sFRP4; early apoptotic cells were found to increase by 16% for HeLa cells, whereas for A549 there was a marginal increase in each quadrant depicting apoptotic cells. Co-therapy resulted in an increase of late apoptotic cell population. Graphical representation of the same is given **Figure 4.12**.

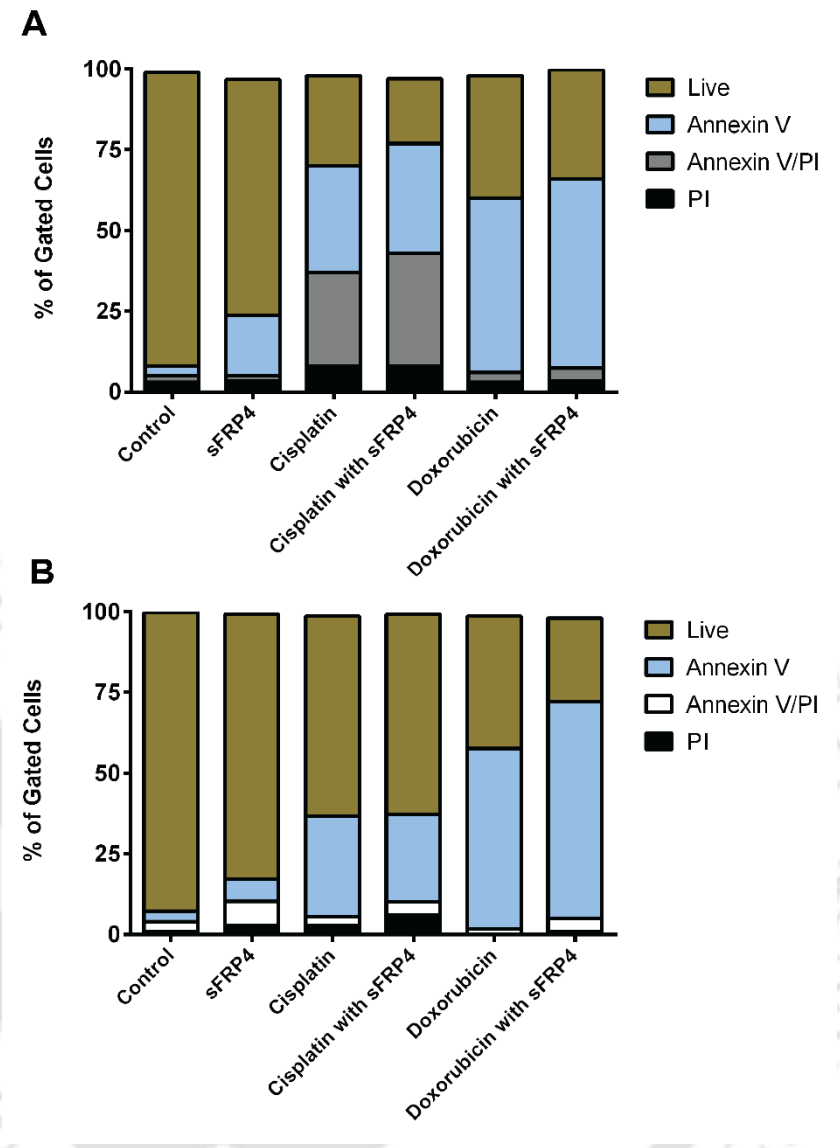

Figure 4.12. Apoptosis detection assays with Annexin V-FITC/PI depict early apoptosis in cells treated with low concentration of GST-sFRP4 and significant apoptotic population after combination therapy; **(A)** HeLa and **(B)** A549.

Apoptosis was also detected by bivariate analysis of dual stained (AO/EB) cancer cells (**Figure 4.13**). Hence, it was established that recombinant sFRP4 as well as combination therapy with cisplatin/doxorubicin induced an apoptotic mode of cell death. This was in accordance with previous reports delineating the mode of action of sFRP4 in keratinocytes [51] and breast cancer cells [151].

A. HeLa cells

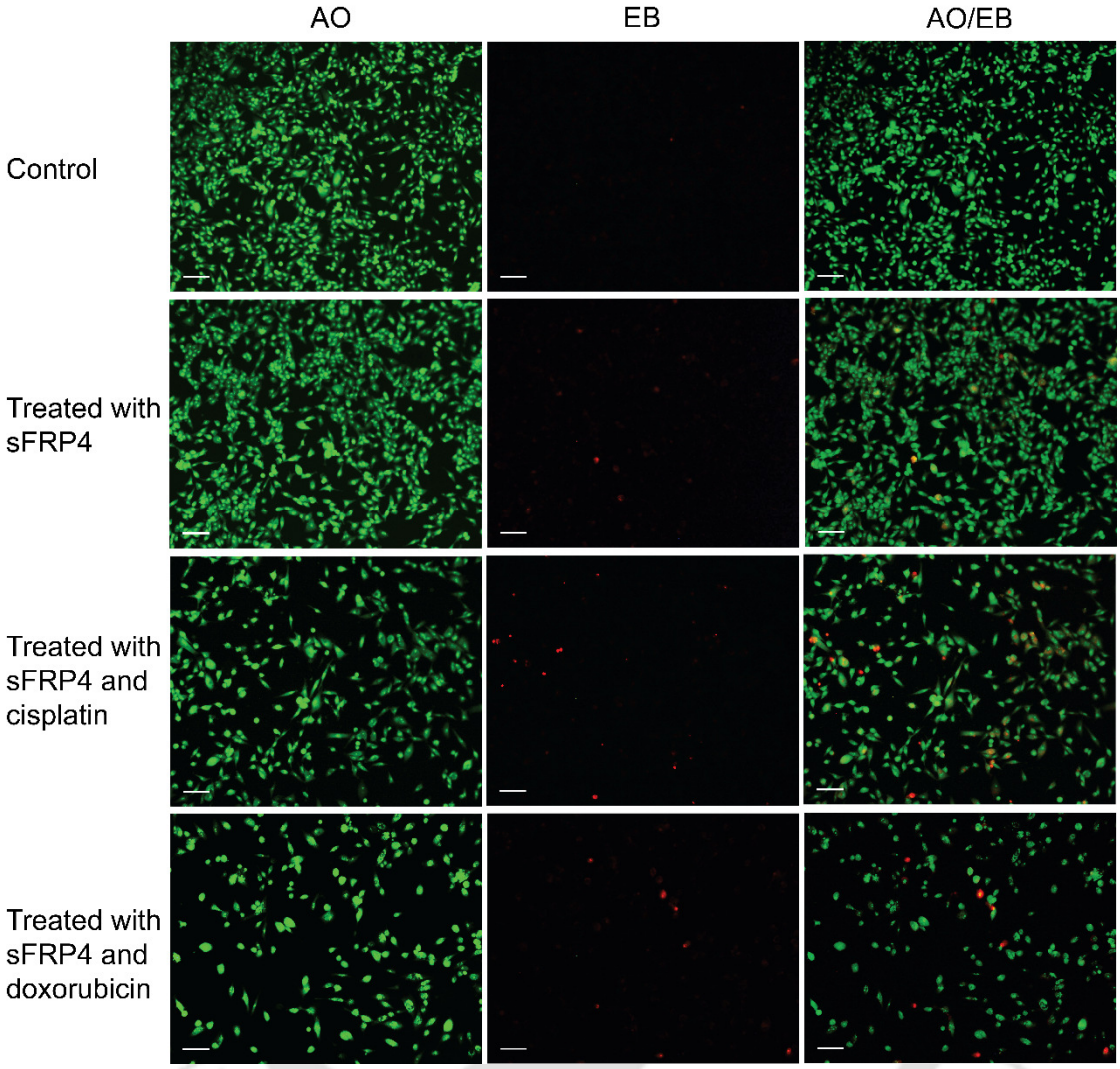

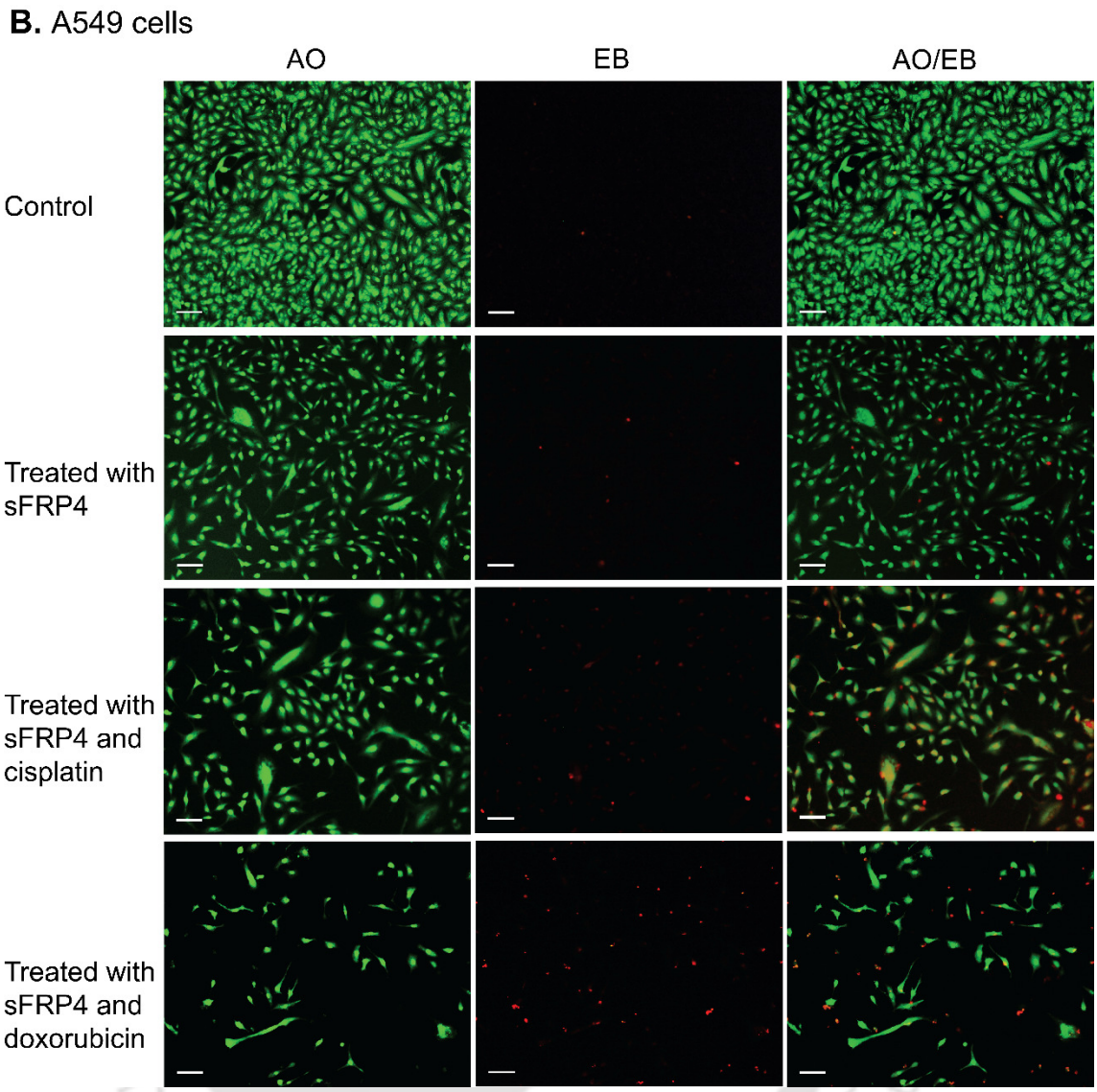

Figure 4.13. Fluorescence microscopic analysis of control and treated cells stained with AO and EB, **(A)** HeLa cells **(B)** A549 cells.

The mode of cell inhibition was determined by flow cytometric and microscopic analyses, which demonstrated cell cycle arrest followed by apoptotic cell death. Programmed cell death is called apoptosis, which is a more desirable form of cell elimination than necrosis. It is conceivable that treatment of HeLa and A549 cells with GST-sFRP4 as well as combination therapy with drugs induced an appreciable arrest in the G2/M phase of cell cycle. This would also be a logical explanation for inhibition of cell proliferation and for the

subsequent apoptosis, which was shown to be mediated by the regulation of cell cycle. This was consistent with previous reports defining the mode of cell death by sFRP4 [51, 151]. Use of low concentration of protein for FACS based analyses may be correlated with the percentage of apoptotic population (20-27%) in case of treatment with protein alone. Also, the fact that sFRP4 affected the cells by holding them in a steady-state population possibly brought about chemosensitization to cisplatin and doxorubicin. Individually, each of the chemotherapeutic drugs induced an arrest in the G2/M phase of the cycle, consistent with previous reports [152]. In cancer, many cell cycle checkpoints, including G2/M checkpoints, are defective, resulting in continuous proliferation and a propensity to acquire chromosomal aberrations causing drug resistance [153]. By causing G2/M arrest, recombinant sFRP4 created an externally imposed cell cycle checkpoint. This not only caused apoptotic cell death by itself, but also made the cells susceptible to chemotherapy, thus ensuring that a very minimal concentration of drug was sufficient to produce massive apoptosis. When applied clinically, this would be advantageous in curtailing the undesirable side-effects of these drugs.

4.3.11 Quantitative expression profiling of Wnt downstream genes by Real-time PCR

To address the mechanism underlying the successful application of co-therapy, the quantitative expressions of pro-proliferative genes cyclin D1, c-myc, and survivin, were checked by quantitative real-time PCR analysis. While all three genes are known to be regulated by the Wnt/β-catenin pathway, their behavior after treatment with combination therapy is unknown. During this investigation, it was observed that in 24 h, cyclin D1 was transcriptionally downregulated by 30% and 10% on treatment with cisplatin alone, in HeLa and A549 cells, respectively (**Figure 4.14A** and **Figure 4.14B**, respectively). However, in both cell types, there was a significant (~50%) difference in expression of cyclin D1 between treatment with cisplatin alone, and its combination with GST-sFRP4, indicating a further inhibition of cell proliferation. From this, it was concluded that the recombinant sFRP4 inhibited the Wnt pathway even in presence of potent anti-cancer drug cisplatin. Also, expression of cyclin D1 was substantially decreased in case of co-therapy, as opposed to either mode of treatment alone. In case of therapy with doxorubicin alone, HeLa cells (**Figure 4.14A**) exhibited reduced levels of cyclin D1 (by 50%). Although there was a further

decrease in expression level on co-therapy with protein, it was marginal, possibly because even in low concentrations, doxorubicin itself is potent enough to substantially inhibit cell proliferation. However for A549 cells, there was a distinct reduction (by nearly 40%) in case of co-therapy, as compared to doxorubicin alone (**Figure 4.14B**). In addition to cyclin D1, the expression of c-myc gene was also probed (**Figure 4.14C** and **Figure 4.14D** for HeLa and A549, respectively). Treatment with cisplatin alone resulted in nearly 20% decrease in the level of c-myc in both cells, compared to untreated cells. In HeLa, this expression was further reduced by 30% on co-therapy of cisplatin with GST-sFRP4; whereas in case of A549 cells, co-therapy brought about a further reduction by 60% compared to treatment with only cisplatin. Doxorubicin treatment yielded a similar effect on c-myc as seen for cyclin D1. Treatment with drug alone lowered gene expression to 60% and 20%, with respect to control, for HeLa and A549 cells, respectively. In both cases, there was a further reduction of approximately 20% for co-therapy of doxorubicin with recombinant sFRP4. Lastly, the expression of survivin gene was determined (**Figure 4.14E** and **Figure 4.14F** for HeLa and A549, respectively). Both the chemotherapeutic drugs had an immense effect in decreasing the levels of survivin. Therefore, the effect of co-therapy on survivin expression was observed to be marginal in both cell lines. These quantitative data revealed that while the recombinant sFRP4 as well as conventional anti-cancer agents individually led to reduced proliferation of cells, their synergistic effect proved to be significantly more fruitful.

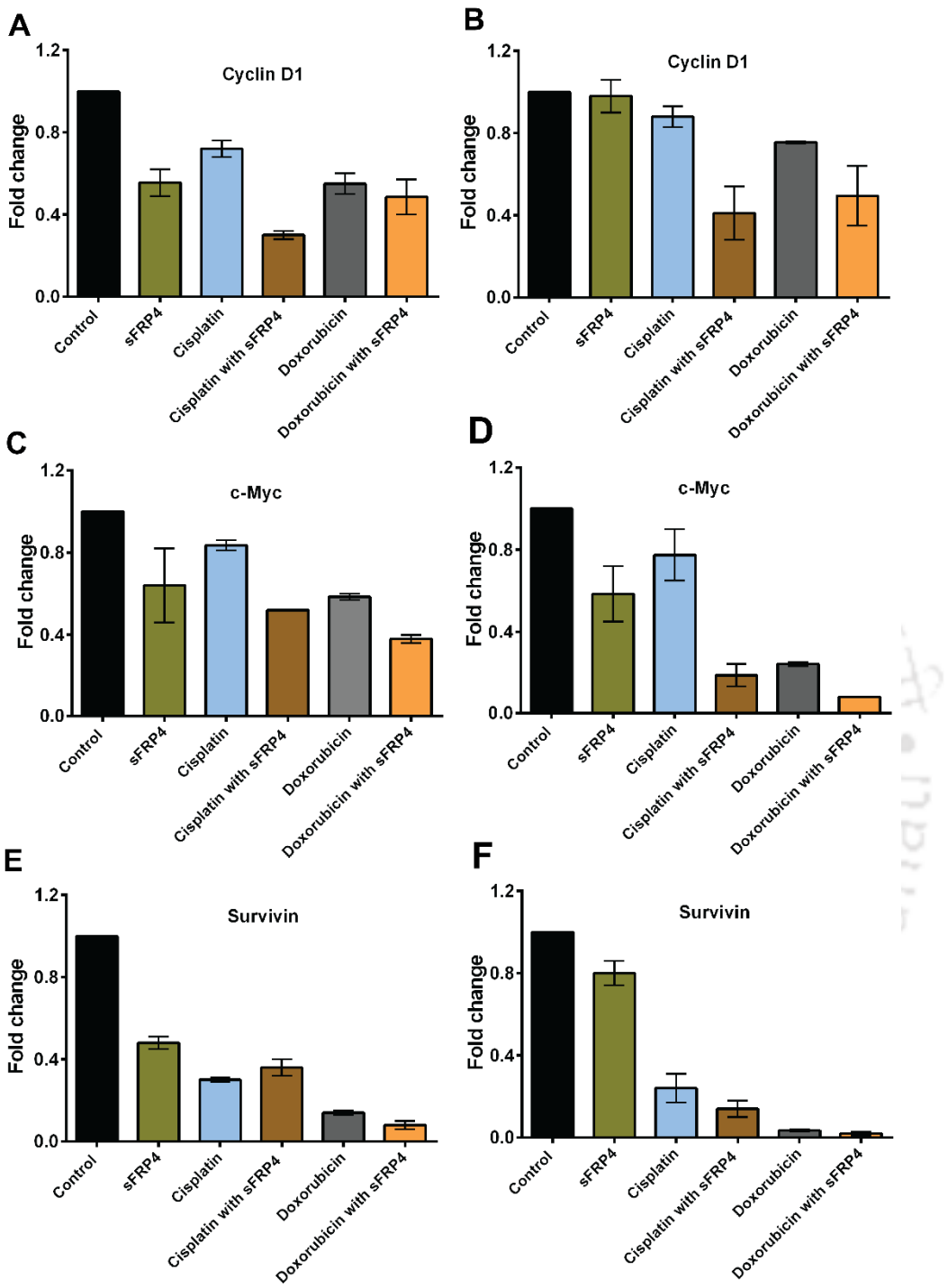

Figure 4.14. Real-time PCR expression analysis of untreated and treated cells, **(A)** cyclin D1 in HeLa, **(B)** cyclin D1 in A549, **(C)** c-myc in HeLa, **(D)** c-myc in A549, **(E)** survivin in HeLa **(F)** survivin in A549.

Binding of recombinant sFRP4 with corresponding Wnt ligands, prevented the signal transduction, which led to phosphorylation and subsequent ubiquitination of β-catenin, as documented by Western blotting. Correspondingly, downregulation of downstream genes, namely cyclin D1, c-myc, and survivin, was observed by real-time PCR. These experiments proved that recombinant sFRP4 executed its anti-proliferative activity by binding to Wnts and blocking the downstream signal cascade. However, treatment with traditional anti-tumor drugs, cisplatin and doxorubicin also suppressed expression of these genes. As there is no known link directly connecting Wnt cascade and these drugs, it was hypothesized that the drugs could be inhibiting these oncogenes via other signaling pathways. For instance, cisplatin has been reported to induce apoptosis mediated by p53 [154, 155], which in turn is known to suppress cyclin D1 [156] as well as c-myc [157]. Cisplatin is also known to be implicated in Ras/Akt/ERK pathways, which have cyclin D1 and c-myc as their downstream targets [158]. Survivin belongs to the Inhibitor of Apoptosis (IAP) protein family and has been reported to be suppressed by p53 [159]. Doxorubicin, an inhibitor of topoisomerase II, has been known to downregulate cyclin D1 [152], c-myc [160-162], and survivin [163, 164]. However, it should be noted here that signaling pathways are complicated, interlinked, obscure, and often behave in conflicting manner. Hence, detailed mechanism of action by cisplatin or doxorubicin was beyond the scope of this study. Herein, it was established that recombinant sFRP4 repressed the expression of key members of the Wnt pathway involved in aberrant proliferation of cancer cells. It should also be mentioned here that significant enhancement of inhibition of these oncogenes was observed after combination therapy, as compared to individual treatment modality. Notably, effect of sFRP4 in blocking of the Wnt signaling was not violated even in course of combination module.

4.3.12 Effect on GST-sFRP4 on normal cell line 3T3-L1

Finally, the effect of GST-sFRP4 was determined on normal mouse fibroblast cell line 3T3-L1. As expected, no significant reduction in cell viability was observed (**Figure 4.15**).

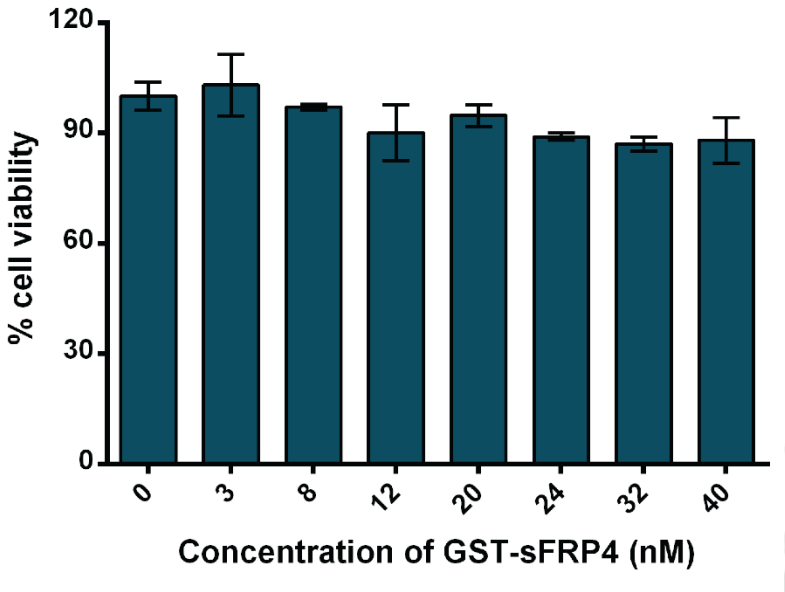

Figure 4.15. Cell viability assay of 3T3-L1 cells showed that there is no significant effect of recombinant sFRP4.

Further detailed studying of the molecular mechanisms involved in the dynamics of this pathway will pave the way for its clinical usage. Recently, Wnt pathway inhibitors have been studied successfully to block Wnt signaling in mouse models [165, 166]. From this, it may be inferred that the bacterially expressed recombinant sFRP4 holds immense potential for *in vivo* cancer therapy.

4.4 Conclusions

In order to implement the existing literature on Wnt to concoct a novel approach of employing bacterially expressed recombinant human protein to inhibit this signaling pathway, human sFRP4 was cloned and purified the GST tagged protein from bacterial host. The proficiency displayed by recombinant sFRP4 in impeding the Wnt signaling may open up new possibilities for recombinant protein therapeutics. The functionality demonstrated by the bacterially expressed human sFRP4 could also be exploited for studying its interactions with various Wnt isoforms. It could also be used to resolve the discrepancies

regarding blocking of canonical or non-canonical or any other intersecting signaling due to binding of sFRP4 to different Wnt ligands. Further, efficacy of the treatment module was augmented significantly by co-therapy with traditional chemotherapeutic drugs. The approach of compiling the benefits of recombinant protein therapy to lower the dosage of drugs has the potential to minimize side effects and circumvent the development of resistance, making it a tremendously fascinating solution for tackling a complex disease like cancer. The highlights of this investigation encompass the identification and possible application of a novel mode of recombinant protein therapeutics via sFRP4.

CHAPTER 5

Recombinant sFRP4 bound Chitosan-Alginate Composite Nanoparticles Embedded with Silver Nanoclusters for Wnt/ β-Catenin targeting in Cancer Theranostics

CHAPTER 5

5.1 Introduction

Major headway in the fields of biology, nanotechnology and electronics has culminated in the emergence of 'theranostics'- having potential to facilitate medical diagnosis and therapy. The advent of theranostics has a positive impact on cancer treatment, where various approaches of probing, detection and delivery of chemotherapeutic drugs have been witnessed in recent years. However, targeting specific signaling pathways with recombinant protein-functionalized nanoparticles (NPs) has seldom been accomplished in cancer therapy. Although using recombinant proteins as a signal modulator presents a challenge in itself; however, their immune acceptance and ability to regulate specific pathways help to surmount the major problem of adverse side-effects of conventional drugs [1].

Active targeting has been achieved by specific recognition between antigen-antibody [167] in order to inhibit molecular pathways aberrant in cancer, such as HER2, MAPK, Akt, EGF, p53 [168, 169]. In addition, cell surface receptors overexpressed in cancer cells, such as transferrin receptors and folate receptors, have been exploited for targeted delivery of a particular gene, siRNA or drugs [170-173]. While delivery of a therapeutic protein with nanocarriers has been deemed prudent [68], the interaction of therapeutic protein with its corresponding cell surface receptor has also been exploited for delivery of the cytotoxic composite nanoparticles [69].

One pathway that has rarely been explored for targeting cancer cells is the Wnt pathway [19]. This signaling pathway is aberrantly upregulated in most cancer types [45], resulting in the activation of downstream pro-proliferative genes [22-24] via stabilization of β-catenin [174], which is a critical molecule central to the Wnt pathway. In non-cancerous cells, it is antagonized by a family of five glycoproteins, called the secreted frizzled-related proteins (sFRPs), which are silenced in cancer cells due to promoter hypermethylation [33]. Of the five known sFRPs, sFRP4 is the most recently discovered one that has exhibited tremendous promise in preliminary investigations. Transfection of sFRP4 gene into prostate cancer [43] and ovarian cancer [98] cells has shown the anti-tumor effect and chemosensitizing property

of sFRP4. Exogenous administration of sFRP4 onto keratinocytes has also been reported to demonstrate positive results [51]. Furthermore, sFRP4 has been found to chemosensitize glioma stem cells toward conventional chemotherapeutic drugs [138].

Equipped with these promising reports, the co-therapeutic value of recombinant sFRP4 decorated silver nanocluster embedded chitosan- nanoparticles (Ag NC-Chi-Alg NPs) was explored. These multifunctional NPs could be designed using components working in tandem, to target the Wnt pathway and specifically inhibit cancer cells. A visual representation of the concept portrays the crux of this investigation in **Scheme 5.1.**

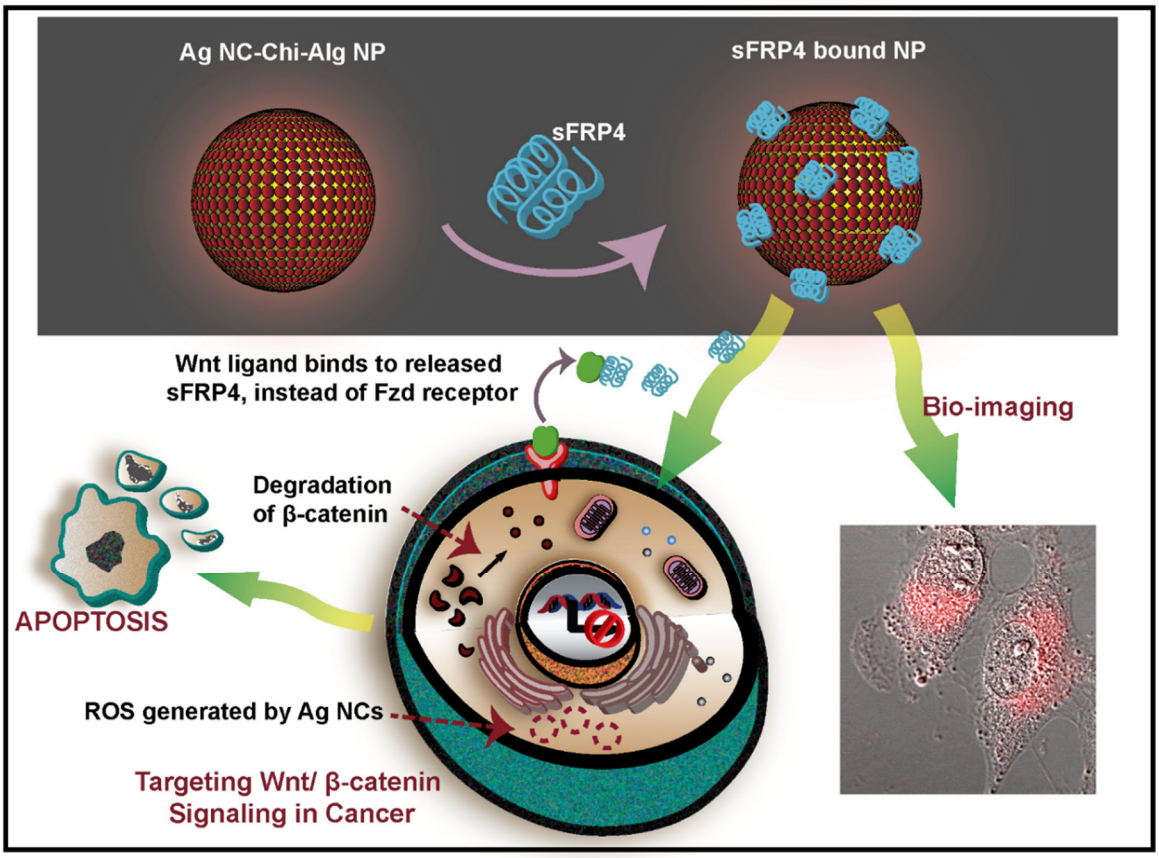

Scheme 5.1. The essence of this study is portrayed in this schematic.

The composite NPs were synthesized by a novel method, to accommodate the size and surface charge requirements of this study. For binding, imaging, and uptake analyses, the extraordinary photoluminescence of Ag NCs was conveniently utilized. Although both gold (Au) and silver (Ag) NCs have attracted tremendous attention of late, Ag NCs hold the added

advantage of being an anti-cell proliferative agent. At low doses, silver has been established to exert minimum toxic effects, as evidenced by its applicability in the biological system [175]. Ag NCs have displayed immense potential in theranostics by virtue of their unique photophysical properties, arising due to their quantum confinement. Moreover, in this study, the interaction of sFRP4 with Wnt ligands would be expected to facilitate the uptake of the Ag NC-Chi-Alg NPs; thus the cytotoxicity of the Ag NCs would be expected to affect the cancer cells, which express Wnt ligands, more than the non-cancerous cells. Furthermore, as the moiety responsible for targeting, that is sFRP4, can play the dual role of specifically inhibiting cancer cells, the composite would possess superior effectuality.

5.2 Material and Methods

5.2.1 Chemicals

All items were purchased from Sigma-Aldrich, unless mentioned otherwise.

5.2.2 Synthesis of Chi-Ag NC-Alg NPs

Ag NCs were engineered by slightly modifying the previous report [176], whereas, the composite NPs were formulated by a novel method of synthesis. Briefly, 200 µl of 0.5% chitosan was dissolved in 2 ml Milli-Q water, to which 5.26 mg of lipoic acid and 5 mg of sodium borohydride were added. The solution was stirred for 30 min, by the end of which, the solution turned brown and the luminescence was observed under UV irradiation. Then 100 µl of 1% sodium alginate was added and pH was adjusted to 7.4. Finally synthesized NPs were centrifuged to remove free clusters.

5.2.3 Expression and Purification of GST tagged sFRP4

The cloning, expression, and purification of human sFRP4 has been described in details in Chapter 4. In brief, recombinant GST tagged protein was purified by affinity chromatography; purified GST-sFRP4 was dialyzed against 10 mM Tris (pH 7.4) and quantified by Bradford assay.

5.2.4 Characterization of Chi-Ag NC-Alg NPs

The Chi-Ag NC-Alg NPs were characterized using fluorescence spectrophotometer (Fluoromax -4) and UV-vis spectrophotometer (Perkin Elmer, Lambda 750). Particle size distribution and surface charge analyses were performed by DLS and zeta potential measurements, respectively, using Malvern Zetasizer Nano ZS. MALDI-TOF analysis was done to ascertain the number of silver atoms constituting a single cluster (Bruker). For imaging the NPs and sFRP4 bound NPs (henceforth referred to as NPs-sFRP4), samples were drop-casted on carbon-coated copper grids and analyzed with TEM (JEM 2100) at an accelerating voltage of 200 kV. Quantum yield was calculated by an established one-step method [117], using the following formula:

$$Q = Q_R \frac{I \quad OD_R \quad n^2}{I_R \; OD \quad n_R^2}$$

Here, Q stands for quantum yield, I denotes integrated fluorescence intensity, OD connotes optical density (absorption), n is the refractive index, and R represents fluorescein, which is the reference dye used here.

5.2.5 Binding and release studies of NPs with GST-sFRP4

Binding of fixed amount of NPs and increasing concentrations of sFRP4 was done for 1 h at 37 ºC. At the end of it, samples were centrifuged and pellet was redispersed in water. Luminescence of NPs was probed using fluorescence spectrophotometer LS55 Perkin-Elmer, at excitation and emission wavelengths of 425 nm and 650 nm, respectively. Binding percentage was calculated by the formula:

$$\text{Binding efficiency (\%)} = \frac{\text{Intensity}_{NP} - \text{Intensity}_{NP\text{-}sFRP4}}{\text{Intensity}_{NP}} \text{ X } 100$$

To further confirm the binding of sFRP4 with NPs, FTIR was done. Lyophilized samples of sFRP4, NPs, and NPs-sFRP4 were mixed potassium bromide to form pellets and spectral analyses were performed in the range of 4000-400 cm^{-1} (Perkin-Elmer Spectral One). Release profile of sFRP4 from NPs was generated after selecting the concentration of protein

at which binding saturation was attained. The intrinsic fluorescence of the protein released in PBS (pH 7.4) was measured over a time span of 48 h at an emission wavelength of 360 nm, on excitation with 280 nm wavelength of light.

5.2.6 Mammalian Cell Culture

Human cervical carcinoma cell line (HeLa) was obtained from National Centre for Cell Sciences, India. Cells were cultured in DMEM, supplemented with 10% FBS, 100 U/ml Penicillin, 100 µg/ml Streptomycin in a 5% carbon dioxide incubator under humid conditions at 37 ºC.

5.2.7 Cytotoxicity assays

The effect of sFRP4-NPs on viability of HeLa cells was gauged by trypan blue and MTT assays. Cells were seeded at a density of $7x10^4$ cells/ well in 12-well plate for trypan blue assay and at 7000 cells/ well in 96-well plates for MTT assay. Cells were allowed to attach overnight, after which sFRP4, NPs, and NP-sFRP4 were added separately to the cells in serum-free media, in triplicates. NP-sFRP4 were added at concentrations ranging from 0.1-0.75 mg/ml, while corresponding concentrations of sFRP4 and NPs were also added separately, for comparison.

Trypan blue assay is based on the concept that the trypan blue dye is membrane impermeable; hence, only the cells with damaged membrane would take up the stain, while healthy cells would remain unstained. For this purpose, control and treated cells were harvested after the treatment period and mixed in equal volume with 0.4% trypan blue (Invitrogen). This was loaded on a counting chamber and mounted on a Countess-automated cell counter (Invitrogen), which calculated the percentage of live cells.

MTT assay was also performed to determine cell viability, in which MTT (HiMedia, India) was converted to purple formazan crystals soluble in DMSO by live cells. Multiplate reader (Tecan) was used to measure the absorbance at 550 nm and the background at 655 nm was subtracted. The following formula was used to ascertain the percentage of cell viability:

$$\% \text{ of cell viability} = \frac{(A_{550} - A_{655})_{\text{sample}}}{(A_{550} - A_{655})_{\text{control}}} x100$$

It should be mentioned here, that while MTT assay gives percentage viability of each treated sample with respect to the untreated control cells, trypan blue provides percentage of live cells in each sample with respect to number of dead cells. Statistical significance was evaluated for both assays.

5.2.8 Estimation of cellular uptake of NPs

To examine the uptake of luminescent Ag NC embedded NPs by the HeLa cells, confocal microscope (LSM 880, Zeiss) was used. Cells were treated with NPs for 2 h and 8 h, before imaging was done. Further, flow cytometric evaluation was done, for which the cells were treated with NPs for varying time durations ranging from 0 h to 48 h. On excitation with 488 nm laser of FACS, red luminescence of the NPs uptaken by cells was detected in the FL3 channel.

5.2.9 Western blotting for confirmation of affected signaling pathway

To confirm whether the recombinant sFRP4 was functional and effectively modulated the Wnt pathway as intended, the expression of a central molecule of the canonical Wnt signaling by Western blotting was probed. Detection of total β-catenin protein as well as its phosphorylated form was done by respective antibodies. For this purpose, HeLa cells were treated for 24 h with sFRP4, NPs, and NP-sFRP4, respectively. Whole cell lysate containing total cytoplasmic protein was prepared with RIPA buffer (with protease inhibitors) and quantified by Lowry's protein estimation assay. 50 µg of each sample was loaded in a 12% SDS-PAGE and electrophoresed. Thereafter, the total protein was transferred onto an activated PVDF membrane. Next, the membrane was blocked with BSA, after which it was incubated overnight at 4 ºC with a primary antibody - β-catenin or phospho ($pSer^{33}$/ $pSer^{37}$)-β-catenin or endogenous control β-actin. Then the blot was washed five times with PBST or TBST and incubated with a corresponding secondary antibody conjugated with HRP. Again it was washed five times, before being developed with Chemiluminiscent Peroxidase Substrate kit, according to manufacturer's protocol. It should be noted that TBS buffer was used in case of phospho- β-catenin only.

5.2.10 Studying the mode of cell death

To delineate the mode of cell death, FACS-based assays, viz., determination of ROS generation, effect on cell cycle, and Annexin V-FITC/PI apoptosis detection were performed. In addition, apoptosis was also deciphered by microscopy-based AO/ EB dual staining and Field Emission Scanning Electron Microscopy (FESEM, Sigma, Zeiss) images.

5.2.11 ROS generation

For determination of reactive oxygen species (ROS) generation, the HeLa cells were treated separately with sFRP4, NPs, and NP-sFRP4 for 4 h. Subsequently, the cells were stained with dichlorofluorescin diacetate (DCFDA) and analyzed by flow cytometry in the FL1 channel.

5.2.12 Cell cycle analysis

For this experiment, the HeLa cells were seeded at a density of $1x10^5$ cells/well in a 6-well plate. Cells were incubated with 0.75 mg/ml NP-sFRP4, along with corresponding concentrations of sFRP4 and NPs. After 48 h of treatment, the cells were harvested by trypsinization and fixed by adding chilled 70% ethanol dropwise while vortexing. After the fixation step of at least 1 h, the cells were centrifuged to wash off the ethanol. Then the pellet was redispersed in 10 mM PBS, supplemented with 0.4 mg/ml DNase-free RNase for 1 h at 37 ºC. Thereafter, each sample was incubated with PI at a final concentration of 10 µg/ml for 15 min in dark, after which samples were analyzed in the FL2 channel of a flow cytometer (BD FACSCalibur).

5.2.13 Annexin V-FITC / PI Apoptosis detection assay

Annexin V-FITC / PI apoptosis detection kit (BD Biosciences) was used to discriminate between healthy and apoptotic cells. While Annexin V binds to phosphatidylserine sites exposed upon membrane flipping, one of the earliest hallmarks of apoptosis, PI can only permeate through membrane compromised cells. Therefore, healthy cells are negative for both FITC (tagged to Annexin V) and PI, early apoptotic cells yet to undergo membrane damage are positive for FITC and negative for PI, late apoptotic cells are positive for both, whereas cells stained with only PI represent the very late apoptotic or necrotic population.

In this pursuit, the cells were seeded and treated in a manner same as above. The assay was performed according to the manufacturer's protocol.

5.2.14 Dual staining with AO/ EB

AO and EB double staining was done to corroborate on the results acquired in the above experiment. While AO is membrane permeable and can stain the entire cell, PI is membrane impermeable and stains the DNA of damaged cells only. Thus double stained cells denote the apoptotic population, whereas only PI stained cells simply represent cell death. For this experiment, cells were treated in a 96-well plate for 48 h. Then the media was discarded and replaced with PBS containing 2 µg/ml AO and 10 µg/ml EB in dark. After 5 min, cells were washed with fresh PBS and imaged with an epi-fluorescence microscope (Nikon ECLIPSE TS100).

5.2.15 FESEM analysis

For capturing the image of apoptotic cells, FESEM analysis was done. To avoid complete disintegration of cellular structure, treatment of the cells with composite NPs was done for only 24 h. The control and treated cells were harvested and fixed with chilled 70% ethanol, following which, they were drop-casted on an aluminium foil wrapped piece of glass slide and allowed to dry. After double coating of the sample with gold film, cells were imaged with FESEM (Sigma, Zeiss).

5.3 Results and Discussion

5.3.1 Expression of functional GST-sFRP4

GST tagged sFRP4 was expressed in *E. coli* BL21(DE3), as described in the previous chapter. Recombinant sFRP4 was purified using glutathione agarose affinity chromatography (**Figure 5.1**). Since the key to the therapeutic application of any recombinant human protein expressed in bacterial system is its functionality, maintaining its functionality by ensuring the proper folding of the GST-sFRP4 by gradient dialysis against Tris-HCl (pH 7.4) was the primary focus. It should be mentioned here that the activity of sFRP4 is known to be independent of post-translational modifications [48, 49]. Confirmation of the proper functioning of the recombinant protein was proven by cell based assays and the Western blotting experiments described later.

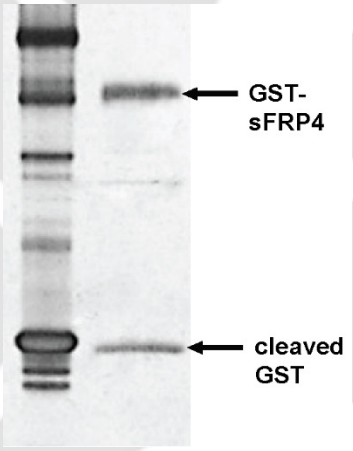

Figure 5.1. Discrete single band of GST-sFRP4 corresponding to its legitimate size of 63 kDa was observed in 12% SDS-PAGE, a cleaved band of GST was also noted.

5.3.2 Binding of sFRP4 with Ag NC-Chitosan-Alginate NPs based on electrostatic interactions

Since the GST-sFRP4 was found to possess an overall positive charge at physiological pH 7.4, as calculated with ExPASy pI calculator, the Ag NC-Chi-Alg NPs were tailored to bind to sFRP4 by endowing a net negative charge upon them, forming the NPs. Zeta potential studies (**Figure 5.2A**) revealed the net surface charge of the as-synthesized NPs to be -27

mV. As sFRP4 affects the Wnt by binding to the extracellular Wnt ligands, sFRP4 was bound onto the surface of the NPs, instead of being encapsulated within. Moreover, to allow the extracellular release of the protein before the uptake of the luminescent NPs, a slow uptake of the NPs was promoted. Hence, in addition to conferring negative charge upon the NPs, their size was also kept relatively large, as illustrated by a hydrodynamic diameter of 774 nm (**Figure 5.2B**) [121].

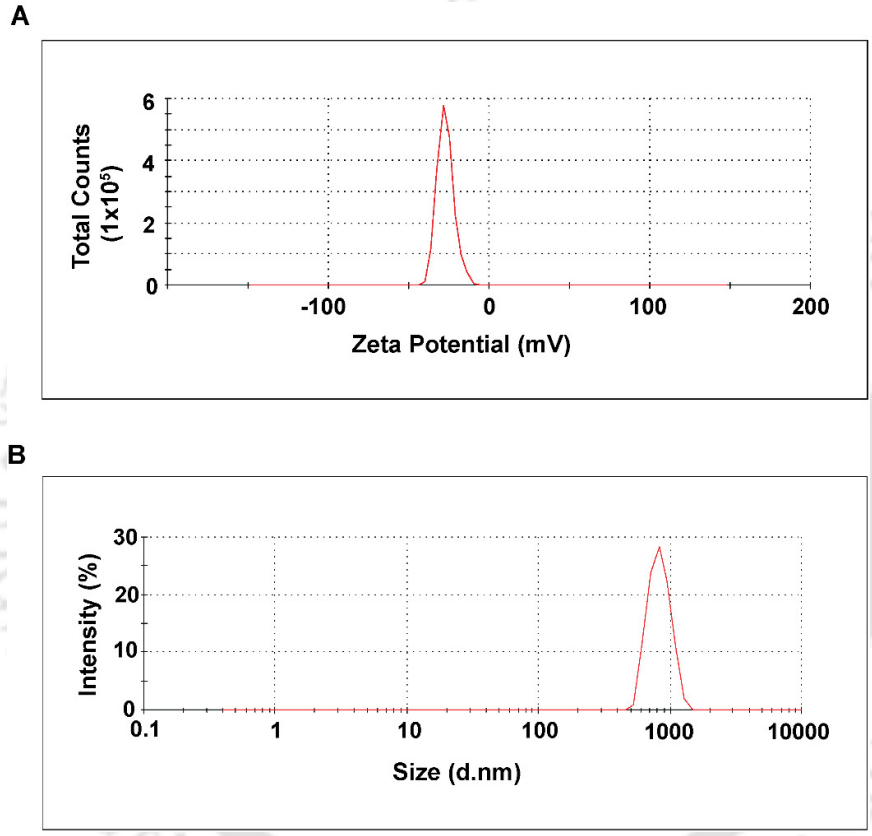

Figure 5.2 (A) Zeta potential studies of Ag NC-Chi-Alg NPs. The single peak shows that the net surface charge of the NPs was -27 mV. **(B)** DLS analysis of Ag NC-Chi-Alg NPs. The hydrodynamic diameter was found to be 774 nm.

5.3.3 Characterization of Ag NC-Chi-Alg NPs

The so-synthesized Ag NC-Chi-Alg NPs displayed characteristic red luminescence emission spectrum of Ag NCs at 650 nm, when excited at a wavelength of 425 nm (**Figure 5.3A**). The intense photoluminescence was evidenced by reasonably higher quantum yield (11.4%) than

many reported Ag NC-based composites, making this composite appropriate for theranostic applications [65, 176, 177]. The mass spectra obtained with MALDI-TOF revealed prominent peaks at m/z equal to 444 and 656 (**Figure 5.3B**), corresponding to the complexes $[Ag_2L + Na^+ + H^+]^+$ and $[Ag_4L + Na^+ - 2H^+]^-$, respectively, where L denotes lipoic acid. Formation of the Ag_4 cluster is in agreement with a previous investigation, where lipoic acid was used as template for synthesis [176]. However, Ag_2 complex has also been reported for red emitting Ag NCs [177]. Additionally, the UV-vis absorption spectra showed the minor peaks at 334 nm and 432 nm (**Figure 5.3C**), possibly due to the formation of extremely small silver nanoparticles [176].

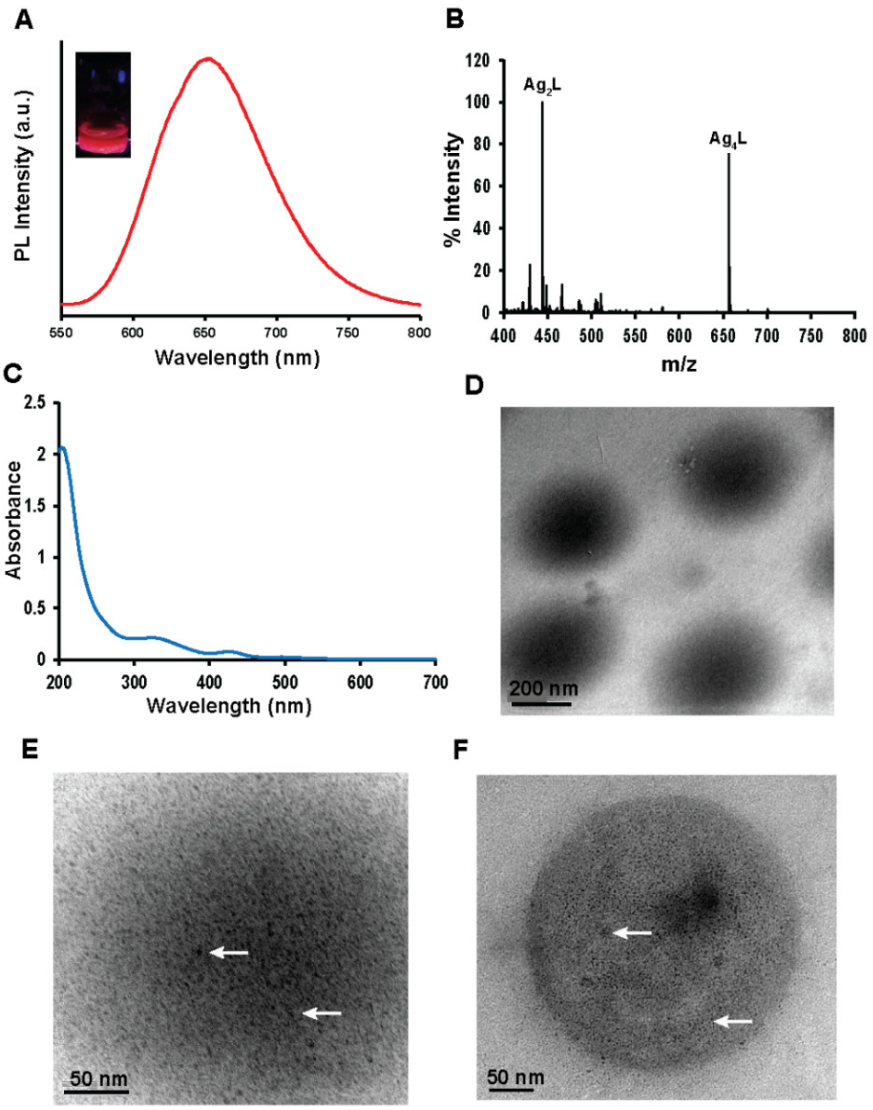

Figure 5.3. (A) Emission spectrum of Ag NC-Chi-Alg NPs connotes red luminescence (650 nm), when excited with 425 nm wavelength of light. **(B)** MALDI-TOF spectra depicted few-atom clusters of silver, with two-atom and four-atom cluster formation being most prominent; L denotes the ligand-lipoic acid. **(C)** UV-visible absorption spectrum of Ag NC-Chi-Alg NPs. The minor peaks at 334 nm and 432 nm were possibly due to the formation of extremely small silver nanoparticles**. (D)** TEM images prove conclusively, the formation of nearly uniform spherical NPs of 350-400 nm in diameter. **(E)** Magnified NP, with distinct Ag NCs. **(F)** Magnified sFRP4 bound NPs, with distinct Ag NCs.

TEM images depicted the formation of spherical NPs with diameters in the range of 350-400 nm (**Figure 5.3D**). The size difference observed between TEM and DLS data was possibly due to swelling of alginate in aqueous environment [122]. Notably, the presence of Ag NCs could be distinctly distinguished for both NPs and sFRP4 bound NPs (henceforth referred to as NPs-sFRP4) samples in the magnified TEM images (**Figure 5.3E** and **Figure 5.3F**, respectively). Interestingly, binding of GST-sFRP4 to the NPs did not alter their spherical structure. Binding was also substantiated by FTIR spectroscopic analysis (**Figure 5.4**), where a shift in amide I and amide II peaks of 1640 and 1560, respectively, confirmed binding of protein with the Chi-Ag NC-Alg NPs. The maximum binding of 71% was recorded by probing the luminescence of Ag NCs (**Figure 5.5A**). Maintaining the same ratio of protein and NPs, this binding efficiency was reaffirmed by probing the intrinsic fluorescence of protein as well (data not shown). Fluorescence of sFRP4 was also exploited to track its release from the NPs over 48 h, where 65% of the bound protein was released immediately in PBS, which increased gradually up to 96% in 48 h (**Figure 5.5B**).

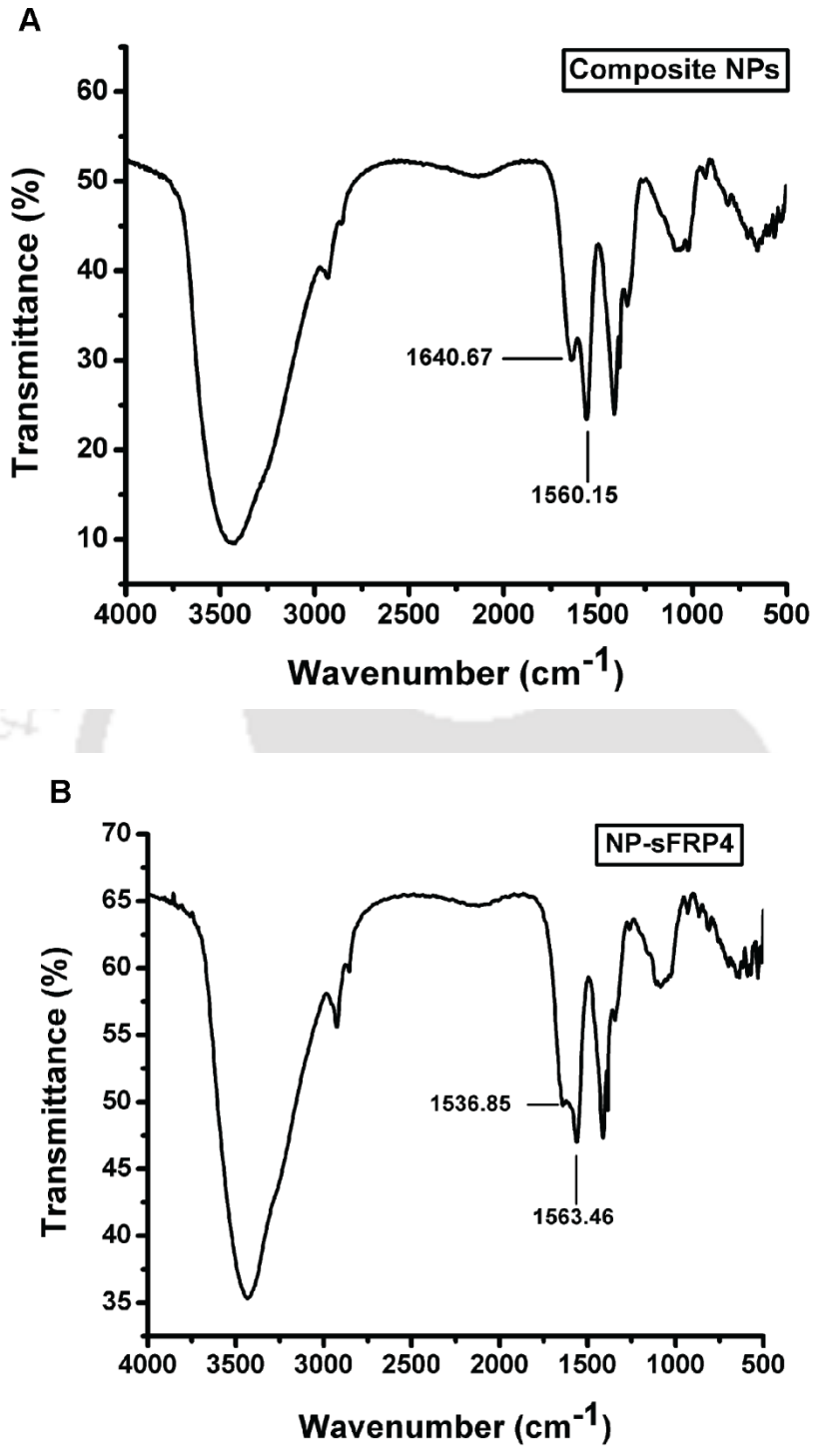

Figure 5.4. FTIR analysis of **(A)** Ag NC-Chi-Alg NPs and **(B)** NP-sFRP4 revealed peak shifts for peaks corresponding to amide I and amide II.

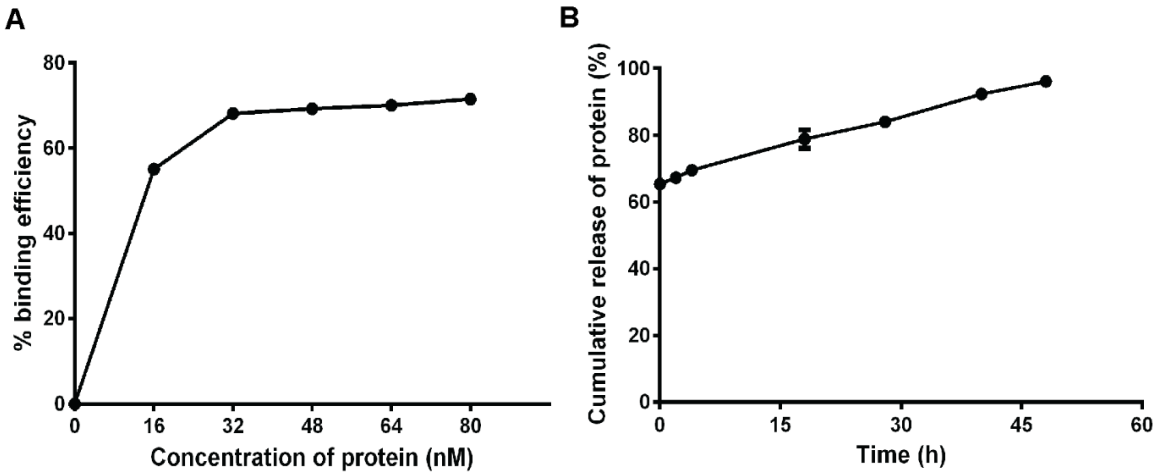

Figure 5.5. (A) Binding efficiency was calculated by incubating fixed concentration of NPs with varying concentrations of sFRP4 for 1 h, maximum binding of 71% was obtained, after which saturation was attained. **(B)** Release profile of sFRP4 from NPs in PBS (pH 7.4). After 1 h of binding in Tris buffer, an instantaneous release of 65% of the protein was documented, which increased gradually up to 96% in 48 h.

5.3.4 Therapeutic efficacy determined by cell viability assays

The therapeutic impact of the NP-sFRP4 was tested on cervical cancer cells (HeLa), which was the primary objective of this work. Although sFRP4 transfection has been reported to exert anti-proliferative effect [178], it is a challenge to ensure that a bacterially expressed human protein retains its functionality. Initial experiments to assess viability of treated cells by trypan blue dye exclusion [179] (**Figure 5.6A**) and MTT (**Figure 5.6B**) assays to confirm the functionality of the purified GST-sFRP4. It should be mentioned here that the absorbance values obtained in the MTT assay appeared to be erroneous, as visual observation under a microscope did not seem to agree with the results of the MTT assay. This could possibly be due to interference by the Ag NCs. Hence, trypan blue dye exclusion assay was performed to determine cell viability. Cytotoxicity of the NPs bestowed by the presence of Ag NCs [180] was also evident. More importantly, trypan blue assay demonstrated the cumulative

effects of sFRP4 and NPs for treatment with sFRP4 bound NPs. At the highest concentration of treatment, viability was significantly lower for NP-sFRP4 (29%), than sFRP4 (55%) or NPs (49%). While 0.75 mg/ml of NPs (containing 22.8 µg/ml of silver) was required to reach the IC_{50} value, only 0.25 mg/ml NP-sFRP4 (containing only 7.6 µg/ml silver) successfully brought about the same effect [181]. These data implied the development of a successful co-therapeutic regime.

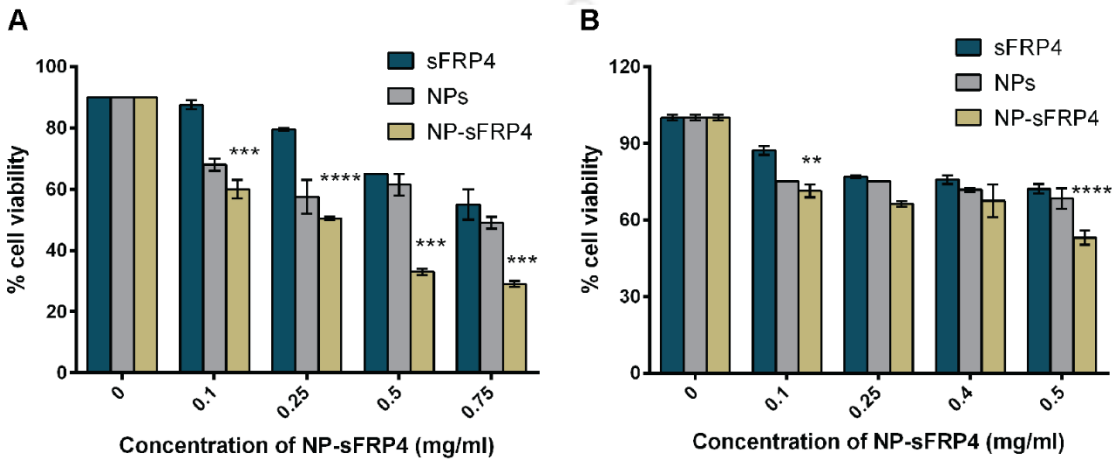

Figure 5.6. (A) Trypan blue dye exclusion assay demonstrated that NP-sFRP4 was more potent in action than either component individually, as depicted by the percentage of viable cells, with the significance being between NP-sFRP4 and sFRP4 treated cells ('***' denotes p value<0.001 and '****' denotes p<0.0001). **(B)** MTT assay of HeLa cells treated with sFRP4, NPs, and NP-sFRP4, separately. It depicted that 0.5 mg/ml of NP-sFRP4 was sufficient to reduce viable cells to nearly 50% ('**' denotes p value<0.01 and '****' denotes p<0.0001).

5.3.5 Cellular uptake of luminescent NPs assessed by Confocal microscopy and Flow cytometry

The cytotoxic effects of the Ag NC embedded NPs attributed to their gradual uptake by the HeLa cells, as divulged by simultaneous confocal microscopy and flow cytometric analysis. The images acquired using confocal microscope illustrated that after 2 h, luminescent NPs were in the process of being uptaken, with NPs prominently visible outside the cells as well (**Figure 5.7A**). However in 8 h, the luminescent NPs were almost completely uptaken by the

cells (**Figure 5.7B**). Z-stacking of image taken at 2 h clearly divulged that NPs remained in the media and on the surface of the cell (**Figure 5.7C**), indicating that the active uptake of the NPs was continuing even after 2 h. From this experiment, it was surmised that the gradual uptake of the NPs would ensure that there was sufficient time for the release of the protein outside the cells, before the NPs were uptaken and Ag NCs began to exert their activity inside the cells. The observation was concurrent with the FACS-based quantitative analysis (**Figure 5.7D**), which connote cellular uptake of NPs over a period of several hours, which is desirable for the release of sFRP4 outside the cells, where it is functional. However, the clusters appear to have been degraded in 48 h, evinced by the lack of luminescence in the cells at the time. Hence, the bright luminescence of these Ag NCs makes them suitable for probing and imaging in biological systems.

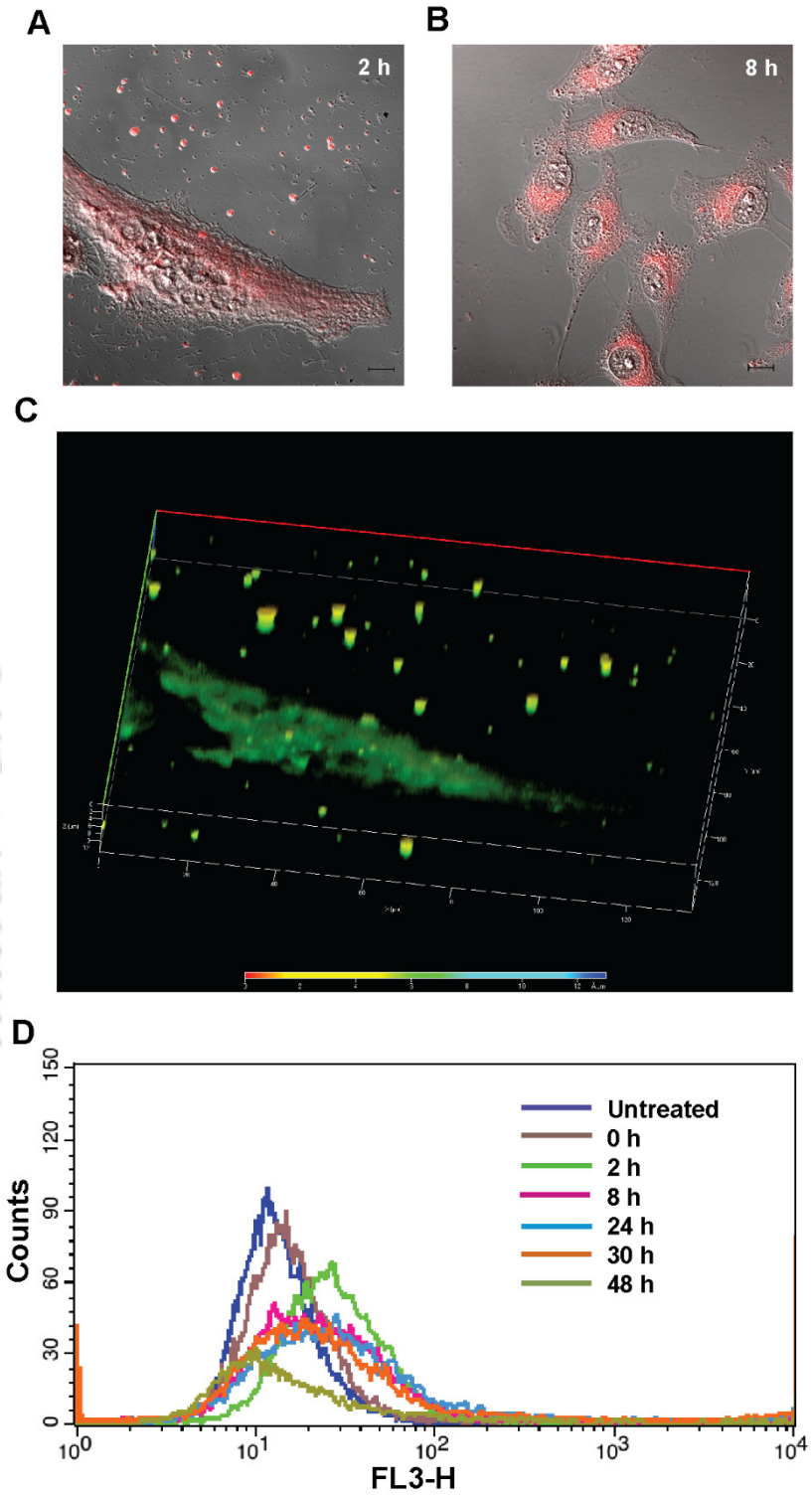

Figure 5.7. (A) Images acquired with confocal microscope showed that in 2 h, luminescent NPs were partially uptaken, with many NPs in the media or on cell surface; **(B)** In 8 h, almost complete cellular uptake of NPs was observed. Scale bar represents 10 µm. The images represent the luminescence of the as-synthesized Ag NCs. **(C)** Confocal microscopic projection of a 12 µm Z-stack (corresponding to Figure 5.7A). This image demonstrates the presence of NPs around and on the surface of the cell. The false colors depict the distance from coverslip to slide (0-12 µm), with red nearest to coverslip (top) and blue being nearest to slide (bottom). The single cell viewed in this field appears green due to uptake of luminescent NPs; green denotes that the NPs are equidistant from slide and coverslip, hence, inside the cell. However, the yellow dots are the NPs possibly on top of the cell, that is, on a different plane than the green layer, closer to the coverslip. Many NPs are also present outside the cell, as denoted by the green-yellow-brown dots. **(D)** Time dependent cellular uptake of luminescent NPs, as studied by flow cytometry. It showed a significant uptake of NPs in 2 h, with the luminescence lasting till 30 h. In 48 h, NPs were degraded inside the cells, as evidenced by lack of luminescence.

5.3.6 Targeting the Wnt/ β-catenin signaling by recombinant sFRP4

As sFRPs are known to block the Wnt pathway in non-cancerous cells, the same effect would be expected in cancer cells if sFRP expression was induced in any manner. With this intent, the mechanism behind the anti-proliferative activity of recombinant sFRP4 was elucidated by examining the downstream Wnt signal cascade. Western blotting experiments were performed to probe the expression of β-catenin, a central molecule of the Wnt signal cascade (**Figure 5.8A**). The sFRP4-treated and NP-sFRP4-treated HeLa cells exhibited a 1.5-fold and 1.75-fold reduction in expression of total β-catenin protein, respectively, denoting inhibition of the downstream Wnt signaling. Furthermore, an upregulation in the phosphorylated form of β-catenin in treated cells signified proteasome mediated degradation of β-catenin. However, this phosphorylated form was not observed in cells treated with NP-sFRP4, possibly due to potent action of the Ag NCs. These results provide categorical evidence in favor of the role of the GST-sFRP4 in antagonizing the Wnt/ β-catenin pathway. Hence the anti-proliferative effect of sFRP4 may be attributed to the degradation of β-

catenin, which is known to downregulate the Wnt downstream pro-proliferative genes [182, 183].

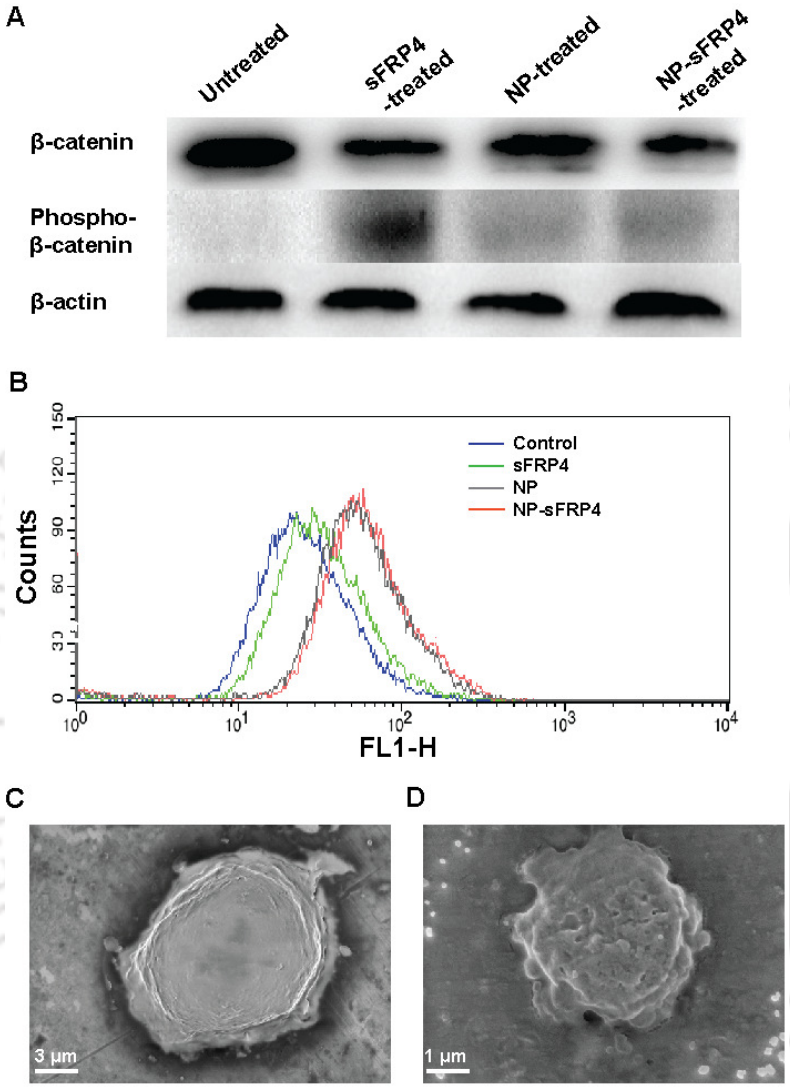

Figure 5.8. (A) Targeting of the canonical Wnt/ β-catenin signaling with functional sFRP4 was proven by Western blotting. β-catenin was significantly downregulated treated HeLa cells, compared to untreated cells; phosphorylated β-catenin, that is, β-catenin marked for degradation, was upregulated in sFRP4-treated cells, however NP-sFRP4 treated cells did not appear to have expressed phospho-β-catenin, possibly due to the presence of potent NPs or due to extremely short half-life of phosphorylated proteins. β-actin antibody was used as endogenous control. **(B)** NP- and NP-sFRP4-treated cells showed significant ROS generation in FACS-based assay, and sFRP4-treated samples generated ROS to a lesser

extent. **(C, D)** FESEM images depict **(C)** untreated HeLa cells and **(D)** HeLa cells treated with NPs with 24 h.

5.3.7 Cytotoxic effect of Ag NC embedded NPs

After elucidating the cause of cell growth inhibition by GST-sFRP4, the mode of effect exerted by the NPs was investigated. Treatment with the Ag NC embedded NPs generated reactive oxygen species (ROS) [184] that directly correlated with cell death (**Figure 5.8B**) [185]. However, treatment with protein alone also resulted in ROS generation, albeit much less than that by Ag NCs. Indeed, onset of apoptosis was documented in FESEM images, depicting membrane blebbing and shrinkage of the cells treated with composite NPs for 24 h (**Figure 5.8C** and **Figure 5.8D**) [186]. This experiment, along with the above Western blotting data were in direct agreement with the results obtained in the cell viability assays. Thus, while Ag NCs induced cell death by ROS generation, recombinant sFRP4 arrested cell growth by blocking the Wnt signaling. Hereby these two components together constituted the co-therapy module, which has been further mechanistically studied.

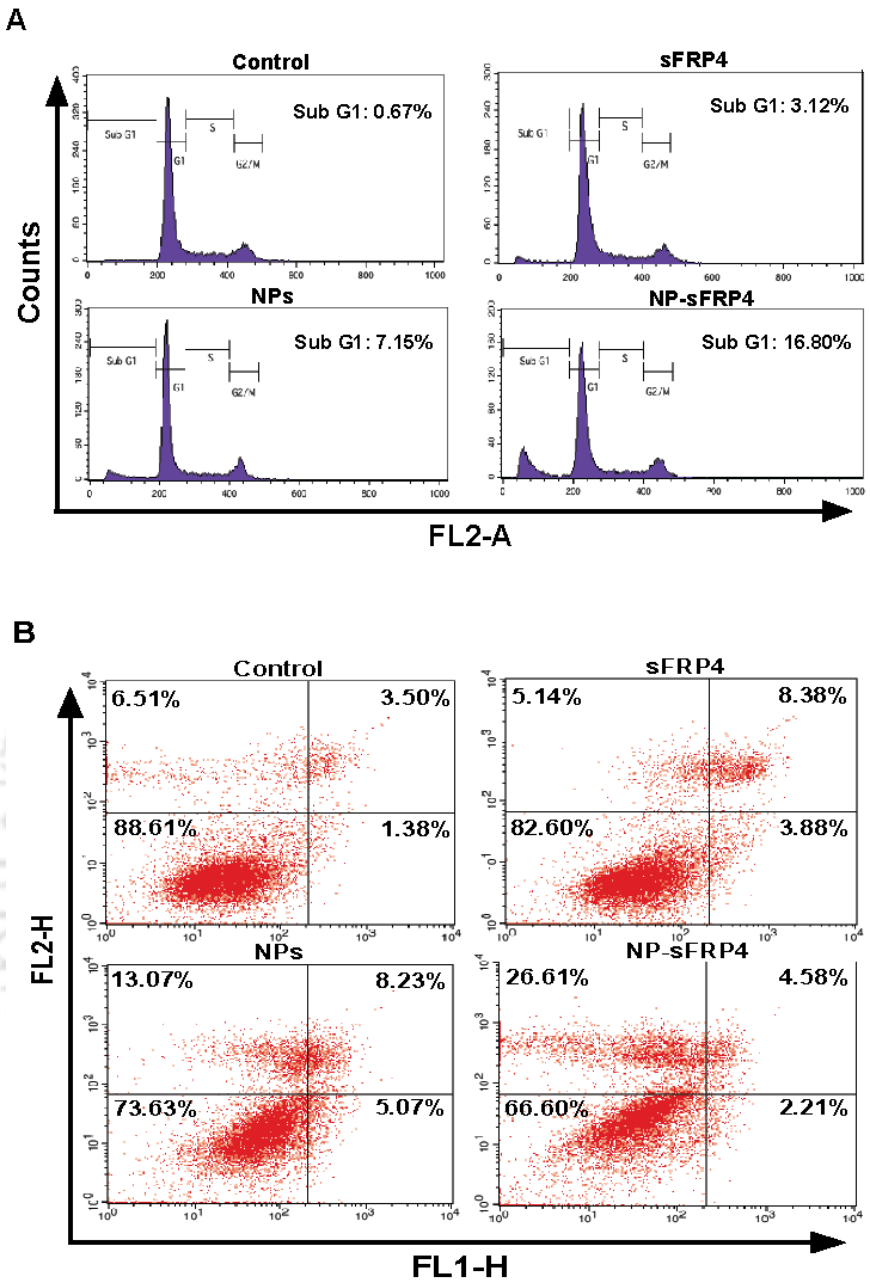

Figure 5.9. **(A)** Cell cycle analysis using PI recorded a significant increase in sub-G1 population in cells treated with NP-sFRP4, as compared to either sFRP4 or NPs individually, indicating apoptosis. **(B)** Annexin V-FITC/PI apoptosis detection assay also depicted a significantly higher population of apoptotic cells in NP-sFRP4-treated cells. These experiments demonstrated the co-therapeutic potential of sFRP4 and NPs in this nanosystem.

5.3.8 Co-therapeutic efficacy of sFRP4 bound NPs

In present regime, combination therapy plays a key role in cancer treatment. To overcome the undesirable side-effects of the chemical drugs currently available in the market, novel co-therapy regimes that can specifically target cancer cells are in the process of being developed. In this chapter, the co-therapeutic potential of the NP-sFRP4 nanosystem was documented. Several flow cytometry-based and microscopy-based assays helped to demonstrate the mechanism of cell death in co-therapy module. FACS-based analysis of cell cycle using PI (**Figure 5.9A**) unveiled that the sub-G1 population, which may be considered as an indicator of apoptosis, was significantly higher in NP-sFRP4-treated cells (16.8%), as compared to control (0.67%), sFRP4-treated (3.12%), or NP-treated cells (7.15%).

Further, FACS-based Annexin V-FITC/PI assay established apoptosis to be the mechanism of cell death (**Figure 5.9B**). The percentage of apoptotic cells was substantially higher in NP-sFRP4-treated cells (33.4%), versus that of control (11%), sFRP4-treated cells (17.5%) [187], and NP-treated cells (26%). These results are in accordance with a previous report, which showed that restoration of expression of sFRP4 in mesothelioma cells induced apoptotic cell death [187]. Also, silver nanoparticles have been proven to induce apoptosis in cancer cells [188].

Visual corroboration of apoptosis was done by dual staining with AO and EB (**Figure 5.10**). The images clearly demonstrated that co-therapy brought about intensive apoptotic cell death.

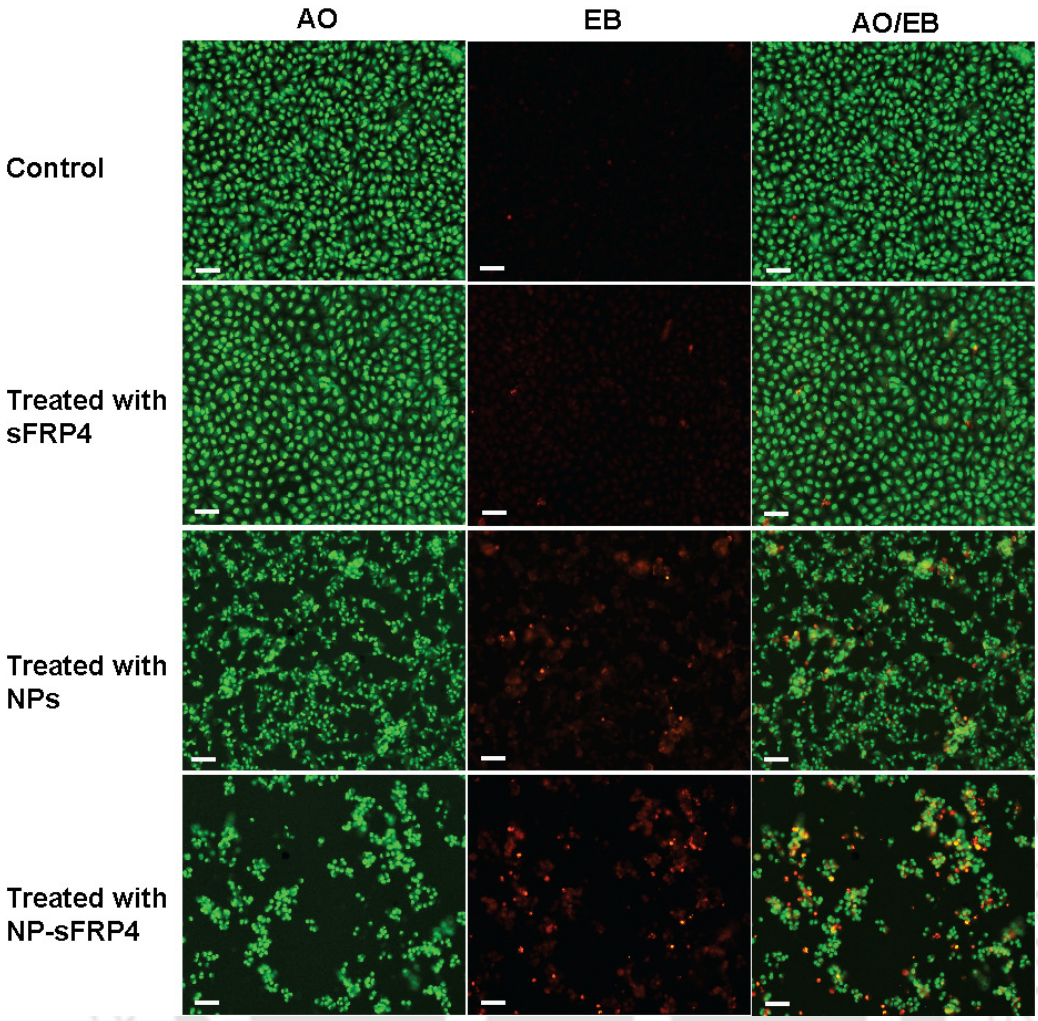

Figure 5.10. AO/EB dual staining of control cells and cells treated with sFRP4, NPs, and NP-sFRP4, respectively. Scale bar represents 100 µm.

This investigation initiates an innovative regimen in cancer theranostics, where recombinant therapeutic sFRP4 bound Ag NC-Chi-Alg NPs induced apoptosis in cervical cancer cells via Wnt/ β-catenin targeted cancer therapy. Moreover, the intense luminescence of the Ag NCs was utilized in imaging, uptake, and binding analyses. This report lays the foundation for *in vivo* studies, which could pave the way for clinical applications of the recombinant sFRP4 bound Ag NC-Chi-Alg NPs.

5.4 Conclusion

In summary, novel multifaceted theranostic recombinant sFRP4-bound Ag NC-Chitosan-Alginate NPs were fabricated to target downstream molecule of Wnt signaling in cancer cells. While chitosan and alginate could tune the size and surface charge of NPs, the remarkable luminescence of the Ag NCs enabled tracking, uptake, and imaging, thus imparting theranostic properties. Moreover, the low toxicity of the Ag NCs [189] ensure that they be possibly employed for *in vivo* therapy, unlike many other toxic nanoclusters [190]. The most intriguing aspect of this chapter was the targeting of the central molecule of active Wnt pathway in cancer cells with recombinant purified sFRP4 bound NPs. Interestingly, the bacterially expressed human sFRP4 retained its functionality post purification and binding, evidenced by its anti-proliferative activity and β–catenin regulation downstream of Wnt signaling. Therapeutic efficacy of the NP-sFRP4 has the potential to engender a new strategy for cancer co-therapy, where the advantages of protein therapy could be implemented to reduce the dosage of Ag NCs. In addition, this luminescence-based platform could lay the foundation for incorporating dynamic perspectives to the area of cancer theranostics. The independent successes of chemical inhibitors of the Wnt pathway [165, 166] as well as the noble metal nanoclusters in biological imaging [105, 189, 191] documented in *in vivo* models have led us to believe that this multifunctional system holds great promise for clinical translation.

CONCLUSION AND FUTURE PROSPECTS

CONCLUSION AND FUTURE PROSPECTS

A final discussion and conclusion of this thesis has been drawn in this section. The highlights of the work done, the significance of this study as well as the prospect of clinical translation of the research presented in this thesis have all been encompassed herein.

An extensive review of literature revealed the progress of research in the field of cancer therapy; more specifically, the prospect of protein therapy and the effectiveness of a repertoire of combination therapies were divulged. Taking into consideration the loopholes of current therapeutic modalities, the canonical Wnt/ β-catenin signaling pathway was targeted in cancer cells by natural inhibitors sFRP1 and sFRP4. These two human sFRP isoforms were cloned into bacterial expression vector pGEX-4T2 and expressed and affinity purified from *E. coli* by methods optimized in this study. It is germane to mention here that sFRP4 was cloned from a novel source- the ACHN (renal carcinoma) cell line. After careful confirmation of the authenticity of the clones by sequencing and restriction digestion, the identity of the subsequently purified and folded recombinant proteins was validated by MALDI-TOF/TOF, Western blot, and circular dichroism analyses. Initial efforts to produce sFRP using histidine tag-containing expression vector pET-28a was not successful. Hence it was assumed that the His tagged sFRP was not stable even for a brief period of time. This drawback was overcome by the GST tag, which possibly imparted stability to the recombinant proteins. Moreover, it was proved during the course of this investigation, that the GST tag itself did not have any effect on the growth of cancer cells, as evidenced by cell viability assays and docking studies. Cleaving of the GST tag using proteolytic enzyme thrombin resulted in very low yield of cleaved sFRP1, which was insufficient to bring about significant anti-proliferative effect on cancer cells. Hence, all further studies were pursued with GST tagged sFRPs.

In vitro cell culture model was employed to ascertain the anti-proliferative effects of the recombinant sFRP1 and sFRP4. HeLa, MCF-7, and A549 cells exhibited significant dose-dependent response upon treatment with either of the two sFRP isoforms. However, IC_{50} values were not attained with protein therapy alone, which could be due to parallel pathways

promoting cell proliferation. Also, it could be possible that blocking of the Wnt pathway inhibited cell proliferation, but did not cause significant cell death. To investigate these possibilities and effectuate an increased reduction in cell viability, further co-therapy experiments using anti-cancer drugs were designed. However, stable cell lines expressing SFRPs was not possible to establish due to enormous cell death post transfection.

The effect of the recombinant sFRPs on the canonical Wnt/ β-catenin signaling was established by Western blot as well as semi-quantitative and quantitative real-time PCR analyses. The expression of β-catenin, which is the central molecule of this pathway, was probed at the protein level. Cytosolic β-catenin was found to be degraded in treated cells, as evidenced by reduced levels of β-catenin and increased levels of phosphorylated β-catenin. Semi-quantitative as well as real-time PCR analyses displayed that downstream targets of β-catenin, viz., cyclin D1, survivin, and c-myc, were also downregulated by the recombinant sFRPs. Since these are pro-proliferative genes, it was concluded that inhibition of these genes engendered the anti-proliferative effect of the sFRPs. The effect of this action was manifested in the form of a G2/M arrest of the cell cycle.

Combination therapy was performed with sFRP and known chemotherapeutic drugs, cisplatin and doxorubicin, which substantially augmented the anti-cancer response of the cancer cells. This effect demonstrated that the cells were chemosensitized toward the drugs, possibly because the sFRPs arrested their growth and made them vulnerable to further treatment. The most crucial benefit derived from this combination therapy was the use of a very low dosage of drug, which would help to reduce their adverse side-effects. The mode of effect of these combination therapy modules was studied by various cell-based assays, which showed that a cell cycle arrest was followed by apoptotic cell death. Indication of apoptosis was observed in the flow cytometry-based cell cycle analysis of PI-stained cells. Apoptosis was further validated by flow cytometry-based Annexin V-FITC/PI assay and fluorescence microscopy-based AO/EB dual staining.

To enhance the stability of the recombinant proteins by achieving sustained release, nanocluster- embedded novel composite nanoparticle systems were fabricated. In this pursuit, biopolymers chitosan and alginate, the latter being FDA approved, were employed for the ease of maneuvering the size and surface charge of the system, according to the

requirements of this study. The remarkable luminescence of the gold and silver nanoclusters, described in Chapters 3 and 5, respectively, was exploited efficiently for binding, uptake, and bio-imaging studies. These multifunctional theranostic nanoparticle-systems brought about augmented anti-cancer responses in the *in vitro* cell culture models and significant apoptotic populations were observed. Additionally, the sFRP component of the nanoparticle systems was responsible for specific targeting of the aberrantly upregulated Wnt pathway in these cancer cells.

This thesis emphasizes on the anti-cancer potential of the recombinant sFRP1 and sFRP4 in clinical translation, alone and in combination therapy. Future prospects include the study of the efficacy of this system in *in vivo* and clinical samples. Targeting the Wnt signal cascade with the sFRPs may serve to combat cancer if exploited clinically.

REFERENCES

1. Leader B, Baca QJ and Golan DE (2008). Protein therapeutics: a summary and pharmacological classification. Nat Rev Drug Discov 7:21-39.

2. Mathé G, Amiel JL, Schwarzenberg L, Schneider M, Cattan A, Schlumberger JR, Hayat M and De Vassal F (1969). Active immunotherapy for acute lymphoblastic leukaemia. The Lancet 293:697-699.

3. Rosenberg SA (2014). IL-2: the first effective immunotherapy for human cancer. J Immunol 192:5451-8.

4. Chacon JA, Sarnaik AA, Chen JQ, Creasy C, Kale C, Robinson J, Weber J, Hwu P, Pilon-Thomas S and Radvanyi L (2015). Manipulating the tumor microenvironment ex vivo for enhanced expansion of tumor-infiltrating lymphocytes for adoptive cell therapy. Clin Cancer Res 21:611-21.

5. Ramu A, Glaubiger D and Fuks Z (1984). Reversal of Acquired Resistance to Doxorubicin in P388 Murine Leukemia Cells by Tamoxifen and Other Triparanol Analogues. Cancer Res 44:4392-4395.

6. O'Brien MER, Wigler N, Inbar M, Rosso R, Grischke E, Santoro A, Catane R, Kieback DG, Tomczak P, Ackland SP, Orlandi F, Mellars L, Alland L and Tendler C (2004). Reduced cardiotoxicity and comparable efficacy in a phase III trial of pegylated liposomal doxorubicin HCl (CAELYX™/Doxil®) versus conventional doxorubicin for first-line treatment of metastatic breast cancer. Ann Oncol 15:440-449.

7. Florea A-M and Büsselberg D (2011). Cisplatin as an Anti-Tumor Drug: Cellular Mechanisms of Activity, Drug Resistance and Induced Side Effects. Cancers 3:1351-1371.

8. Molina MA, Codony-Servat J, Albanell J, Rojo F, Arribas J and Baselga J (2001). Trastuzumab (herceptin), a humanized anti-Her2 receptor monoclonal antibody, inhibits basal and activated Her2 ectodomain cleavage in breast cancer cells. Cancer Res 61:4744-9.

9. Kabbinavar F, Hurwitz HI, Fehrenbacher L, Meropol NJ, Novotny WF, Lieberman G, Griffing S and Bergsland E (2003). Phase II, randomized trial comparing bevacizumab plus fluorouracil (FU)/leucovorin (LV) with FU/LV alone in patients with metastatic colorectal cancer. J Clin Oncol 21:60-5.

10. Yang XD, Jia XC, Corvalan JR, Wang P, Davis CG and Jakobovits A (1999). Eradication of established tumors by a fully human monoclonal antibody to the epidermal growth factor receptor without concomitant chemotherapy. Cancer Res 59:1236-43.

11. Cunningham D, Humblet Y, Siena S, Khayat D, Bleiberg H, Santoro A, Bets D, Mueser M, Harstrick A, Verslype C, Chau I and Van Cutsem E (2004). Cetuximab Monotherapy and Cetuximab plus Irinotecan in Irinotecan-Refractory Metastatic Colorectal Cancer. New Engl J Med 351:337-345.

12. Slamon DJ, Leyland-Jones B, Shak S, Fuchs H, Paton V, Bajamonde A, Fleming T, Eiermann W, Wolter J, Pegram M, Baselga J and Norton L (2001). Use of Chemotherapy plus a Monoclonal Antibody against HER2 for Metastatic Breast Cancer That Overexpresses HER2. New Engl J Med 344:783-792.

13. Vogel CL, Cobleigh MA, Tripathy D, Gutheil JC, Harris LN, Fehrenbacher L, Slamon DJ, Murphy M, Novotny WF, Burchmore M, Shak S, Stewart SJ and Press M (2002). Efficacy and Safety of Trastuzumab as a Single Agent in First-Line Treatment of HER2-Overexpressing Metastatic Breast Cancer. J Clin Oncol 20:719-726.

14. Ferrara N, Hillan KJ, Gerber H-P and Novotny W (2004). Discovery and development of bevacizumab, an anti-VEGF antibody for treating cancer. Nat Rev Drug Discov 3:391-400.

15. Yang JC, Haworth L, Sherry RM, Hwu P, Schwartzentruber DJ, Topalian SL, Steinberg SM, Chen HX and Rosenberg SA (2003). A randomized trial of bevacizumab, an anti-vascular endothelial growth factor antibody, for metastatic renal cancer. N Engl J Med 349:427-34.

16. Wainberg Z and Hecht JR (2006). A phase III randomized, open-label, controlled trial of chemotherapy and bevacizumab with or without panitumumab in the first-line treatment of patients with metastatic colorectal cancer. Clin Colorectal Cancer 5:363-7.

17. Scott AM, Wolchok JD and Old LJ (2012). Antibody therapy of cancer. Nat Rev Cancer 12:278-287.

18. Rachel H. Giles JHvE, Hans Clevers (2003). Caught up in a Wnt storm: Wnt signaling in cancer. Biochim Biophys Acta 1653:1-24.

19. Anastas JN and Moon RT (2013). WNT signalling pathways as therapeutic targets in cancer. Nat Rev Cancer 13:11-26.

20. King TD, Zhang W, Suto MJ and Li Y (2012). Frizzled7 as an emerging target for cancer therapy. Cell Signal 24:846-51.

21. Lustig B and Behrens J (2003). The Wnt signaling pathway and its role in tumor development. J Cancer Res Clin 129:199-221.

22. Zhang T, Otevrel T, Gao Z, Gao Z, Ehrlich SM, Fields JZ and Boman BM (2001). Evidence that APC regulates survivin expression: a possible mechanism contributing to the stem cell origin of colon cancer. Cancer Res 61:8664-7.

23. Tetsu O and McCormick F (1999). Beta-catenin regulates expression of cyclin D1 in colon carcinoma cells. Nature 398:422-6.

24. He TC, Sparks AB, Rago C, Hermeking H, Zawel L, da Costa LT, Morin PJ, Vogelstein B and Kinzler KW (1998). Identification of c-MYC as a target of the APC pathway. Science 281:1509-12.

25. Mann B, Gelos M, Siedow A, Hanski ML, Gratchev A, Ilyas M, Bodmer WF, Moyer MP, Riecken EO, Buhr HJ and Hanski C (1999). Target genes of beta-catenin-T cell-factor/lymphoid-enhancer-factor signaling in human colorectal carcinomas. Proc Natl Acad Sci U S A 96:1603-8.

26. Huang S, Zhong X, Gao J, Song R, Wu H, Zi S, Yang S, Du P, Cui L, Yang C and Li Z (2014). Coexpression of SFRP1 and WIF1 as a prognostic predictor of favorable outcomes in patients with colorectal carcinoma. Biomed Res Int 2014:256723.

27. Ghoshal A and Ghosh SS (2015). Expression, Purification, and Therapeutic Implications of Recombinant sFRP1. Appl Biochem Biotechnol 175:2087-103.

28. Dow Lukas E, O'Rourke Kevin P, Simon J, Tschaharganeh Darjus F, van Es Johan H, Clevers H and Lowe Scott W (2015). Apc Restoration Promotes Cellular Differentiation and Reestablishes Crypt Homeostasis in Colorectal Cancer. Cell 161:1539-1552.

29. Lee AY, He B, You L, Dadfarmay S, Xu Z, Mazieres J, Mikami I, McCormick F and Jablons DM (2004). Expression of the secreted frizzled-related protein gene family is downregulated in human mesothelioma. Oncogene 23:6672-6.

30. Suzuki H, Gabrielson E, Chen W, Anbazhagan R, van Engeland M, Weijenberg MP, Herman JG and Baylin SB (2002). A genomic screen for genes upregulated by demethylation and histone deacetylase inhibition in human colorectal cancer. Nat Genet 31:141-9.

31. Marsit CJ, Karagas MR, Andrew A, Liu M, Danaee H, Schned AR, Nelson HH and Kelsey KT (2005). Epigenetic inactivation of SFRP genes and TP53 alteration act jointly as markers of invasive bladder cancer. Cancer Res 65:7081-5.

32. Hu E, Zhu Y, Fredrickson T, Barnes M, Kelsell D, Beeley L and Brooks D (1998). Tissue restricted expression of two human Frzbs in preadipocytes and pancreas. Biochem Biophys Res Commun 247:287-93.

33. Surana R, Sikka S, Cai W, Shin EM, Warrier SR, Tan HJ, Arfuso F, Fox SA, Dharmarajan AM and Kumar AP (2014). Secreted frizzled related proteins: Implications in cancers. Biochim Biophys Acta 1845:53-65.

34. Finch PW, He X, Kelley MJ, Uren A, Varmus HE and Rubin JS (1997). Purification and molecular cloning of a secreted, Frizzled-related antagonist of Wnt action. Proc Natl Acad Sci U S A 94:6770-6775.

35. Nojima M, Suzuki H, Toyota M, Watanabe Y, Maruyama R, Sasaki S, Sasaki Y, Mita H, Nishikawa N, Yamaguchi K, Hirata K, Itoh F, Tokino T, Mori M, Imai K and Shinomura Y (2007). Frequent epigenetic inactivation of SFRP genes and constitutive activation of Wnt signaling in gastric cancer. Oncogene 26:4699-713.

36. Zhou Z, Wang J, Han X, Zhou J and Linder S (1998). Up-regulation of human secreted frizzled homolog in apoptosis and its down-regulation in breast tumors. Int J Cancer 78:95-9.

37. Rubin JS, Barshishat-Kupper M, Feroze-Merzoug F and Xi ZF (2006). Secreted WNT antagonists as tumor suppressors: pro and con. Front Biosci 11:2093-105.

38. Mii Y and Taira M (2009). Secreted Frizzled-related proteins enhance the diffusion of Wnt ligands and expand their signalling range. Development 136:4083-4088.

39. von Marschall Z and Fisher LW (2010). Secreted Frizzled-related protein-2 (sFRP2) augments canonical Wnt3a-induced signaling. Biochem Bioph Res Co 400:299-304.

40. Fukui T, Kondo M, Ito G, Maeda O, Sato N, Yoshioka H, Yokoi K, Ueda Y, Shimokata K and Sekido Y (2005). Transcriptional silencing of secreted frizzled related protein 1 (SFRP 1) by promoter hypermethylation in non-small-cell lung cancer. Oncogene 24:6323-7.

41. Shih YL, Hsieh CB, Lai HC, Yan MD, Hsieh TY, Chao YC and Lin YW (2007). SFRP1 suppressed hepatoma cells growth through Wnt canonical signaling pathway. Int J Cancer 121:1028-35.

42. Dharmarajan A, McLaren S, White E and Zeps N (2006). Expression of secreted frizzled related protein-4 (sFRP-4) and associated Wnt signalling in breast cancer. Cancer Res 66:1238.

43. Lisa G. Horvath SMH, James G. Kench, et al. (2004). Membranous Expression of Secreted Frizzled-Related Protein 4 Predicts for Good Prognosis in Localized Prostate Cancer and Inhibits PC3 Cellular Proliferation in Vitro. Clin Cancer Res 10:615-625.

44. Urakami S, Shiina H, Enokida H, Hirata H, Kawamoto K, Kawakami T, Kikuno N, Tanaka Y, Majid S, Nakagawa M, Igawa M and Dahiya R (2006). Wnt antagonist family genes as biomarkers for diagnosis, staging, and prognosis of renal cell carcinoma using tumor and serum DNA. Clin Cancer Res 12:6989-97.

45. Suzuki H, Watkins DN, Jair KW, Schuebel KE, Markowitz SD, Chen WD, Pretlow TP, Yang B, Akiyama Y, Van Engeland M, Toyota M, Tokino T, Hinoda Y, Imai K, Herman JG and Baylin SB (2004). Epigenetic inactivation of SFRP genes allows constitutive WNT signaling in colorectal cancer. Nat Genet 36:417-22.

46. Longman D, Arfuso F, Viola HM, Hool LC and Dharmarajan AM (2012). The role of the cysteine-rich domain and netrin-like domain of secreted frizzled-related protein 4 in angiogenesis inhibition in vitro. Oncol Res 20:1-6.

47. Lopez-Rios J, Esteve P, Ruiz JM and Bovolenta P (2008). The Netrin-related domain of Sfrp1 interacts with Wnt ligands and antagonizes their activity in the anterior neural plate. Neural Dev 3:19.

48. Jones SE and Jomary C (2002). Secreted Frizzled-related proteins: searching for relationships and patterns. Bioessays 24:811-20.

49. Dann CE, Hsieh JC, Rattner A, Sharma D, Nathans J and Leahy DJ (2001). Insights into Wnt binding and signalling from the structures of two Frizzled cysteine-rich domains. Nature 412:86-90.

50. Yang ZQ, Liu G, Bollig-Fischer A, Haddad R, Tarca AL and Ethier SP (2009). Methylation-associated silencing of SFRP1 with an 8p11-12 amplification inhibits canonical and non-canonical WNT pathways in breast cancers. Int J Cancer 125:1613-21.

51. Maganga R, Giles N, Adcroft K, Unni A, Keeney D, Wood F, Fear M and Dharmarajan A (2008). Secreted Frizzled related protein-4 (sFRP4) promotes epidermal differentiation and apoptosis. Biochem Biophys Res Commun 377:606-11.

52. Ho YP and Leong KW (2010). Quantum dot-based theranostics. Nanoscale 2:60-8.

53. Janib SM, Moses AS and MacKay JA (2010). Imaging and drug delivery using theranostic nanoparticles. Adv Drug Deliver Rev 62:1052-1063.

54. Cheng K, Peng S, Xu C and Sun S (2009). Porous Hollow Fe3O4 Nanoparticles for Targeted Delivery and Controlled Release of Cisplatin. J Am Chem Soc 131:10637-10644.

55. Medarova Z, Pham W, Farrar C, Petkova V and Moore A (2007). In vivo imaging of siRNA delivery and silencing in tumors. Nat Med 13:372-377.

56. Lee JH, Lee K, Moon SH, Lee Y, Park TG and Cheon J (2009). All-in-one target-cell-specific magnetic nanoparticles for simultaneous molecular imaging and siRNA delivery. Angew Chem Int Ed Engl 48:4174-9.

57. Khandelia R, Jaiswal A, Ghosh SS and Chattopadhyay A (2013). Gold nanoparticle-protein agglomerates as versatile nanocarriers for drug delivery. Small 9:3494-505.

58. Cai W and Chen X (2008). Multimodality molecular imaging of tumor angiogenesis. J Nucl Med 49 Suppl 2:113s-28s.

59. Richardson TP, Murphy WL and Mooney DJ (2001). Polymeric delivery of proteins and plasmid DNA for tissue engineering and gene therapy. Crit Rev Eukaryot Gene Expr 11:47-58.

60. Couvreur P (2013). Nanoparticles in drug delivery: Past, present and future. Adv Drug Deliver Rev 65:21-23.

61. Sharma S, Chockalingam S, Sanpui P, Chattopadhyay A and Ghosh SS (2014). Silver nanoparticles impregnated alginate-chitosan-blended nanocarrier induces apoptosis in human glioblastoma cells. Adv Healthc Mater 3:106-14.

62. Anal AK, Bhopatkar D, Tokura S, Tamura H and Stevens WF (2003). Chitosan-alginate multilayer beads for gastric passage and controlled intestinal release of protein. Drug Dev Ind Pharm 29:713-24.

63. Singh AK, Hahn MA, Gutwein LG, Rule MC, Knapik JA, Moudgil BM, Grobmyer SR and Brown SC (2012). Multi-dye theranostic nanoparticle platform for bioimaging and cancer therapy. Int J Nanomedicine 7:2739-2750.

64. Bardhan R, Lal S, Joshi A and Halas NJ (2011). Theranostic Nanoshells: From Probe Design to Imaging and Treatment of Cancer. Accounts Chem Res 44:936-946.

65. Diez I and Ras RHA (2011). Fluorescent silver nanoclusters. Nanoscale 3:1963-1970.

66. Zhen Z, Tang W, Chen H, Lin X, Todd T, Wang G, Cowger T, Chen X and Xie J (2013). RGD-Modified Apoferritin Nanoparticles for Efficient Drug Delivery to Tumors. ACS Nano 7:4830-4837.

67. Gu Z, Biswas A, Zhao M and Tang Y (2011). Tailoring nanocarriers for intracellular protein delivery. Chem Soc Rev 40:3638-3655.

68. Banerjee S, Sahoo AK, Chattopadhyay A and Ghosh SS (2013). Hydrogel nanocarrier encapsulated recombinant I[small kappa]B[small alpha] as a novel anticancer protein therapeutics. RSC Adv 3:14123-14131.

69. Chaubey N, Sahoo AK, Chattopadhyay A and Ghosh SS (2014). Silver nanoparticle loaded PLGA composite nanoparticles for improving therapeutic efficacy of recombinant IFN[gamma] by targeting the cell surface. Biomater Sci 2:1080-1089.

70. Kim CS, Mout R, Zhao Y, Yeh Y-C, Tang R, Jeong Y, Duncan B, Hardy JA and Rotello VM (2015). Co-Delivery of Protein and Small Molecule Therapeutics Using Nanoparticle-Stabilized Nanocapsules. Bioconjugate Chem 26:950-954.

71. Wang M, Alberti K, Sun S, Arellano CL and Xu Q (2014). Combinatorially Designed Lipid-like Nanoparticles for Intracellular Delivery of Cytotoxic Protein for Cancer Therapy. Angew Chem 126:2937-2942.

72. Mu Q, Kievit FM, Kant RJ, Lin G, Jeon M and Zhang M (2015). Anti-HER2/neu peptide-conjugated iron oxide nanoparticles for targeted delivery of paclitaxel to breast cancer cells. Nanoscale 7:18010-18014.

73. Shi Y, Zhou M, Zhang J and Lu W (2015). Preparation and cellular targeting study of VEGF-conjugated PLGA nanoparticles. J Microencapsul 32:699-704.

74. Cui Y, Xu Q, Chow PK-H, Wang D and Wang C-H (2013). Transferrin-conjugated magnetic silica PLGA nanoparticles loaded with doxorubicin and paclitaxel for brain glioma treatment. Biomaterials 34:8511-8520.

75. Porta F, Lamers GEM, Morrhayim J, Chatzopoulou A, Schaaf M, den Dulk H, Backendorf C, Zink JI and Kros A (2013). Folic Acid-Modified Mesoporous Silica Nanoparticles for Cellular and Nuclear Targeted Drug Delivery. Adv Healthc Mater 2:281-286.

76. Bhattacharyya J, Bellucci JJ, Weitzhandler I, McDaniel JR, Spasojevic I, Li X, Lin C-C, Chi J-TA and Chilkoti A (2015). A paclitaxel-loaded recombinant polypeptide nanoparticle outperforms Abraxane in multiple murine cancer models. Nat Commun 6:8904.

77. Shi P, Aluri S, Lin Y-A, Shah M, Edman M, Dhandhukia J, Cui H and MacKay JA (2013). Elastin-based protein polymer nanoparticles carrying drug at both corona and core suppress tumor growth in vivo. J Control Release 171:330-338.

78. Caldwell GM, Jones C, Gensberg K, Jan S, Hardy RG, Byrd P, Chughtai S, Wallis Y, Matthews GM and Morton DG (2004). The Wnt antagonist sFRP1 in colorectal tumorigenesis. Cancer Res 64:883-8.

79. Veeck J, Niederacher D, An H, Klopocki E, Wiesmann F, Betz B, Galm O, Camara O, Durst M, Kristiansen G, Huszka C, Knuchel R and Dahl E (2006). Aberrant methylation

of the Wnt antagonist SFRP1 in breast cancer is associated with unfavourable prognosis. Oncogene 25:3479-88.

80. Takada T, Yagi Y, Maekita T, Imura M, Nakagawa S, Tsao SW, Miyamoto K, Yoshino O, Yasugi T, Taketani Y and Ushijima T (2004). Methylation-associated silencing of the Wnt antagonist SFRP1 gene in human ovarian cancers. Cancer Sci 95:741-4.

81. Joesting MS, Perrin S, Elenbaas B, Fawell SE, Rubin JS, Franco OE, Hayward SW, Cunha GR and Marker PC (2005). Identification of SFRP1 as a candidate mediator of stromal-to-epithelial signaling in prostate cancer. Cancer Res 65:10423-30.

82. Qu Y, Ray PS, Li J, Cai Q, Bagaria SP, Moran C, Sim MS, Zhang J, Turner RR, Zhu Z, Cui X and Liu B (2013). High levels of secreted frizzled-related protein 1 correlate with poor prognosis and promote tumourigenesis in gastric cancer. Eur J Cancer 49:3718-28.

83. Kelley LA and Sternberg MJ (2009). Protein structure prediction on the Web: a case study using the Phyre server. Nat Protoc 4:363-71.

84. Zhang Y (2008). I-TASSER server for protein 3D structure prediction. BMC Bioinformatics 9:40.

85. Roy A, Kucukural A and Zhang Y (2010). I-TASSER: a unified platform for automated protein structure and function prediction. Nat. Protocols 5:725-738.

86. Roy A, Yang J and Zhang Y (2012). COFACTOR: an accurate comparative algorithm for structure-based protein function annotation. Nucleic Acids Res 40:W471-W477.

87. Tardito S, Isella C, Medico E, Marchio L, Bevilacqua E, Hatzoglou M, Bussolati O and Franchi-Gazzola R (2009). The thioxotriazole copper(II) complex A0 induces endoplasmic reticulum stress and paraptotic death in human cancer cells. J Biol Chem 284:24306-19.

88. Lu DY, Huang M, Xu CH, Yang WY, Hu CX, Lin LP, Tong LJ, Li MH, Lu W, Zhang XW and Ding J (2005). Anti-proliferative effects, cell cycle G2/M phase arrest and

blocking of chromosome segregation by probimane and MST-16 in human tumor cell lines. BMC Pharmacol 5:11.

89. Ferrer-Miralles N, Domingo-Espin J, Corchero J, Vazquez E and Villaverde A (2009). Microbial factories for recombinant pharmaceuticals. Microb Cell Factor 8:17.

90. Mercado-Pimentel ME, Jordan NC and Aisemberg GO (2002). Affinity purification of GST fusion proteins for immunohistochemical studies of gene expression. Protein Expr Purif 26:260-5.

91. Schwanke RC, Renard G, Chies JM, Campos MM, Batista EL, Jr., Santos DS and Basso LA (2009). Molecular cloning, expression in Escherichia coli and production of bioactive homogeneous recombinant human granulocyte and macrophage colony stimulating factor. Int J Biol Macromol 45:97-102.

92. Tsumoto K, Ejima D, Kumagai I and Arakawa T (2003). Practical considerations in refolding proteins from inclusion bodies. Protein Expr Purif 28:1-8.

93. Park DW, Kim SS, Nam MK, Kim GY, Kim J and Rhim H (2011). Improved recovery of active GST-fusion proteins from insoluble aggregates: solubilization and purification conditions using PKM2 and HtrA2 as model proteins. BMB Rep 44:279-84.

94. Achilonu I, Siganunu TP and Dirr HW (2014). Purification and characterisation of recombinant human eukaryotic elongation factor 1 gamma. Protein Expr Purif 99C:70-77.

95. James P, Quadroni M, Carafoli E and Gonnet G (1993). Protein identification by mass profile fingerprinting. Biochem Biophys Res Commun 195:58-64.

96. Pappin DJ, Hojrup P and Bleasby AJ (1993). Rapid identification of proteins by peptide-mass fingerprinting. Curr Biol 3:327-32.

97. Fang HL, Yu ZC, Zhu HB and Jin YT (2012). Effects of 5-Aza-2-deoxycytidine on DNA methylation of anti-oncogenes in non-small cell lung cancer cells. Zhonghua Zhong Liu Za Zhi 34:658-63.

98. Saran U, Arfuso F, Zeps N and Dharmarajan A (2012). Secreted frizzled-related protein 4 expression is positively associated with responsiveness to cisplatin of ovarian cancer cell lines in vitro and with lower tumour grade in mucinous ovarian cancers. BMC Cell Biol 13:25.

99. Ghosh R, Goswami U, Ghosh SS, Paul A and Chattopadhyay A (2015). Synergistic Anticancer Activity of Fluorescent Copper Nanoclusters and Cisplatin Delivered through a Hydrogel Nanocarrier. ACS Appl Mater Interfaces 7:209-22.

100. Ma LL, Feldman MD, Tam JM, Paranjape AS, Cheruku KK, Larson TA, Tam JO, Ingram DR, Paramita V, Villard JW, Jenkins JT, Wang T, Clarke GD, Asmis R, Sokolov K, Chandrasekar B, Milner TE and Johnston KP (2009). Small multifunctional nanoclusters (nanoroses) for targeted cellular imaging and therapy. ACS Nano 3:2686-96.

101. Bian P, Zhou J, Liu Y and Ma Z (2013). One-step fabrication of intense red fluorescent gold nanoclusters and their application in cancer cell imaging. Nanoscale 5:6161-6.

102. Shiang Y-C, Huang C-C, Chen W-Y, Chen P-C and Chang H-T (2012). Fluorescent gold and silver nanoclusters for the analysis of biopolymers and cell imaging. J Mater Chem 22:12972-12982.

103. Tian D, Qian Z, Xia Y and Zhu C (2012). Gold Nanocluster-Based Fluorescent Probes for Near-Infrared and Turn-On Sensing of Glutathione in Living Cells. Langmuir 28:3945-3951.

104. Retnakumari A, Setua S, Menon D, Ravindran P, Muhammed H, Pradeep T, Nair S and Koyakutty M (2010). Molecular-receptor-specific, non-toxic, near-infrared-emitting Au cluster-protein nanoconjugates for targeted cancer imaging. Nanotechnology 21:055103.

105. Wu X, He X, Wang K, Xie C, Zhou B and Qing Z (2010). Ultrasmall near-infrared gold nanoclusters for tumor fluorescence imaging in vivo. Nanoscale 2:2244-9.

106. Wang C, Li J, Amatore C, Chen Y, Jiang H and Wang X-M (2011). Gold Nanoclusters and Graphene Nanocomposites for Drug Delivery and Imaging of Cancer Cells. Angew Chem Int Edit 50:11644-11648.

107. Lin C-AJ, Yang T-Y, Lee C-H, Huang SH, Sperling RA, Zanella M, Li JK, Shen J-L, Wang H-H, Yeh H-I, Parak WJ and Chang WH (2009). Synthesis, Characterization, and Bioconjugation of Fluorescent Gold Nanoclusters toward Biological Labeling Applications. ACS Nano 3:395-401.

108. Bian P, Zhou J, Liu Y and Ma Z (2013). One-step fabrication of intense red fluorescent gold nanoclusters and their application in cancer cell imaging. Nanoscale 5:6161-6166.

109. Sahoo AK, Banerjee S, Ghosh SS and Chattopadhyay A (2014). Simultaneous RGB Emitting Au Nanoclusters in Chitosan Nanoparticles for Anticancer Gene Theranostics. ACS Appl Mater Interfaces 6:712-724.

110. Zhang X-D, Chen J, Luo Z, Wu D, Shen X, Song S-S, Sun Y-M, Liu P-X, Zhao J, Huo S, Fan S, Fan F, Liang X-J and Xie J (2014). Radiosensitizers: Enhanced Tumor Accumulation of Sub-2 nm Gold Nanoclusters for Cancer Radiation Therapy. Adv Healthc Mater 3:152-152.

111. Zhang A, Tu Y, Qin S, Li Y, Zhou J, Chen N, Lu Q and Zhang B (2012). Gold nanoclusters as contrast agents for fluorescent and X-ray dual-modality imaging. J Colloid Interface Sci 372:239-44.

112. Chen AM, Zhang M, Wei D, Stueber D, Taratula O, Minko T and He H (2009). Co-delivery of Doxorubicin and Bcl-2 siRNA by Mesoporous Silica Nanoparticles Enhances the Efficacy of Chemotherapy in Multidrug-Resistant Cancer Cells. Small 5:2673-2677.

113. Solal-Céligny P, Lepage E, Brousse N, Tendler CL, Brice P, Haïoun C, Gabarre J, Pignon B, Tertian G, Bouabdallah R, Rossi JF, Doyen C and Coiffier B (1998). Doxorubicin-containing regimen with or without interferon alfa-2b for advanced follicular lymphomas:

final analysis of survival and toxicity in the Groupe d'Etude des Lymphomes Folliculaires 86 Trial. J Clin Oncol 16:2332-8.

114. Cho K, Wang X, Nie S, Chen Z and Shin DM (2008). Therapeutic Nanoparticles for Drug Delivery in Cancer. Clin Cancer Res 14:1310-1316.

115. Leamon CP and Reddy JA (2004). Folate-targeted chemotherapy. Adv Drug Deliv Rev 56:1127-41.

116. Qian ZM, Li H, Sun H and Ho K (2002). Targeted drug delivery via the transferrin receptor-mediated endocytosis pathway. Pharmacol Rev 54:561-87.

117. Lakowicz JR (2006) Principles of Fluorescence Spectroscopy. Springer, New York.

118. Ugolini F, Charafe-Jauffret E, Bardou VJ, Geneix J, Adelaide J, Labat-Moleur F, Penault-Llorca F, Longy M, Jacquemier J, Birnbaum D and Pebusque MJ (2001). WNT pathway and mammary carcinogenesis: loss of expression of candidate tumor suppressor gene SFRP1 in most invasive carcinomas except of the medullary type. Oncogene 20:5810-7.

119. Liu C, Li NAN, Lu H, Wang Z, Chen C, Wu LIN, Liu J, Lu Y and Wang F (2015). Circulating SFRP1 promoter methylation status in gastric adenocarcinoma and esophageal square cell carcinoma. Biomed Rep 3:123-127.

120. Ricketts CJ, Hill VK and Linehan WM (2014). Tumor-Specific Hypermethylation of Epigenetic Biomarkers, Including <italic>SFRP1</italic>, Predicts for Poorer Survival in Patients from the TCGA Kidney Renal Clear Cell Carcinoma (KIRC) Project. PLoS ONE 9:e85621.

121. Albanese A, Tang PS and Chan WC (2012). The effect of nanoparticle size, shape, and surface chemistry on biological systems. Annu Rev Biomed Eng 14:1-16.

122. Remuñán-López C and Bodmeier R (1997). Mechanical, water uptake and permeability properties of crosslinked chitosan glutamate and alginate films. J Control Release 44:215-225.

123. Xavier Le G, Nicole D and Marc S (2011). Synthesis and characterization of human transferrin-stabilized gold nanoclusters. Nanotechnology 22:275103.

124. Vernejoul F, Ghenassia L, Souque A, Lulka H, Drocourt D, Cordelier P, Pradayrol L, Pyronnet S, Buscail L and Tiraby G (2006). Gene Therapy Based on Gemcitabine Chemosensitization Suppresses Pancreatic Tumor Growth. Mol Ther 14:758-767.

125. Fine HA, Dear KBG, Loeffler JS, Mc Black PL and Canellos GP (1993). Meta-analysis of radiation therapy with and without adjuvant chemotherapy for malignant gliomas in adults. Cancer 71:2585-2597.

126. James ND, Hussain SA, Hall E, Jenkins P, Tremlett J, Rawlings C, Crundwell M, Sizer B, Sreenivasan T, Hendron C, Lewis R, Waters R and Huddart RA (2012). Radiotherapy with or without Chemotherapy in Muscle-Invasive Bladder Cancer. New England Journal of Medicine 366:1477-1488.

127. Moore DH, Ali S, Koh W-J, Michael H, Barnes MN, McCourt CK, Homesley HD and Walker JL (2012). A phase II trial of radiation therapy and weekly cisplatin chemotherapy for the treatment of locally-advanced squamous cell carcinoma of the vulva: A gynecologic oncology group study. Gynecologic Oncology 124:529-533.

128. Cairncross G, Berkey B, Shaw E, Jenkins R, Scheithauer B, Brachman D, Buckner J, Fink K, Souhami L, Laperierre N, Mehta M and Curran W (2006). Phase III Trial of Chemotherapy Plus Radiotherapy Compared With Radiotherapy Alone for Pure and Mixed Anaplastic Oligodendroglioma: Intergroup Radiation Therapy Oncology Group Trial 9402. Journal of Clinical Oncology 24:2707-2714.

129. Peters WA, Liu PY, Barrett RJ, Stock RJ, Monk BJ, Berek JS, Souhami L, Grigsby P, Gordon W and Alberts DS (2000). Concurrent Chemotherapy and Pelvic Radiation Therapy Compared With Pelvic Radiation Therapy Alone as Adjuvant Therapy After Radical Surgery in High-Risk Early-Stage Cancer of the Cervix. J Clin Oncol 18:1606-1613.

130. Miles D, von Minckwitz G and Seidman AD (2002). Combination versus sequential single-agent therapy in metastatic breast cancer. Oncologist 7 Suppl 6:13-9.

131. Sorenson CM, Barry MA and Eastman A (1990). Analysis of Events Associated With Cell Cycle Arrest at G2 Phase and Cell Death Induced by Cisplatin. J Natl Cancer Inst 82:749-755.

132. Ju SM, Pae HO, Kim WS, Kang DG, Lee HS and Jeon BH (2014). Role of reactive oxygen species in p53 activation during cisplatin-induced apoptosis of rat mesangial cells. Eur Rev Med Pharmacol Sci 18:1135-41.

133. Pohl S, Scott R, Arfuso F, Perumal V and Dharmarajan A (2015). Secreted frizzled-related protein 4 and its implications in cancer and apoptosis. Tumour Biol 36:143-52.

134. Carmen J. Marsit MRK, Angeline Andrew, et al. (2005). Epigenetic Inactivation of SFRP Genes and TP53 Alteration Act Jointly as Markers of Invasive Bladder Cancer. Cancer Res 65:7081-7085.

135. Brebi P, Hoffstetter R, Andana A, Ili CG, Saavedra K, Viscarra T, Retamal J, Sanchez R and Roa JC (2014). Evaluation of ZAR1 and SFRP4 methylation status as potentials biomarkers for diagnosis in cervical cancer: exploratory study phase I. Biomarkers 19:181-8.

136. Jacob F, Ukegjini K, Nixdorf S, Ford CE, Olivier J, Caduff R, Scurry JP, Guertler R, Hornung D, Mueller R, Fink DA, Hacker NF and Heinzelmann-Schwarz VA (2012). Loss of Secreted Frizzled-Related Protein 4 Correlates with an Aggressive Phenotype and Predicts Poor Outcome in Ovarian Cancer Patients. PLoS ONE 7:e31885.

137. Huang D, Yu B, Deng Y, Sheng W, Peng Z, Qin W and Du X (2010). SFRP4 was overexpressed in colorectal carcinoma. J Cancer Res Clin Oncol 136:395-401.

138. Warrier S, Balu SK, Kumar AP, Millward M and Dharmarajan A (2013). Wnt antagonist, secreted frizzled-related protein 4 (sFRP4), increases chemotherapeutic response of glioma stem-like cells. Oncol Res 21:93-102.

139. Carmon KS and Loose DS (2008). Secreted frizzled-related protein 4 regulates two Wnt7a signaling pathways and inhibits proliferation in endometrial cancer cells. Mol Cancer Res 6:1017-28.

140. Kozakov D, Beglov D, Bohnuud T, Mottarella SE, Xia B, Hall DR and Vajda S (2013). How good is automated protein docking? Proteins 81:2159-66.

141. Kozakov D, Brenke R, Comeau SR and Vajda S (2006). PIPER: an FFT-based protein docking program with pairwise potentials. Proteins 65:392-406.

142. Comeau SR, Gatchell DW, Vajda S and Camacho CJ (2004). ClusPro: an automated docking and discrimination method for the prediction of protein complexes. Bioinformatics 20:45-50.

143. Comeau SR, Gatchell DW, Vajda S and Camacho CJ (2004). ClusPro: a fully automated algorithm for protein-protein docking. Nucleic Acids Res 32:W96-9.

144. Laskowski RA, Hutchinson EG, Michie AD, Wallace AC, Jones ML and Thornton JM (1997). PDBsum: a Web-based database of summaries and analyses of all PDB structures. Trends Biochem Sci 22:488-90.

145. Laskowski RA (2001). PDBsum: summaries and analyses of PDB structures. Nucleic Acids Res 29:221-2.

146. Huang SM, Mishina YM, Liu S, Cheung A, Stegmeier F, Michaud GA, Charlat O, Wiellette E, Zhang Y, Wiessner S, Hild M, Shi X, Wilson CJ, Mickanin C, Myer V, Fazal A, Tomlinson R, Serluca F, Shao W, Cheng H, Shultz M, Rau C, Schirle M, Schlegl J, Ghidelli S, Fawell S, Lu C, Curtis D, Kirschner MW, Lengauer C, Finan PM, Tallarico JA, Bouwmeester T, Porter JA, Bauer A and Cong F (2009). Tankyrase inhibition stabilizes axin and antagonizes Wnt signalling. Nature 461:614-20.

147. Singh A, Upadhyay V and Panda A (2015) Solubilization and Refolding of Inclusion Body Proteins. In: García-Fruitós E (ed) Insoluble Proteins, Springer New York, pp. 283-291

148. Yip CK, Kimbrough TG, Felise HB, Vuckovic M, Thomas NA, Pfuetzner RA, Frey EA, Brett Finlay B, Miller SI and Strynadka NCJ (2005). Structural characterization of the molecular platform for type III secretion system assembly. Nature 435:702-707.

149. Gattiker A, Bienvenut WV, Bairoch A and Gasteiger E (2002). FindPept, a tool to identify unmatched masses in peptide mass fingerprinting protein identification. Proteomics 2:1435-44.

150. Terpe K (2003). Overview of tag protein fusions: from molecular and biochemical fundamentals to commercial systems. Appl Microbiol Biotechnol 60:523-33.

151. Dharmarajan A, Zeps N and McLaren S (2005). Expression of secreted frizzled related protein-4 (sFRP-4) and associated Wnt signalling in cancer and apoptosis. Reprod Fertil Dev 17:63-63.

152. Rezaei PF, Fouladdel S, Ghaffari SM, Amin G and Azizi E (2012). Induction of G1 cell cycle arrest and cyclin D1 down-regulation in response to pericarp extract of Baneh in human breast cancer T47D cells. DARU 20:1-5.

153. Ahmad N, Feyes DK, Agarwal R, Mukhtar H and Nieminen A-L (1997). Green Tea Constituent Epigallocatechin-3-Gallate and Induction of Apoptosis and Cell Cycle Arrest in Human Carcinoma Cells. J Natl Cancer Inst 89:1881-1886.

154. Bragado P, Armesilla A, Silva A and Porras A (2007). Apoptosis by cisplatin requires p53 mediated p38α MAPK activation through ROS generation. Apoptosis 12:1733-1742.

155. Ikeguchi M, Tatebe S, Kaibara N and Ito H (1997). Changes in Levels of Expression of p53 and the Product of the bcl-2 in Lines of Gastric Cancer Cells during Cisplatin-lnduced Apoptosis. Eur Surg Res 29:396-402.

156. Rocha S, Martin AM, Meek DW and Perkins ND (2003). p53 represses cyclin D1 transcription through down regulation of Bcl-3 and inducing increased association of the p52 NF-kappaB subunit with histone deacetylase 1. Mol Cell Biol 23:4713-27.

157. Ho JS, Ma W, Mao DY and Benchimol S (2005). p53-Dependent transcriptional repression of c-myc is required for G1 cell cycle arrest. Mol Cell Biol 25:7423-31.

158. Luo J, Manning BD and Cantley LC (2003). Targeting the PI3K-Akt pathway in human cancer: Rationale and promise. Cancer Cell 4:257-262.

159. Mirza A, McGuirk M, Hockenberry TN, Wu Q, Ashar H, Black S, Wen SF, Wang L, Kirschmeier P, Bishop WR, Nielsen LL, Pickett CB and Liu S (2002). Human survivin is negatively regulated by wild-type p53 and participates in p53-dependent apoptotic pathway. Oncogene 21:2613-22.

160. Pourquier P, Montaudon D, Huet S, Larrue A, Clary A and Robert J (1998). Doxorubicin-induced alterations of c-myc and c-jun gene expression in rat glioblastoma cells: role of c-jun in drug resistance and cell death. Biochem Pharmacol 55:1963-71.

161. Clary A, Larrue A, Pourquier P and Robert J (1998). Transcriptional down-regulation of c-myc expression in an erythroleukemic cell line, K562, and its doxorubicin-resistant variant by two topoisomerase II inhibitors, doxorubicin and amsacrine. Anti-Cancer Drugs 9:245-254.

162. Fornari FA, Jr., Jarvis WD, Grant S, Orr MS, Randolph JK, White FK, Mumaw VR, Lovings ET, Freeman RH and Gewirtz DA (1994). Induction of differentiation and growth arrest associated with nascent (nonoligosomal) DNA fragmentation and reduced c-myc expression in MCF-7 human breast tumor cells after continuous exposure to a sublethal concentration of doxorubicin. Cell Growth Differ 5:723-33.

163. Lee BS, Kim SH, Jin T, Choi EY, Oh J, Park S, Lee SH, Chung JH and Kang SM (2013). Protective effect of survivin in Doxorubicin-induced cell death in h9c2 cardiac myocytes. Korean Circ J 43:400-7.

164. Estève P-O, Chin HG and Pradhan S (2007). Molecular Mechanisms of Transactivation and Doxorubicin-mediated Repression of survivin Gene in Cancer Cells. J Biol Chem 282:2615-2625.

165. Wickstrom M, Dyberg C, Milosevic J, Einvik C, Calero R, Sveinbjornsson B, Sanden E, Darabi A, Siesjo P, Kool M, Kogner P, Baryawno N and Johnsen JI (2015). Wnt/[beta]-

catenin pathway regulates MGMT gene expression in cancer and inhibition of Wnt signalling prevents chemoresistance. Nat Commun 6:8904.

166. Gurney A, Axelrod F, Bond CJ, Cain J, Chartier C, Donigan L, Fischer M, Chaudhari A, Ji M, Kapoun AM, Lam A, Lazetic S, Ma S, Mitra S, Park I-K, Pickell K, Sato A, Satyal S, Stroud M, Tran H, Yen W-C, Lewicki J and Hoey T (2012). Wnt pathway inhibition via the targeting of Frizzled receptors results in decreased growth and tumorigenicity of human tumors. Proc Natl Acad Sci U S A 109:11717-11722.

167. Stuchinskaya T, Moreno M, Cook MJ, Edwards DR and Russell DA (2011). Targeted photodynamic therapy of breast cancer cells using antibody-phthalocyanine-gold nanoparticle conjugates. Photochem Photobiol Sci 10:822-31.

168. Mock CD, Jordan BC and Selvam C (2015). Recent advances of curcumin and its analogues in breast cancer prevention and treatment. RSC Adv 5:75575-75588.

169. Wang Y, Chen J and Irudayaraj J (2011). Nuclear targeting dynamics of gold nanoclusters for enhanced therapy of HER2+ breast cancer. ACS Nano 5:9718-25.

170. Camp ER, Wang C, Little EC, Watson PM, Pirollo KF, Rait A, Cole DJ, Chang EH and Watson DK (2013). Transferrin receptor targeting nanomedicine delivering wild-type p53 gene sensitizes pancreatic cancer to gemcitabine therapy. Cancer Gene Ther 20:222-228.

171. Zheng M, Zhao P, Luo Z, Gong P, Zheng C, Zhang P, Yue C, Gao D, Ma Y and Cai L (2014). Robust ICG Theranostic Nanoparticles for Folate Targeted Cancer Imaging and Highly Effective Photothermal Therapy. ACS Appl Mater & Interfaces 6:6709-6716.

172. Yhee JY, Lee SJ, Lee S, Song S, Min HS, Kang SW, Son S, Jeong SY, Kwon IC, Kim SH and Kim K (2013). Tumor-targeting transferrin nanoparticles for systemic polymerized siRNA delivery in tumor-bearing mice. Bioconjug Chem 24:1850-60.

173. Balasubramanian S, Girija AR, Nagaoka Y, Iwai S, Suzuki M, Kizhikkilot V, Yoshida Y, Maekawa T and Nair SD (2014). Curcumin and 5-Fluorouracil-loaded, folate-

and transferrin-decorated polymeric magnetic nanoformulation: a synergistic cancer therapeutic approach, accelerated by magnetic hyperthermia. Int J Nanomedicine 9:437-459.

174. Neth P, Ries C, Karow M, Egea V, Ilmer M and Jochum M (2007). The Wnt Signal Transduction Pathway in Stem Cells and Cancer Cells: Influence on Cellular Invasion. Stem Cell Rev 3:18-29.

175. Jiang H, Xu G, Sun Y, Zheng W, Zhu X, Wang B, Zhang X and Wang G (2015). A "turn-on" silver nanocluster based fluorescent sensor for folate receptor detection and cancer cell imaging under visual analysis. Chem Commun 51:11810-11813.

176. Adhikari B and Banerjee A (2010). Facile Synthesis of Water-Soluble Fluorescent Silver Nanoclusters and HgII Sensing. Chem Mater 22:4364-4371.

177. Diez I, Pusa M, Kulmala S, Jiang H, Walther A, Goldmann AS, Muller AH, Ikkala O and Ras RH (2009). Color tunability and electrochemiluminescence of silver nanoclusters. Angew Chem Int Ed Engl 48:2122-5.

178. Lee AY, He B, You L, Dadfarmay S, Xu Z, Mazieres J, Mikami I, McCormick F and Jablons DM (2004). Expression of the secreted frizzled-related protein gene family is downregulated in human mesothelioma. Oncogene 23:6672-6676.

179. Raza A, Kohila V and Ghosh SS (2015). Redesigned Escherichia coli cytosine deaminase: a new facet of suicide gene therapy. J Gene Med 17:132-139.

180. Li J, Zhong X, Cheng F, Zhang J-R, Jiang L-P and Zhu J-J (2012). One-Pot Synthesis of Aptamer-Functionalized Silver Nanoclusters for Cell-Type-Specific Imaging. Anal Chem 84:4140-4146.

181. Foldbjerg R, Dang DA and Autrup H (2011). Cytotoxicity and genotoxicity of silver nanoparticles in the human lung cancer cell line, A549. Arch Toxicol 85:743-750.

182. Zhang J, Gill AJ, Issacs JD, Atmore B, Johns A, Delbridge LW, Lai R and McMullen TP (2012). The Wnt/beta-catenin pathway drives increased cyclin D1 levels in lymph node metastasis in papillary thyroid cancer. Hum Pathol 43:1044-50.

183. Jung H-Y, Jun S, Lee M, Kim H-C, Wang X, Ji H, McCrea Pierre D and Park J-I (2013). PAF and EZH2 Induce Wnt/β-Catenin Signaling Hyperactivation. Mol Cell 52:193-205.

184. Yuan X, Setyawati MI, Tan AS, Ong CN, Leong DT and Xie J (2013). Highly luminescent silver nanoclusters with tunable emissions: cyclic reduction-decomposition synthesis and antimicrobial properties. NPG Asia Mater 5:e39.

185. Guo D, Zhu L, Huang Z, Zhou H, Ge Y, Ma W, Wu J, Zhang X, Zhou X, Zhang Y, Zhao Y and Gu N (2013). Anti-leukemia activity of PVP-coated silver nanoparticles via generation of reactive oxygen species and release of silver ions. Biomaterials 34:7884-7894.

186. Elmore S (2007). Apoptosis: A Review of Programmed Cell Death. Toxicol Pathol 35:495-516.

187. He B, Lee AY, Dadfarmay S, You L, Xu Z, Reguart N, Mazieres J, Mikami I, McCormick F and Jablons DM (2005). Secreted frizzled-related protein 4 is silenced by hypermethylation and induces apoptosis in beta-catenin-deficient human mesothelioma cells. Cancer Res 65:743-8.

188. Sanpui P, Chattopadhyay A and Ghosh SS (2011). Induction of Apoptosis in Cancer Cells at Low Silver Nanoparticle Concentrations using Chitosan Nanocarrier. ACS Appl Mater Interfaces 3:218-228.

189. Gao S, Chen D, Li Q, Ye J, Jiang H, Amatore C and Wang X (2014). Near-infrared fluorescence imaging of cancer cells and tumors through specific biosynthesis of silver nanoclusters. Sci Rep 4:4384.

190. Wu L and Qu X (2015). Cancer biomarker detection: recent achievements and challenges. Chem Soc Rev 44:2963-2997.

191. Liu J-M, Chen J-T and Yan X-P (2013). Near Infrared Fluorescent Trypsin Stabilized Gold Nanoclusters as Surface Plasmon Enhanced Energy Transfer Biosensor and in Vivo Cancer Imaging Bioprobe. Anal Chem 85:3238-3245.

PUBLICATIONS

1. **Archita Ghoshal** and Siddhartha Sankar Ghosh (**2014**). Expression, Purification, and Therapeutic Implications of Recombinant sFRP1, ***Applied Biochemistry and Biotechnology***, Vol 175(4), 2087-2103.

2. **Archita Ghoshal**, Upashi Goswami, Amaresh Kumar Sahoo, Arun Chattopadhyay, and Siddhartha Sankar Ghosh (**2015**). Targeting Wnt Canonical Signaling by Recombinant sFRP1 Bound Luminescent Au-Nanocluster Embedded Nanoparticles in Cancer Theranostics, ***ACS Biomaterials Science and Engineering***, Vol 1(12), 1256-1266.

3. **Archita Ghoshal** and Siddhartha Sankar Ghosh (**2016**). Antagonizing Canonical Wnt Signaling Pathway by Recombinant Human sFRP4 Purified from E. coli and its Implications in Cancer Therapy, ***Molecular and Cellular Biochemistry***, Vol 418 (1-2), 119-135.

4. **Archita Ghoshal**, Upashi Goswami, Asif Raza, Arun Chattopadhyay and Siddhartha Sankar Ghosh (**2016**). Recombinant sFRP4 bound Chitosan-Alginate Composite Nanoparticles Embedded with Silver Nanoclusters for Wnt/ β-catenin targeting in Cancer Theranostics, *Manuscript Communicated*.

Collaborative work:

5. Bandhan Chatterjee, **Archita Ghoshal**, Arun Chattopadhyay, and Siddhartha Sankar Ghosh. Interactive dGTP templated Luminescent Gold Nanocluster and cisplatin PEG coated nanoparticle as novel cancer theranostic. *Manuscript under preparation*.

6. Asif Raza, **Archita Ghoshal**, and Siddhartha Sankar Ghosh. Combination therapy of Artesunate with Connexin-43 via Gap-junction Dependent and Independent Pathways. *Manuscript under preparation*.

CONFERENCES

1. Presented poster and ***won best poster award*** at the International Conference on Biotechnology and Bioinformatics, Pune, **India** (2016)
2. Presented poster in the Research Conclave, Indian Institute of Technology Guwahati, **India** (2016)
3. Presented poster at the International Conference on Advanced Nanomaterial and Nanotechnology, Guwahati, **India** (2015)
4. Presented poster at the 8th Euro Biotechnology Congress, Frankfurt, **Germany** (2015)
5. Presented poster and w***on travel award*** at the International Conference on Stem Cells and Cancer, New Delhi, **India** (2014)
6. Participated in the National Conference on New Advances and Horizons in Nanoscience and Nanotechnology, Institute of Advanced Study in Science and Technology, Guwahati, **India** (2014)

APPENDIX

All chemicals, reagents, and kits were purchased from Sigma-Aldrich, unless mentioned otherwise. Companies and institutes from which items have been procured have been stated at the first mention of each item.

Essential Bacterial strains:

- DH5α (fhuA2, lacΔU169, phoA, glnV44, Φ80', lacZΔM15, gyrA96, recA1, relA1, endA1, thi-1, hsdR17)
- BL21 (dcm, ompT, hsdS (rB^-mB^-), gal) (MTCC, India)

Plasticwares:

- Microcentrifuge tubes- 0.5 mL, 1.5 mL and 2 mL (Tarsons, India), 0.2 mL PCR tube (Grenier BioOne, USA)
- Microtips- 0.2-2 µL, 2-200 µL, 200-1000 µL (Tarsons, India)
- Petridish for bacterial culture (Tarsons, India)
- Mammalian cell culture plates- 35 mm, 60 mm and 100 mm diameter plates (BD Falcon, USA or Tarsons, India or Corning Inc, USA)

Buffers and their compositions:

Buffers	Composition
4X protein loading dye (for 10 mL)	2.0 ml 1 M Tris-HCl (pH 6.8), 0.8 g SDS, 4.0 ml 100% glycerol, 0.4 ml 14.7 M β-mercaptoethanol, 8 mg bromophenol blue in water
6X DNA loading dye	0.25 (%)(w/v) bromophenol blue, 0.25% (w/v) xylene cyanol FF, 30% (v/v) glycerol in water
Alkaline lysis solution for plasmid isolation I	50 mM glucose, 25 mM Tris-Cl (pH-8.0), EDTA (10 mM)
Alkaline lysis solution II	0.2 N NaOH, (freshly diluted from 10 N stock), 1% (w/v) SDS
Alkaline lysis solution III	5 M potassium acetate (60 mL), glacial acetic acid (11.5 mL), water (28.5 mL)
Cleaning buffer 1 for column regeneration (pH-8.5)	0.1 M boric acid, 0.5 M NaCl, adjust the pH 8.5 with sodium hydroxide
Cleaning buffer 2 for column regeneration (pH-4.5)	0.1 M sodium acetate, 0.5 M NaCl, adjust the pH 4.5 with acetic acid
Lysis buffer for protein purification	10 mM PBS (pH-7.4), 1 mM EDTA, 1 mM PMSF, 0.32% N-lauroylsarcosine
Protein elution buffer	50 mM Tris, pH 9.5 and 15 mM L-reduced glutathione
Blocking buffer	3%-5% (w/v) BSA in PBST/TBST
Phosphate buffered saline	137 mM NaCl, 2.68 mM KCl, 7.98 mM Na_2HPO_4, 1.4 mM KH_2PO_4, pH-7.4
Polyacrylamide solution (30%)	29.2% (w/w) acrylamide, 0.8% (w/w) N,N'-methylenebisacrylamide
Tris Buffered Saline Tween-20	Tris-HCl (50 mM), NaCl (150 mM), Tween-20 (0.1% v/v) pH-7.5
Tris-acetate EDTA (TAE) 50X (100 mL)	24.2 g Tris base, 5.71 mL of glacial acetic acid, 10 mL of 0.5 M EDTA (pH-8.0)
Tris-EDTA	10 mM Tris-HCl (pH-8.0), 1 mM Na_2EDTA
TSS buffer for transformation	10% (w/v) PEG 8000, 0.6% (w/v) $MgCl_2.6H_2O$, 5% (v/v) DMSO in LB